

**UNIVERSITY OF THE WESTERN
CAPE**

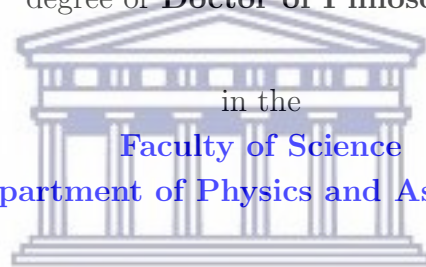
**The observed bispectrum for SKA and
other galaxy surveys**

by

Sheean Jolicoeur

A thesis submitted in partial fulfillment for the
degree of **Doctor of Philosophy**

in the
Faculty of Science
Department of Physics and Astronomy



UNIVERSITY of the
WESTERN CAPE



**UNIVERSITY of the
WESTERN CAPE**

Supervisor: **Prof. Roy Maartens**

Co-supervisor: **Dr. Obinna Umeh**

March 2019

Declaration of Authorship

I, SHEEAN JOLICOEUR, declare that this thesis titled, ‘The observed bispectrum for SKA and other galaxy surveys’ and the work presented in it are my own. I confirm that:

- This work was done wholly or mainly while in candidature for a research degree at this University.
- Where any part of this thesis has previously been submitted for a degree or any other qualification at this University or any other institution, this has been clearly stated.
- Where I have consulted the published work of others, this is always clearly attributed.
- Where I have quoted from the work of others, the source is always given. With the exception of such quotations, this thesis is entirely my own work.
- I have acknowledged all main sources of help.
- Where the thesis is based on work done by myself jointly with others, I have made clear exactly what was done by others and what I have contributed myself.

Signed:

Date:

This thesis is based on the work done by the author who has been supervised by Prof. Roy Maartens and Dr. Obinna Umeh, of the Physics & Astronomy Department, University of the Western Cape. In collaboration with my supervisors and Chris Clarkson, I have published the following papers based on my thesis:

1. O. Umeh, **S. Jolicoeur**, R. Maartens and C. Clarkson, “A general relativistic signature in the galaxy bispectrum: the local effects of observing on the lightcone,” JCAP **1703**, no. 03, 034 (2017) [arXiv:1610.03351 [astro-ph.CO]].
2. **S. Jolicoeur**, O. Umeh, R. Maartens and C. Clarkson, “Imprints of local lightcone projection effects on the galaxy bispectrum. Part II,” JCAP **1709**, no. 09, 040 (2017) [arXiv:1703.09630 [astro-ph.CO]].
3. **S. Jolicoeur**, O. Umeh, R. Maartens and C. Clarkson, “Imprints of local lightcone projection effects on the galaxy bispectrum. Part III. Relativistic corrections from nonlinear dynamical evolution on large-scales,” JCAP **1803**, no. 03, 036 (2018) [arXiv:1711.01812 [astro-ph.CO]].



“Science without religion is lame, religion without science is blind.”

Albert Einstein



UNIVERSITY *of the*
WESTERN CAPE

UNIVERSITY OF THE WESTERN CAPE

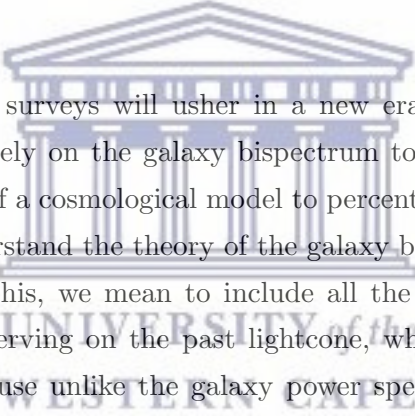
Abstract

Faculty of Science

Department of Physics and Astronomy

Doctor of Philosophy

by Sheean Jolicoeur



Next-generation galaxy surveys will usher in a new era of high precision cosmology. They will increasingly rely on the galaxy bispectrum to provide improved constraints on the key parameters of a cosmological model to percent level or even beyond. Hereby, it is imperative to understand the theory of the galaxy bispectrum to at least the same level of precision. By this, we mean to include all the general relativistic projection effects arising from observing on the past lightcone, which still remains a theoretical challenge. This is because unlike the galaxy power spectrum, the galaxy bispectrum requires these lightcone corrections at second-order. For the first time, this PhD project looks at all the local relativistic lightcone effects in the galaxy bispectrum for a flat Friedmann-Lemaître-Robertson-Walker Universe, giving full details on the second-order scalars, vectors and tensors. These lightcone effects are mostly Doppler and gravitational potential contributions. The vector and tensor modes are induced at second order by scalars. We focus on the squeezed shapes for the monopole of the galaxy bispectrum because non-Gaussianity of the local form shows high signatures for these triangular configurations. In the exact squeezed limit, the contributions from the vectors and tensors vanish. These relativistic projection effects, if not included in the analysis of observations, can be mistaken for primordial non-Gaussianity. For future surveys which will probe equality scales and beyond, all the relativistic corrections will need to be considered for an accurate measurement of primordial non-Gaussianity.

Acknowledgements

This PhD project would not have been accomplished without the support of many people. First of all, I would like to thank in a special way my supervisors, Roy Maartens and Obinna Umeh, for both academic and personal guidance. One simply could not wish for better and friendlier supervisors. I would also like to thank Chris Clarkson for his collaboration in the published works. I also owe special thanks to my mates Vijay P. Chumroo, Rajin Ramphul, Arrykrishna Mootoovaloo, Zafiirah Hosenie, Mika H. Rafieferantsoa, Marc H. F. Yao and Emmanuel F. Ocran for useful discussions and proof-reading. I am grateful to Roselyn Matthews Daniels for her very kind assistance at University of Cape Town. I am very grateful to Kazuya Koyama, Tobias Baldauf, Daniele Bertacca, Ruth Durrer, Sabino Matarrese and David Wands for very helpful discussions and comments.

I am highly indebted to the Physics and Astronomy department of Queen Mary University of London for hospitality during my stay with them. I would like to thank Chris Clarkson, Timothy Clifton, Karim Malik and all the postgraduate students in the group for every special assistance given to me. I also thank the Physics and Astronomy department of University of the Western Cape for all its support. This PhD is fully funded by the South African Square Kilometre Array (SKA) Project. My stay in London was supported by the SKA travel grant.

I thank my parents for their unconditional love, discipline, prayers and support. I would also like to offer my deepest respect to Veera Lakshmi Mandir which has always been my motherhood and special thanks to my uncles Vinod & Vikram Mohabir for their encouragement and guiding principles.

Finally, I would like to thank God Almighty for giving me the knowledge, strength, and opportunity to undertake this research study. Without His blessings, the completion of this work would not have been possible.

Contents

Declaration of Authorship	i
Abstract	iv
Acknowledgements	v
Abbreviations	ix
1 Introduction	1
1.1 The Big Bang model	1
1.2 Inflation	2
1.3 Structure formation in the Universe	3
1.4 Signatures of non-Gaussianity in structure formation	5
1.5 The standard model of cosmology	6
1.5.1 Overview	6
1.5.2 The background Friedmann Universe	7
1.5.3 Conservation equations	9
1.5.4 Dark energy and the cosmic acceleration	10
1.5.5 Distances in a flat FLRW Universe	11
1.5.6 Baryon Acoustic Oscillations	13
1.6 Perturbation theory	15
1.6.1 Overview	15
1.6.2 Linear scalar perturbation theory	16
1.6.2.1 Derivation of Einstein field equations	16
1.6.2.2 Perturbed conservation equations	18
1.6.2.3 Growth in Λ CDM model	19
1.6.3 Second-order scalar perturbations in Λ CDM	24
1.6.4 Solutions to the Einstein field equations	26
1.7 Cosmology with the Square Kilometre Array	27
1.7.1 BAO constraints	27
1.7.2 Redshift space distortion	28
1.7.3 Testing General Relativity and Modified Gravity	29
1.7.4 HI intensity mapping	30
1.8 Thesis outline	31

2	Perturbation theory in the galaxy number counts	32
2.1	The galaxy number count fluctuation	32
2.2	First-order scalars	33
2.2.1	First-order redshift perturbation $\delta z^{(1)}$	36
2.2.2	First-order volume perturbation $\delta \mathcal{V}^{(1)}$	38
2.3	The model of galaxy bias on very large scales	42
2.3.1	The linear model	42
2.3.2	The non-linear model and gauge transformation	43
2.4	Second-order galaxy number counts (scalar modes)	46
2.5	Second-order induced vector and tensor modes	49
2.6	The Newtonian and GR parts of Δ_g	49
3	The Fourier galaxy bispectrum	54
3.1	Fourier space	54
3.2	The galaxy number count fluctuation in Fourier space	55
3.2.1	Fourier transform of the first-order terms	55
3.2.2	Fourier transform of the second-order terms	57
3.2.2.1	Scalars	57
3.2.2.2	Vectors	66
3.2.2.3	Tensors	72
3.3	The galaxy power spectrum	76
3.4	The galaxy bispectrum	81
3.4.1	Wick's theorem	81
3.4.2	The multipoles of the galaxy bispectrum	83
3.4.3	The monopole in the squeezed configuration	86
4	The GR projection effects in the Gaussian galaxy bispectrum	90
4.1	Method of computation	90
4.2	The effect of the tidal term	91
4.3	Correlations in the galaxy bispectrum	93
4.3.1	Quadratic first-order and intrinsic GR second-order scalars	94
4.3.2	Vectors and tensors	97
4.4	The full local relativistic galaxy bispectrum	98
4.5	2-D colour plot	100
5	The GR projection effects in the non-Gaussian galaxy bispectrum	102
5.1	Local primordial non-Gaussianity	102
5.2	Second-order dark matter and velocity kernels in the presence of PNG	103
5.3	Galaxy overdensity with PNG	104
5.4	PNG in the squeezed Newtonian galaxy bispectrum	107
5.5	PNG in the full relativistic galaxy bispectrum	111
6	Conclusion and future work	116
6.1	Summary	116
6.2	Major findings of the project	117
6.3	Upcoming projects	118

Bibliography

120



UNIVERSITY *of the*
WESTERN CAPE

Abbreviations

Acronym	What (it) Stands For
AP	Alcock-Paczynski
BAO	Baryon Acoustic Oscillations
BOSS	Baryon Acoustic Oscillation Spectroscopic Survey
CMB	Cosmic Microwave Background
DES	Dark Energy Survey
EdS	Einstein-de-Sitter
EoS	Equation of State
FLRW	Friedmann-Lemaître-Robertson-Walker
GR	General Relativity
IM	Intensity Mapping
MeerKAT	Karoo Array Telescope
ΛCDM	Lambda Cold Dark Matter
LSS	Large Scale Structure
MG	Modified Gravity
2PCF	2-Point Correlation Function
PNG	Primordial non-Gaussianity
RSD	Redshift Space Distortions
SDSS	Sloan Digital Sky Survey
SR	Special Relativity
SKA	Square Kilometre Array
SNIa	Type Ia SuperNovae

Dedicated to my parents & Veera Lakshmi Mandir



UNIVERSITY *of the*
WESTERN CAPE

Chapter 1

Introduction

1.1 The Big Bang model

The standard model of the expanding Universe predicts a beginning (the ‘Big bang’), 13.8 Gyr ago, of infinite temperature and density. The Big Bang model provides successful explanation for different observed phenomena in the Universe e.g., the Hubble’s law, large scale structure, Cosmic Microwave Background (CMB) radiation and abundance of light elements. Despite of these, the Big Bang model has faced many problems for the major reason that only a decelerating expansion of the Universe is possible for normal matter. The two main problems are:

- *Horizon problem:* Opposite patches of the CMB sky have never been in casual contact, according to the Big Bang model. Yet, the CMB we observe today is statistically isotropic and by the Copernican principle, it is also homogeneous [1]. This shows that the different patches of the sky (10^{90} different regions [2]) appeared to have had enough time to communicate with each other when the CMB photons were emitted at the surface of last scattering.

A possible solution to the horizon problem will be to find a way to shrink the comoving Hubble length, r_H such that the particles could exchange information with each other.

- *Flatness problem:* The spatial Universe today is within a very good approximation, Euclidean i.e., it is flat [3]. However, according to the Big Bang model, this is unlikely to be true for our old Universe since it can be shown that the total energy density of matter, radiation and dark energy is related to the comoving Hubble

radius as [1],

$$1 - \Omega(t) \propto r_{\text{H}}^2(t) , \quad (1.1)$$

where we have set the speed of light, c to 1. The comoving Hubble radius defines that sphere whose expansion follows the Hubble flow. For all world models with a big bang origin, $r_{\text{H}}^2 \propto t$ near the big bang event [1] and this shows that $|\Omega - 1|$ must diverge with increasing time. Hence, the critical point at which $\Omega = 1$ that sets the condition for flatness is an unstable point [4]. Also, at the time of the Big Bang Nucleosynthesis (BBN) the Universe was flat, with $|\Omega - 1| \sim 10^{-18}$ [5]. This is based on extrapolating the CMB constraints to very early times, and is not an independent measurement.

A possible way to address the flatness problem is to decrease r_{H} at early time so that the curvature decreases.

We have seen that the solution to the above two problems is to effectively find a way to shrink the comoving Hubble radius at early time and then, to return the evolution back to the standard Big Bang model. One such realization is done through the theory of cosmic Inflation [6].

1.2 Inflation

Inflation is a brief period of accelerated expansion in early times of the Universe. It aims at improving the explanation of the Big Bang theory on the primordial Universe. There are several ways of defining inflation but, a more geometrical approach of writing it is as follows [7],

$$\frac{dr_{\text{H}}}{dt} < 0 . \quad (1.2)$$

It shows that the rate of change of the comoving Hubble radius is negative, which means a decrease during inflation. This happens over a very short period of time where the Universe undergoes an ultra rapid accelerated expansion. Then, any length scale measurement in the Universe becomes very small relative to this expansion.

The most adopted model of inflation is the slow-roll inflation [8]. It predicts that inflation cannot be an everlasting process. The accelerated expansion ceases when the kinetic energy of the scalar (inflaton) field dominates its potential energy [9]. In addition to addressing the horizon and flatness problems, inflation provides a natural mechanism for generating the primordial perturbations that seed the CMB anisotropies and large-scale structure formation.

1.3 Structure formation in the Universe

The small and large scale structures e.g., stars, galaxies, galaxy clusters and cosmic web, that we observe today have been formed through the gravitational amplification of tiny matter density fluctuations generated at very early times in the Universe [10]. Figure 1.1 shows the distribution of galaxies in the Universe. With our large ground-based

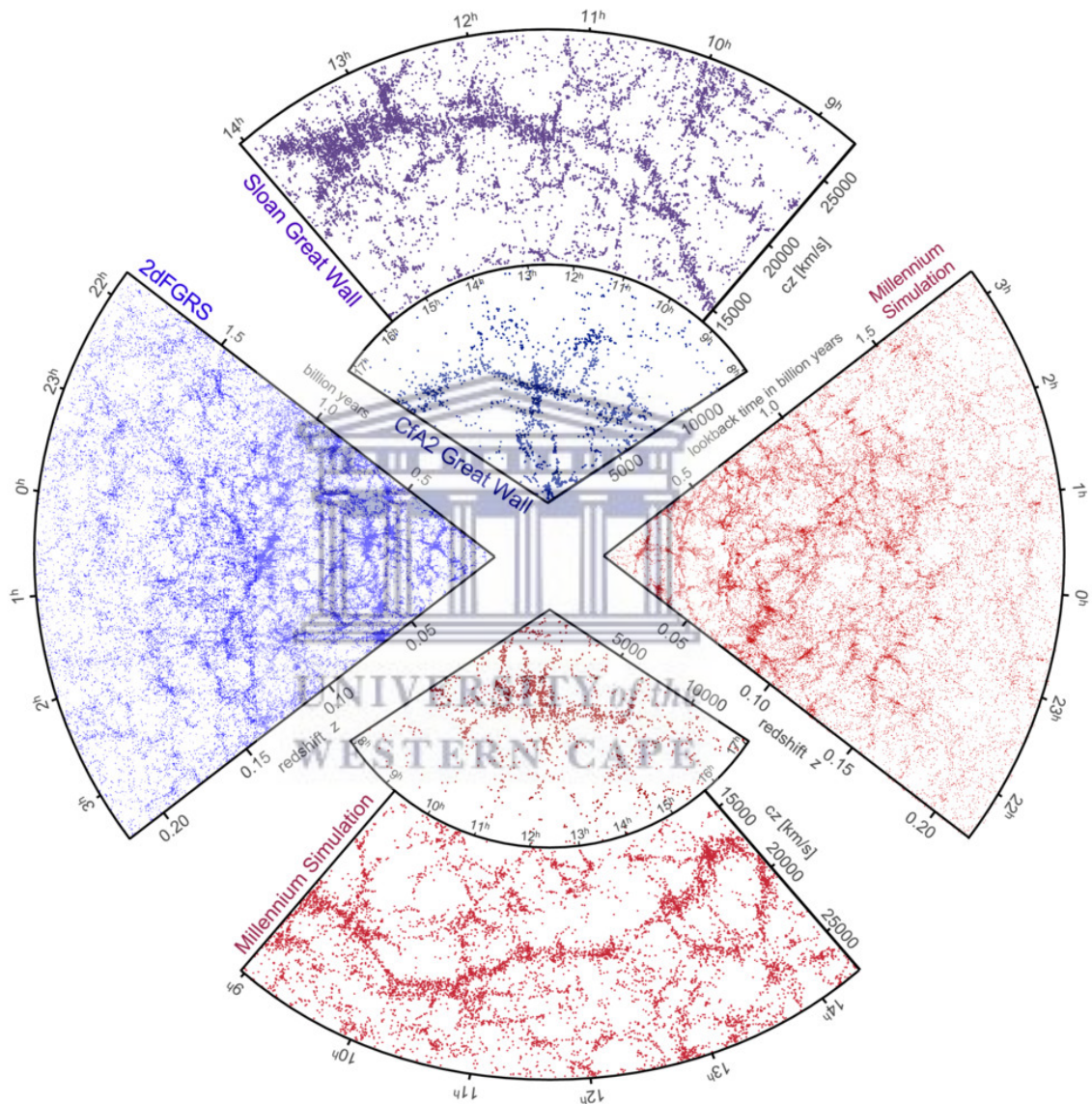


FIGURE 1.1: The distribution of galaxies from spectroscopic redshift surveys (blue and purple) and mock data constructed from cosmological simulations (red) (from [11]).

telescopes, we have been able to observe very distant galaxies and quasars aging ~ 12.8 billion years [12]. We also observe the CMB radiation which is a remnant of the early stage of the Universe [13–16]. The epoch between CMB and the formation of the first stars is called the cosmic Dark Ages [17].

At the recombination epoch which happened $\sim 300,000$ years after the Big Bang event, the first hydrogen atoms were formed and the CMB photons free-streamed through the Universe. It then took a very long time before the first stars were born to terminate the Dark Ages. They were the first sources of light and heavy elements that enabled the formation of more complex bodies e.g., planets and galaxies. This is summarized below in Figure 1.2.

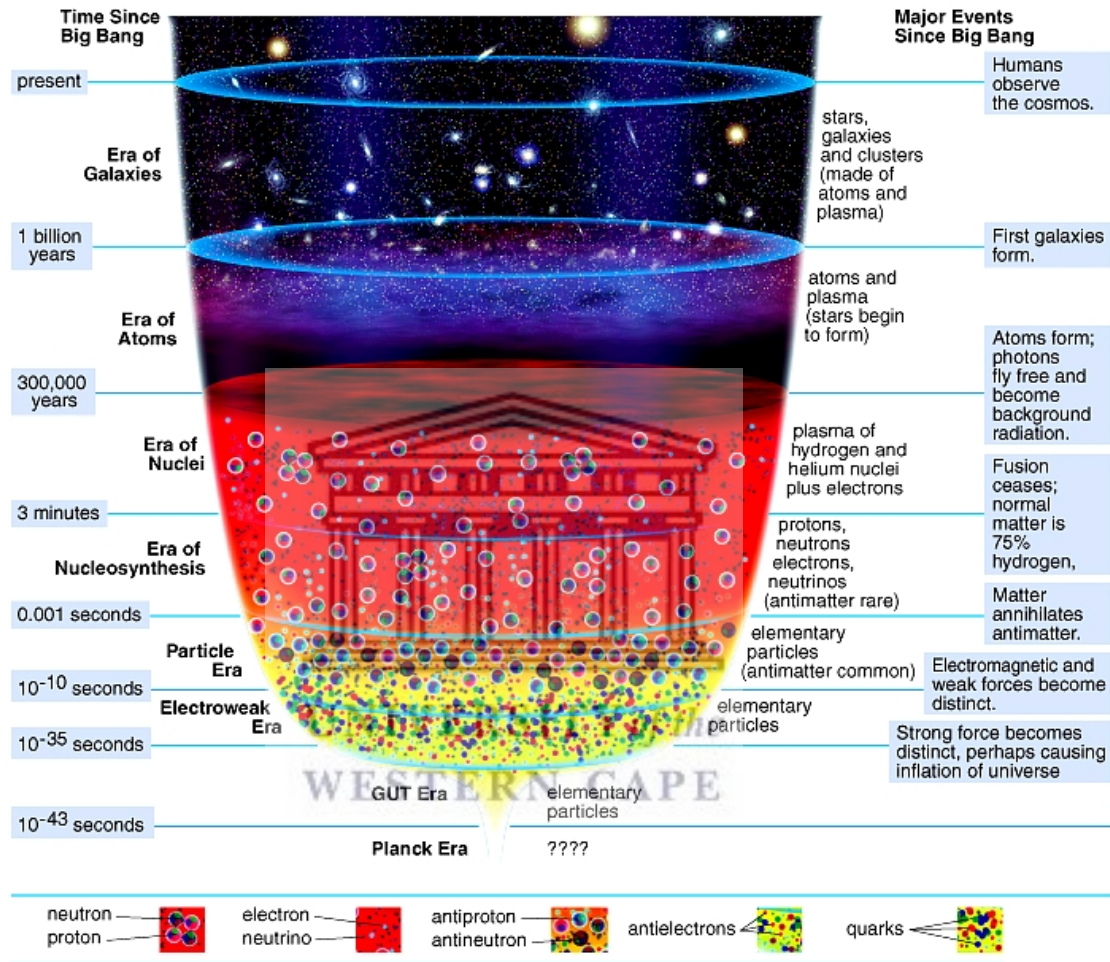


FIGURE 1.2: The cosmic timeline (from [18]).

The characteristics of the primordial density perturbations are predicted from inflation [19]. Most single-field inflationary models describe them as Gaussian random fields with a nearly scale-invariant dimensionless power spectrum [20, 21],

$$\mathcal{P}_\xi(k) = A_s \left(\frac{k}{k_*} \right)^{n_s - 1}, \quad (1.3)$$

where ξ is the primordial curvature perturbation, k is the wavenumber and $n_s \sim 1$ is the spectral index. The perturbations lead to the formation of dark matter halos. The first 'dark' objects are very small dark matter halos that are formed at any mass scales by

gravitational instability from density fluctuations [10]. Then the baryons are pulled in by the strong gravitational force of the halos to form small clumps of baryonic matter. Many of these clumps merge to form galaxies, which are drawn together by gravitation to form galaxy clusters.

1.4 Signatures of non-Gaussianity in structure formation

Cosmic inflation which addresses the basic problems of the Big Bang theory has several generic predictions on the nature of the density perturbations that seed the large scale structures (LSS) [22]:

- They are frozen on superhorizon scales.
- They are nearly scale-invariant because the Fourier modes, \mathbf{k} , experience nearly the same expansion rate as they are stretched across the horizon.
- They are approximately Gaussian in the single-field slow-roll inflationary models [23, 24].

CMB temperature anisotropy experiments and galaxy surveys are the best data sets to test the above predictions. The primordial perturbations are treated as Gaussian if their statistical properties are fully explained by the power spectrum.

To learn more about the interaction details of the primordial perturbations and break degeneracies among several models, we need to go beyond the power spectrum [22]. Deviations from Gaussianity are therefore, encoded in the 3PCF and 4PCF namely, the bispectrum and trispectrum respectively [25, 26]. A way of parameterizing the level of non-Gaussianity is to expand the real space non-Gaussian primordial gravitational potential, Φ_P , as a power series of the linear Gaussian gravitational potential, φ , as follows [27–29],

$$-\Phi_P(\mathbf{x}) = \varphi(\mathbf{x}) + f_{\text{NL}} (\varphi^2(\mathbf{x}) - \langle \varphi^2(\mathbf{x}) \rangle) + \dots, \quad (1.4)$$

where the dimensionless parameter f_{NL} sets the magnitude for the amount of non-Gaussianity. Recent studies on primordial non-Gaussianity (PNG) contributions to correlation functions have shown that they mimic the relativistic effects on large scales [30–34]. This is illustrated for the case of the monopole of the galaxy power spectrum in Figure 1.3 below.

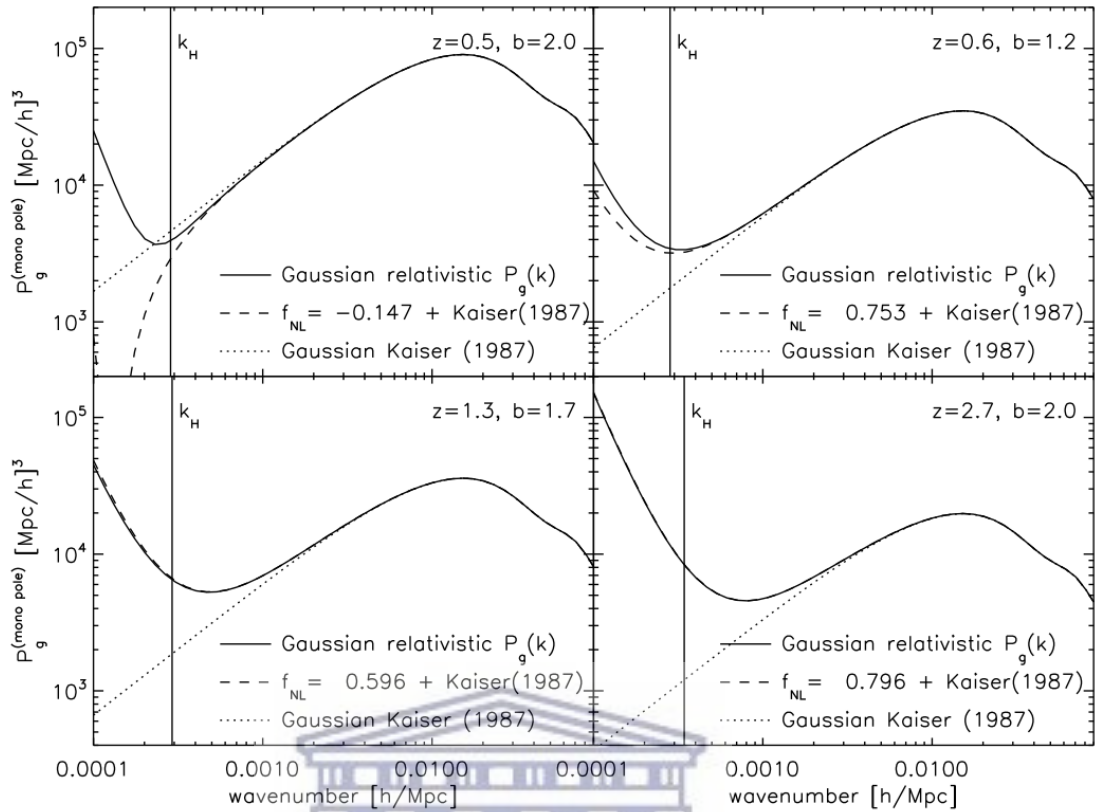


FIGURE 1.3: The Kaiser term constitutes the galaxy bias and RSD. $f_{\text{NL}}+\text{Kaiser}$ (dashed) mimics the Gaussian GR+Kaiser corrections (solid) on large scales for $f_{\text{NL}} \rightarrow 1$ (from [32]).

1.5 The standard model of cosmology

1.5.1 Overview

In the standard model of cosmology, the fundamental assumption is that the Universe is homogeneous and isotropic on sufficiently large scales ($\gtrsim 100$ Mpc). This is known as the Cosmological Principle and it is supported by ‘Occam’s razor’ hypothesis. This hypothesis is used as a heuristic technique to set up theoretical models and imposes that a good model is the one with the fewest assumptions. Therefore, it puts strong constraints on the geometry of spacetime and the type of underlying matter field that can describe the Universe on large scales. Among the constraints are two important ones and they are [35]:

1. The Universe when averaged over sufficiently large scales is isotropic i.e., every observable must be invariant under rotation on large scales.
2. All comoving observers experience the same history of the Universe i.e., they observe the same properties of averaged observables if they set their clocks suitably.

This is known as a homogeneous Universe which implies that every observable must be invariant under translation.

The first point above is observationally supported by the CMB where the averaged temperature of the photons arriving from different parts of the sky is nearly the same ($T_{\text{CMB}} = 2.73 \text{ K}$) [36]. The second point is supported by the fact that we understand the small angular scale Physics of the CMB using linear perturbations of a homogeneous background.

1.5.2 The background Friedmann Universe

The only metric which satisfies the constraints of isotropy and homogeneity is the Friedmann-Lemaître-Robertson-Walker (FLRW) and it is given by [37],

$$\bar{d}s^2 = -dt^2 + a^2(t) \left(\frac{d\bar{\chi}^2}{1 - K\bar{\chi}^2} + \bar{\chi}^2 d\theta^2 + \bar{\chi}^2 \sin^2 \theta d\phi^2 \right), \quad (1.5)$$

where t is the cosmic time, a is the scale factor which accounts for the background expansion of the Universe, $(\bar{\chi}, \theta, \phi)$ are the comoving radial and angular spherical coordinates and K is the curvature parameter. The latter can take a positive, zero or a negative value corresponding to a closed (spherical), flat or open (hyperbolic) Universe respectively. The evolution of the scale factor is determined by solving the Einstein field equations,

$$\bar{G}_{\mu\nu} + \Lambda \bar{g}_{\mu\nu} = 8\pi G \bar{T}_{\mu\nu}, \quad (1.6)$$

where Λ is the cosmological constant. The Einstein tensor is defined as,

$$\bar{G}_{\mu\nu} = \bar{R}_{\mu\nu} - \frac{1}{2} \bar{g}_{\mu\nu} R, \quad (1.7)$$

where $\bar{R}_{\mu\nu}$ and R are the Ricci tensor and Ricci scalar respectively. The Ricci tensor is obtained from the Christoffel symbol $\bar{\Gamma}^\lambda_{\mu\nu}$ as follows [38],

$$\bar{R}_{\mu\nu} = \partial_\lambda \bar{\Gamma}^\lambda_{\mu\nu} - \partial_\nu \bar{\Gamma}^\lambda_{\lambda\mu} + \bar{\Gamma}^\lambda_{\lambda\sigma} \bar{\Gamma}^\sigma_{\mu\nu} - \bar{\Gamma}^\lambda_{\sigma\nu} \bar{\Gamma}^\sigma_{\lambda\mu}. \quad (1.8)$$

The Christoffel symbol is related to metric tensor $\bar{g}_{\mu\nu}$ as [36, 38],

$$\bar{\Gamma}^\lambda_{\mu\nu} = \frac{1}{2} \bar{g}^{\lambda\sigma} (\partial_\mu \bar{g}_{\nu\sigma} + \partial_\nu \bar{g}_{\mu\sigma} - \partial_\sigma \bar{g}_{\mu\nu}), \quad (1.9)$$

and for the metric given in (1.5) the non-zero Christoffel symbols are found to be,

$$\begin{aligned}
\bar{\Gamma}^0_{11} &= \frac{a\dot{a}}{1 - K\bar{\chi}^2}, & \bar{\Gamma}^0_{22} &= a\dot{a}\bar{\chi}^2, \\
\bar{\Gamma}^0_{33} &= a\dot{a}\bar{\chi}^2 \sin^2 \theta, & \bar{\Gamma}^1_{01} &= \bar{\Gamma}^2_{02} = \bar{\Gamma}^3_{03} = \frac{\dot{a}}{a}, \\
\bar{\Gamma}^1_{11} &= \frac{K\bar{\chi}}{1 - K\bar{\chi}^2}, & \bar{\Gamma}^1_{22} &= -\bar{\chi}(1 - K\bar{\chi}^2), \\
\bar{\Gamma}^1_{33} &= -\bar{\chi}(1 - K\bar{\chi}^2) \sin^2 \theta, & \bar{\Gamma}^2_{33} &= -\sin \theta \cos \theta, \\
\bar{\Gamma}^2_{12} &= \bar{\Gamma}^3_{13} = \frac{1}{\bar{\chi}}, & \bar{\Gamma}^3_{23} &= \cot \theta.
\end{aligned} \tag{1.10}$$

Then, the non-zero elements of the Ricci tensor can be calculated from (1.8) and they are,

$$\begin{aligned}
\bar{R}_{00} &= -3(\dot{H} + H^2), & \bar{R}_{11} &= \frac{a^2}{1 - K\bar{\chi}^2} \left(\dot{H} + 3H^2 + \frac{2K}{a^2} \right), \\
\bar{R}_{22} &= a^2\bar{\chi}^2 \left(\dot{H} + 3H^2 + \frac{2K}{a^2} \right), & \bar{R}_{33} &= a^2\bar{\chi}^2 \sin^2 \theta \left(\dot{H} + 3H^2 + \frac{2K}{a^2} \right),
\end{aligned} \tag{1.11}$$

where $H = \dot{a}/a$ is the Hubble parameter and $\dot{a} = da/dt$. The Ricci scalar is then obtained as,

$$\bar{R} = 6 \left(\dot{H} + 2H^2 + \frac{K^2}{a^2} \right). \tag{1.12}$$

The metric given in (1.5) admits a perfect fluid whose energy momentum tensor is given by [38],

$$\bar{T}_{\mu\nu} = (\bar{\rho} + \bar{p})\bar{U}_\mu\bar{U}_\nu + \bar{p}g_{\mu\nu}, \tag{1.13}$$

where we have absorbed the Λ term of (1.7) in $\bar{T}_{\mu\nu}$. Here, \bar{U}_μ is the 4-velocity vector of the fluid and, $\bar{\rho}$ and \bar{p} are the energy density and pressure. For a comoving observer, $\bar{U}_\mu = (-1, \mathbf{0})$ and we find that,

$$\begin{aligned}
\bar{T}_{00} &= \bar{\rho}, & \bar{T}_{11} &= \frac{\bar{p}a^2}{1 - K\bar{\chi}^2}, \\
\bar{T}_{22} &= \bar{p}a^2\bar{\chi}^2, & \bar{T}_{33} &= \bar{p}a^2\bar{\chi}^2 \sin^2 \theta.
\end{aligned} \tag{1.14}$$

It is then easy to solve the Einstein field equations by using (1.10), (1.11) and (1.14) and we obtain a system of equations for the evolution of the scale factor as,

$$H^2 = \frac{8\pi G\bar{\rho}}{3} - \frac{K}{a^2}, \tag{1.15}$$

$$H^2 + \dot{H} = -\frac{4\pi G}{3}(\bar{\rho} + 3\bar{p}). \tag{1.16}$$

Equation (1.15) is known as the Friedmann equation and (1.16) is the Raychaudhuri equation. By assuming that matter in the Universe can be treated as a barotropic fluid, then its equation of state (EoS) is given by [36, 38],

$$\bar{p} = w\bar{\rho}, \quad (1.17)$$

where w is the EoS parameter. For a Universe dominated by:

- a non-relativistic matter, we have $w = 0$,
- a gas of relativistic particles, we have $w = 1/3$, and
- a cosmological constant, we have $w = -1$.

Therefore we can express (1.16) in terms of w as,

$$H^2 + \dot{H} = -\frac{4\pi G}{3} (1 + 3w) \bar{\rho}. \quad (1.18)$$

1.5.3 Conservation equations

The Bianchi identity requires that the covariant divergence of the Einstein tensor vanishes i.e.,

$$\bar{\nabla}_\nu \bar{G}^{\mu\nu} = 0, \quad (1.19)$$

and from the Einstein field equations in (1.6) it implies that,

$$\bar{\nabla}_\nu \bar{T}^{\mu\nu} = 0, \quad (1.20)$$

which is the conservation of the energy-momentum tensor. The continuity equation is then obtained by contracting (1.20) with \bar{U}_μ . This yields the following equation,

$$\dot{\bar{\rho}} + \bar{\Theta} (1 + w) \bar{\rho} = 0, \quad (1.21)$$

where $\dot{\bar{\rho}} = \bar{U}^\nu \nabla_\nu \bar{\rho}$ and $\bar{\Theta}$ is the volume expansion rate given by,

$$\bar{\Theta} = \partial_\nu \bar{U}^\nu + \bar{\Gamma}^\nu_{\nu\alpha} \bar{U}^\alpha. \quad (1.22)$$

For a comoving observer $\bar{\Theta} = 3H$ and by using the Christoffel symbol given in (1.10) we find that,

$$\dot{\bar{\rho}} + 3H (1 + w) \bar{\rho} = 0. \quad (1.23)$$

The other conservative equation is the Euler equation. We can re-express the energy-momentum tensor in terms of the spatial tensor \bar{h}_μ^α as follows,

$$\bar{T}_\mu^\alpha = \bar{\rho} \bar{U}_\mu \bar{U}^\alpha + \bar{h}_\mu^\alpha \bar{p}, \quad (1.24)$$

where $\bar{h}_\mu^\alpha = \bar{U}_\mu \bar{U}^\alpha + \delta_\mu^\alpha$. Then the Euler equation is obtained by contracting (1.20) with \bar{h}_μ^α . This gives the following equation,

$$(1 + w) \bar{\rho} \dot{\bar{U}}^\alpha + \bar{h}^{\alpha\nu} \bar{\nabla}_\nu \bar{p} = 0, \quad (1.25)$$

where $\dot{\bar{U}}^\alpha$ is the 4-acceleration vector given by $\dot{\bar{U}}^\alpha = \bar{U}^\nu \bar{\nabla}_\nu \bar{U}^\alpha$. Because of isotropy there can be no non-zero physical spatial vectors and this means that $\dot{\bar{U}}^\alpha$ and the spatial gradient of the pressure, $\bar{\nabla}_\nu \bar{p}$ must both be zero. Therefore, (1.25) is identically satisfied in a FLRW background. We summarize the solutions for the evolution of the scale factor and energy density in different Universe scenarios with $K = 0$ in Table 1.1 below. They are obtained by solving (1.15) and (1.23).

TABLE 1.1: Possible FLRW solutions for each fluid dominating the energy budget of a flat Universe.

	w	$\bar{\rho}(a)$	$a(t)$
Radiation	1/3	a^{-4}	$t^{1/2}$
Matter	0	a^{-3}	$t^{3/2}$
Λ	-1	a^0	e^{Ht}

1.5.4 Dark energy and the cosmic acceleration

If there is only ordinary matter present in the Universe, then the expansion rate of the cosmos is expected to slow down with time since gravitational interaction is attractive. However, this is not the case because the expansion rate is growing faster. This is observationally supported from the measurement of luminosity distances of type Ia supernovae (SNIa) which shows that the Universe is not only expanding but the expansion is accelerating [39]. Many efforts are still being made to explain the nature of this acceleration both observationally and theoretically using data from CMB measurements down to galaxy surveys e.g., Baryon Acoustic Oscillation Spectroscopic Survey (BOSS) [40] and Dark Energy Survey (DES) [41].

From the Raychaudhuri equation given in (1.18), the condition required for an accelerated expansion is found to be when $w < -1/3$. Thus, a negative pressure,

$$\bar{p} < -\frac{1}{3} \bar{\rho}, \quad (1.26)$$

is needed to create the acceleration. This violates the strong energy condition (SEC) [42],

$$\bar{\rho} + 3\bar{p} \geq 0, \quad (1.27)$$

but does not inhibit the causality for particle interactions. The cosmological constant, Λ has effective $w = -1$ and is interpreted as a vacuum energy model for dark energy. However, quantum field theory predicts a much larger amplitude for the vacuum energy than is observed. If dark energy (DE) is no the cosmological constant, then $w \neq -1$ and $\bar{\rho}_{\text{DE}}$ is no longer constant. But there is also no satisfactory model for this dynamical DE.

1.5.5 Distances in a flat FLRW Universe

In our Universe several fluids obeying different equation of states coexist and for the current standard model of cosmology which is the Lambda Cold Dark Matter (Λ CDM) model, dark energy is parametrized by Λ and we can write the Friedmann equation (1.15) as,

$$H^2 = \frac{8\pi G}{3} (\bar{\rho}_m + \bar{\rho}_r + \bar{\rho}_\Lambda), \quad (1.28)$$

where $\bar{\rho}_m$, $\bar{\rho}_r$ (photons and neutrinos), $\bar{\rho}_\Lambda$ are the energy densities of matter (cold dark matter + baryons), radiation and dark energy respectively. It is more convenient to express (1.28) in terms of the dimensionless density parameters,

$$\Omega_{(i)}(a) = \frac{8\pi G \bar{\rho}_{(i)}(a)}{3H^2}, \quad (1.29)$$

where $\bar{\rho}_{(i)}$ denotes the energy densities. Hence, we have the Friedmann equation expressed as,

$$1 = \Omega_m + \Omega_r + \Omega_\Lambda, \quad (1.30)$$

or as,

$$H(a) = H_0 \sqrt{\Omega_{m_0} a^{-3} + \Omega_{r_0} a^{-4} + \Omega_{\Lambda_0}}, \quad (1.31)$$

where the dimensionless density parameters at present time are given by the Planck data 2018: $\Omega_{m_0} = 0.308$, $\Omega_{r_0} = 9.24 \times 10^{-5}$, $\Omega_{\Lambda_0} = 0.692$ and the Hubble constant, $H_0 = 67.8 \text{ km s}^{-1} \text{ Mpc}^{-1} = 100 h \text{ km s}^{-1} \text{ Mpc}^{-1}$ [43].

The comoving distance, $\bar{\chi}$ between two comoving points is the distance measured along the path joining the two points at a defined cosmological time t divided by $a(t)$. It remains unchanged as the Universe expands because the comoving coordinates are frozen on the background. The only distance which changes is the physical distance and it is

written as,

$$\mathcal{D}(t) = a(t)\bar{\chi} . \quad (1.32)$$

In Figure 1.4, we show a spacetime diagram where the vertical axis represents time and the horizontal axis is 3-dimensional space. We consider a distant galaxy receding from

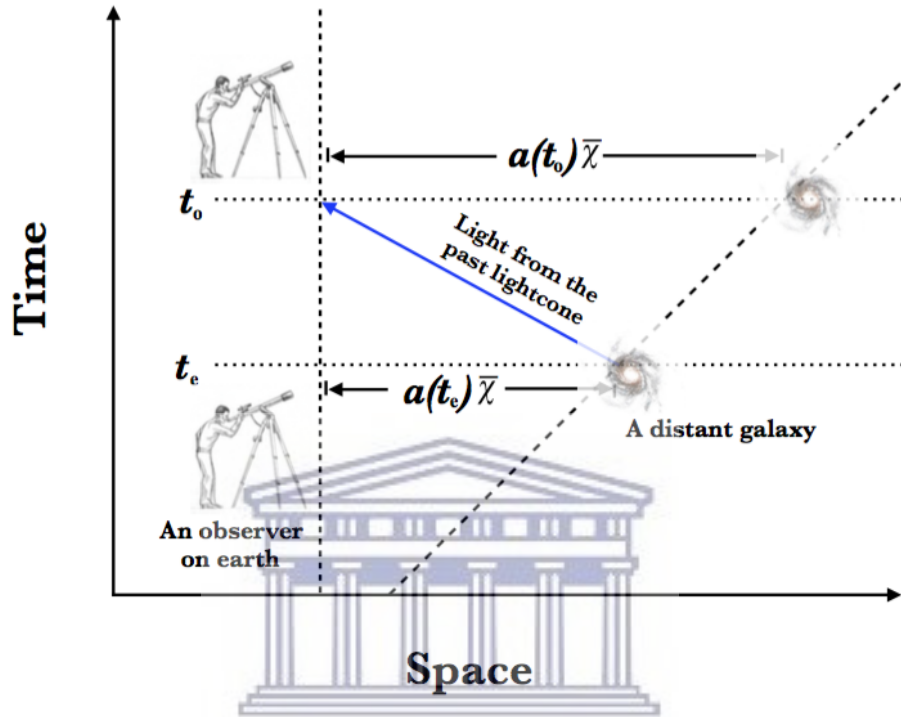


FIGURE 1.4: A worldline diagram showing light emitted by a distance galaxy from the past lightcone reaching an observer on earth.

an observer on earth. It emits a ray of light at time t_e which reaches the observer at time t_o . We choose the unit of time such that the speed of light, c is given by the gradient of the inclined line (solid blue) at a fixed angle of 45° with respect to the horizontal axis. In that case, if we consider a small element of the blue line we can write the following,

$$a d\bar{\chi} = -dt , \quad (1.33)$$

and therefore we obtain,

$$\bar{\chi} = \int_{t_e}^{t_o} \frac{dt}{a(t)} , \quad (1.34)$$

where we have set $c = 1$. The motion of the galaxy induces a change in the wavelength of the light ray reaching the observer at t_o . We characterize this change by the redshift \bar{z} and it is related to the scale factor as [38],

$$1 + \bar{z} = \frac{a_0}{a(t)} , \quad (1.35)$$

where a_0 is the scale factor defined at present time and is usually taken to be 1. Hence, we can express (1.34) in terms of redshift and we obtain,

$$\bar{\chi}(\bar{z}) = \int_0^{\bar{z}} \frac{dz'}{H(z')} \equiv \int_0^{\bar{z}} \frac{dz'}{H_0 \sqrt{\Omega_{m_0}(1+z')^3 + \Omega_{r_0}(1+z')^4 + \Omega_{\Lambda_0}}} . \quad (1.36)$$

The angular diameter distance, \bar{D}_A follows directly from (1.36) as [44, 45],

$$\bar{D}_A = \frac{\bar{\chi}}{1 + \bar{z}} . \quad (1.37)$$

We show the numerical results below in Figure 1.5. The comoving distance, $\bar{\chi}$ increases

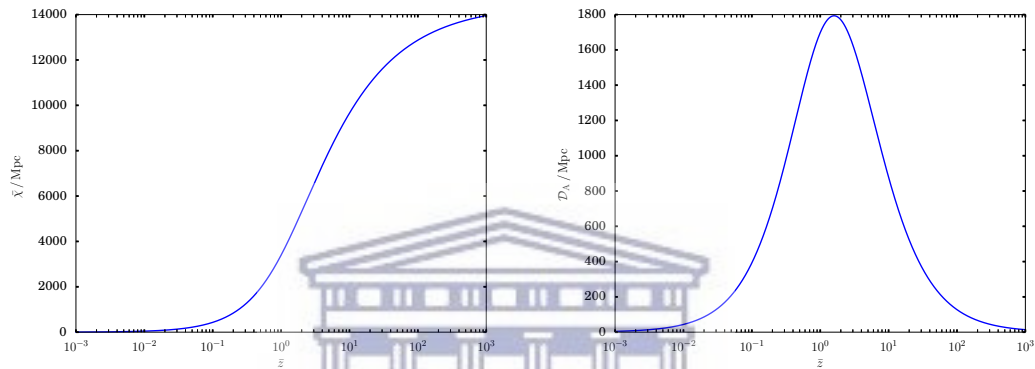


FIGURE 1.5: *Left panel:* The comoving distance, $\bar{\chi}$ plotted as a function of the background redshift \bar{z} . *Right panel:* The angular diameter distance, \mathcal{D}_A and its maximum value occurs at $\bar{z} \sim 1.6$.

sharply at low redshifts and gently asymptotes to a maximum at high redshifts. The angular diameter distance, \bar{D}_A has a maximum in an FLRW background which shows that it is possible to have objects with same \bar{D}_A at two different redshifts.

1.5.6 Baryon Acoustic Oscillations

Baryon Acoustic Oscillations (BAO) are frozen relics of the early Universe at time of decoupling. During that time, photons, protons and electrons were coupled by Thomson scattering and the Coulomb interaction, behaving as a single fluid namely the primordial plasma. When the Universe was sufficiently cooled down, the protons and electrons could interact electromagnetically to form the first atoms i.e., neutral Hydrogen. The photons could no longer interact with the electrons and therefore, could decouple from them leaving a slight excess of baryonic matter at a fixed distance from the centre of each dark matter clump as shown in Figure 1.6.

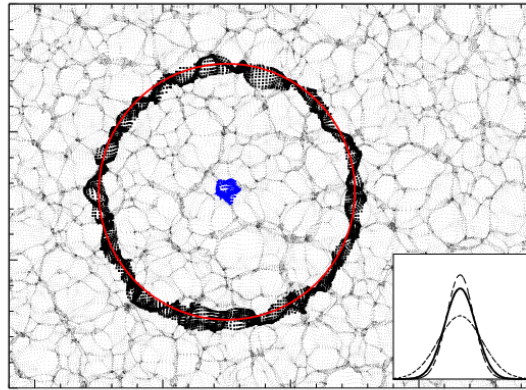


FIGURE 1.6: A ring of excess baryons around the lump of dark matter. It is also known as the BAO ring. (from [46])

This distance is used as a standard ruler and corresponds to a specific scale r_{BAO} given by,

$$r_{\text{BAO}} \approx \frac{105 h^{-1}}{(1+z)} \text{ Mpc} . \quad (1.38)$$

This scale can also be expressed in terms of an angular scale,

$$\theta_{\text{BAO}} = \frac{r_{\text{BAO}}}{D_{\text{A}}} . \quad (1.39)$$

For this particular scale of r_{BAO} , we observe the BAO features as:

1. a bump in the galaxy 2-Point Correlation function (2PCF) or,
2. wiggles in the galaxy power spectrum which is the Fourier transform of the 2PCF.

We show the results in Figure 1.7. For the case of the CMB angular power spectrum,

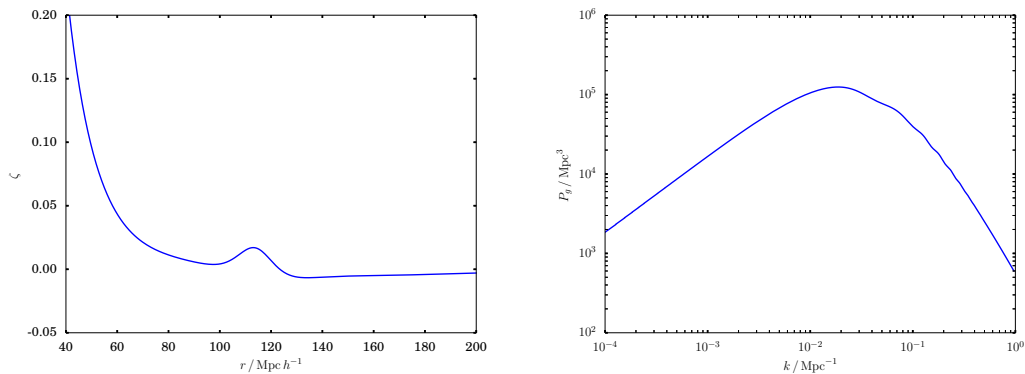


FIGURE 1.7: *Left panel:* The galaxy 2PCF with the BAO bump at $r_{\text{BAO}} = 105 h^{-1} \text{ Mpc}$. *Right panel:* The galaxy power spectrum with the first BAO peak occurring at $k_{\text{BAO}} \sim 0.03 \text{ Mpc}^{-1}$. Both plots are at $z = 0$ and the linear galaxy bias b_1 has been taken to be 1.0.

the first BAO peak is observed at $\theta_{\text{BAO}} \sim 0.6^\circ$ as shown in Figure 1.8.

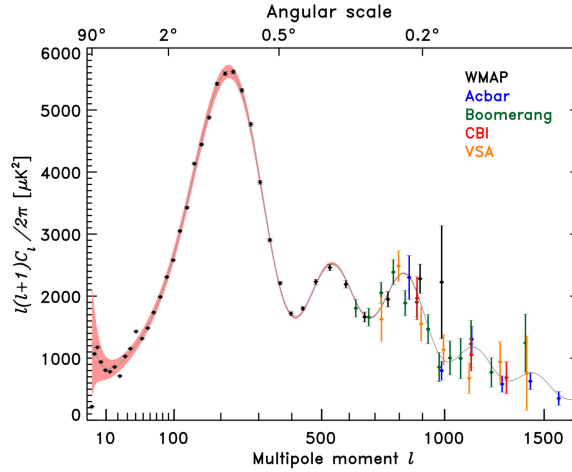


FIGURE 1.8: The angular power spectrum of the CMB (from [47]).

1.6 Perturbation theory

1.6.1 Overview

Cosmological perturbation theory is starting to take a new kind of interest. Linear or first-order theory is still actively used in the field of research, though now the focus is aiming towards higher order or even fully non-linear theory. This is because we have been able to greatly improve our data sets with the latest engineering at our disposal. At the beginning, linear theory or the power spectrum was sufficient to describe the observables in the Universe but, at present the data are such that higher order observables e.g., the bispectrum is possible to be compared to theoretical predictions [48].

Perturbation theory can be illustrated by using an example for which we define the full metric tensor, $g_{\mu\nu}$ in the standard model of cosmology. We assume that we can approximate $g_{\mu\nu}$ by a Taylor expansion,

$$g_{\mu\nu} = \bar{g}_{\mu\nu} + \delta g_{\mu\nu}^{(1)} + \frac{1}{2} \delta g_{\mu\nu}^{(2)} + \dots, \quad (1.40)$$

where $\bar{g}_{\mu\nu}$ is the background FLRW metric given in (1.5) and the remaining terms are treated as perturbations. To zeroth-order we have,

$$g_{\mu\nu} = \bar{g}_{\mu\nu}, \quad (1.41)$$

and to first-order,

$$g_{\mu\nu} = \bar{g}_{\mu\nu} + \delta g_{\mu\nu}^{(1)}. \quad (1.42)$$

Therefore, with the approximation of (1.40) we are going to solve the Einstein field equations given by (1.6), to obtain solutions at the required order of perturbations we wish to work with.

This is not quite a straightforward calculation because perturbations of the metric implies perturbations of the energy-momentum tensor, Christoffel symbols and Ricci tensor. These will involve terms at different orders and also, they will require raising or lowering indices at several stages of the calculation. We do not have any problem for the zeroth- and first-order calculations but, at higher orders the steps are complicated and therefore, the choice of a gauge for the metric becomes important. For this reason, we restrict our choice to the Poisson gauge. The most general metric for a perturbed FLRW Universe, allowing the evolution of gravitational waves and induced vector modes is written as [49, 50],

$$ds^2 = a^2 \left[\underbrace{-(1 + 2\Phi)d\eta^2 + (1 - 2\Psi)\gamma_{ij}dx^i dx^j}_{\text{scalar part}} + \underbrace{2w_i dx^i d\eta}_{\text{vector part}} + \underbrace{\frac{1}{2}h_{ij}dx^i dx^j}_{\text{tensor part}} \right], \quad (1.43)$$

where η is the conformal time and is related to the cosmic time as, $a d\eta = dt$ [38]. The vector and tensor parts are later considered in Chapter 2.

1.6.2 Linear scalar perturbation theory

1.6.2.1 Derivation of Einstein field equations

We start with the metric,

$$ds^2 = a^2 \left[-(1 + 2\Phi)d\eta^2 + (1 - 2\Psi)\delta_{ij}dx^i dx^j \right], \quad (1.44)$$

where we now admit that the Bardeen potentials Φ and Ψ are at first-order. Hence, we omit the superscript (1) and will continue to do so except when there is ambiguity. By using (1.9) we find that the non-zero Christoffel symbols are,

$$\begin{aligned} \Gamma^0_{00} &= \mathcal{H} + \Phi', & \Gamma^0_{0i} &= \partial_i \Phi, \\ \Gamma^i_{00} &= \delta^{ij} \partial_j \Phi, & \Gamma^0_{ij} &= [\mathcal{H} - \Psi' - 2\mathcal{H}(\Psi + \Phi)] \delta_{ij}, \\ \Gamma^i_{j0} &= (\mathcal{H} - \Psi') \delta^i_j, & \Gamma^i_{jk} &= -2\delta^i_j \partial_k \Psi + \delta_{jk} \delta^{il} \partial_l \Psi, \end{aligned} \quad (1.45)$$

where $'$ denotes the derivative with respect to η and \mathcal{H} is the conformal Hubble parameter given by $\mathcal{H} = a'/a = aH$. Then, the Friedmann equation as given by (1.28) becomes,

$$\mathcal{H}^2 = \frac{8\pi G a^2}{3}(\bar{\rho}_m + \bar{\rho}_r) + \frac{a^2 \Lambda}{3}, \quad (1.46)$$

where $\Lambda = 8\pi G \bar{\rho}_\Lambda$. The Raychaudhuri equation (1.18) becomes,

$$\mathcal{H}' = -\frac{4\pi G a^2}{3} \left(\bar{\rho}_m + \frac{2}{3} \bar{\rho}_r \right) + \frac{a^2 \Lambda}{3}. \quad (1.47)$$

Using (1.45) in (1.8) leads to the following non-zero elements of the Ricci tensor,

$$R_{00} = -3\mathcal{H}' + \nabla^2 \Phi + 3\mathcal{H}(\Phi' + \Psi') + 3\Psi'', \quad (1.48)$$

$$R_{0i} = 2\partial_i \Psi + 2\mathcal{H}\partial_i \Phi, \quad (1.49)$$

$$R_{ij} = [\mathcal{H}' + 2\mathcal{H}^2 - \Psi'' + \nabla^2 \Psi - 2(\mathcal{H}' + 2\mathcal{H}^2)(\Phi + \Psi) - \mathcal{H}\Phi' - 5\mathcal{H}\Psi'] \delta_{ij} + \partial_i \partial_j (\Psi - \Phi). \quad (1.50)$$

The Ricci scalar is then obtained as,

$$R = \frac{1}{a^2} [6(\mathcal{H}' + \mathcal{H}^2) - 2\nabla^2 \Phi + 4\nabla^2 \Psi - 12(\mathcal{H}' + \mathcal{H}^2)\Phi - 6\Psi'' - 6\mathcal{H}(\Phi' + 3\Psi')]. \quad (1.51)$$

For the perturbed 4-velocity vector we write,

$$U^\mu = \frac{1}{a}(1 + \vartheta, v^i), \quad (1.52)$$

where the peculiar velocity v^i is curl-free such that,

$$v^i = \partial^i v. \quad (1.53)$$

We use the normalizing condition for time-like particles, $g_{\mu\nu}U^\mu U^\nu = -1$ [38] to obtain this useful relation,

$$\vartheta = -\Phi. \quad (1.54)$$

By defining the following perturbations for the energy density and pressure,

$$\rho = \bar{\rho} + \delta\rho, \quad p = \bar{p} + \delta p, \quad (1.55)$$

and using the result for U^μ , we find that the perturbed energy-momentum tensor $T_{\mu\nu}$ of (1.13) gives the following non-zero components,

$$T_{00} = a^2(\bar{\rho} + 2\Phi\bar{\rho} + \delta\rho), \quad (1.56)$$

$$T_{0i} = -a^2(\bar{\rho} + \bar{p})v_i, \quad (1.57)$$

$$T_{ij} = a^2(\bar{p} + \delta p - 2\Psi\bar{p})\delta_{ij}. \quad (1.58)$$

Implementing (1.48)-(1.51) and (1.56)-(1.58) in the Einstein field equations gives the following set of linear scalar perturbation equations,

$$\nabla^2\Psi - 3\mathcal{H}(\Psi' + \mathcal{H}\Phi) = 4\pi G a^2 \delta\rho, \quad (1.59)$$

$$\Psi' + \mathcal{H}\Phi = -4\pi G a^2 (\bar{\rho} + \bar{p})v, \quad (1.60)$$

$$\Psi'' + 2\mathcal{H}\Psi' + \mathcal{H}\Phi + (2\mathcal{H}' + \mathcal{H}^2)\Phi = 4\pi G a^2 \delta p, \quad (1.61)$$

$$\partial_i\partial_j(\Psi - \Phi) = 0, \quad (1.62)$$

where in the last equation we find that,

$$\Psi = \Phi, \quad (1.63)$$

because we have assumed zero anisotropic stress in the energy-momentum tensor.

1.6.2.2 Perturbed conservation equations

Following the argument presented on the background conservation equations in Section 1.5, we perform a similar derivation for the perturbed energy-momentum tensor $T_{\mu\nu}$. The energy conservation equation is written as,

$$\nabla_\mu T^\mu_\nu = \partial_\mu T^\mu_\nu + \Gamma^\mu_{\mu\alpha} T^\alpha_\nu - \Gamma^\beta_{\mu\nu} T^\mu_\beta = 0. \quad (1.64)$$

Since (1.56)-(1.58) give the non-zero components of the energy-momentum tensor in the form of $T_{\alpha\beta}$, we can use the metric given by (1.44) to raise the index and finally obtain,

$$T^0_0 = -(\bar{\rho} + \delta\rho), \quad T^0_i = (\bar{\rho} + \bar{p})\partial_i v, \quad T^i_j = (\bar{p} + \delta p)\delta^i_j. \quad (1.65)$$

We then use (1.65) in (1.64) to derive the following set of equations,

$$\delta\rho' + 3\mathcal{H}(\delta\rho + \delta p) = (\bar{\rho} + \bar{p})[3\Psi' - \nabla^2 v], \quad (1.66)$$

$$[(\bar{\rho} + \bar{p})v]' + 4\mathcal{H}(\bar{\rho} + \bar{p})v^{(1)} = -[\delta p + (\bar{\rho} + \bar{p})\Phi]. \quad (1.67)$$

To obtain the first equation we have:

- expressed the continuity equation (1.23) in conformal form i.e.,

$$\bar{\rho}' + 3\mathcal{H}(\bar{\rho} + \bar{p}) = 0, \quad (1.68)$$

and used it to eliminate the background contribution.

- used $\nabla^2 = \partial_i \partial^i$.

The left hand side of (1.66) is similar to that of (1.68). It is the perturbed version of the continuity equation with a source term that depends on the potential Ψ' and peculiar velocity $\nabla^2 v^{(1)}$. The perturbed Euler equation is given by (1.67) and it shows that the driving mechanism for the peculiar velocity depends on the pressure perturbation δp and a gravitational potential term Φ .

1.6.2.3 Growth in Λ CDM model

We are going to focus at late times in the Universe where the radiation density is negligible as compared to the dark matter and dark energy densities. This is illustrated in Figure 1.9. It shows the different era of the Universe starting from radiation to matter

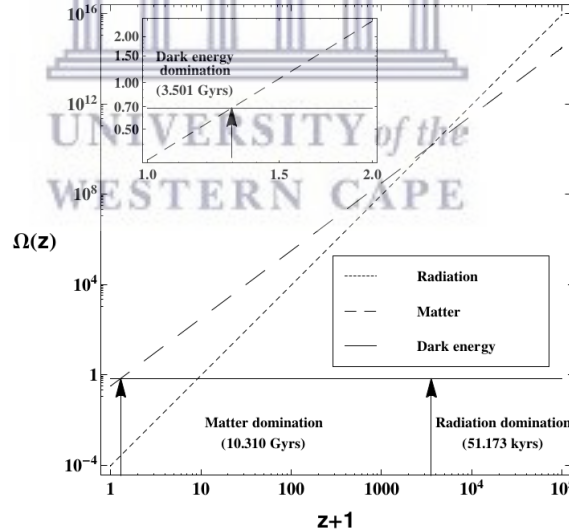


FIGURE 1.9: The dimensionless energy densities as a function of redshift (from [51]).

dominance and then lately, dark energy takes over. We hereafter neglect the radiation contribution i.e., $\bar{\rho}_r = \delta\rho_r = 0$ and also, $\delta\rho_\Lambda = 0$ because its energy density is constant through time (no perturbations). Hence, we have only perturbations in dark matter and we define the Poisson dark matter density contrast as,

$$\delta = \frac{\delta\rho_m}{\bar{\rho}_m}. \quad (1.69)$$

We also introduce the adiabatic acoustic speed c_a as [52, 53],

$$c_a^2 = \frac{\bar{p}'_m}{\bar{\rho}'_m} = \frac{\delta p_m}{\delta \rho_m}, \quad (1.70)$$

where in the last equality we assume adiabatic perturbations. We can use (1.69), (1.70) and the definition of the EoS parameter w given in (1.17) to write the set of linear perturbation equations as,

$$\nabla^2 \Psi - 3\mathcal{H}(\Psi' + \mathcal{H}\Phi) = 4\pi G a^2 \bar{\rho}_m \delta, \quad (1.71)$$

$$\Psi' + \mathcal{H}\Phi = -4\pi G a^2 \bar{\rho}_m (1+w)v, \quad (1.72)$$

$$\Psi'' + 2\mathcal{H}\Psi' + \mathcal{H}\Phi' + (2\mathcal{H}' + \mathcal{H}^2)\Phi = 4\pi G a^2 c_a^2 \bar{\rho}_m \delta, \quad (1.73)$$

$$\Psi = \Phi, \quad (1.74)$$

and the perturbed conservation equations as,

$$\delta' + 3\mathcal{H}(c_a^2 - w)\delta = (1+w)[3\Psi' - \nabla^2 v], \quad (1.75)$$

$$[\bar{\rho}_m(1+w)v]' + c_a^2 \bar{\rho}_m \delta = -\bar{\rho}_m(1+w)[\Phi + 4\mathcal{H}v]. \quad (1.76)$$

In Λ CDM model, dark matter particles are treated as cold particles i.e., they are practically at rest (non-interacting) and therefore, exert no pressure. This leads to $c_a = w = \bar{p}_m = \delta p_m = 0$ and thus (1.71)-(1.76) become,

$$\nabla^2 \Psi - 3\mathcal{H}(\Psi' + \mathcal{H}\Phi) = 4\pi G a^2 \bar{\rho}_m \delta, \quad (1.77)$$

$$\Psi' + \mathcal{H}\Phi = -4\pi G a^2 \bar{\rho}_m v, \quad (1.78)$$

$$\Psi'' + 2\mathcal{H}\Psi' + \mathcal{H}\Phi' + (2\mathcal{H}' + \mathcal{H}^2)\Phi = 0, \quad (1.79)$$

$$\Psi = \Phi, \quad (1.80)$$

$$\delta^{(1)'} = 3\Psi' - \nabla^2 v, \quad (1.81)$$

$$v^{(1)'} = -\Phi - \mathcal{H}v. \quad (1.82)$$

Using (1.77), (1.78), (1.80) and the definition of Ω_m as given by (1.29) we can show the following,

$$\nabla^2 \Phi = \frac{3}{2}\Omega_m \mathcal{H}^2 [\delta - 3\mathcal{H}v], \quad (1.83)$$

where the term in the square bracket is the comoving dark matter overdensity, δ_C which is described in detail in Chapter 2. Hence we obtain the Poisson equation,

$$\nabla^2 \Phi = \frac{3}{2}\Omega_m \mathcal{H}^2 \delta_C = \frac{3}{2a}\Omega_{m0} H_0^2 \delta_C. \quad (1.84)$$

The perturbation Φ evolves through both time and space i.e., $\Phi = \Phi(a, \mathbf{x})$. To describe its time evolution, we define the linear growth suppression function [54, 55],

$$\frac{D_\Phi}{a} = \frac{\Phi}{\Phi_d}, \quad (1.85)$$

which is normalized at time of decoupling i.e., $a = a_d \sim 10^{-3}$. In Fourier space, (1.84) reads as,

$$-k^2 \Phi = \frac{3}{2a} \Omega_{m0} H_0^2 \delta_C. \quad (1.86)$$

This is discussed in more detail in Chapter 3. At decoupling,

$$-k^2 \Phi_d = \frac{3}{2a_d} \Omega_{m0} H_0^2 \delta_{C_d}. \quad (1.87)$$

Dividing (1.86) by (1.87) yields,

$$a \frac{\Phi}{\Phi_d} = a_d \frac{\delta_C}{\delta_{C_d}} = D_\Phi. \quad (1.88)$$

We can then define a linear growth function for the comoving dark matter overdensity as,

$$D = a_d \frac{\delta_C}{\delta_{C_d}}, \quad (1.89)$$

such that in Λ CDM,

$$D_\Phi = D. \quad (1.90)$$

The matter growth function or growth factor, D , describes the linear growth of matter perturbations after matter-radiation equality [55]. We use the word ‘‘suppression’’ for D_Φ/a because of the Λ term which causes Φ to decay. For δ , Λ slows down the growth since it inhibits clustering.

We begin with time evolution equation of the Bardeen potentials Ψ and Φ given by (1.79). The condition for zero anisotropic stress is set by (1.80) and hence, we write (1.79) as,

$$\Phi'' + 3\mathcal{H}\Phi' + (2\mathcal{H}' + \mathcal{H}^2)\Phi = 0. \quad (1.91)$$

Using the Friedmann and Raychaudhuri equations as given in (1.46) and (1.47) respectively, with $\bar{\rho}_r = 0$ since we are neglecting radiation, we can show that,

$$2\mathcal{H}' + \mathcal{H}^2 = a^2 \Lambda, \quad (1.92)$$

and therefore (1.91) becomes,

$$\Phi'' + 3\mathcal{H}\Phi' + \underbrace{a^2\Lambda\Phi}_{\text{damping term}} = 0. \quad (1.93)$$

We can derive these useful relations,

$$\frac{d}{d\eta} = a\mathcal{H}\frac{d}{da}, \quad \frac{d^2}{d\eta^2} = a^2\mathcal{H}^2\frac{d^2}{da^2} + a\mathcal{H}^2\left(1 + \frac{\mathcal{H}'}{\mathcal{H}^2}\right)\frac{d}{da}, \quad (1.94)$$

and use them in (1.93) to show,

$$\frac{d^2\Phi}{da^2} + \frac{1}{a}\left(4 + \frac{\mathcal{H}'}{\mathcal{H}^2}\right)\frac{d\Phi}{da} + \frac{\Lambda}{\mathcal{H}^2}\Phi = 0. \quad (1.95)$$

We now use the definition for the gravitational growth function given in (1.85) to finally obtain,

$$\frac{d^2D_\Phi}{da^2} + \frac{3}{a}\left(1 - \frac{\Omega_m}{2}\right)\frac{dD_\Phi}{da} - \frac{3}{2a^2}\Omega_m D_\Phi = 0. \quad (1.96)$$

In deriving (1.96) we have done the following:

- Starting with (1.46) and (1.47), we have re-written \mathcal{H}' in terms of \mathcal{H}^2 by using the definition of Ω_m given in (1.29). This gives,

$$\mathcal{H}' = \left(1 - \frac{3}{2}\Omega_m\right)\mathcal{H}^2. \quad (1.97)$$

- We have used the definition of Ω_Λ given by (1.29) and the dimensionless Friedmann equation at late times,

$$1 = \Omega_m + \Omega_\Lambda. \quad (1.98)$$

Since $D_\Phi = D$, we therefore have,

$$\frac{d^2D}{da^2} + \frac{3}{a}\left(1 - \frac{\Omega_m}{2}\right)\frac{dD}{da} - \frac{3}{2a^2}\Omega_m D = 0. \quad (1.99)$$

We initialize (1.99) at time of decoupling i.e., $a_d = 10^{-3}$. For an Einstein-de Sitter (EdS) Universe, $\Omega_m = 1$ and $\Omega_r = \Omega_\Lambda = 0$. Therefore, the gravitational potential Φ is a constant through time i.e., $\Phi = \Phi_d$ such that by (1.85),

$$D_\Phi^{(\text{EdS})} = a \quad \text{and} \quad \frac{dD_\Phi^{(\text{EdS})}}{da} = 1. \quad (1.100)$$

The relation $D_\Phi = D$ is still valid for the EdS Universe and this implies that,

$$D^{(\text{EdS})} = a \quad \text{and} \quad \frac{dD^{(\text{EdS})}}{da} = 1. \quad (1.101)$$

The initial conditions for finding the solution to (1.99) are then,

$$D_d^{(\text{EdS})} = a_d \quad \text{and} \quad \left. \frac{dD^{(\text{EdS})}}{da} \right|_d = 1. \quad (1.102)$$

We show the result of the numerical integration below in Figure 1.10. Matter clumps together because of gravity and since dark energy competes against clustering at late times, D is suppressed. This effect is captured by the deviation of the Λ CDM curve from the EdS curve.

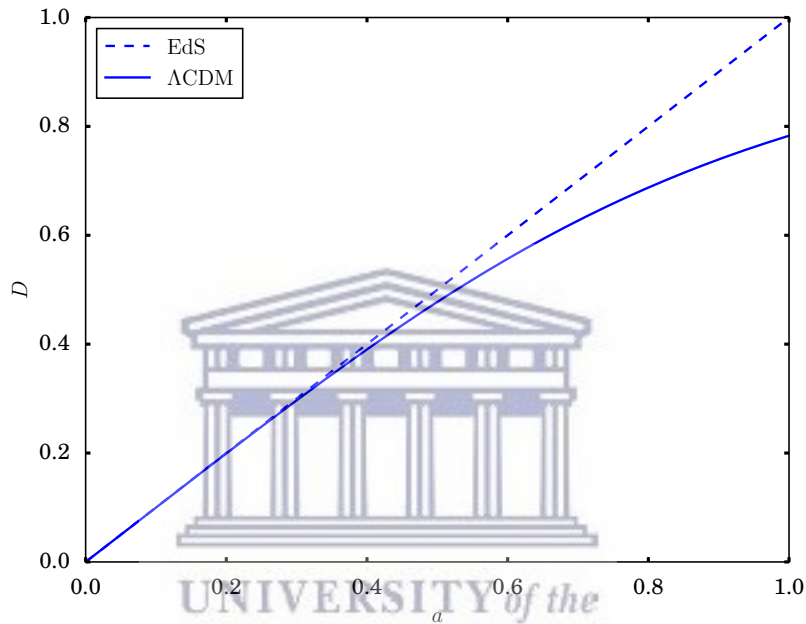


FIGURE 1.10: The time evolution of the matter growth factor for EdS (dashed) and Λ CDM (solid). The effect of Λ suppresses D at late times ($a \rightarrow 1$).

It is helpful to convert the second-order differential equation for D into a first-order equation for the linear growth rate, f , which is defined as [56],

$$f = \frac{d \ln \delta_C}{d \ln a}. \quad (1.103)$$

Since δ_C is proportional to D (see (1.89)), we can show that (1.103) becomes,

$$f = \frac{d \ln D}{d \ln a} = \frac{a}{D} \frac{dD}{da}. \quad (1.104)$$

The above definition leads to the following,

$$\frac{df}{da} = \frac{f}{a} - \frac{f^2}{a} + \frac{a}{D} \frac{d^2 D}{da^2}. \quad (1.105)$$

Using (1.104) and (1.105) in (1.99), we obtain the first-order equation for f as,

$$a \frac{df}{da} + f^2 + \frac{1}{2} (4 - 3\Omega_m) f - \frac{3}{2} \Omega_m = 0. \quad (1.106)$$

The above result is consistent with [56, 57]. The initial condition is given by considering the EdS Universe and by (1.101), we find that (1.104) leads to,

$$f^{(\text{EdS})} = 1. \quad (1.107)$$

An analytical solution to (1.106) does exist and can be found in [56, 58, 59]. We introduce a new parameter, γ , which is the growth index and relates to f as,

$$f(a) = [\Omega_m(a)]^\gamma. \quad (1.108)$$

This parameterization provides a very good fit to the numerical solution of (1.106) for the Λ CDM model when $\gamma \sim 0.55$ [58, 60]. This is shown in Figure 1.11.

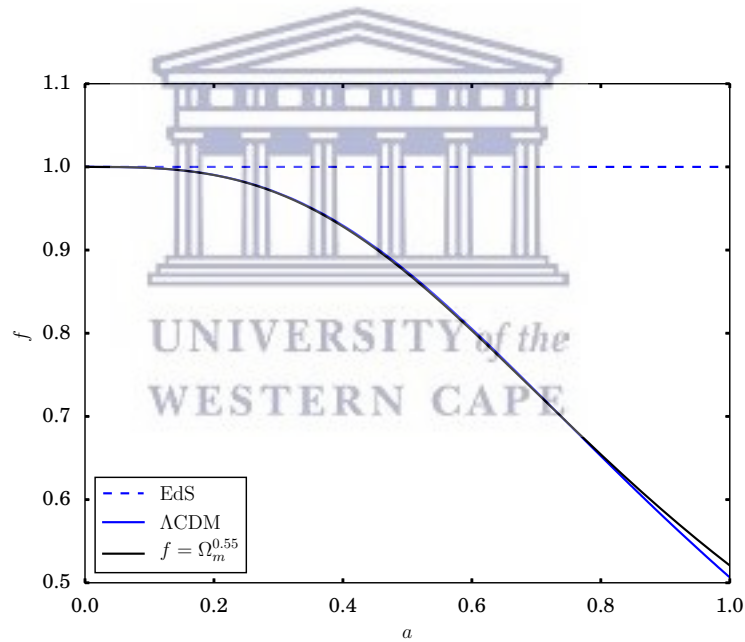


FIGURE 1.11: The linear growth rate f for EdS (dashed) and Λ CDM (solid blue). The analytical approximation with $\gamma = 0.55$ is shown as the black curve. The effect of Λ suppresses f at late times.

1.6.3 Second-order scalar perturbations in Λ CDM

The derivation of the Einstein field equations at second-order is not as easy as that of the first-order. The scalar second-order terms split into two parts:

- The intrinsic second-order terms e.g., $\Phi^{(2)}$, $\Psi^{(2)}$, $v^{(2)}$ and others.

- The quadratic first-order terms e.g., Φ^2 , Ψ^2 , v^2 , $\Phi\delta$, $\Psi\delta$ and many other possible combinations.

Then we can write the second-order Einstein field equations as,

$$G_{\mu\nu}^{(2)} + G_{\mu\nu}^{\text{II}} = 8\pi GT_{\mu\nu}^{(2)}, \quad (1.109)$$

where $G_{\mu\nu}^{(2)}$ is the Einstein tensor for the intrinsic second-order terms and $G_{\mu\nu}^{\text{II}}$ is for the quadratic first-order terms. We still work in the Poisson gauge with the FLRW metric,

$$ds^2 = a^2 [- (1 + 2\Phi + \Phi^{(2)})d\eta^2 + (1 - 2\Phi + \Psi^{(2)})\delta_{ij}dx^i dx^j], \quad (1.110)$$

where we maintain the condition of zero anisotropic stress in the first-order scalar perturbations i.e., $\Phi = \Psi$. The non-zero components of $G_{\mu\nu}^{(2)}$ and $G_{\mu\nu}^{\text{II}}$ are then [61],

$$G_{00}^{(2)} = -\frac{1}{a^2} [-6\mathcal{H}\Psi^{(2)'} + 2\nabla^2\Psi^{(2)} - 6\mathcal{H}^2\Phi^{(2)}], \quad (1.111)$$

$$G_{i0}^{(2)} = \frac{1}{a^2} [2\partial_i\Psi^{(2)'} + 2\mathcal{H}\partial_i\Phi^{(2)}], \quad (1.112)$$

$$G_{0i}^{(2)} = \frac{1}{a^2} [2\partial^j\Psi^{(2)'} + 2\mathcal{H}\partial^j\Phi^{(2)}] \delta_{ij}, \quad (1.113)$$

$$G_{ij}^{(2)} = \frac{1}{a^2} \left\{ \partial_i\partial^k(\Psi^{(2)} - \Phi^{(2)})\delta_{jk} + [2\Psi^{(2)''} - \nabla^2\Psi^{(2)} + 4\mathcal{H}\Psi^{(2)'} + 2\mathcal{H}\Phi^{(2)'} + 2(2\mathcal{H}' + \mathcal{H}^2)\Phi^{(2)} + \nabla^2\Phi^{(2)}] \delta_{ij} \right\}, \quad (1.114)$$

$$G_{00}^{\text{II}} = \frac{2}{a^2} [3\partial_k\Phi\partial^k\Phi + 3(\Phi')^2 + 8\Phi\nabla^2\Phi + 12\mathcal{H}^2\Phi^2], \quad (1.115)$$

$$G_{i0}^{\text{II}} = \frac{4}{a^2} [4\mathcal{H}\Phi\partial_i\Phi - \Phi'\partial_i\Phi], \quad (1.116)$$

$$G_{0i}^{\text{II}} = \frac{4}{a^2} [\Phi'\partial^j\Phi + 4\Phi\partial^j\Phi'] \delta_{ij}, \quad (1.117)$$

$$G_{ij}^{\text{II}} = \frac{4}{a^2} \left\{ [\partial_i\Phi\partial^k\Phi + 2\Phi\partial_i\partial^k\Phi] \delta_{jk} - [3\partial_k\Phi\partial^k\Phi + 4\Phi\nabla^2\Phi + (\Phi')^2 + 8\mathcal{H}\Phi\Phi' + 4(2\mathcal{H}' + \mathcal{H}^2)\Phi^2] \delta_{ij} \right\}. \quad (1.118)$$

Since we are considering Λ CDM, the second-order pressure perturbation, $\delta p^{(2)} = 0$.

For the peculiar velocity we have,

$$v^i = \partial^i \left(v + \frac{1}{2}v^{(2)} \right). \quad (1.119)$$

The energy-momentum tensor then gives,

$$T_{00}^{(2)} = -2\bar{\rho}_m \partial^i v \partial_i v - \delta\rho_m^{(2)}, \quad (1.120)$$

$$T_{i0}^{(2)} = \bar{\rho}_m [\partial_i v^{(2)} - 2\Phi \partial_i v] + 2\delta\rho_m \partial_i v, \quad (1.121)$$

$$T_{0i}^{(2)} = -[\bar{\rho}_m (\partial^j v^{(2)} - 6\Phi \partial^j v) + 2\delta\rho_m \partial^j v] \delta_{ij}, \quad (1.122)$$

$$T_{ij}^{(2)} = 2\bar{\rho}_m \partial_i v \partial^k v \delta_{jk}. \quad (1.123)$$

Implementing (1.111)-(1.118) and (1.120)-(1.123) in (1.109) leads to the following set of second-order scalar perturbation equations,

$$3\mathcal{H}\Psi^{(2)'} - \nabla^2\Psi^{(2)} + 3\mathcal{H}^2\Phi^{(2)} - 3\partial_k\Phi\partial^k\Phi - 3(\Phi')^2 + 8\Phi\nabla^2\Phi - 12\mathcal{H}^2\Phi^2 = S_0, \quad (1.124)$$

$$2\partial_i\Psi^{(2)'} + 2\mathcal{H}\partial_i\Phi^{(2)} - 12\mathcal{H}\Phi\partial_i\Phi + 4\Phi\partial_i\Phi' - 4\Phi'\partial_i\Phi = S_i, \quad (1.125)$$

$$[\partial_i\partial^k(\Psi^{(2)} - \Phi^{(2)}) + 4(\partial_i\Phi\partial^k\Phi + 2\Phi\partial_i\partial^k\Phi')] \gamma_{jk} = S_{ij}, \quad (1.126)$$

$$\begin{aligned} & \partial_i\partial^k(\Psi^{(2)} - \Phi^{(2)}) \gamma_{ik} + 2\Psi^{(2)''} - \nabla^2\Psi^{(2)} + 4\mathcal{H}\Psi^{(2)'} + 2\mathcal{H}\Phi^{(2)'} \\ & + 2(2\mathcal{H}' + \mathcal{H}^2)\Phi^{(2)} + \nabla^2\Phi^{(2)} + 4[\partial_i\Phi\partial^k\Phi + 2\Phi\partial_i\partial^k\Phi'] \delta_{ik} \\ & - 2[3\partial_k\Phi\partial^k\Phi + 4\Phi\nabla^2\Phi + (\Phi')^2 + 8\mathcal{H}\Phi\Phi' + 4(2\mathcal{H}' + \mathcal{H}^2)\Phi^2] = S_1, \end{aligned} \quad (1.127)$$

where,

$$\begin{aligned} S_0 &= 8\pi G a^2 \bar{\rho}_m [\partial^i v \partial_i v - \delta^{(2)}], & S_{ij} &= 16\pi G a^2 \bar{\rho}_m \partial_i v \partial^k v \gamma_{jk}, \\ S_i &= -8\pi G a^2 \bar{\rho}_m [\delta \partial_i v + \partial_i v^{(2)}], & S_1 &= 16\pi G a^2 \bar{\rho}_m \partial_i v \partial^k v \gamma_{ik}. \end{aligned} \quad (1.128)$$

In S_0 we have introduced the second-order Poisson dark matter overdensity, $\delta^{(2)} = \delta\rho_m^{(2)}/\bar{\rho}_m$. The results of (1.124)-(1.127) are consistent with [61, 62]. From (1.126) we can see that,

$$\Phi^{(2)} \neq \Psi^{(2)}. \quad (1.129)$$

1.6.4 Solutions to the Einstein field equations

The solutions to the Einstein field equations both at linear and non-linear orders are usually given in Fourier space. This is because Fourier analysis provides an easy platform to solve the perturbation equations. If we refer to the first- and second-order perturbation equations given by (1.77)-(1.82) and (1.124)-(1.127) respectively, we find that the evolution equations for the Bardeen potentials are written in terms of the dark matter overdensity, $\delta^{(n)}$, and velocity potential, $v^{(n)}$, where n is the order of the perturbations.

In Fourier space, these quantities have perturbative solutions [28, 63, 64],

$$\delta^{(n)}(\eta, \mathbf{k}) = \sum_n \int \frac{dk_1}{(2\pi)^3} \cdots \frac{dk_{n-1}}{(2\pi)^3} \int dk_n \delta^D(\mathbf{k}_1 + \dots + \mathbf{k}_n - \mathbf{k}) F_n(\mathbf{k}_1, \dots, \mathbf{k}_n) \times \delta_C^{(1)}(\eta, \mathbf{k}_1) \delta_C^{(1)}(\eta, \mathbf{k}_2) \dots \delta_C^{(1)}(\eta, \mathbf{k}_n), \quad (1.130)$$

$$\theta^{(n)}(\eta, \mathbf{k}) = -\mathcal{H}f \sum_n \int \frac{dk_1}{(2\pi)^3} \cdots \frac{dk_{n-1}}{(2\pi)^3} \int dk_n \delta^D(\mathbf{k}_1 + \dots + \mathbf{k}_n - \mathbf{k}) G_n(\mathbf{k}_1, \dots, \mathbf{k}_n) \times \delta_C^{(1)}(\eta, \mathbf{k}_1) \delta_C^{(1)}(\eta, \mathbf{k}_2) \dots \delta_C^{(1)}(\eta, \mathbf{k}_n), \quad (1.131)$$

where $\theta^{(n)} = \nabla \cdot \mathbf{v}^{(n)}(\mathbf{x})$ is the velocity divergence and δ^D is the Dirac-delta function. F_n and G_n are known as the Fourier kernels. More details on Fourier calculations are presented in Chapter 3.

Once we have (1.130) and (1.131), we can obtain the Fourier solutions for $\Phi^{(n)}$ and $\Psi^{(n)}$ which are used to compute their N -point correlation functions.

1.7 Cosmology with the Square Kilometre Array

The Square Kilometre Array (SKA) will be the world's largest radio telescope project to be built in South Africa and Western Australia. It will have a collecting area of nearly a million square metres. The pre-construction phase has already started in 2012 and the main bulk of the SKA will be done in two phases. For the SKA phase 1, Australia will operate on approximately 130,000 low frequency antennas and South Africa will host 200 dishes among which will be the 64 dishes of the Karoo Array Telescope (MeerKAT) precursor telescope. This will constitute $\sim 10\%$ of the total collecting area at low and mid frequencies and will be operational by 2023. For the SKA phase 2, all the low and mid frequency arrays will be completed across both South Africa and Australia and will be fully operational by 2030.

1.7.1 BAO constraints

The SKA HI (neutral atomic Hydrogen) redshift galaxy survey will measure the BAO in both the radial and transverse directions over a very large volume of the sky. The radial measurements will probe the expansion rate of the Universe as a function of redshift and therefore we will be capable of constraining the Hubble parameter, $H(z)$. This will allow us to obtain key information on the energy content of the Universe and hence,

the nature of dark energy. The transverse measurements will enable us to measure the angular diameter distance, \mathcal{D}_A accurately which we can use to produce good estimates of distances in the Universe [65]. The predictions on the expansion rate and angular diameter distance are shown in Figure 1.12.

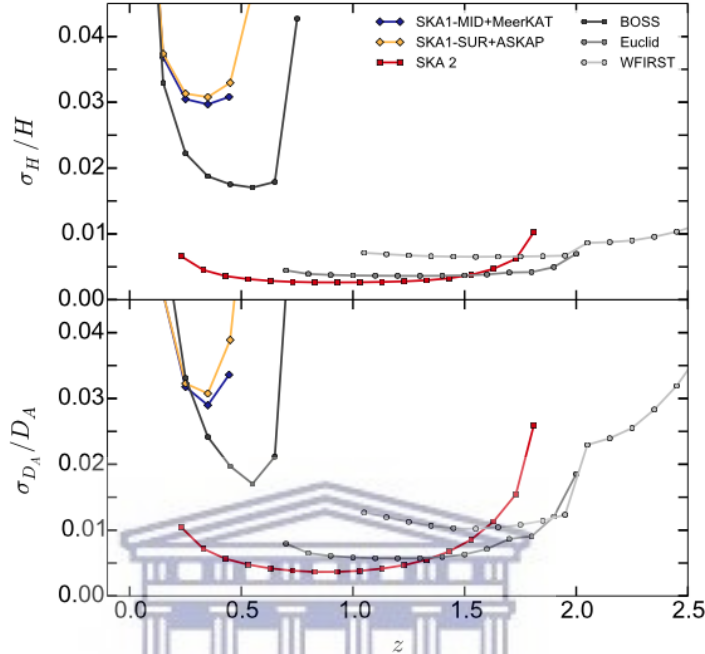


FIGURE 1.12: Forecasts on the expansion rate and angular diameter distance. SKA phase 2 will provide the best constraints for both quantities up to $z \sim 1.4$ with a fractional error of $\lesssim 1\%$. (from [65])

UNIVERSITY of the
WESTERN CAPE

1.7.2 Redshift space distortion

We are confronted to several competing theories of dark energy which are degenerate in their explanation of the late time cosmic acceleration. It is possible to break these degeneracies by looking at the growth of structures predicted by these models. The study of the peculiar motion of the galaxies is the ideal candidate to understand gravitational collapse and hence the formation of structure. The name given to the effect due to the peculiar motion of the galaxies is redshift space distortion (RSD) where the positions of the galaxies are “shifted” or more precisely, the distribution of galaxies along the line of sight appears to be squashed. This effect will modify the shape of the galaxy correlation function (or power spectrum). If we are able to measure the effect of the peculiar velocities of the galaxies, we can put constraint on the various dark energy models by looking at the changes in the shape of the correlation function [65].

This method to probe the nature of dark energy from RSD constraints is to extract

the growth rate parameter, f which is the logarithmic derivative of the matter overdensity with respect to the scale factor (see (1.103)). This can be done by expanding the redshift space galaxy 2PCF into multipole moments using the Legendre polynomials [66]. The growth rate parameter can then be obtained from the monopole and quadrupole. Using the 2PCF or power spectrum requires us to assume a background cosmological model, leading to errors. We cannot measure galaxy clustering but we can measure galaxy redshifts and angles to infer their distances. Therefore, a wrong cosmological model will lead to incorrect estimates of the distances. The information that we will then retrieve from the galaxy clusters will be inaccurate. This is the Alcock-Paczynski (AP) effect [65, 67]. The AP effect can weaken the constraints that one can obtain from RSD measurements but, by measuring its amplitude we may calculate the AP factor, F which is related to the ratio of the transverse to radial distances. The forecasts for f and F are shown in Figure 1.13.

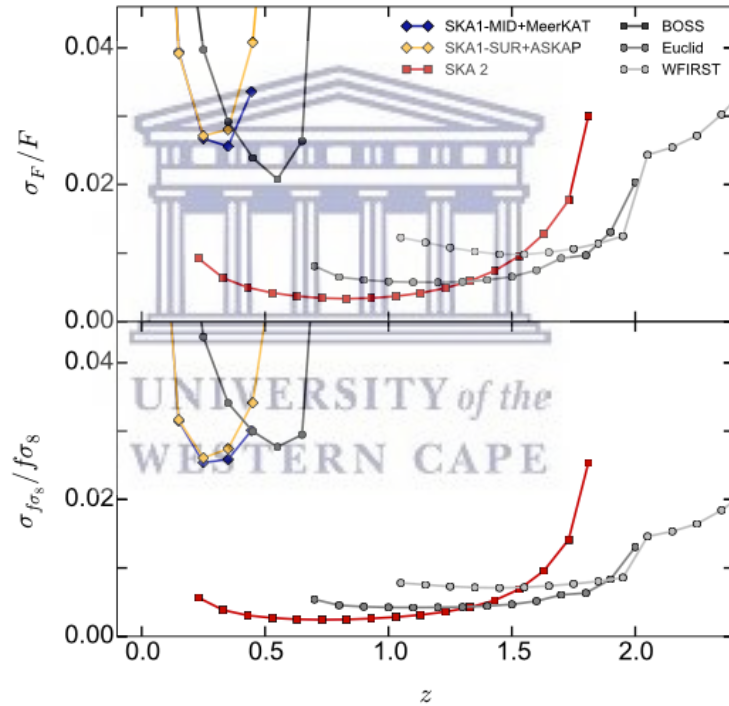


FIGURE 1.13: Forecasts on the AP factor, F and the observable growth rate parameter, $f\sigma_8$ which is the linear growth rate $f(z)$ multiplied by the normalisation of the power spectrum, σ_8 . Again, SKA phase 2 will provide the best constraints for both quantities up to $z \sim 1.4$ with a fractional error of $\lesssim 1\%$. (from [65])

1.7.3 Testing General Relativity and Modified Gravity

With the SKA HI surveys we will be able to put constraint on the EoS parameter, w for dark energy. Λ CDM predicts that $w = -1$ for dark energy and any departure from this value will indicate [65]:

- dynamical dark energy or,
- failure of GR

For a dynamical model of dark energy the parameter, w is usually parameterized as [68],

$$w(a) = w_0 + w_a(1 - a) , \quad (1.132)$$

where in Λ CDM, $w_0 = -1$ and $w_a = 0$. Also, a scale-independent linear growth rate f can be parameterized as [56, 58, 59],

$$f(a) = [\Omega_m(a)]^\gamma , \quad (1.133)$$

where for Λ CDM, $\gamma = 0.554$ and for standard dynamical DE models, γ is close to this value. Theories of Modified Gravity (MG) predict different values for γ and therefore, by putting constraint on it we can test GR. The predictions for w_a , w_0 and γ are shown below in Figure 1.14.

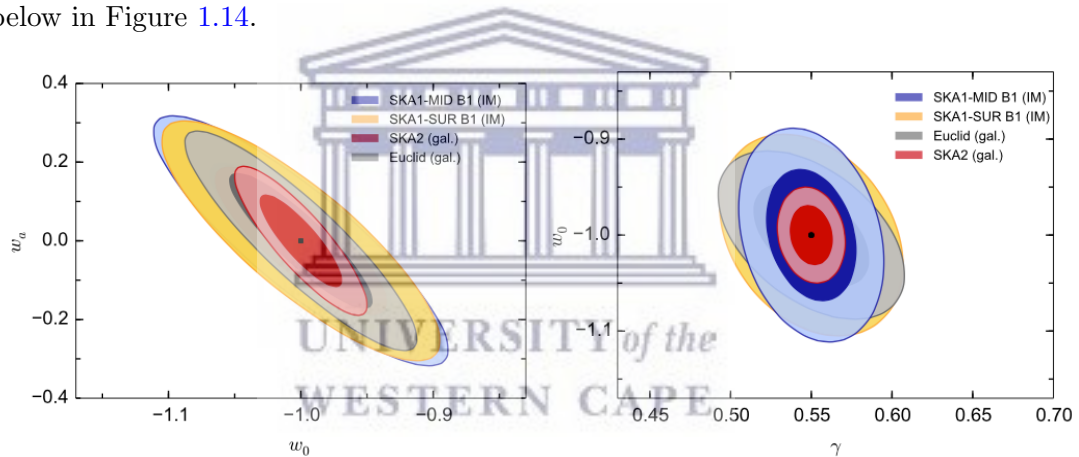


FIGURE 1.14: *Left panel:* Constraints on dark energy EoS parameters w_a and w_0 . *Right panel:* Constraints on w_0 and γ . SKA phase 2 will be far more powerful than the Euclid galaxy survey. (from [68])

1.7.4 HI intensity mapping

HI intensity mapping (IM) after reionization is a new technique of mapping large-scale structure (LSS) of the Universe using the integrated 21 cm emission from HI gas in galaxies, without trying to detect individual galaxies. In this method, we do not require high resolution because we create a map of the Universe by measuring the intensity of the redshifted 21 cm line over a range of redshifts without the need to resolve the individual galaxies [69]. SKA phase 1 will be able to generate HI maps out to redshift $z \sim 3$ for a great fraction of the sky. The scales at which we will focus will be the

BAO scale and large scales past the equality peak ($k_{\text{eq.}} \sim 0.01 \text{ Mpc}^{-1}$). The large scale IM measurements will be important for detecting primordial non-Gaussianity (PNG). Putting strong constraints on PNG will help to rule out a large number of the existing models of inflation.

1.8 Thesis outline

The structure of the thesis is as follows:

- Chapter 1 is a condensed introductory chapter on the background of cosmology. It gives a full derivation on the FLRW background Universe. It also shows the details on the first- and second-order perturbation theory in the Λ CDM model. In the end, it summarizes the relevant scientific goals of the SKA.
- Chapter 2 is on the theory of the galaxy number counts. It shows a full explanation on the first- and second-order perturbation theory in the galaxy number count fluctuations, taking into account all the local scalars, vectors and tensors. The initial condition for the primordial gravitational potential is Gaussian.
- Chapter 3 is on Fourier space. It has a full explanation on the geometry of the galaxy bispectrum and derives the first- and second-order Fourier kernels for the relativistic lightcone projection effects given in Chapter 2.
- Chapter 4 shows the numerical analysis of the galaxy bispectrum, starting with the scalars, and building towards a more general case i.e. including the vectors and tensors.
- Chapter 5 is on primordial non-Gaussianity. It looks at the effect of f_{NL} in the Newtonian as well as the full local relativistic galaxy bispectrum.
- Chapter 6 is on the conclusion. It summarizes all the key findings of the project and the assumptions we have used in our methods. It also shows the future work that can be done with the galaxy bispectrum.

Chapter 2

Perturbation theory in the galaxy number counts

2.1 The galaxy number count fluctuation

We consider an observer looking down on the past lightcone. S/he counts $d\mathcal{N}$ number of galaxies above a threshold luminosity L , within a redshift bin of width dz about the observed redshift z , subtending a solid angle $d\Omega_o$ about the direction of observation \mathbf{n} . Then, we can write an equation for $d\mathcal{N}$ as [32, 49, 70–72],

$$d\mathcal{N}(z, \mathbf{n}, > \ln L) = \rho_g(z, \mathbf{n}, > \ln L) D_A^2(z, \mathbf{n}) K_\mu U^\mu \frac{d\lambda}{dz} dz d\Omega_o, \quad (2.1)$$

where D_A is the angular diameter distance given in the background by (1.37), U^μ is the 4-velocity of the galaxy, $K^\mu = dx^\mu/d\lambda$ is the geodesic photon 4-momentum, λ is the affine parameter and ρ_g is the flux-limited number density of galaxies given by,

$$\rho_g(z, \mathbf{n}, > \ln L) = \int_{\ln L}^{\infty} d \ln \tilde{L} n_g(z, \mathbf{n}, \ln \tilde{L}). \quad (2.2)$$

In the above integral, n_g is the proper galaxy number density i.e., it is defined in the rest frame of the galaxies. Only galaxies above luminosity L are detected by the observer. Then using (2.1), we define the observed galaxy number count fluctuation Δ_g as,

$$\frac{d\mathcal{N}(z, \mathbf{n}, > \ln L)}{dz d\Omega_o} = \frac{dV(z, \mathbf{n})}{dz d\Omega_o} \bar{\rho}_g(z, > \ln L) [1 + \Delta_g(z, \mathbf{n}, > \ln L)], \quad (2.3)$$

where $\bar{\rho}_g$ is the background flux-limited galaxy number density. The small element of volume $dV(z, \mathbf{n})$ is given by (2.1) as,

$$dV(z, \mathbf{n}) = D_A^2(z, \mathbf{n}) K_\mu U^\mu \frac{d\lambda}{dz} dz d\Omega_o . \quad (2.4)$$

In the background,

$$\begin{aligned} d\bar{V}(z) &= \frac{\bar{D}_A^2(z)}{(1+z)^2 \mathcal{H}(z)} dz d\Omega_o \\ &= \frac{\bar{\chi}^2(z)}{(1+z)^4 \mathcal{H}(z)} dz d\Omega_o . \end{aligned} \quad (2.5)$$

Henceforth, we suppress the $\ln L$ dependence to reduce clutter and write (2.3) in the following way,

$$N(z, \mathbf{n}) = \bar{N}(z) [1 + \Delta_g(z, \mathbf{n})] , \quad (2.6)$$

such that [20, 73],

$$\Delta_g(z, \mathbf{n}) = \frac{N(z, \mathbf{n}) - \bar{N}(z)}{\bar{N}(z)} , \quad (2.7)$$

where $N(z, \mathbf{n}) = d\mathcal{N}/[dzd\Omega_o]$ is the number of galaxies per unit redshift interval dz and per unit solid angle $d\Omega_o$ about the direction \mathbf{n} . $\bar{N}(z) = \bar{\rho}_g(z) d\bar{V}(z)/[dzd\Omega_o]$ is the average number galaxies in the same redshift interval dz . We can expand (2.7) perturbatively up to second-order as,

$$\Delta_g(z, \mathbf{n}) = \Delta_g^{(1)}(z, \mathbf{n}) + \frac{1}{2} [\Delta_g^{(2)}(z, \mathbf{n}) - \langle \Delta_g^{(2)}(z, \mathbf{n}) \rangle] , \quad (2.8)$$

where we subtract off the average of $\Delta_g^{(2)}$ in order to satisfy the condition $\langle \Delta_g \rangle = 0$. In the next section, we work out the expression for $\Delta_g^{(1)}$.

2.2 First-order scalars

Here, we give a full derivation for $\Delta_g^{(1)}$. The number of galaxies $N(z, \mathbf{n})$ in the given volume $\mathcal{V}(z, \mathbf{n}) \equiv dV(z, \mathbf{n})/[dzd\Omega_o]$ can be written as,

$$N(z, \mathbf{n}) = \rho_g(z, \mathbf{n}) \mathcal{V}(z, \mathbf{n}) . \quad (2.9)$$

We can expand ρ_g and \mathcal{V} about their mean values $\bar{\rho}_g$ and $\bar{\mathcal{V}}$ respectively by allowing for a small deviation of the form,

$$\rho_g(z, \mathbf{n}) = \bar{\rho}_g(z) + \delta\rho_g^{(1)}(z, \mathbf{n}) \quad \text{and} \quad \mathcal{V}(z, \mathbf{n}) = \bar{\mathcal{V}}(z) + \delta\mathcal{V}^{(1)}(z, \mathbf{n}) , \quad (2.10)$$

and replacing (2.10) in (2.9) we have at linear order,

$$\begin{aligned} N(z, \mathbf{n}) &= \bar{\rho}_g(z)\bar{\mathcal{V}}(z) + \bar{\mathcal{V}}(z)\delta\rho_g^{(1)}(z, \mathbf{n}) + \bar{\rho}_g(z)\delta\mathcal{V}^{(1)}(z, \mathbf{n}) \\ &= \bar{N}(z) + \bar{\mathcal{V}}(z)\delta\rho_g^{(1)}(z, \mathbf{n}) + \bar{\rho}_g(z)\delta\mathcal{V}^{(1)}(z, \mathbf{n}). \end{aligned} \quad (2.11)$$

By substituting (2.11) in the expression for the fluctuation in the galaxy number count as given in (2.7) we have,

$$\Delta_g^{(1)}(z, \mathbf{n}) = \frac{\delta\rho_g^{(1)}(z, \mathbf{n})}{\bar{\rho}_g(z)} + \frac{\delta\mathcal{V}^{(1)}(z, \mathbf{n})}{\bar{\mathcal{V}}(z)}. \quad (2.12)$$

In a perturbed Universe, the redshift z has also fluctuations with respect to its background value \bar{z} and we can write,

$$z = \bar{z} + \delta z^{(1)}. \quad (2.13)$$

Therefore, we can Taylor expand $\bar{\rho}_g(z)$ as,

$$\bar{\rho}_g(z) = \bar{\rho}_g(\bar{z}) + \frac{\partial\bar{\rho}_g(z)}{\partial z}\delta z^{(1)}, \quad (2.14)$$

and we can show that,

$$\delta\rho_g^{(1)}(z, \mathbf{n}) = \rho_g(z, \mathbf{n}) - \bar{\rho}_g(z) = \rho_g(z, \mathbf{n}) - \bar{\rho}_g(\bar{z}) - \frac{\partial\bar{\rho}_g(z)}{\partial z}\delta z^{(1)}. \quad (2.15)$$

Since Δ_g is an observable, it must be gauge-independent and therefore, we can use any gauge to compute it. We choose to work in the Poisson gauge because it can be easily transformed to any gauge we want later on. The linear galaxy density contrast in the Poisson gauge is given by,

$$\delta_g^{(1)}(z, \mathbf{n}) = \frac{\rho_g(z, \mathbf{n}) - \bar{\rho}_g(\bar{z})}{\bar{\rho}_g(\bar{z})}. \quad (2.16)$$

We can combine (2.15) and (2.16) and use the result together with (2.14) to finally write (2.12) as,

$$\Delta_g^{(1)}(z, \mathbf{n}) = \delta_g^{(1)}(z, \mathbf{n}) - \frac{1}{\bar{\rho}_g(z)}\frac{\partial\bar{\rho}_g(z)}{\partial z}\delta z^{(1)} + \frac{\delta\mathcal{V}^{(1)}(z, \mathbf{n})}{\bar{\mathcal{V}}(z)}. \quad (2.17)$$

Galaxies are found in dark matter halos which cannot be observed directly. The distribution of the galaxies gives us information about the dark matter profile of the halos. In other words, galaxies are tracers for the underlying dark matter distribution. These two are related by the galaxy bias, b which is defined in the comoving-synchronous gauge [74]. Therefore, we need to relate $\delta_g^{(1)}$ to the comoving-synchronous (C), $\delta_{gC}^{(1)}$ by using

the result [75],

$$\delta\beta_C = \delta\beta - \bar{\beta}'v, \quad (2.18)$$

for any $\delta\beta$. The transformation involves a derivative of the quantity β with respect to the conformal time η multiplied by the velocity potential v along the direction of observation \mathbf{n} . In the case of the first-order galaxy number density $\rho_g^{(1)}$,

$$\delta\rho_g^{(1)}(z, \mathbf{n}) = \delta\rho_{gC}^{(1)}(z, \mathbf{n}) + \bar{\rho}_g'(\bar{z})v^{(1)}, \quad (2.19)$$

and we can divide (2.19) by $\bar{\rho}_g(\bar{z})$ to obtain the transformation relation for the galaxy overdensity contrast,

$$\delta_g^{(1)}(z, \mathbf{n}) = \delta_{gC}^{(1)}(z, \mathbf{n}) + \frac{\bar{\rho}_g'(\bar{z})}{\bar{\rho}_g(\bar{z})}v^{(1)}. \quad (2.20)$$

Now, we can introduce the first-order galaxy bias b_1 given by [31, 74],

$$\delta_{gC}^{(1)}(z, \mathbf{n}) = b_1\delta_C^{(1)}(z, \mathbf{n}), \quad (2.21)$$

where $\delta_C^{(1)}$ is the first-order dark matter overdensity contrast in comoving-synchronous gauge. We can replace (2.21) in (2.20) and use the result in (2.17) to show that,

$$\Delta_g^{(1)}(z, \mathbf{n}) = b_1\delta_C^{(1)}(z, \mathbf{n}) + \frac{\bar{\rho}_g'(\bar{z})}{\bar{\rho}_g(\bar{z})}v^{(1)} - \frac{1}{\bar{\rho}_g(z)}\frac{\partial\bar{\rho}_g(z)}{\partial z}\delta z^{(1)} + \frac{\delta\mathcal{V}^{(1)}(z, \mathbf{n})}{\bar{\mathcal{V}}(z)}. \quad (2.22)$$

For conserved sources,

$$\frac{\bar{\rho}_g'(\bar{z})}{\bar{\rho}_g(\bar{z})} = -3\mathcal{H}, \quad (2.23)$$

which is given by the continuity equation [76, 77]. However, in the real picture of the Universe we observe galaxy formation and mergers and therefore, the galaxy number density $\bar{\rho}_g$ changes with time. We account for this time evolution by defining the evolution bias [32, 33],

$$b_e = \frac{\partial \ln(a^3 \bar{\rho}_g)}{\partial \ln a}. \quad (2.24)$$

We can use the following transformation rules, $\partial/\partial\eta = a\mathcal{H}\partial/\partial a$ and $\partial/\partial \ln a = a\partial/\partial a$ to show that for non-conserved sources,

$$\frac{\bar{\rho}_g'(\bar{z})}{\bar{\rho}_g(\bar{z})} = \mathcal{H}(b_e - 3) \quad \text{and} \quad \frac{1}{\bar{\rho}_g(z)}\frac{\partial\bar{\rho}_g(z)}{\partial z} = -\frac{(b_e - 3)}{1+z} = -\frac{(b_e - 3)}{1+\bar{z}} \left[1 - \frac{\delta z^{(1)}}{(1+\bar{z})} + \dots \right]. \quad (2.25)$$

Hence, the expression given in (2.22) becomes,

$$\Delta_g^{(1)}(z, \mathbf{n}) = b_1\delta_C^{(1)}(z, \mathbf{n}) + \mathcal{H}(b_e - 3)v^{(1)} + \frac{(b_e - 3)}{1+\bar{z}}\delta z^{(1)} + \frac{\delta\mathcal{V}^{(1)}(z, \mathbf{n})}{\bar{\mathcal{V}}(z)}. \quad (2.26)$$

2.2.1 First-order redshift perturbation $\delta z^{(1)}$

We consider a perturbed and non-expanding FLRW Universe with a metric,

$$ds^2 = -\left(1 + 2\Phi^{(1)}\right)d\eta^2 + \left(1 - 2\Psi^{(1)}\right)\delta_{ij}dx^i dx^j, \quad (2.27)$$

where galactic objects are free to move relative to a fixed background. Let us take a fixed observer with 4-velocity vector $U_{(o)}^\mu = (1, \mathbf{0})$ looking at a source having a peculiar velocity \mathbf{v} with respect to the background. The 4-velocity vector of the source is defined as $U_{(s)}^\mu = (1 - \Phi^{(1)}, v^{(1)})$ [20]. If the source emits a photon and the positive direction of \mathbf{n} is taken to be towards the fixed observer, then the 4-momentum vector K^μ of the photon as seen by the fixed observer will be,

$$K_{(o)}^\mu = (1, n^i), \quad (2.28)$$

with $\sum_{i=1}^3 n^i n_i = 1$. On the other hand, an observer at the source will see the photon going away from him and in that case, the 4-momentum vector of the photon at the source will be,

$$K_{(s)}^\mu = (1 + \delta\gamma, -n^i + \delta n^i), \quad (2.29)$$

where $\delta\gamma$ and δn^i are the perturbations in the time-time and space-space components of K^μ due to the motion of the source. Then, the photon as observed by the fixed observer will be redshifted as [20],

$$1 + z = \frac{U_{(s)}^\mu K_{\mu(s)}}{U_{(o)}^\mu K_{\mu(o)}}. \quad (2.30)$$

To restore the effect of the expanding Universe we put back the scale factor a and the definition for the redshift becomes,

$$1 + z = \frac{1}{a} \left[\frac{U_{(s)}^\mu K_{\mu(s)}}{U_{(o)}^\mu K_{\mu(o)}} \right]. \quad (2.31)$$

We can apply the result $K^\mu K_\mu = 0$ [38] to obtain the expressions for $K_{\mu(o)}$ and $K_{\mu(s)}$ respectively. Using (2.31) we can show,

$$1 + z = \frac{1}{a} \left(1 - \Phi^{(1)} + \mathbf{v} \cdot \mathbf{n} - \delta\gamma \right). \quad (2.32)$$

We now consider the geodesic equation [38],

$$\frac{dK^\mu}{d\lambda} + \Gamma^\mu_{\alpha\beta} K^\alpha K^\beta = 0, \quad (2.33)$$

which gives,

$$\frac{d\delta K^\mu}{d\lambda} + \delta\Gamma^\mu_{\alpha\beta} \bar{K}^\alpha \bar{K}^\beta = 0, \quad (2.34)$$

at linear order in perturbation. We can obtain $\delta\gamma$ by solving the time-time component of (2.34) i.e., we set $\mu = 0$ and we have,

$$\frac{d\delta K^0}{d\lambda} \equiv \frac{d\delta\gamma}{d\lambda} = -\left(\delta\Gamma^0_{00} \bar{K}^0 \bar{K}^0 + 2\delta\Gamma^0_{0i} \bar{K}^0 \bar{K}^i + \delta\Gamma^0_{ij} \bar{K}^i \bar{K}^j \right). \quad (2.35)$$

For the perturbed FLRW metric given in (2.27),

$$\delta\Gamma^0_{00} = \Phi^{(1)'}, \quad \delta\Gamma^0_{0i} = \partial_i \Phi^{(1)}, \quad \delta\Gamma^0_{ij} = -\delta_{ij} \Psi^{(1)'}. \quad (2.36)$$

By replacing (2.36) in (2.35) and knowing that $\bar{K}^\mu = (1, n^i)$ we have,

$$\frac{d\delta\gamma}{d\lambda} = -\Phi^{(1)'} - 2\bar{n}^i \partial_i \Phi^{(1)} + \Psi^{(1)'}. \quad (2.37)$$

The derivative along light rays is a sum of a time derivative and a radial derivative so that,

$$\frac{d\Phi^{(1)}}{d\lambda} = \Phi^{(1)'} + n^i \partial_i \Phi^{(1)}, \quad (2.38)$$

By substituting (2.38) in (2.37) we can show that,

$$\delta\gamma = -2\Phi^{(1)} + \int_0^\lambda d\tilde{\lambda} \left(\Phi^{(1)'} + \Psi^{(1)'} \right). \quad (2.39)$$

We can then replace (2.39) in (2.32) to obtain the expression for the redshift as,

$$1 + z = \frac{1}{a} \left[1 + \Phi^{(1)} + \mathbf{v} \cdot \mathbf{n} - \int_0^\lambda d\tilde{\lambda} \left(\Phi^{(1)'} + \Psi^{(1)'} \right) \right]. \quad (2.40)$$

The first term on the right-hand side of (2.40) is just $(1 + \bar{z})$ and therefore, we can further simplify using $\delta z^{(1)} = z - \bar{z}$ to obtain [78],

$$\delta z^{(1)} = (1 + \bar{z}) \left[\Phi^{(1)} + \mathbf{v} \cdot \mathbf{n} - \int_0^\lambda d\tilde{\lambda} \left(\Phi^{(1)'} + \Psi^{(1)'} \right) \right]. \quad (2.41)$$

We can now substitute (2.41) in (2.26) to show that the first-order fluctuation in the galaxy number count becomes,

$$\begin{aligned} \Delta_g^{(1)}(z, \mathbf{n}) &= b_1 \delta_C^{(1)}(z, \mathbf{n}) + \mathcal{H}(b_e - 3) v^{(1)} \\ &+ (b_e - 3) \left[\Phi^{(1)} + \partial_{\parallel} v^{(1)} - \int_0^\lambda d\tilde{\lambda} \left(\Phi^{(1)'} + \Psi^{(1)'} \right) \right] + \frac{\delta \mathcal{V}^{(1)}(z, \mathbf{n})}{\bar{\mathcal{V}}(z)}, \end{aligned} \quad (2.42)$$

where $\partial_{\parallel} v^{(1)}$ is the Doppler term¹.

2.2.2 First-order volume perturbation $\delta\mathcal{V}^{(1)}$

We consider a source moving with the 4-velocity $U_{(s)}^{\mu} = (1 - \Phi^{(1)}, v^{(1)})$ with respect to a background observer. The definition for a small element of volume dV_s as measured in the frame of reference of the source is given by [20, 73],

$$dV_s = \sqrt{-g} \epsilon_{\mu\alpha\beta\gamma} U_{(s)}^{\mu} dx^{\alpha} dx^{\beta} dx^{\gamma}, \quad (2.43)$$

where g is the determinant of the perturbed FLRW metric,

$$ds^2 = a^2(\eta) \left[- \left(1 + 2\Phi^{(1)} \right) d\eta^2 + \left(1 - 2\Psi^{(1)} \right) \delta_{ij} dx^i dx^j \right], \quad (2.44)$$

and $\epsilon_{\mu\alpha\beta\gamma}$ is called the Levi-Civita symbol [79]. We will need to perform a coordinate transformation of (2.43) to include the mapping between the coordinates at the source and the observer. Such a transformation involves a Jacobian determinant \mathcal{J} and we have [20, 73],

$$dV_s = \sqrt{-g} \epsilon_{\mu\alpha\beta\gamma} U_{(s)}^{\mu} \frac{\partial x^{\alpha}}{\partial z} \frac{\partial x^{\beta}}{\partial \theta_o} \frac{\partial x^{\gamma}}{\partial \phi_o} \mathcal{J} dz d\theta_o d\phi_o, \quad (2.45)$$

where z is the observed redshift and,

$$\mathcal{J} = \left| \frac{\partial(\theta_s, \phi_s)}{\partial(\theta_o, \phi_o)} \right|, \quad (2.46)$$

is the Jacobian transformation between the polar angles (θ_s, ϕ_s) and (θ_o, ϕ_o) which are the angular coordinates measured at the position of the source and observer respectively. If $\bar{\chi}_s$ is the radial comoving distance to dV as measured in the source's frame, then in spherical coordinates the small element of length is given as $dx^{\mu} = (-d\eta, d\bar{\chi}_s, \bar{\chi}_s d\theta_s, \bar{\chi}_s \sin \theta_s d\phi_s)$. In a perturbed Universe, both the radial and angular coordinates are perturbed with respect to the background observer and therefore we have at first-order,

$$\theta_s = \theta_o + \delta\theta^{(1)}, \quad \phi_s = \phi_o + \delta\phi^{(1)}, \quad \bar{\chi}_s = \bar{\chi} + \delta\bar{\chi}^{(1)}. \quad (2.47)$$

¹ $\mathbf{v} \cdot \mathbf{n} = n^i \partial_i v^{(1)} = \partial_{\parallel} v^{(1)}$ where $n^i \partial_i \equiv \partial_{\parallel}$.

On expanding the right-hand side expression of (2.45), $\delta\theta^{(1)}$, $\delta\phi^{(1)}$ and $\delta\bar{\chi}^{(1)}$ directly translate into the volume fluctuation as [20, 73],

$$\begin{aligned} \frac{\delta\mathcal{V}^{(1)}(z, \mathbf{n})}{\bar{\mathcal{V}}(z)} &= -3\Psi^{(1)} + \left(\cot\theta_o + \frac{\partial}{\partial\theta_o} \right) \delta\theta^{(1)} + \frac{\partial\delta\phi^{(1)}}{\partial\phi_o} - \mathbf{v} \cdot \mathbf{n} + 2\frac{\delta\bar{\chi}^{(1)}}{\bar{\chi}} - \frac{\partial\delta\bar{\chi}^{(1)}}{\partial\lambda} \\ &+ \frac{1}{\mathcal{H}(1+\bar{z})} \frac{\partial\delta z^{(1)}}{\partial\lambda} - \left(-4 + \frac{2}{\bar{\chi}\mathcal{H}} + \frac{\mathcal{H}'}{\mathcal{H}^2} \right) \frac{\delta z^{(1)}}{(1+\bar{z})}. \end{aligned} \quad (2.48)$$

We can solve for $\delta\theta^{(1)}$, $\delta\phi^{(1)}$ and $\delta\bar{\chi}^{(1)}$ by finding the deviation vector [20],

$$\delta x^i = \int_0^\lambda d\tilde{\lambda} (\delta K^i - n^i \delta K^0), \quad (2.49)$$

which relates the perturbed geodesic to the unperturbed one. The space-space component of the geodesic equation (2.34) gives,

$$\frac{d\delta K^i}{d\lambda} = - \left(\delta\Gamma_{00}^i \bar{K}^0 \bar{K}^0 + 2\delta\Gamma_{j0}^i \bar{K}^j \bar{K}^0 + \delta\Gamma_{jk}^i \bar{K}^j \bar{K}^k \right). \quad (2.50)$$

For the perturbed FLRW metric given in (2.44),

$$\delta\Gamma_{00}^i = \partial^i \Phi^{(1)}, \quad \delta\Gamma_{j0}^i = -\Psi^{(1)'} \delta_j^i, \quad \delta\Gamma_{jk}^i = -\delta_j^i \partial_k \Psi^{(1)} + \delta_{jk} \delta^{il} \partial_l \Psi^{(1)}, \quad (2.51)$$

and (2.50) becomes,

$$\frac{d\delta K^i}{d\lambda} = -\partial^i \Phi^{(1)} + 2\Psi^{(1)'} n^i + n^i \partial_{\parallel} \Psi^{(1)}. \quad (2.52)$$

where we have made use of $\bar{K}^\mu = (1, n^i)$. We can further simplify (2.52) by using (2.38) and $\partial^i = n^i \partial_{\parallel} + \nabla_{\perp}^i$ to show that,

$$\delta K^i = n^i \left[\Psi^{(1)} - \Phi^{(1)} + \int_0^\lambda d\tilde{\lambda} (\Phi^{(1)'} + \Psi^{(1)'}) \right] - \int_0^\lambda d\tilde{\lambda} \tilde{\nabla}_{\perp}^i (\Phi^{(1)} + \Psi^{(1)}). \quad (2.53)$$

The expression for δK^0 is $\delta\gamma$ which is given in (2.39) and by substituting (2.53) in (2.49) we obtain,

$$\delta x^i = n^i \int_0^\lambda d\tilde{\lambda} (\Phi^{(1)} + \Psi^{(1)}) - \int_0^\lambda d\tilde{\lambda} (\lambda - \tilde{\lambda}) \tilde{\nabla}_{\perp}^i (\Phi^{(1)} + \Psi^{(1)}). \quad (2.54)$$

We can also write (2.54) as,

$$\delta x^i = \delta x_{\parallel}^i + \delta x_{\perp}^i, \quad (2.55)$$

where

$$\delta x_{\parallel}^i = n^i \int_0^\lambda d\tilde{\lambda} (\Phi^{(1)} + \Psi^{(1)}), \quad \delta x_{\perp}^i = - \int_0^\lambda d\tilde{\lambda} (\lambda - \tilde{\lambda}) \tilde{\nabla}_{\perp}^i (\Phi^{(1)} + \Psi^{(1)}). \quad (2.56)$$

To obtain $\delta\theta^{(1)}$, $\delta\phi^{(1)}$ and $\delta\bar{\chi}^{(1)}$, we need to do the projections of δx_{\perp}^i and δx_{\parallel}^i on the unit vectors $e_{\theta i}$, $e_{\phi i}$ and $e_{\bar{\chi} i}$ accordingly. These unit vectors have the following characteristics [20],

$$n^i e_{\theta i} = 0, \quad \bar{n}^i e_{\phi i} = 0, \quad n^i e_{\bar{\chi} i} = 1, \quad (2.57)$$

and,

$$e_{\theta i} \tilde{\nabla}_{\perp}^i = \frac{1}{\tilde{\chi}} \tilde{\partial}_{\theta_o}, \quad e_{\phi i} \tilde{\nabla}_{\perp}^i = \frac{1}{\tilde{\chi} \sin \theta_o} \tilde{\partial}_{\phi_o}. \quad (2.58)$$

Therefore we have,

$$\begin{aligned} \delta\bar{\chi}^{(1)} &= \delta x_{\parallel}^i e_{\bar{\chi} i} = \int_0^{\lambda} d\tilde{\lambda} \left(\Phi^{(1)} + \Psi^{(1)} \right), \\ \delta\theta^{(1)} &= \frac{1}{\tilde{\chi}} \delta x_{\perp}^i e_{\theta i} = - \int_0^{\lambda} d\tilde{\lambda} \frac{\lambda - \tilde{\lambda}}{\tilde{\chi} \tilde{\chi}} \tilde{\partial}_{\theta_o} \left(\Phi^{(1)} + \Psi^{(1)} \right), \\ \delta\phi^{(1)} &= \frac{1}{\tilde{\chi} \sin \theta_o} \delta x_{\perp}^i e_{\phi i} = - \frac{1}{\sin^2 \theta_o} \int_0^{\lambda} d\tilde{\lambda} \frac{\lambda - \tilde{\lambda}}{\tilde{\chi} \tilde{\chi}} \tilde{\partial}_{\phi_o} \left(\Phi^{(1)} + \Psi^{(1)} \right). \end{aligned} \quad (2.59)$$

The redshift contribution $\partial\delta z^{(1)}/\partial\lambda$ can be obtained by taking the derivative of (2.41) with respect to the affine parameter λ . Then, by using the results of (2.41) and (2.59) in (2.48) we can show that the volume fluctuation becomes,

$$\begin{aligned} \frac{\delta\mathcal{V}^{(1)}(z, \mathbf{n})}{\bar{\mathcal{V}}(z)} &= -\frac{1}{\mathcal{H}} \frac{\partial}{\partial\lambda} (\mathbf{v} \cdot \mathbf{n}) + \left(3 - \frac{\mathcal{H}'}{\mathcal{H}^2} - \frac{2}{\tilde{\chi}\mathcal{H}} \right) \mathbf{v} \cdot \mathbf{n} + \Phi^{(1)} - 2\Psi^{(1)} + \frac{1}{\mathcal{H}} \Psi^{(1)'} \\ &+ \left(3 - \frac{\mathcal{H}'}{\mathcal{H}^2} - \frac{2}{\tilde{\chi}\mathcal{H}} \right) \Phi^{(1)} - \left(3 - \frac{\mathcal{H}'}{\mathcal{H}^2} - \frac{2}{\tilde{\chi}\mathcal{H}} \right) \int_0^{\lambda} d\tilde{\lambda} \left(\Phi^{(1)'} + \Psi^{(1)'} \right) \\ &+ \frac{2}{\tilde{\chi}} \int_0^{\lambda} d\tilde{\lambda} \left(\Phi^{(1)} + \Psi^{(1)} \right) - \int_0^{\lambda} d\tilde{\lambda} \frac{\lambda - \tilde{\lambda}}{\tilde{\chi} \tilde{\chi}} \tilde{\nabla}_{\Omega}^2 \left(\Phi^{(1)} + \Psi^{(1)} \right), \end{aligned} \quad (2.60)$$

where $\tilde{\nabla}_{\Omega}^2 = \cot \theta_o \partial_{\theta_o} + \partial_{\theta_o}^2 + (1/\sin^2 \theta_o) \partial_{\phi_o}$ is the angular part of the Laplacian operator. We can substitute (2.60) in (2.42) to show that the fluctuation in the observed galaxy number count at first-order is given by,

$$\begin{aligned} \Delta_g^{(1)}(z, \mathbf{n}) &= \underbrace{b_1 \delta_C^{(1)}}_{\text{Density term}} - \frac{1}{\mathcal{H}} \frac{\partial}{\partial\lambda} (\mathbf{v} \cdot \mathbf{n}) + \underbrace{\mathcal{H}(b_e - 3)v^{(1)} + \left(b_e - \frac{\mathcal{H}'}{\mathcal{H}^2} - \frac{2}{\tilde{\chi}\mathcal{H}} \right) \partial_{\parallel} v^{(1)}}_{\text{Doppler}} \\ &- \underbrace{\left(b_e - \frac{\mathcal{H}'}{\mathcal{H}^2} - \frac{2}{\tilde{\chi}\mathcal{H}} \right) \Phi^{(1)} + \Phi^{(1)} - 2\Psi^{(1)} + \frac{1}{\mathcal{H}} \Psi^{(1)'}}_{\text{Sachs-Wolfe}} \\ &- \underbrace{\left(b_e - \frac{\mathcal{H}'}{\mathcal{H}^2} - \frac{2}{\tilde{\chi}\mathcal{H}} \right) \int_0^{\lambda} d\tilde{\lambda} \left(\Phi^{(1)'} + \Psi^{(1)'} \right)}_{\text{Integrated Sachs-Wolfe}} + \underbrace{\frac{2}{\tilde{\chi}} \int_0^{\lambda} d\tilde{\lambda} \left(\Phi^{(1)} + \Psi^{(1)} \right)}_{\text{Time-delay (Shapiro)}} \\ &- \underbrace{\int_0^{\lambda} d\tilde{\lambda} \frac{\lambda - \tilde{\lambda}}{\tilde{\chi} \tilde{\chi}} \tilde{\nabla}_{\Omega}^2 \left(\Phi^{(1)} + \Psi^{(1)} \right)}_{\text{Lensing}}. \end{aligned} \quad (2.61)$$

The result of (2.61) shows the fluctuation of the galaxy number count obtained from the redshift and volume perturbations on the sky. However, in observations the number of observed sources depend also on their apparent fluxes [32]. This is because any survey has its own flux sensitivity and therefore, objects above the threshold flux will be detected by the telescope. This flux dependence leads to either the magnification or demagnification of the observed sources because their apparent fluxes are either amplified or de-amplified [80]. We can compute the effect of this distortion in magnification and we find that it contributes to corrections in the Doppler, Sachs-Wolfe, integrated Sachs-Wolfe, time-delay (Shapiro effect) and lensing terms as [32, 80, 81],

$$\begin{aligned} \Delta_{\mathcal{M}}^{(1)}(z, \mathbf{n}) &= -2\mathcal{Q}\left(1 - \frac{1}{\bar{\chi}\mathcal{H}}\right)\partial_{\parallel}v^{(1)} + \mathcal{Q}\int_0^\lambda d\tilde{\lambda}\frac{\lambda - \tilde{\lambda}}{\lambda\tilde{\lambda}}\tilde{\nabla}_\Omega^2\left(\Phi^{(1)} + \Psi^{(1)}\right) \\ &\quad - 2\mathcal{Q}\left(\Phi^{(1)} - 2\Psi^{(1)}\right) - 2\mathcal{Q}\left(1 - \frac{1}{\bar{\chi}\mathcal{H}}\right)\Phi^{(1)} \\ &\quad - \frac{2\mathcal{Q}}{\bar{\chi}}\int_0^\lambda d\tilde{\lambda}\left(\Phi^{(1)} + \Psi^{(1)}\right) + 2\mathcal{Q}\left(1 - \frac{1}{\bar{\chi}\mathcal{H}}\right)\int_0^\lambda d\tilde{\lambda}\left(\Phi^{(1)'} + \Psi^{(1)'}\right), \end{aligned} \quad (2.62)$$

where $\Delta_{\mathcal{M}}^{(1)}(z, \mathbf{n})$ is the magnification correction and \mathcal{Q} is the magnification bias. It is given by the logarithmic derivative of the background galaxy number density with respect to the threshold luminosity as [33],

$$\mathcal{Q} = -\frac{\partial \ln(a^3 \bar{\rho}_g)}{\partial \ln \bar{L}}. \quad (2.63)$$

Therefore, we can add the result of (2.62) to (2.61) and show that,

$$\begin{aligned} \Delta_g^{(1)}(z, \mathbf{n}) &= \underbrace{b_1 \delta_C^{(1)}}_{\text{Density term}} - \frac{1}{\mathcal{H}} \frac{\partial}{\partial \lambda} (\mathbf{v} \cdot \mathbf{n}) \\ &\quad + \underbrace{\mathcal{H}(b_e - 3)v^{(1)} + \left[b_e - \frac{\mathcal{H}'}{\mathcal{H}^2} - 2\mathcal{Q} - \frac{2(1 - \mathcal{Q})}{\bar{\chi}\mathcal{H}} \right] \partial_{\parallel}v^{(1)}}_{\text{Doppler}} \\ &\quad - \underbrace{\left[b_e - \frac{\mathcal{H}'}{\mathcal{H}^2} + 2\mathcal{Q} - \frac{2(1 - \mathcal{Q})}{\bar{\chi}\mathcal{H}} \right] \Phi^{(1)} + (1 - 2\mathcal{Q}) \left(\Phi^{(1)} - 2\Psi^{(1)} \right) + \frac{1}{\mathcal{H}} \Psi^{(1)'}}_{\text{Sachs-Wolfe}} \\ &\quad - \underbrace{\left[b_e - \frac{\mathcal{H}'}{\mathcal{H}^2} - 2\mathcal{Q} - \frac{2(1 - \mathcal{Q})}{\bar{\chi}\mathcal{H}} \right] \int_0^\lambda d\tilde{\lambda} \left(\Phi^{(1)'} + \Psi^{(1)'} \right)}_{\text{Integrated Sachs-Wolfe}} \\ &\quad + \underbrace{\frac{2(1 - \mathcal{Q})}{\bar{\chi}} \int_0^\lambda d\tilde{\lambda} \left(\Phi^{(1)} + \Psi^{(1)} \right)}_{\text{Time-delay (Shapiro)}} \\ &\quad - \underbrace{(1 - \mathcal{Q}) \int_0^\lambda d\tilde{\lambda} \frac{\lambda - \tilde{\lambda}}{\bar{\chi}\tilde{\lambda}} \tilde{\nabla}_\Omega^2 \left(\Phi^{(1)} + \Psi^{(1)} \right)}_{\text{Lensing}}. \end{aligned} \quad (2.64)$$

The second term in $\partial/\partial\lambda$ is simplified as follows:

$$\frac{\partial}{\partial\lambda}(\mathbf{v} \cdot \mathbf{n}) = \frac{\partial}{\partial\eta}(\mathbf{v} \cdot \mathbf{n}) + \partial_{\parallel}(\mathbf{v} \cdot \mathbf{n}) = \mathbf{v}' \cdot \mathbf{n} + \partial_{\parallel}(\mathbf{v} \cdot \mathbf{n}). \quad (2.65)$$

The $\mathbf{v}' \cdot \mathbf{n}$ is eliminated using the Euler equation (refer to (1.25)). Therefore (2.64) becomes [49],

$$\begin{aligned} \Delta_g^{(1)}(z, \mathbf{n}) = & \underbrace{b_1 \delta_C^{(1)}}_{\text{Density term}} - \underbrace{\frac{1}{\mathcal{H}} \partial_{\parallel}^2 v^{(1)}}_{\text{Redshift space distortion}} \\ & + \underbrace{\mathcal{H}(b_e - 3)v^{(1)} + \left[b_e - \frac{\mathcal{H}'}{\mathcal{H}^2} - 2\mathcal{Q} - \frac{2(1-\mathcal{Q})}{\bar{\chi}\mathcal{H}} \right] \partial_{\parallel} v^{(1)}}_{\text{Doppler}} \\ & - \underbrace{\left[b_e - \frac{\mathcal{H}'}{\mathcal{H}^2} + 2\mathcal{Q} - \frac{2(1-\mathcal{Q})}{\bar{\chi}\mathcal{H}} \right] \Phi^{(1)} + (1-2\mathcal{Q}) \left(\Phi^{(1)} - 2\Psi^{(1)} \right) + \frac{1}{\mathcal{H}} \Psi^{(1)'}}_{\text{Sachs-Wolfe}} \\ & - \underbrace{\left[b_e - \frac{\mathcal{H}'}{\mathcal{H}^2} - 2\mathcal{Q} - \frac{2(1-\mathcal{Q})}{\bar{\chi}\mathcal{H}} \right] \int_0^{\bar{\chi}} d\tilde{\lambda} \left(\Phi^{(1)'} + \Psi^{(1)'} \right)}_{\text{Integrated Sachs-Wolfe}} \\ & + \underbrace{\frac{2(1-\mathcal{Q})}{\bar{\chi}} \int_0^{\bar{\chi}} d\tilde{\lambda} \left(\Phi^{(1)} + \Psi^{(1)} \right)}_{\text{Time-delay(Shapiro)}} \\ & - \underbrace{(1-\mathcal{Q}) \int_0^{\bar{\chi}} d\tilde{\lambda} \frac{\bar{\lambda} - \tilde{\lambda}}{\chi\tilde{\chi}} \tilde{\nabla}_{\Omega}^2 \left(\Phi^{(1)} + \Psi^{(1)} \right)}_{\text{Lensing}}, \end{aligned} \quad (2.66)$$

where $\partial_{\parallel}^2 v^{(1)}$ is the same as $\partial_{\parallel}(\mathbf{v} \cdot \mathbf{n})^2$. For brevity we can write (2.66) as follows,

$$\Delta_g^{(1)}(z, \mathbf{n}) = \Delta^{(1)} + \Delta_{\text{RSD}}^{(1)} + \Delta_{\text{Dop.}}^{(1)} + \Delta_{\text{pot.}}^{(1)} + \Delta_{\kappa}^{(1)}, \quad (2.67)$$

where $\Delta^{(1)}$ is the galaxy density term, $\Delta_{\text{RSD}}^{(1)}$ is the redshift space distortion term, $\Delta_{\text{Dop.}}^{(1)}$ is the Doppler term, $\Delta_{\text{pot.}}^{(1)}$ are the potential terms (non-integrated and integrated terms) and $\Delta_{\kappa}^{(1)}$ is the lensing term.

2.3 The model of galaxy bias on very large scales

2.3.1 The linear model

The model of galaxy bias which we are going to use is the local-in-mass-density (LIMD) model [64]. We first consider the linear galaxy density contrast $\delta_g^{(1)}$ which is defined in

$${}^2\partial_{\parallel}(\mathbf{v} \cdot \mathbf{n}) = n^i \partial_i \left[n^j \partial_j v^{(1)} \right] = (n^i \partial_i)^2 v^{(1)} = \partial_{\parallel}^2 v^{(1)}$$

the Poisson gauge as given in (2.16). This is related to the dark matter density contrast $\delta^{(1)}$ via the galaxy bias. We must make sure that the definition for scale-independent galaxy bias has to be gauge-independent and is consistent on very large scales. The definition for scale-independent bias is given in the matter rest-frame [31, 32, 70], which coincide with the galaxy rest-frame on large scales where, there is no velocity bias. The matter rest-frame coincides with the comoving-synchronous (C) gauge such that the correct definition of the linear galaxy bias is,

$$\delta_{gC}^{(1)}(z, \mathbf{x}, < \ln L) = b_1(z, \ln L) \delta_C^{(1)}(z, \mathbf{x}) . \quad (2.68)$$

The transformation from the Poisson gauge to the C-gauge is obtained from (2.18) and for $\delta_g^{(1)}$ we have [70],

$$\begin{aligned} \delta_g^{(1)} &= \delta_{gC}^{(1)} + (3 - b_e) \mathcal{H}v^{(1)} \\ &= b_1 \delta_C^{(1)} + (3 - b_e) \mathcal{H}v^{(1)} . \end{aligned} \quad (2.69)$$

It is the velocity potential term that ensures the gauge-independence on very large scales. It is the GR part of $\delta_g^{(1)}$ and its effect is suppressed on small scales but grows on large scales [72].

In GR, the C-gauge is treated as the Lagrangian frame [82, 83]. However, there is no unique gauge defined for the Eulerian frame but, the total matter (T) gauge is a convenient choice. The mapping from T- to C-gauge is via a pure spatial coordinate transformation so that at first-order [82],

$$\delta_C^{(1)} = \delta_T^{(1)} , \quad (2.70)$$

and from (2.69) it implies that,

$$\delta_{gC}^{(1)} = \delta_{gT}^{(1)} = b_1 \delta_T^{(1)} . \quad (2.71)$$

2.3.2 The non-linear model and gauge transformation

We assume that the galaxy density contrast is only a local function of the dark matter density contrast and extend (2.68) to higher powers in δ_C as,

$$\delta_{gC} = b_1 \delta_C + \frac{1}{2} b_2 [\delta_C]^2 + \dots \quad (2.72)$$

This is why the model is called the local-in-mass-density model [64]. To be valid on very large scales, we need the bias coefficients to be scale-independent in the galaxy

rest-frame (C-gauge). At first-order, we recover (2.68) and at second-order we obtain,

$$\delta_{gC}^{(2)} = b_1 \delta_C^{(2)} + b_2 \left[\delta_C^{(1)} \right]^2. \quad (2.73)$$

The second-order C- and T-gauge matter densities are related by [82, 83],

$$\delta_T^{(2)} = \delta_C^{(2)} + 2 \left[\partial_i \delta_C^{(1)} \right] \nabla^{-2} \partial^i \delta_C^{(1)}, \quad (2.74)$$

where $-2\nabla^{-2} \partial^i \delta_C^{(1)}$ is a gauge generator. Since the coordinate transformation from C- to T-gauge is purely spatial, (2.74) can directly be translated to the galaxy overdensities as,

$$\delta_{gT}^{(2)} = \delta_{gC}^{(2)} + 2 \left[\partial_i \delta_{gC}^{(1)} \right] \nabla^{-2} \partial^i \delta_C^{(1)}. \quad (2.75)$$

Using (2.70), (2.71), (2.73) and (2.74) we can show that (2.75) becomes,

$$\delta_{gT}^{(2)} = b_1 \left[\delta_C^{(2)} + 2 \left[\partial_i \delta_C^{(1)} \right] \nabla^{-2} \partial^i \delta_C^{(1)} \right] + b_2 \left[\delta_C^{(1)} \right]^2, \quad (2.76)$$

which can be written as,

$$\delta_{gT}^{(2)} = b_1 \delta_T^{(2)} + b_2 \left[\delta_T^{(1)} \right]^2. \quad (2.77)$$

By comparing (2.73) with (2.77), we find that local-in-mass-density and scale-independent bias in the C- and T-gauge are equivalent up to second-order, with the same bias coefficients which are Eulerian. The second-order galaxy overdensities in the Poisson and C-gauge are related by [84],

$$\begin{aligned} \delta_g^{(2)} = & \delta_{gC}^{(2)} + (3 - b_e) \mathcal{H} v^{(2)} + \left[(b_e - 3) \mathcal{H}' + b_e' \mathcal{H} + (b_e - 3)^2 \mathcal{H}^2 \right] \left[v^{(1)} \right]^2 + (b_e - 3) \mathcal{H} v^{(1)} v^{(1)'} \\ & - (b_e - 3) \mathcal{H} \nabla^{-2} \left[v^{(1)} \nabla^2 v^{(1)'} - v^{(1)'} \nabla^2 v^{(1)} - 6 \partial_i \Phi^{(1)} \partial^i v^{(1)} - 6 \Phi^{(1)} \nabla^2 v^{(1)} \right] \\ & + 2(3 - b_e) \mathcal{H} v^{(1)} \delta_{gC}^{(1)} - 2v^{(1)} \delta_{gC}^{(1)'} - \frac{1}{2} \partial^i \xi^{(1)} \left[(3 - b_e) \mathcal{H} \partial_i v^{(1)} + 2 \partial_i \delta_{gC}^{(1)} \right] \\ & - \frac{1}{2} (b_e - 3) \mathcal{H} \nabla^{-2} \left[\partial_i \xi^{(1)} \partial^i \nabla^2 v^{(1)} + \partial_i v^{(1)} \partial^i \nabla^2 \xi^{(1)} + 2 \partial_i \partial_j \xi^{(1)} \partial^i \partial^j v^{(1)} \right], \quad (2.78) \end{aligned}$$

where $\xi^{(1)}$ is a gauge generator and $\xi^{(1)'} = 2v^{(1)}$ is the gauge fixing condition [84]. Using the identity,

$$\nabla^2 \left[\partial_i \xi^{(1)} \cdot \partial^i v^{(1)} \right] = \partial^i v^{(1)} \cdot \nabla^2 \left[\partial_i \xi^{(1)} \right] + \partial_i \xi^{(1)} \cdot \nabla^2 \left[\partial^i v^{(1)} \right] + 2 \partial_j \partial_i \xi^{(1)} \cdot \partial^j \partial^i v^{(1)}, \quad (2.79)$$

we find that the last line of (2.78) gives,

$$- \frac{1}{2} (b_e - 3) \mathcal{H} \partial_i \xi^{(1)} \partial^i v^{(1)}, \quad (2.80)$$

which cancels with the first term of the expansion of the square bracket on the third line. Therefore (2.78) simplifies to,

$$\begin{aligned} \delta_g^{(2)} &= \delta_{gC}^{(2)} + (3 - b_e)\mathcal{H}v^{(2)} + \left[(b_e - 3)\mathcal{H}' + b'_e\mathcal{H} + (b_e - 3)^2\mathcal{H}^2 \right] [v^{(1)}]^2 + (b_e - 3)\mathcal{H}v^{(1)}v^{(1)'} \\ &\quad - (b_e - 3)\mathcal{H}\nabla^{-2} \left[v^{(1)}\nabla^2 v^{(1)'} - v^{(1)'}\nabla^2 v^{(1)} - 6\partial_i\Phi^{(1)}\partial^i v^{(1)} - 6\Phi^{(1)}\nabla^2 v^{(1)} \right] \\ &\quad + 2(3 - b_e)\mathcal{H}v^{(1)}\delta_{gC}^{(1)} - 2v^{(1)}\delta_{gC}^{(1)'} - \left[\partial_i\delta_{gC}^{(1)} \right] \partial^i \xi^{(1)}. \end{aligned} \quad (2.81)$$

By using the continuity equation,

$$\delta_C^{(1)'} = -\nabla^2 v^{(1)}, \quad (2.82)$$

the gauge fixing condition implies that,

$$\partial^i \xi^{(1)} = -2\nabla^{-2} \partial^i \delta_C^{(1)}. \quad (2.83)$$

By (2.74) we can show that,

$$\delta_{gT}^{(2)} = \delta_{gC}^{(2)} - \left[\partial_i \delta_{gC}^{(1)} \right] \partial^i \xi^{(1)}, \quad (2.84)$$

and therefore, replacing (2.84) in (2.81) we can write the second-order Poisson galaxy overdensity $\delta_g^{(2)}$ in terms of the second-order T-gauge galaxy overdensity $\delta_{gT}^{(2)}$ as,

$$\begin{aligned} \delta_g^{(2)} &= \delta_{gT}^{(2)} + (3 - b_e)\mathcal{H}v^{(2)} + \left[(b_e - 3)\mathcal{H}' + b'_e\mathcal{H} + (b_e - 3)^2\mathcal{H}^2 \right] [v^{(1)}]^2 + (b_e - 3)\mathcal{H}v^{(1)}v^{(1)'} \\ &\quad - (b_e - 3)\mathcal{H}\nabla^{-2} \left[v^{(1)}\nabla^2 v^{(1)'} - v^{(1)'}\nabla^2 v^{(1)} - 6\partial_i\Phi^{(1)}\partial^i v^{(1)} - 6\Phi^{(1)}\nabla^2 v^{(1)} \right] \\ &\quad + 2(3 - b_e)\mathcal{H}v^{(1)}\delta_{gT}^{(1)} - 2v^{(1)}\delta_{gT}^{(1)'} . \end{aligned} \quad (2.85)$$

We can further simplify by using (2.71) and (2.77) to express the galaxy overdensities in terms of the dark matter overdensities as,

$$\begin{aligned} \delta_g^{(2)} &= b_1\delta_T^{(2)} + b_2[\delta_T^{(1)}]^2 + (3 - b_e)\mathcal{H}v^{(2)} + \left[(b_e - 3)\mathcal{H}' + b'_e\mathcal{H} + (b_e - 3)^2\mathcal{H}^2 \right] [v^{(1)}]^2 \\ &\quad - (b_e - 3)\mathcal{H}\nabla^{-2} \left[v^{(1)}\nabla^2 v^{(1)'} - v^{(1)'}\nabla^2 v^{(1)} - 6\partial_i\Phi^{(1)}\partial^i v^{(1)} - 6\Phi^{(1)}\nabla^2 v^{(1)} \right] \\ &\quad + (b_e - 3)\mathcal{H}v^{(1)}v^{(1)'} + 2b_1(3 - b_e)\mathcal{H}v^{(1)}\delta_T^{(1)} - 2v^{(1)} \left[b_1\delta_T^{(1)'} + b'_1\delta_T^{(1)} \right]. \end{aligned} \quad (2.86)$$

which is the second-order generalization of (2.69). The velocity and metric potentials ensure the gauge-independence on very large scales. The LIMD model does not include the tidal field. The local bias model includes the tidal field - the tidal operator which forms part of the leading *local gravitational observables* of long-wavelength spacetime

perturbation [64]. It is defined through the scaled dimensionless quantity [64],

$$K_{ij} = \mathcal{D}_{ij}\delta_C^{(1)} = \mathcal{D}_{ij}\delta_T^{(1)}, \quad \mathcal{D}_{ij} = \left(\frac{\partial_i \partial_j}{\nabla^2} - \frac{1}{3}\delta_{ij} \right), \quad (2.87)$$

and using the Poisson equation (1.84) we have,

$$K_{ij} = \frac{2}{3\Omega_m \mathcal{H}^2} \partial_i \partial_j \Phi^{(1)} - \frac{1}{3} \delta_{ij} \delta_T^{(1)}. \quad (2.88)$$

K_{ij} enters (2.86) via the square of the tidal operator i.e., $[K_{ij}]^2$. This is because the latter is a local observable which is of the same order in perturbations as $[\delta_T^{(1)}]^2$. Therefore, it is expected to hold similar relevance as the term in $b_2 [\delta_T^{(1)}]^2$. We can then generalize the LIMD model (2.86), to the local model of bias as,

$$\begin{aligned} \delta_g^{(2)} = & b_1 \delta_T^{(2)} + b_2 [\delta_T^{(1)}]^2 + (3 - b_e) \mathcal{H} v^{(2)} + [(b_e - 3) \mathcal{H}' + b_e' \mathcal{H} + (b_e - 3)^2 \mathcal{H}^2] [v^{(1)}]^2 \\ & - (b_e - 3) \mathcal{H} \nabla^{-2} \left[v^{(1)} \nabla^2 v^{(1)'} - v^{(1)'} \nabla^2 v^{(1)} - 6 \partial_i \Phi^{(1)} \partial^i v^{(1)} - 6 \Phi^{(1)} \nabla^2 v^{(1)} \right] \\ & + (b_e - 3) \mathcal{H} v^{(1)} v^{(1)'} + 2b_1 (3 - b_e) \mathcal{H} v^{(1)} \delta_T^{(1)} - 2v^{(1)} [b_1 \delta_T^{(1)'} + b_1' \delta_T^{(1)}] \\ & + b_{\text{Tidal}} [K_{ij}]^2, \end{aligned} \quad (2.89)$$

where b_{Tidal} is the tidal bias coefficient. The tidal field cannot enter the bias expansion at first-order because it is traceless ($\text{tr}[K_{ij}] = 0$) [64]. The simplest local bias model is when the Lagrangian tidal bias vanishes:

$$b_{\text{Tidal}} = \frac{2}{7} (b_1 - 1). \quad (2.90)$$

2.4 Second-order galaxy number counts (scalar modes)

At second-order we have many more terms. The metric is,

$$a^{-2} ds^2 = -[1 + 2\Phi^{(1)} + \Phi^{(2)}] d\eta^2 + [1 - 2\Phi^{(1)} - \Psi^{(2)}] dx^2, \quad (2.91)$$

and the peculiar velocity of the galaxies which we are assuming to be equal to the dark matter velocity on scales of interest are,

$$v^i = \partial^i \left[v^{(1)} + \frac{1}{2} v^{(2)} \right]. \quad (2.92)$$

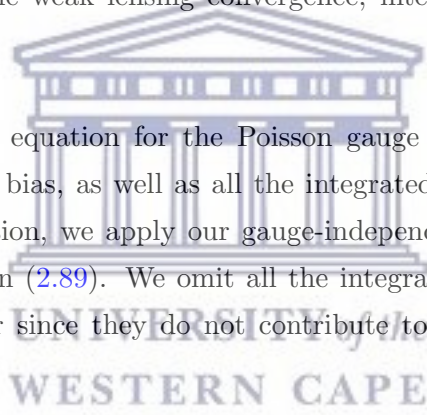
We have taken zero anisotropic stress at first-order, which implies $\Psi^{(1)} = \Phi^{(1)}$ in GR. The observed comoving coordinates of a galaxy are given by $\mathbf{x} = \bar{\chi}(z) \mathbf{n}$ [84]. The expression for $\Delta_g^{(2)}$ contains second-order generalizations of the dark matter, RSD, Doppler,

potentials and lensing terms, together with correlating terms which are quadratic in all the first-order terms. This can be shown as follows,

$$\begin{aligned}
\Delta_{gS}^{(2)}(z, \boldsymbol{x}) = & \underbrace{\Delta_m^{(2)} + \Delta_{\text{RSD}}^{(2)} + \Delta_{\text{Dop.}}^{(2)} + \Delta_{\text{pot.}}^{(2)} + \Delta_{\kappa}^{(2)}}_{\text{Second order dynamical terms}} \\
& + \underbrace{\Delta_{m \times m}^{(2)} + \Delta_{\text{RSD} \times \text{RSD}}^{(2)} + \Delta_{\text{Dop.} \times \text{Dop.}}^{(2)} + \Delta_{\text{pot.} \times \text{pot.}}^{(2)} + \Delta_{\kappa \times \kappa}^{(2)}}_{\text{Auto correlations between first order terms}} \\
& + \underbrace{\Delta_{m \times \text{RSD}}^{(2)} + \Delta_{m \times \text{Dop.}}^{(2)} + \Delta_{m \times \kappa}^{(2)} + \Delta_{m \times \text{pot.}}^{(2)} + \Delta_{\text{RSD} \times \text{Dop.}}^{(2)}}_{\text{Cross correlations between first order terms}} \\
& + \underbrace{\Delta_{\text{RSD} \times \kappa}^{(2)} + \Delta_{\text{RSD} \times \text{pot.}}^{(2)} + \Delta_{\text{Dop.} \times \kappa}^{(2)} + \Delta_{\text{Dop.} \times \text{pot.}}^{(2)} + \Delta_{\kappa \times \text{pot.}}^{(2)}}_{\text{Cross correlations between first order terms}}. \quad (2.93)
\end{aligned}$$

In the next chapter we are going to derive the galaxy bispectrum in Fourier space which is at fixed redshift, so that all the correlations are computed in the same redshift bin. For this purpose, we hereby neglect all the GR integrated contributions of $\Delta_g^{(1)}$ and $\Delta_g^{(2)}$. These include the weak lensing convergence, integrated Sachs-Wolfe and time-delay terms.

We can find a general equation for the Poisson gauge $\Delta_g^{(2)}$, including the evolution bias and magnification bias, as well as all the integrated and observer's terms in [49]. To this general expression, we apply our gauge-independent model of the galaxy bias at second-order given in (2.89). We omit all the integrated terms and also, the terms defined at the observer since they do not contribute to the galaxy bispectrum. The



result is as follows [49],

$$\begin{aligned}
\Delta_{gS}^{(2)}(z, \mathbf{x}) = & b_1 \delta_T^{(2)} + b_2 [\delta_T^{(1)}]^2 + \left[(b_e - 3)^2 \mathcal{H}^2 + b'_e \mathcal{H} + (b_e - 3) \mathcal{H}' \right] [v^{(1)}]^2 \\
& + (b_e - 3) \mathcal{H} v^{(1)} v^{(1)'} + 2b_1 (3 - b_e) \mathcal{H} v^{(1)} \delta_T^{(1)} - 2v^{(1)} \left[b_1 \delta_T^{(1)'} + b'_1 \delta_T^{(1)} \right] \\
& + (3 - b_e) \mathcal{H} \nabla^{-2} \left[v^{(1)} \nabla^2 v^{(1)'} - v^{(1)'} \nabla^2 v^{(1)} - 6 \partial_i \Phi^{(1)} \partial^i v^{(1)} - 6 \Phi^{(1)} \nabla^2 v^{(1)} \right] \\
& - \frac{1}{\mathcal{H}} \partial_{\parallel}^2 v^{(2)} + (3 - b_e) \mathcal{H} v^{(2)} + \left[b_e - 2\mathcal{Q} - \frac{2(1 - \mathcal{Q})}{\bar{\chi} \mathcal{H}} - \frac{\mathcal{H}'}{\mathcal{H}^2} \right] \left[\partial_{\parallel} v^{(2)} - \Phi^{(2)} \right] \\
& + b_{\text{Tidal}} [K_{ij}]^2 + 2(\mathcal{Q} - 1) \Psi^{(2)} + \Phi^{(2)} + \frac{1}{\mathcal{H}} \Psi^{(2)'} \\
& + \left[b_e - 2\mathcal{Q} - \frac{\mathcal{H}'}{\mathcal{H}^2} - (1 - \mathcal{Q}) \frac{2}{\bar{\chi} \mathcal{H}} \right] \left[3[\Phi^{(1)}]^2 - [\partial_{\parallel} v^{(1)}]^2 + \partial_{\perp i} v^{(1)} \partial_{\perp}^i v^{(1)} \right. \\
& \left. - 2 \partial_{\parallel} v^{(1)} \Phi^{(1)} - \frac{2}{\mathcal{H}} \left(\Phi^{(1)} - \partial_{\parallel} v^{(1)} \right) \left(\Phi^{(1)'} - \partial_{\parallel}^2 v^{(1)} \right) \right] + 2(2\mathcal{Q} - 1) \Phi^{(1)} \delta_g^{(1)} \\
& - \frac{2}{\mathcal{H}} \delta_g^{(1)} \partial_{\parallel}^2 v^{(1)} + \frac{2}{\mathcal{H}} \delta_g^{(1)} \Phi^{(1)'} + \left(4\mathcal{Q} - 5 + 4\mathcal{Q}^2 - 4 \frac{\partial \mathcal{Q}}{\partial \ln \bar{L}} \right) [\Phi^{(1)}]^2 \\
& + \frac{2}{\mathcal{H}} \left(2\mathcal{Q} + \frac{\mathcal{H}'}{\mathcal{H}^2} \right) \Phi^{(1)} \Phi^{(1)'} - \frac{2}{\mathcal{H}} \left(1 + 2\mathcal{Q} + \frac{\mathcal{H}'}{\mathcal{H}^2} \right) \Phi^{(1)} \partial_{\parallel}^2 v^{(1)} + \frac{2}{\mathcal{H}^2} [\Phi^{(1)'}]^2 \\
& + \frac{2}{\mathcal{H}^2} [\partial_{\parallel}^2 v^{(1)}]^2 + \frac{2}{\mathcal{H}^2} \partial_{\parallel} v^{(1)} \partial_{\parallel}^2 \Phi^{(1)} + \frac{4}{\mathcal{H}} \partial_{\parallel} v^{(1)} \partial_{\parallel} \Phi^{(1)} - \frac{2}{\mathcal{H}^2} \Phi^{(1)} \partial_{\parallel}^3 v^{(1)} \\
& + \frac{2}{\mathcal{H}^2} \Phi^{(1)} \frac{d\Phi^{(1)'}}{d\bar{\chi}} - \frac{2}{\mathcal{H}^2} \partial_{\parallel} v^{(1)} \frac{d\Phi^{(1)'}}{d\bar{\chi}} + \frac{2}{\mathcal{H}} \left(1 + \frac{\mathcal{H}'}{\mathcal{H}^2} \right) \partial_{\parallel} v^{(1)} \partial_{\parallel}^2 v^{(1)} \\
& + \frac{2}{\mathcal{H}} \left(1 - \frac{\mathcal{H}'}{\mathcal{H}^2} \right) \partial_{\parallel} v^{(1)} \Phi^{(1)'} - \frac{4}{\mathcal{H}^2} \partial_{\parallel}^2 v^{(1)} \Phi^{(1)'} + \frac{2}{\mathcal{H}} \partial_{\perp i} v^{(1)} \partial_{\perp}^i \Phi^{(1)} \\
& + \left(\frac{4}{\bar{\chi} \mathcal{H}} - 1 \right) \partial_{\perp i} v^{(1)} \partial_{\perp}^i v^{(1)} + \frac{2}{\mathcal{H}^2} \partial_{\parallel} v^{(1)} \partial_{\parallel}^3 v^{(1)} + \left\{ \left[4b_e \mathcal{Q} - 2b_e - 4\mathcal{Q} - 8\mathcal{Q}^2 \right. \right. \\
& \left. \left. + 8 \frac{\partial \mathcal{Q}}{\partial \ln \bar{L}} + 4 \frac{\partial \mathcal{Q}}{\partial \ln a} + 2 \frac{\mathcal{H}'}{\mathcal{H}^2} (1 - 2\mathcal{Q}) + \frac{4}{\bar{\chi} \mathcal{H}} \left(\mathcal{Q} - 1 + 2\mathcal{Q}^2 - 2 \frac{\partial \mathcal{Q}}{\partial \ln \bar{L}} \right) \right] \Phi^{(1)} \right. \\
& \left. + 2 \left[b_e - 2\mathcal{Q} - \frac{\mathcal{H}'}{\mathcal{H}^2} - \frac{2}{\bar{\chi} \mathcal{H}} (1 - \mathcal{Q}) \right] \delta_g^{(1)} - \frac{2}{\mathcal{H}} \frac{d\delta_g^{(1)}}{d\bar{\chi}} - \frac{2}{\mathcal{H}} \Phi^{(1)} \partial_{\parallel} \Phi^{(1)} \right. \\
& \left. + \frac{2}{\mathcal{H}} \left[2\mathcal{Q} - b_e + \frac{\mathcal{H}'}{\mathcal{H}^2} + \frac{2}{\bar{\chi} \mathcal{H}} (1 - \mathcal{Q}) \right] \partial_{\parallel}^2 v^{(1)} - \frac{2}{\mathcal{H}^2} \Phi^{(1)} \partial_{\parallel}^2 \Phi^{(1)} \right. \\
& \left. + \frac{2}{\mathcal{H}} \left[b_e - 2 - \frac{2}{\bar{\chi} \mathcal{H}} (1 - \mathcal{Q}) - \frac{\mathcal{H}'}{\mathcal{H}^2} \right] \Phi^{(1)'} - \frac{4}{\mathcal{H}} \mathcal{Q} \partial_{\parallel} \Phi \right\} \left[\partial_{\parallel} v^{(1)} - \Phi^{(1)} \right] \\
& + \left\{ b_e^2 - b_e + \frac{\partial b_e}{\partial \ln a} + 6\mathcal{Q} - 4\mathcal{Q} b_e + 4\mathcal{Q}^2 - 4 \frac{\partial \mathcal{Q}}{\partial \ln \bar{L}} - 4 \frac{\partial \mathcal{Q}}{\partial \ln a} + \frac{6}{\bar{\chi}} \frac{\mathcal{H}'}{\mathcal{H}^3} (1 - \mathcal{Q}) \right. \\
& \left. + (1 - 2b_e + 4\mathcal{Q}) \frac{\mathcal{H}'}{\mathcal{H}^2} - \frac{\mathcal{H}''}{\mathcal{H}^3} + 3 \frac{\mathcal{H}'^2}{\mathcal{H}^4} + \frac{2}{\bar{\chi}^2 \mathcal{H}^2} \left(1 - \mathcal{Q} + 2\mathcal{Q}^2 - 2 \frac{\partial \mathcal{Q}}{\partial \ln \bar{L}} \right) \right. \\
& \left. + \frac{2}{\bar{\chi} \mathcal{H}} \left[1 - 2b_e - \mathcal{Q} + 2b_e \mathcal{Q} - 4\mathcal{Q}^2 + 4 \frac{\partial \mathcal{Q}}{\partial \ln \bar{L}} + 2 \frac{\partial \mathcal{Q}}{\partial \ln a} \right] \right\} \left[\partial_{\parallel} v^{(1)} - \Phi^{(1)} \right]^2 \\
& - \frac{4}{\mathcal{H}} \partial_{\perp i} v^{(1)} \partial_{\perp}^i \partial_{\parallel} v^{(1)} + 4 \left[\left(1 - \frac{1}{\bar{\chi} \mathcal{H}} \right) \partial_{\parallel} v^{(1)} - \left(2 - \frac{1}{\bar{\chi} \mathcal{H}} \right) \Phi^{(1)} \right] \frac{\partial \delta_g^{(1)}}{\partial \ln \bar{L}}. \quad (2.94)
\end{aligned}$$

2.5 Second-order induced vector and tensor modes

The local vector and tensor perturbations at second-order, are generated by the second-order scalars [85, 86]. We start with (1.43) which is the most general metric for a flat FLRW Universe,

$$ds^2 = a^2 \left[- (1 + 2\Phi)d\eta^2 + (1 - 2\Psi)\gamma_{ij}dx^i dx^j + 2w_i^{(2)}dx^i d\eta + \frac{1}{2}h_{ij}^{(2)}dx^i dx^j \right], \quad (2.95)$$

where $w_i^{(2)}$ and $h_{ij}^{(2)}$ are the second-order vector and tensor perturbations respectively. We neglect the first-order vector and tensor modes because they are purely decaying modes and contribute negligibly to the second-order density perturbations [87–90]. The vector contributions to the second-order galaxy number count fluctuation is given by [49],

$$\Delta_{gV}^{(2)}(z, \mathbf{x}) = \left[b_e - 2\mathcal{Q} - \frac{2(1 - \mathcal{Q})}{\bar{\chi}\mathcal{H}} - \frac{\mathcal{H}'}{\mathcal{H}^2} \right] \hat{v}_{\parallel}^{(2)} - \frac{1}{\mathcal{H}} \partial_{\parallel} \hat{v}_{\parallel}^{(2)}, \quad (2.96)$$

where $\hat{v}_{\parallel}^{(2)} = n^i \hat{v}_i^{(2)}$ is the longitudinal component of the vector perturbations. In the Λ CDM model, $\hat{v}_i^{(2)} = -2\omega_i^{(2)}$ [90] and (2.96) becomes,

$$\Delta_{gV}^{(2)}(z, \mathbf{x}) = 2 \left[-b_e + 2\mathcal{Q} + \frac{2(1 - \mathcal{Q})}{\bar{\chi}\mathcal{H}} + \frac{\mathcal{H}'}{\mathcal{H}^2} + \frac{1}{\mathcal{H}} \partial_{\parallel} \right] \omega_{\parallel}^{(2)}(\mathbf{x}). \quad (2.97)$$

where $\omega_{\parallel}^{(2)} = n^i \omega_i^{(2)}$. For the tensors we have [49],

$$\Delta_{gT}^{(2)}(z, \mathbf{x}) = -\frac{1}{2}(1 - \mathcal{Q})h_{\parallel}^{(2)}(\mathbf{x}) - \frac{1}{2\mathcal{H}}h_{\parallel}^{(2)'}(\mathbf{x}), \quad (2.98)$$

where $h_{\parallel}^{(2)} = h_{ij}^{(2)}n^i n^j$. Therefore, the galaxy number count fluctuation at second-order can be written as,

$$\Delta_g^{(2)}(z, \mathbf{x}) = \Delta_{gS}^{(2)}(z, \mathbf{x}) + \Delta_{gV}^{(2)}(z, \mathbf{x}) + \Delta_{gT}^{(2)}(z, \mathbf{x}). \quad (2.99)$$

2.6 The Newtonian and GR parts of Δ_g

We start with (2.66) which shows the general expression for $\Delta_g^{(1)}$ in C-gauge. We transform to T-gauge by using (2.69) and neglect the integrated terms. We then split $\Delta_g^{(1)}$

into Newtonian (N) and GR parts as,

$$\Delta_{gN}^{(1)} = \underbrace{b_1 \delta_T^{(1)}}_{\text{DM term}} - \underbrace{\frac{1}{\mathcal{H}} \partial_{\parallel}^2 v^{(1)}}_{\text{Redshift space distortion}}, \quad (2.100)$$

$$\begin{aligned} \Delta_{gGR}^{(1)} = & \underbrace{\mathcal{H}(b_e - 3)v^{(1)} + \left[b_e - \frac{\mathcal{H}'}{\mathcal{H}^2} - 2\mathcal{Q} - \frac{2(1-\mathcal{Q})}{\bar{\chi}\mathcal{H}} \right] \partial_{\parallel} v^{(1)}}_{\text{Doppler}} \\ & - \underbrace{\left[b_e - \frac{\mathcal{H}'}{\mathcal{H}^2} + 2\mathcal{Q} - \frac{2(1-\mathcal{Q})}{\bar{\chi}\mathcal{H}} \right] \Phi^{(1)} + (2\mathcal{Q} - 1)\Phi^{(1)} + \frac{1}{\mathcal{H}} \Phi^{(1)'}}_{\text{Sachs-Wolfe}}, \end{aligned} \quad (2.101)$$

where we have imposed $\Phi^{(1)} = \Psi^{(1)}$. The Newtonian part is the T-gauge density contrast and the Kaiser RSD term. The remaining terms i.e., Doppler and Sachs-Wolfe, are the GR parts. For $\Delta_{gS}^{(2)}$ given in (2.94), the Newtonian part constitutes the density contrast, tidal term, Kaiser RSD term and their couplings. The dark matter density contrast $\delta_T^{(2)}$ has a GR part which is of the order [83],

$$\delta_{TGR}^{(2)} \sim [\nabla\Phi]^2 + \Phi\nabla^2\Phi. \quad (2.102)$$

For a fixed physical scale R corresponding to fixed halo-mass formation, $\delta_T^{(2)}$ is smoothed and if we assume Gaussianity for the primordial metric perturbation, then the small scale density contrast is not affected by the long-wavelength mode $\delta_{TGR}^{(2)}$. A local observer at the galaxy sees no effect of the long mode and therefore, $\delta_{TGR}^{(2)}$ does not enter the bias relation of (2.89) [91–93],

$$\delta_{gT}^{(2)} = b_1 \delta_T^{(2)} + b_2 [\delta_T^{(1)}]^2 + b_{\text{Tidal}} [K_{ij}]^2 + \text{many other terms to ensure gauge-independence}. \quad (2.103)$$

Therefore we may write,

$$\begin{aligned} \Delta_{gN}^{(2)} = & b_1 \delta_T^{(2)} + b_2 [\delta_T^{(1)}]^2 - \frac{1}{\mathcal{H}} \partial_{\parallel}^2 v^{(2)} - 2 \frac{b_1}{\mathcal{H}} \left[\delta_T^{(1)} \partial_{\parallel}^2 v^{(1)} + \partial_{\parallel} v^{(1)} \partial_{\parallel} \delta_T^{(1)} \right] \\ & + \frac{2}{\mathcal{H}^2} \left[[\partial_{\parallel}^2 v^{(1)}]^2 + \partial_{\parallel} v^{(1)} \partial_{\parallel}^3 v^{(1)} \right] + b_{\text{Tidal}} [K_{ij}]^2. \end{aligned} \quad (2.104)$$

The remaining terms of (2.94), (2.97) and (2.98) constitute the GR part,

$$\begin{aligned}
\Delta_{g\text{GR}}^{(2)} = & \mathcal{H}(3 - b_e)v^{(2)} + \left[(9 - 6b_e + b_e^2)\mathcal{H}^2 + b_e'\mathcal{H} + (b_e - 3)\mathcal{H}' \right] [v^{(1)}]^2 \\
& - (b_e - 3)\mathcal{H}\nabla^{-2} \left[v^{(1)}\nabla^2 v^{(1)'} - v^{(1)'}\nabla^2 v^{(1)} - 6\partial_i\Phi^{(1)}\partial^i v^{(1)} - 6\Phi^{(1)}\nabla^2 v^{(1)} \right] \\
& + 2(3 - b_e)b_1\mathcal{H}v^{(1)}\delta_{\text{T}}^{(1)} - 2v^{(1)} \left(b_1'\delta_{\text{T}}^{(1)} + b_1\delta_{\text{T}}^{(1)'} \right) + (b_e - 3)\mathcal{H}v^{(1)}v^{(1)'} \\
& + \left[b_e - 2\mathcal{Q} - \frac{2(1 - \mathcal{Q})}{\bar{\chi}\mathcal{H}} - \frac{\mathcal{H}'}{\mathcal{H}^2} \right] \partial_{\parallel}v^{(2)} + \left[1 - b_e + 2\mathcal{Q} + \frac{2(1 - \mathcal{Q})}{\bar{\chi}\mathcal{H}} + \frac{\mathcal{H}'}{\mathcal{H}^2} \right] \Phi^{(2)} \\
& - 2(1 - \mathcal{Q})\Psi^{(2)} + \frac{1}{\mathcal{H}}\Psi^{(2)'} + \frac{2}{\mathcal{H}} \left[b_1\delta_{\text{T}}^{(1)'}\partial_{\parallel}v^{(1)} + (f - 2 + 2\mathcal{Q})\Phi^{(1)}\partial_{\parallel}\Phi^{(1)} \right. \\
& + (2 - f - 2\mathcal{Q})\partial_{\parallel}v^{(1)}\partial_{\parallel}\Phi^{(1)} - b_1\Phi^{(1)}\delta_{\text{T}}^{(1)'} + b_1\Phi^{(1)}\partial_{\parallel}\delta_{\text{T}}^{(1)} - 2\partial_i v^{(1)}\partial_{\parallel}\partial^i v^{(1)} \\
& \left. + \partial_i v^{(1)}\partial^i\Phi^{(1)} \right] + \frac{2}{\mathcal{H}^2} \left[\partial_{\parallel}v^{(1)}\partial_{\parallel}^2\Phi^{(1)} - \Phi^{(1)}\partial_{\parallel}^2\Phi^{(1)} - \Phi^{(1)}\partial_{\parallel}^3v^{(1)} \right] \\
& + 2 \left[b_1 \left(b_e - 2\mathcal{Q} - \frac{2(1 - \mathcal{Q})}{\bar{\chi}\mathcal{H}} - \frac{\mathcal{H}'}{\mathcal{H}^2} \right) + \frac{b_1'}{\mathcal{H}} + 2 \left(1 - \frac{1}{\bar{\chi}\mathcal{H}} \right) \frac{\partial b_1}{\partial \ln \bar{L}} \right] \delta_{\text{T}}^{(1)}\partial_{\parallel}v^{(1)} \\
& + \frac{2}{\mathcal{H}} \left[3 - 2b_e + 4\mathcal{Q} + \frac{4(1 - \mathcal{Q})}{\mathcal{H}\bar{\chi}} + \frac{3\mathcal{H}'}{\mathcal{H}} \right] \partial_{\parallel}v^{(1)}\partial_{\parallel}^2v^{(1)} + 2 \left[b_1 \left(f - 2 - b_e + 4\mathcal{Q} \right. \right. \\
& \left. \left. + \frac{2(1 - \mathcal{Q})}{\bar{\chi}\mathcal{H}} + \frac{\mathcal{H}'}{\mathcal{H}^2} \right) - \frac{b_1'}{\mathcal{H}} - 2 \left(2 - \frac{1}{\bar{\chi}\mathcal{H}} \right) \frac{\partial b_1}{\partial \ln \bar{L}} \right] \Phi^{(1)}\delta_{\text{T}}^{(1)} - 2(3 - b_e)v^{(1)}\partial_{\parallel}^2v^{(1)} \\
& + \left[b_e - 1 - 2\mathcal{Q} - \frac{2(1 - \mathcal{Q})}{\bar{\chi}\mathcal{H}} - \frac{\mathcal{H}'}{\mathcal{H}^2} \right] \partial_i v^{(1)}\partial^i v^{(1)} + \frac{2}{\mathcal{H}} \left[1 - 2f + 2b_e - 6\mathcal{Q} \right. \\
& \left. - \frac{4(1 - \mathcal{Q})}{\bar{\chi}\mathcal{H}} - \frac{3\mathcal{H}'}{\mathcal{H}^2} \right] \Phi^{(1)}\partial_{\parallel}^2v^{(1)} + \mathcal{A}_1[\Phi^{(1)}]^2 + \mathcal{A}_2v^{(1)}\partial_{\parallel}v^{(1)} + \mathcal{A}_3\Phi^{(1)}v^{(1)} \\
& + \mathcal{A}_4\Phi^{(1)}\partial_{\parallel}v^{(1)} + \mathcal{A}_5[\partial_{\parallel}v^{(1)}]^2 + 2 \left[-b_e + 2\mathcal{Q} + \frac{2(1 - \mathcal{Q})}{\bar{\chi}\mathcal{H}} + \frac{\mathcal{H}'}{\mathcal{H}^2} + \frac{1}{\mathcal{H}}\partial_{\parallel} \right] \omega_{\parallel}^{(2)} \\
& - \frac{1}{2}(1 - \mathcal{Q})h_{\parallel}^{(2)} - \frac{1}{2\mathcal{H}}h_{\parallel}^{(2)}, \tag{2.105}
\end{aligned}$$

where the background coefficients are,

$$\begin{aligned}
\mathcal{A}_1 = & -3 + 2f \left(2 - 2b_e + 4\mathcal{Q} + \frac{4(1 - \mathcal{Q})}{\bar{\chi}\mathcal{H}} + \frac{2\mathcal{H}'}{\mathcal{H}^2} \right) - \frac{2f'}{\mathcal{H}} + b_e^2 + 6b_e - 8b_e\mathcal{Q} + 4\mathcal{Q} \\
& + 16\mathcal{Q}^2 - 16\frac{\partial\mathcal{Q}}{\partial \ln \bar{L}} - 8\frac{\mathcal{Q}'}{\mathcal{H}} + \frac{b_e'}{\mathcal{H}} + \frac{2}{\bar{\chi}^2\mathcal{H}^2} \left(1 - \mathcal{Q} + 2\mathcal{Q}^2 - 2\frac{\partial\mathcal{Q}}{\partial \ln \bar{L}} \right) \\
& - \frac{2}{\bar{\chi}\mathcal{H}} \left[4 + 2b_e - 2b_e\mathcal{Q} - 4\mathcal{Q} + 8\mathcal{Q}^2 - \frac{3\mathcal{H}'}{\mathcal{H}^2}(1 - \mathcal{Q}) - 8\frac{\partial\mathcal{Q}}{\partial \ln \bar{L}} - 2\frac{\mathcal{Q}'}{\mathcal{H}} \right] \\
& + \frac{\mathcal{H}'}{\mathcal{H}^2} \left(-8 - 2b_e + 8\mathcal{Q} + \frac{3\mathcal{H}'}{\mathcal{H}^2} \right) - \frac{\mathcal{H}''}{\mathcal{H}^3}, \tag{2.106}
\end{aligned}$$

$$\begin{aligned}
\mathcal{A}_2 = & 2\mathcal{H} \left[-3 + 4b_e + \frac{2b_e(1 - \mathcal{Q})}{\bar{\chi}\mathcal{H}} - b_e^2 + 2b_e\mathcal{Q} - 6\mathcal{Q} - \frac{b_e'}{\mathcal{H}} - \frac{6(1 - \mathcal{Q})}{\bar{\chi}\mathcal{H}} \right. \\
& \left. + 2 \left(1 - \frac{1}{\bar{\chi}\mathcal{H}} \right) \frac{\mathcal{Q}'}{\mathcal{H}} \right], \tag{2.107}
\end{aligned}$$

$$\begin{aligned} \mathcal{A}_3 = & 2\mathcal{H} \left[-3 + f(3 - b_e) - 3b_e - 2b_e \frac{(1 - \mathcal{Q})}{\bar{\chi}\mathcal{H}} + \frac{b'_e}{\mathcal{H}} + b_e^2 - 4b_e\mathcal{Q} + 12\mathcal{Q} + \frac{6(1 - \mathcal{Q})}{\bar{\chi}\mathcal{H}} \right. \\ & \left. - 2 \left(2 - \frac{1}{\bar{\chi}\mathcal{H}} \right) \frac{\mathcal{Q}'}{\mathcal{H}} \right], \end{aligned} \quad (2.108)$$

$$\begin{aligned} \mathcal{A}_4 = & 4 + 2f \left[-3 + f + 2b_e - 3\mathcal{Q} - \frac{4(1 - \mathcal{Q})}{\bar{\chi}\mathcal{H}} - \frac{2\mathcal{H}'}{\mathcal{H}^2} \right] + \frac{2f'}{\mathcal{H}} - 6b_e - 2b_e^2 + 12b_e\mathcal{Q} - 8\mathcal{Q} \\ & - 16\mathcal{Q}^2 + 16 \frac{\partial \mathcal{Q}}{\partial \ln \bar{L}} + 12 \frac{\mathcal{Q}'}{\mathcal{H}} - 2 \frac{b'_e}{\mathcal{H}} - \frac{4}{\bar{\chi}^2 \mathcal{H}^2} \left(1 - \mathcal{Q} + 2\mathcal{Q}^2 - 2 \frac{\partial \mathcal{Q}}{\partial \ln \bar{L}} \right) \\ & - \frac{4}{\bar{\chi}\mathcal{H}} \left(-1 - 2b_e + 2b_e\mathcal{Q} + \mathcal{Q} - 6\mathcal{Q}^2 + \frac{3\mathcal{H}'}{\mathcal{H}^2} (1 - \mathcal{Q}) + 6 \frac{\partial \mathcal{Q}}{\partial \ln \bar{L}} + 2 \frac{\mathcal{Q}'}{\mathcal{H}} \right) \\ & + \frac{2\mathcal{H}'}{\mathcal{H}^2} \left(3 + 2b_e - 6\mathcal{Q} - \frac{3\mathcal{H}'}{\mathcal{H}^2} \right) + \frac{2\mathcal{H}''}{\mathcal{H}^3}, \end{aligned} \quad (2.109)$$

$$\begin{aligned} \mathcal{A}_5 = & -4 - b_e + b_e^2 - 4b_e\mathcal{Q} + 6\mathcal{Q} + 4\mathcal{Q}^2 - 4 \frac{\partial \mathcal{Q}}{\partial \ln \bar{L}} - 4 \frac{\mathcal{Q}'}{\mathcal{H}} + \frac{b'_e}{\mathcal{H}} \\ & + \frac{2}{\bar{\chi}^2 \mathcal{H}^2} \left(1 - \mathcal{Q} + 2\mathcal{Q}^2 - 2 \frac{\partial \mathcal{Q}}{\partial \ln \bar{L}} \right) \\ & + \frac{2}{\bar{\chi}\mathcal{H}} \left[3 - 2b_e + 2b_e\mathcal{Q} - 3\mathcal{Q} - 4\mathcal{Q}^2 + \frac{3\mathcal{H}'}{\mathcal{H}^2} (1 - \mathcal{Q}) + 4 \frac{\partial \mathcal{Q}}{\partial \ln \bar{L}} + 2 \frac{\mathcal{Q}'}{\mathcal{H}} \right] \\ & + \frac{\mathcal{H}'}{\mathcal{H}^2} \left(3 - 2b_e + 4\mathcal{Q} + \frac{3\mathcal{H}'}{\mathcal{H}^2} \right) - \frac{\mathcal{H}''}{\mathcal{H}^3}. \end{aligned} \quad (2.110)$$

In deriving (2.104)-(2.110), we have done the following:

- We have eliminated $d/d\bar{\chi}$ and $\partial_{\perp i}$ by using [49, 72],

$$\frac{d}{d\bar{\chi}} = -\frac{d}{d\eta} = -\partial_{\eta} + \partial_{\parallel} \quad \text{and} \quad \partial_{\perp i} = \partial_i - n_i \partial_{\parallel}, \quad (2.111)$$

where the first equation is the total derivative along the past lightcone and second equation is the transverse derivative. ∂_{\parallel} is the radial derivative and is defined as [49, 72],

$$\partial_{\parallel} = n^i \partial_i. \quad (2.112)$$

- From the commutator relation $[\partial_{\perp i}, \partial_{\parallel}] = \bar{\chi}^{-1} \partial_{\perp i}$ we have shown that,

$$\partial_{\perp i} v^{(1)} \partial_{\perp}^i \partial_{\parallel} v^{(1)} = \partial_i v^{(1)} \partial_{\parallel} \partial^i v^{(1)} - \partial_{\parallel} v^{(1)} \partial_{\parallel}^2 v^{(1)} + \frac{1}{\bar{\chi}} \left[\partial_i v^{(1)} \partial^i v^{(1)} - [\partial_{\parallel} v^{(1)}]^2 \right]. \quad (2.113)$$

- We have expressed the Poisson gauge galaxy overdensity, $\delta_g^{(1)}$ in terms of the T-gauge dark matter overdensity, $\delta_{\text{T}}^{(1)}$ and the velocity potential, $v^{(1)}$ by using (2.69), (2.70) and (2.71).
- Using (2.68)-(2.71), we have re-written the term $\partial \delta_g^{(1)} / \partial \ln \bar{L}$ as,

$$\frac{\partial \delta_g^{(1)}}{\partial \ln \bar{L}} = \frac{\partial b_1}{\partial \ln \bar{L}} \delta_{\text{T}}^{(1)} - \frac{\partial b_e}{\partial \ln \bar{L}} \mathcal{H} v^{(1)}. \quad (2.114)$$

When we use (2.24), (2.63) and $\partial/\partial \ln a = \mathcal{H}^{-1}\partial/\partial \eta$, we can further simplify (2.114) to,

$$\frac{\partial \delta_g^{(1)}}{\partial \ln \bar{L}} = \frac{\partial b_1}{\partial \ln \bar{L}} \delta_T^{(1)} + \mathcal{Q}' v^{(1)}. \quad (2.115)$$



UNIVERSITY *of the*
WESTERN CAPE

Chapter 3

The Fourier galaxy bispectrum

3.1 Fourier space

We only consider correlations at the same observed redshift z . Then the metric potentials (Φ, Ψ) and velocity potential, v depend on the spatial coordinates,

$$\begin{aligned} \mathbf{x} &= \bar{\chi} \mathbf{n} + \mathbf{x}_0 \\ &= [\eta_0 - \eta(z)] \mathbf{n} + \mathbf{x}_0, \end{aligned} \quad (3.1)$$

and can be computed in Fourier space at fixed $\eta(z)$. The position of the observer is defined above as \mathbf{x}_0 . We transform from the configuration space i.e., \mathbf{x} -space, to Fourier space which is the \mathbf{k} -space as follows,

$$f(\mathbf{x}) = \int \frac{d^3 k}{(2\pi)^3} e^{i\mathbf{k}\cdot\mathbf{x}} f(\mathbf{k}), \quad (3.2)$$

where we suppress the redshift dependence. The inverse Fourier transform is then,

$$\begin{aligned} f(\mathbf{k}) &= \int d^3 x e^{-i\mathbf{k}\cdot\mathbf{x}} f(\mathbf{x}) \\ &= \int d^3 x \int \frac{d^3 k'}{(2\pi)^3} e^{-i(\mathbf{k}-\mathbf{k}')\cdot\mathbf{x}} f(\mathbf{k}') \\ &= \int d^3 k' \delta^D(\mathbf{k} - \mathbf{k}') f(\mathbf{k}'), \end{aligned} \quad (3.3)$$

where $\delta^D(\mathbf{k} - \mathbf{k}')$ is the Dirac-delta function defined as,

$$(2\pi)^3 \delta^D(\mathbf{k} - \mathbf{k}') = \int d^3 x e^{-i(\mathbf{k}-\mathbf{k}')\cdot\mathbf{x}}. \quad (3.4)$$

For the case of the radial derivative we have,

$$\partial_{\parallel} f(\mathbf{x}) = \int \frac{d^3k}{(2\pi)^3} \partial_{\parallel} e^{i\mathbf{k}\cdot\mathbf{x}} f(\mathbf{k}) . \quad (3.5)$$

We can simplify (3.5) as follows,

$$\begin{aligned} \int \frac{d^3k}{(2\pi)^3} \partial_{\parallel} e^{i\mathbf{k}\cdot\mathbf{x}} f(\mathbf{k}) &= \int \frac{d^3k}{(2\pi)^3} \partial_{\parallel} e^{i[(k\hat{\mathbf{k}})\cdot(\bar{\chi}\hat{\mathbf{n}})]} f(\mathbf{k}) \\ &= \int \frac{d^3k}{(2\pi)^3} \partial_{\parallel} e^{ik\bar{\chi}\mu} f(\mathbf{k}) , \end{aligned} \quad (3.6)$$

where $\mu = \hat{\mathbf{k}} \cdot \hat{\mathbf{n}}$. The above leads to,

$$\int \frac{d^3k}{(2\pi)^3} (ik\mu) e^{ik\bar{\chi}\mu} f(\mathbf{k}) , \quad \text{i.e.,} \quad \partial_{\parallel} = \frac{\partial}{\partial \bar{\chi}} \rightarrow ik\mu . \quad (3.7)$$

Hence, we find that $\partial_{\parallel}^2 \rightarrow -k^2\mu^2$ and $\partial_{\parallel}^3 \rightarrow -ik^3\mu^3$. Lastly, the Fourier transform of a product $h(\mathbf{x}) = f(\mathbf{x})g(\mathbf{x})$ is a convolution,

$$\begin{aligned} h(\mathbf{k}) &= f(\mathbf{k}) \otimes g(\mathbf{k}) \\ &= \int \frac{d^3k_1}{(2\pi)^3} \int d^3k_2 f(\mathbf{k}_1) g(\mathbf{k}_2) \delta^D(\mathbf{k}_1 + \mathbf{k}_2 - \mathbf{k}) . \end{aligned} \quad (3.8)$$

3.2 The galaxy number count fluctuation in Fourier space

3.2.1 Fourier transform of the first-order terms

We express all the perturbed variables $\Phi^{(1)}$ and $v^{(1)}$ in terms of the T-gauge dark matter overdensity $\delta_{\text{T}}^{(1)}$. We start with the first-order Poisson equation [72, 94, 95],

$$\nabla^2 \Phi^{(1)}(z, \mathbf{x}) = \frac{3}{2} \Omega_m \mathcal{H}^2 \delta_{\text{T}}^{(1)}(z, \mathbf{x}) . \quad (3.9)$$

In Fourier space, $\nabla^2 \rightarrow -k^2$ and therefore we have,

$$\Phi^{(1)}(\mathbf{k}) = -\frac{3}{2} \Omega_m \frac{\mathcal{H}^2}{k^2} \delta_{\text{T}}^{(1)}(\mathbf{k}) . \quad (3.10)$$

For the velocity potential we use (2.82) which is the first-order continuity equation,

$$\delta_{\text{T}}^{(1)'}(z, \mathbf{x}) = -\nabla^2 v^{(1)}(z, \mathbf{x}) , \quad (3.11)$$

and we can show that,

$$\delta_{\text{T}}^{(1)'}(z, \mathbf{x}) = \mathcal{H} f \delta_{\text{T}}^{(1)}(z, \mathbf{x}) , \quad (3.12)$$

where $f = d \ln D / d \ln a$ is the matter growth rate and is given by the logarithmic time derivative of the matter growth factor D . In Λ CDM model, D and f obey (see (1.104) and (1.106) in Chapter 1),

$$D' = \mathcal{H}fD \quad \text{and} \quad \frac{f'}{\mathcal{H}} = \frac{1}{2}(3\Omega_m - 4)f - f^2 + \frac{3}{2}\Omega_m. \quad (3.13)$$

Therefore, the Fourier version of (3.11) is,

$$\mathcal{H}v^{(1)}(\mathbf{k}) = f \frac{\mathcal{H}^2}{k^2} \delta_{\text{T}}^{(1)}(\mathbf{k}). \quad (3.14)$$

Then, by using (3.10) and (3.14) in,

$$\Delta_g^{(1)}(z, \mathbf{x}) = \underbrace{\Delta_{g\text{N}}^{(1)}(z, \mathbf{x})}_{\text{Newtonian}} + \underbrace{\Delta_{g\text{GR}}^{(1)}(z, \mathbf{x})}_{\text{GR effects}}, \quad (3.15)$$

where $\Delta_{g\text{N}}^{(1)}$ and $\Delta_{g\text{GR}}^{(1)}$ are given in (2.100) and (2.101) respectively, we obtain the Fourier transform as follows,

$$\Delta_g^{(1)}(\mathbf{k}) = \mathcal{K}^{(1)}(\mathbf{k}) \delta_{\text{T}}^{(1)}(\mathbf{k}), \quad (3.16)$$

where $\mathcal{K}^{(1)} = \mathcal{K}_{\text{N}}^{(1)} + \mathcal{K}_{\text{GR}}^{(1)}$ is the first-order kernel. The Newtonian part is [96],

$$\mathcal{K}_{\text{N}}^{(1)}(\mathbf{k}) = b_1 + f\mu^2, \quad (3.17)$$

and the GR part is [72, 96],

$$\mathcal{K}_{\text{GR}}^{(1)}(\mathbf{k}) = i \frac{\mu}{k} \gamma_1 + \frac{\gamma_2}{k^2}, \quad (3.18)$$

where γ_1 and γ_2 are functions of redshift given by [72, 96, 97],

$$\frac{\gamma_1}{\mathcal{H}} = f \left[b_e - 2\mathcal{Q} - \frac{2(1-\mathcal{Q})}{\bar{\chi}\mathcal{H}} - \frac{\mathcal{H}'}{\mathcal{H}^2} \right], \quad (3.19)$$

$$\frac{\gamma_2}{\mathcal{H}^2} = f(3 - b_e) + \frac{3}{2}\Omega_m \left[2 + b_e - f - 4\mathcal{Q} - 2 \frac{(1-\mathcal{Q})}{\bar{\chi}\mathcal{H}} - \frac{\mathcal{H}'}{\mathcal{H}^2} \right]. \quad (3.20)$$

3.2.2 Fourier transform of the second-order terms

3.2.2.1 Scalars

We begin with the intrinsic second-order scalars $\delta_{\text{T}}^{(2)}$, $v^{(2)}$, $\Phi^{(2)}$ and $\Psi^{(2)}$. They can be split into Newtonian (N) and GR parts. Their Newtonian expressions are [63],

$$\delta_{\text{T}\text{N}}^{(2)}(\mathbf{k}_3) = \int d(\mathbf{k}_1, \mathbf{k}_2, \mathbf{k}_3) F_2(\mathbf{k}_1, \mathbf{k}_2), \quad \Phi_{\text{N}}^{(2)}(\mathbf{k}_3) = -\frac{3}{2}\Omega_m \frac{\mathcal{H}^2}{k_3^2} \delta_{\text{T}\text{N}}^{(2)}(\mathbf{k}_3), \quad (3.21)$$

$$v_{\text{N}}^{(2)}(\mathbf{k}_3) = f \frac{\mathcal{H}}{k_3^2} \int d(\mathbf{k}_1, \mathbf{k}_2, \mathbf{k}_3) G_2(\mathbf{k}_1, \mathbf{k}_2), \quad \Psi_{\text{N}}^{(2)}(\mathbf{k}_3) = \Phi_{\text{N}}^{(2)}(\mathbf{k}_3), \quad (3.22)$$

where we define,

$$\int d(\mathbf{k}_1, \mathbf{k}_2, \mathbf{k}_3) \equiv \int \frac{d^3 k_1}{(2\pi)^3} \int d^3 k_2 \delta_{\text{T}}^{(1)}(\mathbf{k}_1) \delta_{\text{T}}^{(1)}(\mathbf{k}_2) \delta^{\text{D}}(\mathbf{k}_1 + \mathbf{k}_2 - \mathbf{k}_3). \quad (3.23)$$

The second-order kernels for the dark matter (F_2) and velocity (G_2) perturbations in T-gauge are given by [83],

$$F_2(\mathbf{k}_1, \mathbf{k}_2) = 1 + \frac{F}{D^2} + \frac{\mathbf{k}_1 \cdot \mathbf{k}_2}{k_1 k_2} \left(\frac{k_1}{k_2} + \frac{k_2}{k_1} \right) + \left(1 - \frac{F}{D^2} \right) \left(\frac{\mathbf{k}_1 \cdot \mathbf{k}_2}{k_1 k_2} \right)^2, \quad (3.24)$$

$$G_2(\mathbf{k}_1, \mathbf{k}_2) = \frac{F'}{DD'} + \frac{\mathbf{k}_1 \cdot \mathbf{k}_2}{k_1 k_2} \left(\frac{k_1}{k_2} + \frac{k_2}{k_1} \right) + \left(2 - \frac{F'}{DD'} \right) \left(\frac{\mathbf{k}_1 \cdot \mathbf{k}_2}{k_1 k_2} \right)^2. \quad (3.25)$$

F is the second-order growth factor and satisfies the growing mode solution of [83],

$$F'' + \mathcal{H}F' - \frac{1}{\alpha a} F = \frac{1}{\alpha a} D^2, \quad \text{with} \quad \alpha \equiv \frac{2}{3H_0^2 \Omega_{m0}} = \frac{2}{3\Omega_m \mathcal{H}^2 a}. \quad (3.26)$$

In an Einstein-de Sitter (EDS) background, $F = 3D^2/7$ which is a very good approximation in Λ CDM [98]. Then (3.24) and (3.25) becomes,

$$F_2(\mathbf{k}_1, \mathbf{k}_2) = \frac{10}{7} + \frac{\mathbf{k}_1 \cdot \mathbf{k}_2}{k_1 k_2} \left(\frac{k_1}{k_2} + \frac{k_2}{k_1} \right) + \frac{4}{7} \left(\frac{\mathbf{k}_1 \cdot \mathbf{k}_2}{k_1 k_2} \right)^2, \quad (3.27)$$

$$G_2(\mathbf{k}_1, \mathbf{k}_2) = \frac{6}{7} + \frac{\mathbf{k}_1 \cdot \mathbf{k}_2}{k_1 k_2} \left(\frac{k_1}{k_2} + \frac{k_2}{k_1} \right) + \frac{8}{7} \left(\frac{\mathbf{k}_1 \cdot \mathbf{k}_2}{k_1 k_2} \right)^2. \quad (3.28)$$

For the GR parts, the real space equations in the Poisson gauge are [83],

$$\delta_{\text{TGR}}^{(2)}(\mathbf{x}) = \frac{20}{3}\alpha D g_{\text{in}} \left[\left(\frac{3}{4} - a_{\text{NL}} \right) [\nabla\varphi_0(\mathbf{x})]^2 + (2 - a_{\text{NL}})\varphi_0(\mathbf{x})\nabla^2\varphi_0(\mathbf{x}) \right], \quad (3.29)$$

$$v_{\text{GR}}^{(2)}(\mathbf{x}) = \alpha D' \left[\left(-\frac{4}{3}g + \frac{5}{3}g_{\text{in}}(2a_{\text{NL}} - 1) - \alpha\mathcal{H}D' \right) \varphi_0^2(\mathbf{x}) - 12\Theta_0(\mathbf{x}) \right], \quad (3.30)$$

$$\Phi_{\text{GR}}^{(2)}(\mathbf{x}) = \left(3g^2 + \frac{5}{3}gg_{\text{in}}(1 - 2a_{\text{NL}}) + \frac{\alpha D'^2}{a} \right) \varphi_0^2(\mathbf{x}) + 12 \left(2g^2 - \frac{5}{3}gg_{\text{in}} + \frac{\alpha D'^2}{a} \right) \Theta_0(\mathbf{x}), \quad (3.31)$$

$$\Psi_{\text{GR}}^{(2)}(\mathbf{x}) = \left(-g^2 + \frac{5}{3}gg_{\text{in}}(1 - 2a_{\text{NL}}) + \frac{\alpha D'^2}{a} \right) \varphi_0^2(\mathbf{x}) + 12 \left(g^2 - \frac{5}{3}gg_{\text{in}} \right) \Theta_0(\mathbf{x}), \quad (3.32)$$

where,

$$\Theta_0(\mathbf{x}) = \frac{1}{2}\nabla^{-2} \left[\frac{1}{3}\varphi_0^l\varphi_{0,l} - \nabla^{-2} \left(\varphi_0^l\varphi_0^m \right)_{,lm} \right], \quad (3.33)$$

and,

$$\Psi^{(1)} = \Phi^{(1)} = g\varphi_0, \quad g = \frac{D}{a}, \quad \delta_{\text{T}}^{(1)} = \alpha D \nabla^2 \varphi_0, \quad a_{\text{NL}} = 1 + \frac{3}{5}f_{\text{NL}}, \quad \frac{g_{\text{in}}}{g} = \frac{1}{5} \left(3 + \frac{2f}{\Omega_m} \right). \quad (3.34)$$

f_{NL} is the non-Gaussian parameter, g_{in} is the initial value of the growth factor in the matter-dominated era and “0” denotes redshift $z = 0$ where $a_0 = D_0 = g_0 = 1$. We now simplify (3.29)-(3.32) by using (3.34) and obtain,

$$\mathcal{H}^2 \delta_{\text{TGR}}^{(2)}(\mathbf{x}) = \frac{2g^2}{3\Omega_m} \left\{ \left[1 + \frac{2f}{3\Omega_m} + \frac{12}{5}f_{\text{NL}} \left(1 + \frac{2f}{3\Omega_m} \right) \right] [\nabla\varphi_0(\mathbf{x})]^2 - 12 \left[1 + \frac{2f}{3\Omega_m} - \frac{3}{5}f_{\text{NL}} \left(1 + \frac{2f}{3\Omega_m} \right) \right] \varphi_0(\mathbf{x})\nabla^2\varphi_0(\mathbf{x}) \right\}, \quad (3.35)$$

$$\mathcal{H}v_{\text{GR}}^{(2)}(\mathbf{x}) = -\frac{2g^2f}{3\Omega_m} \left\{ \left[3 - \frac{6}{5}f_{\text{NL}} \left(1 + \frac{2f}{3\Omega_m} \right) \right] \varphi_0^2(\mathbf{x}) + 12\Theta_0(\mathbf{x}) \right\}, \quad (3.36)$$

$$\Phi_{\text{GR}}^{(2)}(\mathbf{x}) = g^2 \left[2 - \frac{2f}{3\Omega_m} + \frac{2f^2}{3\Omega_m} - \frac{6}{5}f_{\text{NL}} \left(1 + \frac{2f}{3\Omega_m} \right) \right] \varphi_0^2(\mathbf{x}) + 12g^2 \left[1 - \frac{2f}{3\Omega_m} + \frac{2f^2}{3\Omega_m} \right] \Theta_0(\mathbf{x}), \quad (3.37)$$

$$\Psi_{\text{GR}}^{(2)}(\mathbf{x}) = -2g^2 \left[1 + \frac{f}{3\Omega_m} - \frac{f^2}{3\Omega_m} + \frac{3}{5}f_{\text{NL}} \left(1 + \frac{2f}{3\Omega_m} \right) \right] \varphi_0^2(\mathbf{x}) - 8g^2 \frac{f}{\Omega_m} \Theta_0(\mathbf{x}). \quad (3.38)$$

We consider (3.33) which can be re-written as follows,

$$\begin{aligned}\Theta_0(\mathbf{x}) &= \frac{1}{2}\nabla^{-2}\left[\frac{1}{3}\partial^l\varphi_0\partial_l\varphi_0 - \nabla^{-2}\partial_l\partial_m\left(\partial^l\varphi_0\partial^m\varphi_0\right)\right] \\ &= \frac{1}{2}\nabla^{-2}\left\{\frac{1}{3}\partial^l\varphi_0\partial_l\varphi_0 - \nabla^{-2}\left[\partial_l(\partial_m\partial^l\varphi_0)\partial^m\varphi_0 + (\partial^m\partial^l\varphi_0)(\partial_l\partial^m\varphi_0)\right.\right. \\ &\quad \left.\left.+ \partial_l\partial^l\varphi_0(\partial_m\partial^m\varphi_0) + \partial^l\varphi_0\partial_l(\partial_m\partial^m\varphi_0)\right]\right\}.\end{aligned}\quad (3.39)$$

In Fourier space, $\nabla^{-2} \rightarrow -1/k^2$ and $\partial^l \rightarrow ik^l$. We use the convolution theorem given in (3.8) to show that the Fourier transform of the first term is,

$$\frac{1}{6k_3^2}\int\frac{d^3k_1}{(2\pi)^3}\int d^3k_2(\mathbf{k}_1\cdot\mathbf{k}_2)\varphi_0(\mathbf{k}_1)\varphi_0(\mathbf{k}_2)\delta^D(\mathbf{k}_1+\mathbf{k}_2-\mathbf{k}_3),\quad (3.40)$$

where we have used $k_1^l k_{2l} = \mathbf{k}_1 \cdot \mathbf{k}_2$. The Fourier transform of the second term gives,

$$-\frac{1}{2k_3^2}\int\frac{d^3k_1}{(2\pi)^3}\int d^3k_2\left[k_1^2k_2^2+(\mathbf{k}_1\cdot\mathbf{k}_2)(k_1^2+k_2^2)+(\mathbf{k}_1\cdot\mathbf{k}_2)^2\right]\varphi_0(\mathbf{k}_1)\varphi_0(\mathbf{k}_2)\delta^D(\mathbf{k}_1+\mathbf{k}_2-\mathbf{k}_3).\quad (3.41)$$

Using the definition of α given in (3.26) we can show from (3.34) that,

$$\varphi_0(\mathbf{k}) = -\frac{3}{2g}\Omega_m\frac{\mathcal{H}^2}{k^2}\delta_T^{(1)}(\mathbf{k}).\quad (3.42)$$

Together with the results of (3.40), (3.41), (3.42) and the definition of the integral given in (3.23) the Fourier transform of (3.39) is,

$$\Theta_0(\mathbf{k}_3) = \left(\frac{3\Omega_m\mathcal{H}^2}{2gk_3}\right)^2\int d(\mathbf{k}_1, \mathbf{k}_2, \mathbf{k}_3)\left\{\frac{\mathbf{k}_1\cdot\mathbf{k}_2}{6k_1^2k_2^2}-\frac{1}{2k_3^2}\left[1+\frac{\mathbf{k}_1\cdot\mathbf{k}_2}{k_1k_2}\left(\frac{k_1}{k_2}+\frac{k_2}{k_1}\right)+\frac{(\mathbf{k}_1\cdot\mathbf{k}_2)^2}{k_1^2k_2^2}\right]\right\}.\quad (3.43)$$

The Fourier transforms of the other terms, $[\nabla\varphi_0]^2$, $\varphi_0\nabla^2\varphi_0$ and φ_0^2 can be worked as follows,

$$[\nabla\varphi_0]^2(\mathbf{k}_3) = -\left(\frac{3\Omega_m\mathcal{H}^2}{2g}\right)^2\int d(\mathbf{k}_1, \mathbf{k}_2, \mathbf{k}_3)\frac{\mathbf{k}_1\cdot\mathbf{k}_2}{k_1^2k_2^2},\quad (3.44)$$

$$[\varphi_0\nabla^2\varphi_0](\mathbf{k}_3) = -\left(\frac{3\Omega_m\mathcal{H}^2}{2g}\right)^2\int d(\mathbf{k}_1, \mathbf{k}_2, \mathbf{k}_3)\frac{k_1^2+k_2^2}{2k_1^2k_2^2},\quad (3.45)$$

$$\varphi_0^2(\mathbf{k}_3) = \left(\frac{3\Omega_m\mathcal{H}^2}{2g}\right)^2\int d(\mathbf{k}_1, \mathbf{k}_2, \mathbf{k}_3)\frac{1}{k_1^2k_2^2}.\quad (3.46)$$

We now have all the tools to Fourier transform (3.35)-(3.38). For the second-order T-gauge dark matter overdensity we have,

$$\begin{aligned} \mathcal{H}^2 \delta_{\text{TGR}}^{(2)}(\mathbf{k}_3) = & 3\Omega_m \mathcal{H}^4 \int d(\mathbf{k}_1, \mathbf{k}_2, \mathbf{k}_3) \frac{1}{k_1^2 k_2^2} \left\{ \left[\frac{1}{2} + \frac{f}{3\Omega_m} + \frac{6}{5} f_{\text{NL}} \left(1 + \frac{2f}{3\Omega_m} \right) \right] \mathbf{k}_1 \cdot \mathbf{k}_2 \right. \\ & \left. - \left[1 + \frac{2f}{3\Omega_m} - \frac{3}{5} f_{\text{NL}} \left(1 + \frac{2f}{3\Omega_m} \right) \right] (k_1^2 + k_2^2) \right\}. \end{aligned} \quad (3.47)$$

For the velocity potential we obtain,

$$\mathcal{H} v_{\text{GR}}^{(2)}(\mathbf{k}_3) = 3\Omega_m \mathcal{H}^4 f \int d(\mathbf{k}_1, \mathbf{k}_2, \mathbf{k}_3) \frac{1}{k_1^2 k_2^2} \left[-\frac{3}{2} + \frac{3}{5} f_{\text{NL}} \left(1 + \frac{2f}{3\Omega_m} \right) + E_2(\mathbf{k}_1, \mathbf{k}_2, \mathbf{k}_3) \right], \quad (3.48)$$

where we have defined a new kernel,

$$E_2(\mathbf{k}_1, \mathbf{k}_2, \mathbf{k}_3) = \frac{k_1^2 k_2^2}{k_3^4} \left[3 + 2 \frac{\mathbf{k}_1 \cdot \mathbf{k}_2}{k_1 k_2} \left(\frac{k_1}{k_2} + \frac{k_2}{k_1} \right) + \frac{(\mathbf{k}_1 \cdot \mathbf{k}_2)^2}{k_1^2 k_2^2} \right], \quad (3.49)$$

which is scale independent as E_2 and G_2 [see (3.27) and (3.28)]. For the metric potentials $\Phi^{(2)}$ and $\Psi^{(2)}$ we have,

$$\begin{aligned} \Phi_{\text{GR}}^{(2)}(\mathbf{k}_3) = & 3\Omega_m \mathcal{H}^4 \int d(\mathbf{k}_1, \mathbf{k}_2, \mathbf{k}_3) \frac{1}{k_1^2 k_2^2} \left[\frac{1}{2} (3\Omega_m - f + f^2) - \frac{3}{10} f_{\text{NL}} (2f + 3\Omega_m) \right. \\ & \left. - \frac{1}{2} (3\Omega_m - 2f + f^2) E_2(\mathbf{k}_1, \mathbf{k}_2, \mathbf{k}_3) \right], \end{aligned} \quad (3.50)$$

$$\begin{aligned} \Psi_{\text{GR}}^{(2)}(\mathbf{k}_3) = & 3\Omega_m \mathcal{H}^4 \int d(\mathbf{k}_1, \mathbf{k}_2, \mathbf{k}_3) \frac{1}{k_1^2 k_2^2} \left[-\frac{1}{2} (3\Omega_m + f - f^2) - \frac{3}{10} f_{\text{NL}} (2f - 3\Omega_m) \right. \\ & \left. + f E_2(\mathbf{k}_1, \mathbf{k}_2, \mathbf{k}_3) \right]. \end{aligned} \quad (3.51)$$

For the time derivative of (3.51) we find that,

$$\begin{aligned} \Psi_{\text{GR}}^{(2)'}(\mathbf{k}_3) = & 3\Omega_m \mathcal{H}^5 \int d(\mathbf{k}_1, \mathbf{k}_2, \mathbf{k}_3) \frac{1}{k_1^2 k_2^2} \left\{ \frac{1}{2} (1 - f) \left[6\Omega_m + f(1 - 2f) - 2f \frac{\mathcal{H}'}{\mathcal{H}^2} \right] \right. \\ & + \frac{1}{2} (2f - 1) \frac{f'}{\mathcal{H}} \\ & - \frac{3}{5} f_{\text{NL}} \left[3\Omega_m (1 - f) + f \left(2f - 1 + \frac{2\mathcal{H}'}{\mathcal{H}^2} \right) + \frac{f'}{\mathcal{H}} \right] \\ & \left. + \left[f \left(2f - 1 + \frac{2\mathcal{H}'}{\mathcal{H}^2} \right) + \frac{f'}{\mathcal{H}} \right] E_2(\mathbf{k}_1, \mathbf{k}_2, \mathbf{k}_3) \right\}. \end{aligned} \quad (3.52)$$

We neglect the long modes $\delta_{\text{TGR}}^{(2)}$ and $v_{\text{GR}}^{(2)}$ because we are assuming *Gaussianity* i.e., $f_{\text{NL}} = 0$. More details on the removal of the long mode are given in [99]. From (3.50)–(3.52), it follows that the potential terms proportional to $\Phi^{(2)}$, $\Psi^{(2)}$ and $\Psi^{(2)'}$ in (2.105), lead to relativistic corrections proportional to $\Phi_{\text{GR}}^{(2)}$, $\Psi_{\text{GR}}^{(2)}$ and $\Psi_{\text{GR}}^{(2)'}$, which sum up to a term of the form,

$$[\tilde{\Gamma}_1(z) + E_2(\mathbf{k}_1, \mathbf{k}_2, \mathbf{k}_3) \tilde{\Gamma}_2(z)] / (k_1 k_2)^2. \quad (3.53)$$

where,

$$\begin{aligned} \frac{\tilde{\Gamma}_1}{\mathcal{H}^4} &= \frac{9}{4} \Omega_m^2 \left[9 - 4f - b_e - 2\mathcal{Q} + \frac{2(1-\mathcal{Q})}{\bar{\chi}\mathcal{H}} + \frac{\mathcal{H}'}{\mathcal{H}^2} \right] + \frac{3}{2} \Omega_m f \left[2 - 2f + \frac{2f'}{\mathcal{H}} + b_e \right. \\ &\quad \left. - 4\mathcal{Q} - \frac{2(1-\mathcal{Q})}{\bar{\chi}\mathcal{H}} - \frac{3\mathcal{H}'}{\mathcal{H}^2} \right] + \frac{3}{2} \Omega_m f^2 \left[-2 + 2f - b_e + 4\mathcal{Q} + \frac{2(1-\mathcal{Q})}{\bar{\chi}\mathcal{H}} + \frac{3\mathcal{H}'}{\mathcal{H}^2} \right] \\ &\quad - \frac{3}{2} \Omega_m \frac{f'}{\mathcal{H}}, \end{aligned} \quad (3.54)$$

$$\begin{aligned} \frac{\tilde{\Gamma}_2}{\mathcal{H}^4} &= \frac{9}{2} \Omega_m^2 \left[-1 + b_e - 2\mathcal{Q} - \frac{2(1-\mathcal{Q})}{\bar{\chi}\mathcal{H}} - \frac{\mathcal{H}'}{\mathcal{H}^2} \right] + 3\Omega_m f \left[-2 + 2f - b_e + 4\mathcal{Q} \right. \\ &\quad \left. + \frac{2(1-\mathcal{Q})}{\bar{\chi}\mathcal{H}} + \frac{3\mathcal{H}'}{\mathcal{H}^2} \right] + 3\Omega_m f^2 \left[-1 + b_e - 2\mathcal{Q} - \frac{2(1-\mathcal{Q})}{\bar{\chi}\mathcal{H}} - \frac{\mathcal{H}'}{\mathcal{H}^2} \right] \\ &\quad + 3\Omega_m \frac{f'}{\mathcal{H}}. \end{aligned} \quad (3.55)$$

Other typical second-order terms are those which are quadratic in first-order terms e.g., $v^{(1)}(\mathbf{x})\delta_g^{(1)}(\mathbf{x})$. Its Fourier transform is as follows,

$$\left[v^{(1)}\delta_g^{(1)} \right] (\mathbf{k}_3) = \frac{1}{2} \int \frac{d^3 k_1}{(2\pi)^3} \int d^3 k_2 \left[v^{(1)}(\mathbf{k}_1)\delta_g^{(1)}(\mathbf{k}_2) + v^{(1)}(\mathbf{k}_2)\delta_g^{(1)}(\mathbf{k}_1) \right] \delta^{\text{D}}(\mathbf{k}_1 + \mathbf{k}_2 - \mathbf{k}_3), \quad (3.56)$$

where the factor of 1/2 follows from symmetrization. We express the perturbative variables in terms of $\delta_{\text{T}}^{(1)}$ by using (2.69), (2.70) and (3.14). This leads to,

$$v^{(1)}(\mathbf{k}_1)\delta_g^{(1)}(\mathbf{k}_2) + v^{(1)}(\mathbf{k}_2)\delta_g^{(1)}(\mathbf{k}_1) = \left[b_1 f \mathcal{H} \left(\frac{1}{k_1^2} + \frac{1}{k_2^2} \right) + 2f^2 (3 - b_e) \mathcal{H}^3 \frac{1}{k_1^2 k_2^2} \right] \delta_{\text{T}}^{(1)}(\mathbf{k}_1) \delta_{\text{T}}^{(1)}(\mathbf{k}_2). \quad (3.57)$$

Then (3.56) becomes,

$$\left[v^{(1)}\delta_g^{(1)} \right] (\mathbf{k}_3) = \mathcal{H} f \int d(\mathbf{k}_1, \mathbf{k}_2, \mathbf{k}_3) \frac{[b_1 (k_1^2 + k_2^2) + 2(3 - b_e) f \mathcal{H}^2]}{2k_1^2 k_2^2}. \quad (3.58)$$

Table 3.1 shows the Fourier kernels of all the scalars in $\Delta_g^{(2)}$. For convenience, the superscript (1) is dropped from first-order variables $\delta_{\text{T}}^{(1)}$, $v^{(1)}$ and $\Phi^{(1)}$.

TABLE 3.1: Fourier transform kernel and coefficient of the scalars in (2.104) and (2.105), ordered according to their k -dependence. N denotes a Newtonian term (k^0), Γ_1 is for k^{-4} , Γ_2 is for k^{-3} , Γ_3 to Γ_8 are for k^{-2} and Γ_9 to Γ_{14} are for k^{-1} .

Term	Γ	Fourier kernel \mathcal{F}	Coefficient
$\delta_{\text{T}}^{(2)}$	N	$F_2(\mathbf{k}_1, \mathbf{k}_2)$	b_1
$\partial_{\parallel}^2 v^{(2)}$	N	$f^2 \mathcal{H} \mu_3^2 G_2(\mathbf{k}_1, \mathbf{k}_2)$	$-1/\mathcal{H}$
$\delta_{\text{T}} \partial_{\parallel}^2 v$	N	$-f \mathcal{H} (\mu_1^2 + \mu_2^2)/2$	$-2b_1/\mathcal{H}$
$\partial_{\parallel} v \partial_{\parallel} \delta_{\text{T}}$	N	$-f \mathcal{H} \mu_1 \mu_2 (k_1^2 + k_2^2)/(2k_1 k_2)$	$-2b_1/\mathcal{H}$
$\partial_{\parallel} v \partial_{\parallel}^3 v$	N	$f^2 \mathcal{H}^2 (\mu_1 \mu_2^3 k_2^2 + \mu_2 \mu_1^3 k_1^2)/(k_1 k_2)$	$2/\mathcal{H}^2$
$[\partial_{\parallel}^2 v]^2$	N	$f^2 \mathcal{H}^2 \mu_1^2 \mu_2^2$	$2/\mathcal{H}^2$
$[\Phi]^2$	Γ_1	$9\Omega_m^2 \mathcal{H}^4/(4k_1^2 k_2^2)$	\mathcal{A}_1
Φv	Γ_1	$-3\Omega_m \mathcal{H}^3 f/(2k_1^2 k_2^2)$	\mathcal{A}_3
$\nabla^{-2} [v \nabla^2 v' - v' \nabla^2 v - 6\partial_i \Phi \partial^i v - 6\Phi \nabla^2 v]$	Γ_1	$9\Omega_m \mathcal{H}^3 f/(2k_1^2 k_2^2)$	$(3 - b_e)\mathcal{H}$
vv'	Γ_1	$f \mathcal{H}^3 (3\Omega_m - 2f)/(2k_1^2 k_2^2)$	$(b_e - 3)\mathcal{H}$
$[v]^2$	Γ_1	$f^2 \mathcal{H}^2/(k_1^2 k_2^2)$	$(b_e - 3)^2 \mathcal{H}^2 + b'_e \mathcal{H} + (b_e - 3)\mathcal{H}'$
$v \partial_{\parallel} v$	Γ_2	$i f^2 \mathcal{H}^2 (\mu_1 k_1 + \mu_2 k_2)/(2k_1^2 k_2^2)$	\mathcal{A}_2
$\Phi \partial_{\parallel} v$	Γ_2	$-3i f \Omega_m \mathcal{H}^3 (\mu_1 k_1 + \mu_2 k_2)/(4k_1^2 k_2^2)$	\mathcal{A}_4
$\Phi \partial_{\parallel} \Phi$	Γ_2	$9i \Omega_m^2 \mathcal{H}^4 (\mu_1 k_1 + \mu_2 k_2)/(8k_1^2 k_2^2)$	$2(f - 2 + 2\mathcal{Q})/\mathcal{H}$
$\Psi^{(2)} = \Phi^{(2)}$	Γ_3	$-3\Omega_m \mathcal{H}^2 F_2(\mathbf{k}_1, \mathbf{k}_2)/(2k_3^2)$	$4\mathcal{Q} - 1 - b_e + R$
$\Phi^{(2)'}$	Γ_3	$-3\Omega_m \mathcal{H}^3 (2f - 1) F_2(\mathbf{k}_1, \mathbf{k}_2)/(2k_3^2)$	$1/\mathcal{H}$
$v^{(2)}$	Γ_4	$f \mathcal{H} G_2(\mathbf{k}_1, \mathbf{k}_2)/k_3^2$	$(3 - b_e)\mathcal{H}$
$[\partial_{\parallel} v]^2$	Γ_5	$-f^2 \mathcal{H}^2 \mu_1 \mu_2/(k_1 k_2)$	\mathcal{A}_5
$\partial_{\parallel} v \partial_{\parallel} \Phi$	Γ_5	$3f \Omega_m \mathcal{H}^3 \mu_1 \mu_2/(2k_1 k_2)$	$2(2 - f - 2\mathcal{Q})/\mathcal{H}$
$\partial_i v \partial^i v$	Γ_6	$-f^2 \mathcal{H}^2 \mathbf{k}_1 \cdot \mathbf{k}_2/(k_1^2 k_2^2)$	$b_e - 1 - 2\mathcal{Q} - \mathcal{R}$
$\partial_i v \partial^i \Phi$	Γ_6	$3f \Omega_m \mathcal{H}^3 \mathbf{k}_1 \cdot \mathbf{k}_2/(2k_1^2 k_2^2)$	$2/\mathcal{H}$
$\Phi \delta_{\text{T}}$	Γ_7	$-3\Omega_m \mathcal{H}^2 (k_1^2 + k_2^2)/(4k_1^2 k_2^2)$	$2b_1(f - 2 - b_e + 4\mathcal{Q} + \mathcal{R}) - S$
$\Phi \delta'_{\text{T}}$	Γ_7	$-3f \Omega_m \mathcal{H}^3 (k_1^2 + k_2^2)/(4k_1^2 k_2^2)$	$-2b_1/\mathcal{H}$
$v \delta_{\text{T}}$	Γ_7	$f \mathcal{H} (k_1^2 + k_2^2)/(2k_1^2 k_2^2)$	$b'_1 + 2b_1(3 - b_e)\mathcal{H}$
$v \delta'_{\text{T}}$	Γ_7	$f^2 \mathcal{H}^2 (k_1^2 + k_2^2)/(2k_1^2 k_2^2)$	$-2b_1$
$\Phi \partial_{\parallel}^2 v$	Γ_8	$3f \Omega_m \mathcal{H}^3 (\mu_1^2 k_1^2 + \mu_2^2 k_2^2)/(4k_1^2 k_2^2)$	$2(1 - 2f + 2b_e - 6\mathcal{Q} - 2R - \mathcal{H}'/\mathcal{H}^2)/\mathcal{H}$
$\Phi \partial_{\parallel}^2 \Phi$	Γ_8	$-9\Omega_m^2 \mathcal{H}^4 (\mu_1^2 k_1^2 + \mu_2^2 k_2^2)/(4k_1^2 k_2^2)$	$-2/\mathcal{H}^2$
$v \partial_{\parallel}^2 v$	Γ_8	$-f^2 \mathcal{H}^3 (\mu_1^2 k_1^2 + \mu_2^2 k_2^2)/(2k_1^2 k_2^2)$	$2(b_e - 3)/\mathcal{H}$
$\Phi \partial_{\parallel} \delta_{\text{T}}$	Γ_9	$-3i \Omega_m \mathcal{H}^2 (\mu_1 k_1^3 + \mu_2 k_2^3)/(4k_1^2 k_2^2)$	$2b_1/\mathcal{H}$
$\partial_i v \partial_{\parallel} \partial^i v$	Γ_{10}	$-i f^2 \mathcal{H}^2 \mathbf{k}_1 \cdot \mathbf{k}_2 (\mu_1 k_1 + \mu_2 k_2)/(2k_1^2 k_2^2)$	$-4/\mathcal{H}$
$\delta'_{\text{T}} \partial_{\parallel} v$	Γ_{11}	$i f^2 \mathcal{H}^2 (\mu_1 k_2 + \mu_2 k_1)/(2k_1 k_2)$	$2b_1/\mathcal{H}$
$\delta_{\text{T}} \partial_{\parallel} v$	Γ_{11}	$i f \mathcal{H} (\mu_1 k_2 + \mu_2 k_1)/(2k_1 k_2)$	$2b_1(b_e - 2\mathcal{Q} - \mathcal{R}) + S$
$\Phi \partial_{\parallel}^3 v$	Γ_{12}	$3i f \Omega_m \mathcal{H}^3 (\mu_1^3 k_1^3 + \mu_2^3 k_2^3)/(4k_1^2 k_2^2)$	$-2/\mathcal{H}^2$
$\partial_{\parallel} v \partial_{\parallel}^2 v$	Γ_{13}	$-i f^2 \mathcal{H}^2 (\mu_1 \mu_2^2 k_2 + \mu_2 \mu_1^2 k_1)/(2k_1 k_2)$	$2(3 - 2b_e + 4\mathcal{Q} + 2R + \mathcal{H}'/\mathcal{H}^2)/\mathcal{H}$
$\partial_{\parallel} v \partial_{\parallel}^2 \Phi$	Γ_{13}	$3i f \Omega_m \mathcal{H}^3 (\mu_1 \mu_2^2 k_2 + \mu_2 \mu_1^2 k_1)/(4k_1 k_2)$	$2/\mathcal{H}^2$
$\partial_{\parallel} v^{(2)}$	Γ_{14}	$i f \mathcal{H} \mu_3 G_2(\mathbf{k}_1, \mathbf{k}_2)/k_3$	$b_e - 2\mathcal{Q} - \mathcal{R}$

The coefficients $\mathcal{A}_1, \mathcal{A}_2, \mathcal{A}_3, \mathcal{A}_4, \mathcal{A}_5$ are given in (2.106)-(2.110) and,

$$\mathcal{R} \equiv \frac{2(1 - \mathcal{Q})}{\bar{\chi}\mathcal{H}} + \frac{\mathcal{H}'}{\mathcal{H}^2}, \quad \mathcal{S} \equiv 4 \left(2 - \frac{1}{\bar{\chi}\mathcal{H}} \right) \frac{\partial b_1}{\partial \ln \bar{L}}. \quad (3.59)$$

The Fourier kernels for the quadratic terms in Table 3.1 can be represented by the following algorithm,

$$D^n X D^m Y, \quad (3.60)$$

where $D = \partial_i$ or ∂_{\parallel} , and $X, Y = \delta_{\Gamma}, v$ or Φ . Then the corresponding term in the kernel is formed as follows,

$$\begin{aligned} & \left\{ \frac{1}{2} (i k_1)^n (i k_2)^m \text{ for } D = \partial_{\parallel} \text{ OR } \frac{1}{2} (i \mathbf{k}_1 \cdot i \mathbf{k}_2)^n \text{ for } D = \partial_i, m = n \right. \\ & \times [k_1^{-2} \text{ if } X \text{ is } v \text{ or } \Phi] \times [k_2^{-2} \text{ if } Y \text{ is } v \text{ or } \Phi] \\ & \times [\text{a factor of } \mu_1 \text{ for each } \partial_{\parallel} \text{ acting on } X] \times [\text{a factor of } \mu_2 \text{ for each } \partial_{\parallel} \text{ acting on } Y] \\ & \times [\text{a factor of } f\mathcal{H} \text{ for each } v] \\ & \times [\text{a factor of } -\frac{3}{2}\Omega_m\mathcal{H}^2 \text{ for each } \Phi] \left. \right\} \\ & + \{1 \leftrightarrow 2\} \end{aligned} \quad (3.61)$$

Therefore, we use the results of (3.54), (3.55) and Table 3.1 to obtain the Fourier transform of the second-order scalars in the galaxy number count fluctuation as,

$$\Delta_{gS}^{(2)}(\mathbf{k}_3) = \int d(\mathbf{k}_1, \mathbf{k}_2, \mathbf{k}_3) \mathcal{K}^{(1)}(\mathbf{k}_1) \mathcal{K}^{(1)}(\mathbf{k}_2) \mathcal{K}_{\text{Sca.}}^{(2)}(\mathbf{k}_1, \mathbf{k}_2, \mathbf{k}_3) - \delta^D(\mathbf{k}_3) \langle \Delta_g^{(2)} \rangle. \quad (3.62)$$

where we subtract off the second term which is the ensemble average of $\Delta_g^{(2)}$ to ensure that $\langle \Delta_g^{(2)} \rangle = 0$. The first-order kernel $\mathcal{K}^{(1)}$ is given by (3.17) and (3.18). $\mathcal{K}_{\text{Sca.}}^{(2)}$ is the second-order kernel for scalar perturbations and is cyclically symmetrical over the \mathbf{k}_i 's. The Newtonian part is,

$$\begin{aligned} \mathcal{K}_{\text{N}}^{(2)}(\mathbf{k}_1, \mathbf{k}_2, \mathbf{k}_3) &= b_1 F_2(\mathbf{k}_1, \mathbf{k}_2) + b_2 + f G_2(\mathbf{k}_1, \mathbf{k}_2) \mu_3^2 + b_{\text{Tidal}} S_2(\mathbf{k}_1, \mathbf{k}_2) \\ &+ f^2 \frac{\mu_1 \mu_2}{k_1 k_2} (\mu_1 k_1 + \mu_2 k_2)^2 + b_1 \frac{f}{k_1 k_2} \left[(\mu_1^2 + \mu_2^2) k_1 k_2 + \mu_1 \mu_2 (k_1^2 + k_2^2) \right], \end{aligned} \quad (3.63)$$

where the first line is the second-order generalizations of the dark matter overdensity and Kaiser RSD terms respectively. S_2 is the Fourier kernel for the tidal term and is of the form [27, 100],

$$S_2(\mathbf{k}_1, \mathbf{k}_2) = \frac{(\mathbf{k}_1 \cdot \mathbf{k}_2)^2}{k_1^2 k_2^2} - \frac{1}{3}. \quad (3.64)$$

The terms in the second line are the non-linear RSD contributions. The GR part of $\mathcal{K}_{\text{Sca.}}^{(2)}$ is,

$$\begin{aligned} \mathcal{K}_{\text{S}}^{(2)}(\mathbf{k}_1, \mathbf{k}_2, \mathbf{k}_3) = & \frac{1}{k_1^2 k_2^2} \left\{ \Gamma_1 + \tilde{\Gamma}_1 + E_2(\mathbf{k}_1, \mathbf{k}_2, \mathbf{k}_3) \tilde{\Gamma}_2 \right. \\ & + i(\mu_1 k_1 + \mu_2 k_2) \Gamma_2 + \frac{k_1^2 k_2^2}{k_3^2} \left[F_2(\mathbf{k}_1, \mathbf{k}_2) \Gamma_3 + G_2(\mathbf{k}_1, \mathbf{k}_2) \Gamma_4 \right] \\ & + (\mu_1 k_1 \mu_2 k_2) \Gamma_5 + (\mathbf{k}_1 \cdot \mathbf{k}_2) \Gamma_6 + (k_1^2 + k_2^2) \Gamma_7 + (\mu_1^2 k_1^2 + \mu_2^2 k_2^2) \Gamma_8 \\ & + i \left[(\mu_1 k_1^3 + \mu_2 k_2^3) \Gamma_9 + (\mu_1 k_1 + \mu_2 k_2) (\mathbf{k}_1 \cdot \mathbf{k}_2) \Gamma_{10} \right. \\ & \quad + k_1 k_2 (\mu_1 k_2 + \mu_2 k_1) \Gamma_{11} + (\mu_1^3 k_1^3 + \mu_2^3 k_2^3) \Gamma_{12} \\ & \quad \left. + \mu_1 \mu_2 k_1 k_2 (\mu_1 k_1 + \mu_2 k_2) \Gamma_{13} + \mu_3 \frac{k_1^2 k_2^2}{k_3} G_2(\mathbf{k}_1, \mathbf{k}_2) \Gamma_{14} \right] \left. \right\}, \end{aligned} \quad (3.65)$$

where the Γ -coefficients are as follows,

$$\begin{aligned} \frac{\Gamma_1}{\mathcal{H}^4} = & \frac{9}{4} \Omega_m^2 \left[-3 + 2f \left(2 - 2b_e + 4\mathcal{Q} + \frac{4(1-\mathcal{Q})}{\bar{\chi}\mathcal{H}} + \frac{2\mathcal{H}'}{\mathcal{H}^2} \right) - \frac{2f'}{\mathcal{H}} + b_e^2 + 6b_e - 8b_e \mathcal{Q} \right. \\ & + 4\mathcal{Q} + 16\mathcal{Q}^2 - 16 \frac{\partial \mathcal{Q}}{\partial \ln \bar{L}} - 8 \frac{\mathcal{Q}'}{\mathcal{H}} + \frac{b_e'}{\mathcal{H}} + \frac{2}{\bar{\chi}^2 \mathcal{H}^2} \left(1 - \mathcal{Q} + 2\mathcal{Q}^2 - 2 \frac{\partial \mathcal{Q}}{\partial \ln \bar{L}} \right) \\ & - \frac{2}{\bar{\chi}\mathcal{H}} \left(4 + 2b_e - 2b_e \mathcal{Q} - 4\mathcal{Q} + 8\mathcal{Q}^2 - \frac{3\mathcal{H}'}{\mathcal{H}^2} (1 - \mathcal{Q}) - 8 \frac{\partial \mathcal{Q}}{\partial \ln \bar{L}} - 2 \frac{\mathcal{Q}'}{\mathcal{H}} \right) \\ & + \frac{\mathcal{H}'}{\mathcal{H}^2} \left(-8 - 2b_e + 8\mathcal{Q} + \frac{3\mathcal{H}'}{\mathcal{H}^2} \right) - \frac{\mathcal{H}''}{\mathcal{H}^3} \left. \right] \\ & + 3\Omega_m f \left[6 - f(3 - b_e) + b_e \left(3 + \frac{2(1-\mathcal{Q})}{\bar{\chi}\mathcal{H}} \right) - \frac{b_e'}{\mathcal{H}} - b_e^2 + 4b_e \mathcal{Q} - 12\mathcal{Q} \right. \\ & \left. - \frac{6(1-\mathcal{Q})}{\bar{\chi}\mathcal{H}} + 2 \left(2 - \frac{1}{\bar{\chi}\mathcal{H}} \right) \frac{\mathcal{Q}'}{\mathcal{H}} \right] + f^2 \left[12 - 7b_e + b_e^2 + \frac{b_e'}{\mathcal{H}} + (b_e - 3) \frac{\mathcal{H}'}{\mathcal{H}^2} \right], \end{aligned} \quad (3.66)$$

$$\begin{aligned}
\frac{\Gamma_2}{\mathcal{H}^3} &= \frac{9}{4}\Omega_m^2(f-2+2\mathcal{Q}) + \frac{3}{2}\Omega_m f \left[-2-f \left(-3+f+2b_e-3\mathcal{Q} - \frac{4(1-\mathcal{Q})}{\bar{\chi}\mathcal{H}} - \frac{2\mathcal{H}'}{\mathcal{H}^2} \right) \right. \\
&\quad - \frac{f'}{\mathcal{H}} + 3b_e + b_e^2 - 6b_e\mathcal{Q} + 4\mathcal{Q} + 8\mathcal{Q}^2 - 8\frac{\partial\mathcal{Q}}{\partial\ln\bar{L}} - 6\frac{\mathcal{Q}'}{\mathcal{H}} + \frac{b'_e}{\mathcal{H}} \\
&\quad + \frac{2}{\bar{\chi}^2\mathcal{H}^2} \left(1-\mathcal{Q}+2\mathcal{Q}^2 - 2\frac{\partial\mathcal{Q}}{\partial\ln\bar{L}} \right) + \frac{2}{\bar{\chi}\mathcal{H}} \left(-1-2b_e+2b_e\mathcal{Q} + \mathcal{Q} - 6\mathcal{Q}^2 \right. \\
&\quad + \frac{3\mathcal{H}'}{\mathcal{H}^2}(1-\mathcal{Q}) + 6\frac{\partial\mathcal{Q}}{\partial\ln\bar{L}} + 2\frac{\mathcal{Q}'}{\mathcal{H}} \left. \right) - \frac{\mathcal{H}'}{\mathcal{H}^2} \left(3+2b_e-6\mathcal{Q} - \frac{3\mathcal{H}'}{\mathcal{H}^2} \right) - \frac{\mathcal{H}''}{\mathcal{H}^3} \left. \right] \\
&\quad + f^2 \left[-3+2b_e \left(2 + \frac{(1-\mathcal{Q})}{\bar{\chi}\mathcal{H}} \right) - b_e^2 + 2b_e\mathcal{Q} - 6\mathcal{Q} - \frac{b'_e}{\mathcal{H}} - \frac{6(1-\mathcal{Q})}{\bar{\chi}\mathcal{H}} \right. \\
&\quad \left. + 2 \left(1 - \frac{1}{\bar{\chi}\mathcal{H}} \right) \frac{\mathcal{Q}'}{\mathcal{H}} \right], \tag{3.67}
\end{aligned}$$

$$\frac{\Gamma_3}{\mathcal{H}^2} = \frac{3}{2}\Omega_m \left[2-2f+b_e-4\mathcal{Q} - \frac{2(1-\mathcal{Q})}{\bar{\chi}\mathcal{H}} - \frac{\mathcal{H}'}{\mathcal{H}^2} \right], \tag{3.68}$$

$$\frac{\Gamma_4}{\mathcal{H}^2} = f(3-b_e), \tag{3.69}$$

$$\begin{aligned}
\frac{\Gamma_5}{\mathcal{H}^2} &= 3\Omega_m f(2-f-2\mathcal{Q}) + f^2 \left[4+b_e-b_e^2+4b_e\mathcal{Q}-6\mathcal{Q}-4\mathcal{Q}^2+4\frac{\partial\mathcal{Q}}{\partial\ln\bar{L}}+4\frac{\mathcal{Q}'}{\mathcal{H}} \right. \\
&\quad - \frac{b'_e}{\mathcal{H}} - \frac{2}{\bar{\chi}^2\mathcal{H}^2} \left(1-\mathcal{Q}+2\mathcal{Q}^2 - 2\frac{\partial\mathcal{Q}}{\partial\ln\bar{L}} \right) - \frac{2}{\bar{\chi}\mathcal{H}} \left(3-2b_e+2b_e\mathcal{Q} - \mathcal{Q} - 4\mathcal{Q}^2 \right. \\
&\quad + \frac{3\mathcal{H}'}{\mathcal{H}^2}(1-\mathcal{Q}) + 4\frac{\partial\mathcal{Q}}{\partial\ln\bar{L}} + 2\frac{\mathcal{Q}'}{\mathcal{H}} \left. \right) - \frac{\mathcal{H}'}{\mathcal{H}^2} \left(3-2b_e+4\mathcal{Q} + \frac{3\mathcal{H}'}{\mathcal{H}^2} \right) + \frac{\mathcal{H}''}{\mathcal{H}^3} \left. \right], \tag{3.70}
\end{aligned}$$

$$\frac{\Gamma_6}{\mathcal{H}^2} = 3\Omega_m f - f^2 \left[-1+b_e-2\mathcal{Q} - \frac{2(1+\mathcal{Q})}{\bar{\chi}\mathcal{H}} - \frac{\mathcal{H}'}{\mathcal{H}^2} \right], \tag{3.71}$$

$$\begin{aligned}
\frac{\Gamma_7}{\mathcal{H}^2} &= \frac{3}{2}\Omega_m \left[b_1 \left(2+b_e-4\mathcal{Q} - \frac{2(1-\mathcal{Q})}{\bar{\chi}\mathcal{H}} - \frac{\mathcal{H}'}{\mathcal{H}^2} \right) + \frac{b'_1}{\mathcal{H}} + 2 \left(2 - \frac{1}{\bar{\chi}\mathcal{H}} \right) \frac{\partial b_1}{\partial\ln\bar{L}} \right] \\
&\quad - f \left[b_1(f-3+b_e) + \frac{b'_1}{\mathcal{H}} \right], \tag{3.72}
\end{aligned}$$

$$\frac{\Gamma_8}{\mathcal{H}^2} = \frac{9}{4}\Omega_m^2 + \frac{3}{2}\Omega_m f \left[-2f+2b_e-6\mathcal{Q} - \frac{4(1-\mathcal{Q})}{\bar{\chi}\mathcal{H}} - \frac{3\mathcal{H}'}{\mathcal{H}^2} \right] + f^2(5-b_e), \tag{3.73}$$

$$\frac{\Gamma_9}{\mathcal{H}} = -\frac{3}{2}\Omega_m b_1, \tag{3.74}$$

$$\frac{\Gamma_{10}}{\mathcal{H}} = 2f^2, \tag{3.75}$$

$$\frac{\Gamma_{11}}{\mathcal{H}} = f \left[b_1 \left(f+b_e-2\mathcal{Q} - \frac{2(1-\mathcal{Q})}{\bar{\chi}\mathcal{H}} - \frac{\mathcal{H}'}{\mathcal{H}^2} \right) + \frac{b'_1}{\mathcal{H}} + 2 \left(1 - \frac{1}{\bar{\chi}\mathcal{H}} \right) \frac{\partial b_1}{\partial\ln\bar{L}} \right], \tag{3.76}$$

$$\frac{\Gamma_{12}}{\mathcal{H}} = -\frac{3}{2}\Omega_m f, \tag{3.77}$$

$$\frac{\Gamma_{13}}{\mathcal{H}} = \frac{3}{2}\Omega_m f - f^2 \left[3-2b_e+4\mathcal{Q} + \frac{4(1-\mathcal{Q})}{\bar{\chi}\mathcal{H}} + \frac{3\mathcal{H}'}{\mathcal{H}^2} \right], \tag{3.78}$$

$$\frac{\Gamma_{14}}{\mathcal{H}} = f \left[b_e-2\mathcal{Q} - \frac{2(1-\mathcal{Q})}{\bar{\chi}\mathcal{H}} - \frac{\mathcal{H}'}{\mathcal{H}^2} \right]. \tag{3.79}$$

3.2.2.2 Vectors

The Fourier transform of a pure vector can be written in terms of two independent polarization vectors as [85],

$$\omega_i^{(2)}(\mathbf{x}) = \int \frac{d^3k}{(2\pi)^3} [\omega(\mathbf{k})e_i(\mathbf{k}) + \bar{\omega}(\mathbf{k})\bar{e}_i(\mathbf{k})] e^{i\mathbf{k}\cdot\mathbf{x}}, \quad (3.80)$$

with,

$$\omega(\mathbf{k}) = \int d^3x \omega_i(\mathbf{x}) e^i(\mathbf{k}) e^{-i\mathbf{k}\cdot\mathbf{x}}, \quad \bar{\omega}(\mathbf{k}) = \int d^3x \omega_i(\mathbf{x}) \bar{e}^i(\mathbf{k}) e^{-i\mathbf{k}\cdot\mathbf{x}}. \quad (3.81)$$

The polarization vectors satisfy the following conditions,

$$\mathbf{e}(\mathbf{k}) \cdot \mathbf{k} = \bar{\mathbf{e}}(\mathbf{k}) \cdot \mathbf{k} = 0 \quad \text{and} \quad \mathbf{e}(\mathbf{k}) \cdot \bar{\mathbf{e}}(\mathbf{k}) = 0. \quad (3.82)$$

Taking (3.80) we can write,

$$\omega_{\parallel}^{(2)}(\mathbf{x}) = n^i \omega_i^{(2)}(\mathbf{x}) = \int \frac{d^3k}{(2\pi)^3} [\omega(\mathbf{k})n^i e_i(\mathbf{k}) + \bar{\omega}(\mathbf{k})n^i \bar{e}_i(\mathbf{k})] e^{i\mathbf{k}\cdot\mathbf{x}}, \quad (3.83)$$

where the solution for $\omega_i^{(2)}(\mathbf{x})$ is given by [85],

$$\nabla^2 \omega_i(\mathbf{x}) = \frac{16f}{3\Omega_m \mathcal{H}} \left[\nabla^2 \Phi^{(1)}(\mathbf{x}) \partial_i \Phi^{(1)}(\mathbf{x}) \right]^V. \quad (3.84)$$

The superscript ‘V’ denotes the vector part. The Fourier transform of (3.84) gives,

$$\omega_i(\mathbf{k}_3) = -i \frac{6\Omega_m \mathcal{H}^3 f}{k_3^2} \int d(\mathbf{k}_1, \mathbf{k}_2, \mathbf{k}_3) \left[\frac{k_{1i}}{k_1^2} + \frac{k_{2i}}{k_2^2} \right]. \quad (3.85)$$

Then,

$$\omega(\mathbf{k}_3) = e^i(\mathbf{k}_3) \omega_i(\mathbf{k}_3) = -i \frac{6\Omega_m \mathcal{H}^3 f}{k_3^2} \int d(\mathbf{k}_1, \mathbf{k}_2, \mathbf{k}_3) \left[\frac{\mathbf{k}_1 \cdot \mathbf{e}(\mathbf{k}_3)}{k_1^2} + \frac{\mathbf{k}_2 \cdot \mathbf{e}(\mathbf{k}_3)}{k_2^2} \right]. \quad (3.86)$$

The other parity $\bar{\omega}(\mathbf{k}_3)$ has a similar Fourier solution with \mathbf{e} being replaced by $\bar{\mathbf{e}}$. The second-order vectors in the expression for the galaxy number count fluctuation is given by (2.97),

$$\Delta_{gV}^{(2)}(z, \mathbf{x}) = 2 \left[-b_e + 2\mathcal{Q} + \frac{2(1-\mathcal{Q})}{\bar{\chi}\mathcal{H}} + \frac{\mathcal{H}'}{\mathcal{H}^2} + \frac{1}{\mathcal{H}} \partial_{\parallel} \right] \omega_{\parallel}^{(2)}(\mathbf{x}). \quad (3.87)$$

Together with (3.83) and (3.86) we find that (3.87) Fourier transforms as follows,

$$\Delta_{gV}^{(2)}(\mathbf{x}) = \int \frac{d^3k_3}{(2\pi)^3} \Delta_{gV}^{(2)}(\mathbf{k}_3) e^{i\mathbf{k}_3\cdot\mathbf{x}}, \quad (3.88)$$

where,

$$\Delta_{gV}^{(2)}(\mathbf{k}_3) = \int d(\mathbf{k}_1, \mathbf{k}_2, \mathbf{k}_3) \mathcal{K}_V^{(2)}(\mathbf{k}_1, \mathbf{k}_2, \mathbf{k}_3) . \quad (3.89)$$

We have suppressed the redshift dependence to reduce clutter. $\mathcal{K}_V^{(2)}$ is the second-order kernel for the vector perturbations and takes the form,

$$\mathcal{K}_V^{(2)}(\mathbf{k}_1, \mathbf{k}_2, \mathbf{k}_3) = 12\Omega_m \mathcal{H}^2 f \frac{\mu_3}{k_3} \mathcal{V}_{123} - i 12\Omega_m \mathcal{H}^3 f \left[-b_e + 2\mathcal{Q} + \frac{2(1-\mathcal{Q})}{\bar{\chi}\mathcal{H}} + \frac{\mathcal{H}'}{\mathcal{H}^2} \right] \frac{\mathcal{V}_{123}}{k_3^2} , \quad (3.90)$$

where,

$$\mathcal{V}_{123} = \left[\mathbf{n} \cdot \mathbf{e}(\mathbf{k}_3) \left(\frac{\mathbf{k}_1 \cdot \mathbf{e}(\mathbf{k}_3)}{k_1^2} + \frac{\mathbf{k}_2 \cdot \mathbf{e}(\mathbf{k}_3)}{k_2^2} \right) + \mathbf{n} \cdot \bar{\mathbf{e}}(\mathbf{k}_3) \left(\frac{\mathbf{k}_1 \cdot \bar{\mathbf{e}}(\mathbf{k}_3)}{k_1^2} + \frac{\mathbf{k}_2 \cdot \bar{\mathbf{e}}(\mathbf{k}_3)}{k_2^2} \right) \right] . \quad (3.91)$$

At this stage, we introduce coordinates in Fourier space and this breaks the algebraic cyclic symmetry of the kernel when we permute the \mathbf{k}_i 's. We consider \mathbf{k}_1 along the z -axis as shown in Figure 3.1. For the direction of observation \mathbf{n} , we use two angles: an angle θ_1 and an azimuthal angle ϕ_n with respect to the z - and x -axes respectively. This places \mathbf{n} in a different plane which we consider to be the fixed frame of reference.

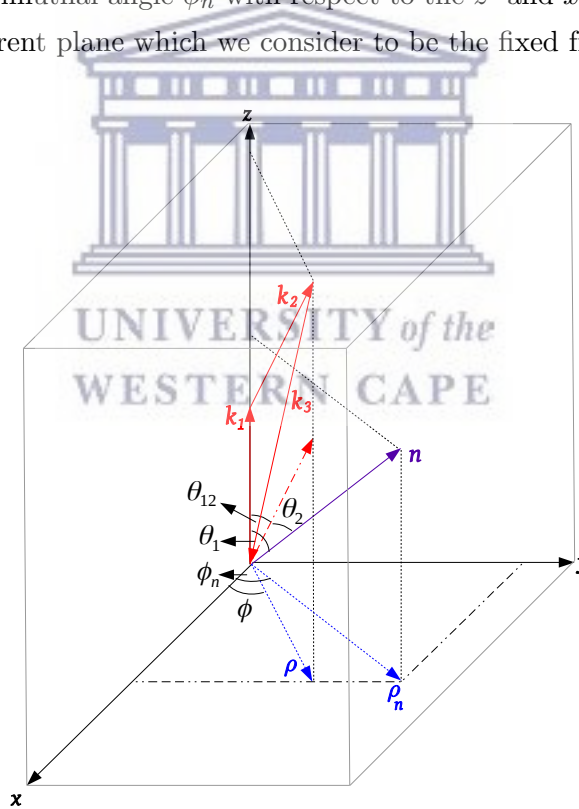


FIGURE 3.1: The geometry of the galaxy bispectrum without the polarization vectors.

We use a right-handed coordinate system and a tail-tail configuration for the angles (θ_i, θ_{ij}) throughout. We start with \mathbf{k}_1 on the z -axis,

$$\mathbf{k}_1 = k_1 [0\hat{x} + 0\hat{y} + \hat{z}] , \quad (3.92)$$

and choose \mathbf{k}_2 to be in the plane controlled by the azimuthal angle ϕ (with respect to the x -axis) such that,

$$\mathbf{k}_2 = k_2 [\sin \theta_{12} \cos \phi \hat{\mathbf{x}} + \sin \theta_{12} \sin \phi \hat{\mathbf{y}} + \cos \theta_{12} \hat{\mathbf{z}}], \quad (3.93)$$

where θ_{12} is the angle between the \mathbf{k}_1 and \mathbf{k}_2 . For \mathbf{k}_3 we obtain,

$$\mathbf{k}_3 = k_3 [-\sin \theta_{31} \cos \phi \hat{\mathbf{x}} - \sin \theta_{31} \sin \phi \hat{\mathbf{y}} + \cos \theta_{31} \hat{\mathbf{z}}], \quad (3.94)$$

where θ_{31} is the angle between the \mathbf{k}_1 and \mathbf{k}_3 . The conservation of the mode vectors,

$$\mathbf{k}_1 + \mathbf{k}_2 + \mathbf{k}_3 = \mathbf{0}, \quad (3.95)$$

ensures a closed triangle. Using (3.92) and (3.93) in (3.95) we obtain,

$$\mathbf{k}_3 = -k_2 \left[\sin \theta_{12} \cos \phi \hat{\mathbf{x}} + \sin \theta_{12} \sin \phi \hat{\mathbf{y}} + \left(\frac{k_1}{k_2} + \cos \theta_{12} \right) \hat{\mathbf{z}} \right]. \quad (3.96)$$

Then (3.94) and (3.96) imply that,

$$k_3 \sin \theta_{31} = k_2 \sin \theta_{12}, \quad (3.97)$$

$$k_3 \cos \theta_{31} = -k_2 \left(\frac{k_1}{k_2} + \cos \theta_{12} \right). \quad (3.98)$$

For \mathbf{n} we have,

$$\mathbf{n} = \sin \theta_1 \cos \phi_n \hat{\mathbf{x}} + \sin \theta_1 \sin \phi_n \hat{\mathbf{y}} + \cos \theta_1 \hat{\mathbf{z}}, \quad (3.99)$$

where θ_i is the angle between \mathbf{n} and \mathbf{k}_i and, ϕ_n is the azimuthal angle with respect to the x -axis. Taking the dot product with \mathbf{n} on both sides of (3.95) leads to,

$$\mu_1 k_1 + \mu_2 k_2 + \mu_3 k_3 = 0, \quad (3.100)$$

where $\mu_i = \hat{\mathbf{k}}_i \cdot \mathbf{n}$. This shows that two of the μ_i are independent, where $k_3 = |\mathbf{k}_1 + \mathbf{k}_2|$. One of the μ_i can be expressed in terms of the other one and the choice of independent μ_{ij} where $\mu_{ij} = \hat{\mathbf{k}}_i \cdot \hat{\mathbf{k}}_j$. Here, we choose μ_1 and μ_{12} . We consider the plane containing $[\mathbf{k}_1, \mathbf{k}_2]$. We decompose $\hat{\mathbf{k}}_2$ in the direction of $\hat{\mathbf{k}}_1$ and perpendicular to $\hat{\mathbf{k}}_1$ in the $[\mathbf{k}_1, \mathbf{k}_2]$ plane as,

$$\hat{\mathbf{k}}_2 = \mu_{12} \hat{\mathbf{k}}_1 + \sqrt{1 - \mu_{12}^2} \hat{\boldsymbol{\rho}}, \quad (3.101)$$

where $\hat{\boldsymbol{\rho}}$ is the projection of \mathbf{k}_2 in the x - y plane. We do the same thing for the plane $[\mathbf{k}_1, \mathbf{n}]$,

$$\mathbf{n} = \mu_1 \hat{\mathbf{k}}_1 + \sqrt{1 - \mu_1^2} \hat{\boldsymbol{\rho}}_n, \quad (3.102)$$

where $\hat{\rho}_n$ is the projection of \mathbf{n} in the x - y plane. Taking the dot product between (3.101) and (3.102) gives,

$$\mu_2 = \mu_1\mu_{12} + \sqrt{1 - \mu_1^2}\sqrt{1 - \mu_{12}^2}\hat{\rho} \cdot \hat{\rho}_n . \quad (3.103)$$

From Figure 3.1, the angle between $\hat{\rho}$ and $\hat{\rho}_n$ is $\omega = \phi_n - \phi$. Hence (3.103) becomes,

$$\mu_2 = \mu_1\mu_{12} + \sqrt{1 - \mu_1^2}\sqrt{1 - \mu_{12}^2}\cos\omega . \quad (3.104)$$

Using (3.100) we find that,

$$\mu_3 = -\frac{1}{k_3} [\mu_1 k_1 + \mu_2 k_2] . \quad (3.105)$$

For the mode vectors, let us consider Figure 3.2.

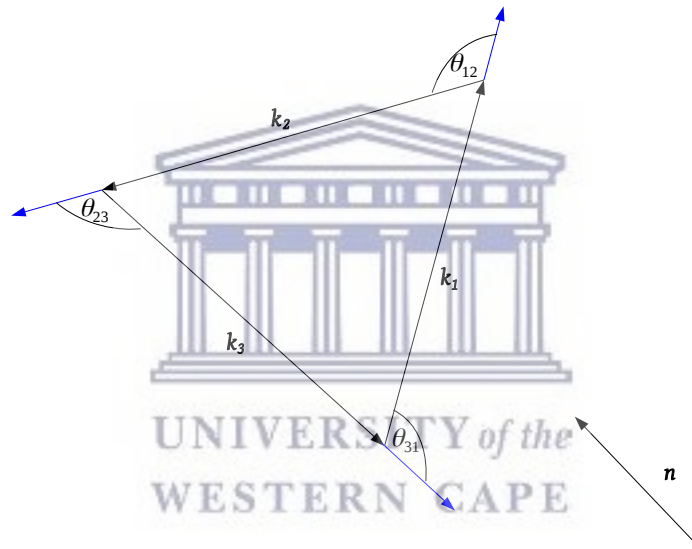


FIGURE 3.2: A closed triangle with \mathbf{k}_1 , \mathbf{k}_2 and \mathbf{k}_3 flowing in one direction. The direction of observation is \mathbf{n} and all the angles are defined in a tail-tail configuration.

From (3.95) it follows that,

$$\mathbf{k}_3 \cdot \mathbf{k}_3 = k_3^2 = k_1^2 + k_2^2 + 2k_1k_2\mu_{12} , \quad (3.106)$$

and if we define $k_2 = rk_1$, we can show that (3.106) becomes,

$$k_3 = k_1\sqrt{1 + r^2 + 2r\mu_{12}} . \quad (3.107)$$

Then for $\mathbf{k}_1 \cdot \mathbf{k}_1$ and $\mathbf{k}_2 \cdot \mathbf{k}_2$ we show that,

$$\mu_{23} = \frac{-(r + \mu_{12})}{\sqrt{1 + r^2 + 2r\mu_{12}}} \quad \text{and} \quad \mu_{31} = \frac{-(1 + r\mu_{12})}{\sqrt{1 + r^2 + 2r\mu_{12}}}. \quad (3.108)$$

Hence, changing the values of r and μ_{12} control the magnitudes of the \mathbf{k} -vectors and the angles among them. This leads to different triangular shapes as shown in Figure 3.3.

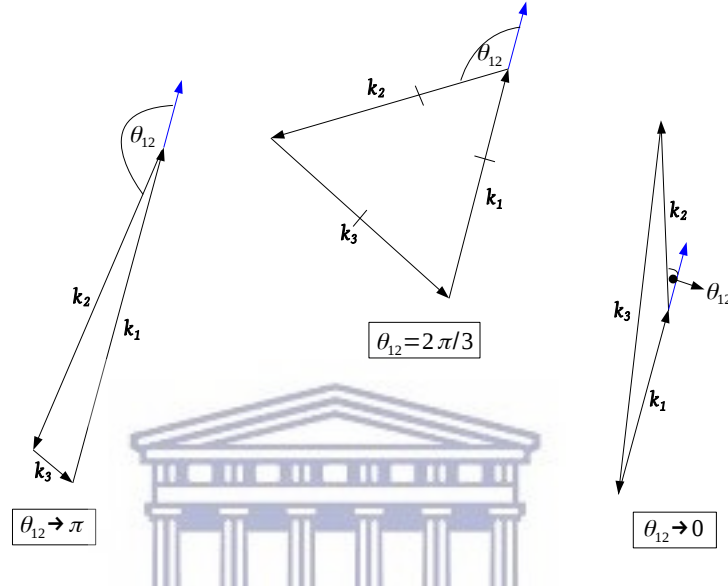


FIGURE 3.3: These are examples of different triangular configurations. *Left figure:* The squeezed triangle with $k_1 \approx k_2 \gg k_3$. *Middle figure:* The equilateral triangle with $k_1 = k_2 = k_3$. *Right figure:* The folded triangle with $k_1 \approx k_2 \approx k_3/2$.

We now modify Figure 3.1 to include the polarization vectors as shown in Figure 3.4. We start by defining the triplet $[\mathbf{k}_1, \mathbf{e}(\mathbf{k}_1), \bar{\mathbf{e}}(\mathbf{k}_1)]$ as follows,

$$\mathbf{k}_1 = k_1 [0\hat{\mathbf{x}} + 0\hat{\mathbf{y}} + \hat{\mathbf{z}}], \quad \mathbf{e}(\mathbf{k}_1) = \hat{\mathbf{x}} + 0\hat{\mathbf{y}} + 0\hat{\mathbf{z}}, \quad \bar{\mathbf{e}}(\mathbf{k}_1) = 0\hat{\mathbf{x}} + \hat{\mathbf{y}} + 0\hat{\mathbf{z}}. \quad (3.109)$$

For $(\mathbf{e}, \bar{\mathbf{e}})(\mathbf{k}_2)$ we choose the triplet $[\mathbf{k}_2, \mathbf{e}(\mathbf{k}_2), \bar{\mathbf{e}}(\mathbf{k}_2)]$ to coincide with $[\mathbf{k}_1, \mathbf{e}(\mathbf{k}_1), \bar{\mathbf{e}}(\mathbf{k}_1)]$ when $\theta_{12} = \phi = 0$ and this implies,

$$\mathbf{e}(\mathbf{k}_2) = \mu_{12} \cos \phi \hat{\mathbf{x}} + \mu_{12} \sin \phi \hat{\mathbf{y}} - \sqrt{1 - \mu_{12}^2} \hat{\mathbf{z}}, \quad \bar{\mathbf{e}}(\mathbf{k}_2) = -\sin \phi \hat{\mathbf{x}} + \cos \phi \hat{\mathbf{y}} + 0\hat{\mathbf{z}}, \quad (3.110)$$

where $(\mathbf{e}, \bar{\mathbf{e}})(\mathbf{k}_2)$ has the same handedness as $(\mathbf{e}, \bar{\mathbf{e}})(\mathbf{k}_1)$ with respect to their \mathbf{k} -vectors. We specify $(\mathbf{e}, \bar{\mathbf{e}})(\mathbf{k}_3)$ in the same way and obtain,

$$\mathbf{e}(\mathbf{k}_3) = -\frac{k_2}{k_3} \left[\left(\frac{k_1}{k_2} + \mu_{12} \right) \cos \phi \hat{\mathbf{x}} + \left(\frac{k_1}{k_2} + \mu_{12} \right) \sin \phi \hat{\mathbf{y}} - \sqrt{1 - \mu_{12}^2} \hat{\mathbf{z}} \right], \quad (3.111)$$

$$\bar{\mathbf{e}}(\mathbf{k}_3) = -\sin \phi \hat{\mathbf{x}} + \cos \phi \hat{\mathbf{y}} + 0\hat{\mathbf{z}}. \quad (3.112)$$

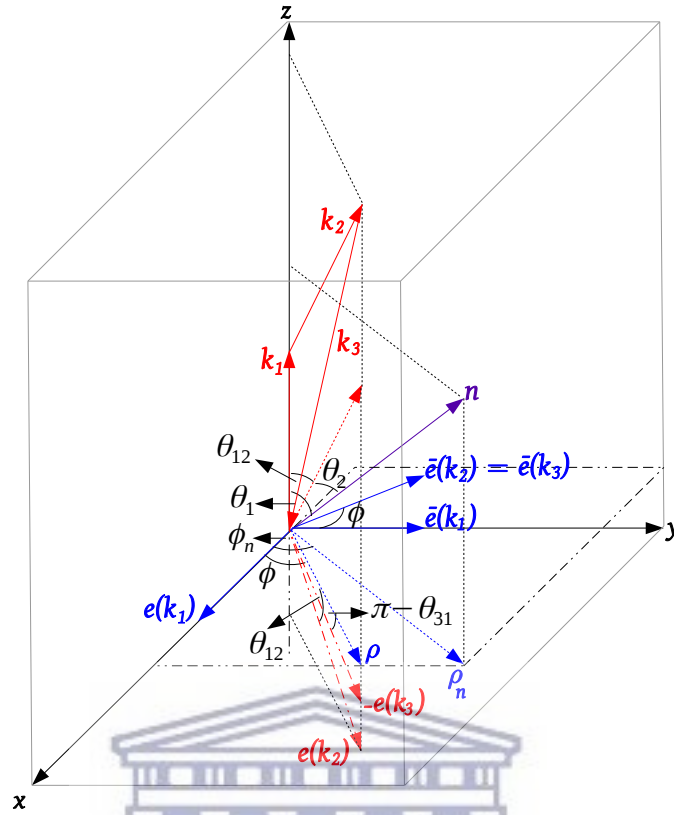


FIGURE 3.4: The geometry of the galaxy bispectrum with the polarization vectors satisfying the conditions in (3.82).

Then the projection along \mathbf{n} gives,

$$\mathbf{n} \cdot \mathbf{e}(\mathbf{k}_1) = \sqrt{1 - \mu_1^2} \cos \phi_n, \quad (3.113)$$

$$\mathbf{n} \cdot \bar{\mathbf{e}}(\mathbf{k}_1) = \sqrt{1 - \mu_1^2} \sin \phi_n, \quad (3.114)$$

$$\mathbf{n} \cdot \mathbf{e}(\mathbf{k}_2) = \mu_{12} \sqrt{1 - \mu_1^2} \cos(\phi_n - \phi) - \mu_1 \sqrt{1 - \mu_{12}^2}, \quad (3.115)$$

$$\mathbf{n} \cdot \bar{\mathbf{e}}(\mathbf{k}_2) = \sqrt{1 - \mu_1^2} \sin \omega, \quad (3.116)$$

$$\mathbf{n} \cdot \mathbf{e}(\mathbf{k}_3) = \frac{k_2}{k_3} \left[-\sqrt{1 - \mu_1^2} \left(\frac{k_1}{k_2} + \mu_{12} \right) \cos \omega + \mu_1 \sqrt{1 - \mu_{12}^2} \right], \quad (3.117)$$

$$\mathbf{n} \cdot \bar{\mathbf{e}}(\mathbf{k}_3) = \sqrt{1 - \mu_1^2} \sin \omega, \quad (3.118)$$

and the dot products with \mathbf{k} -vectors yield,

$$\mathbf{k}_1 \cdot \mathbf{e}(\mathbf{k}_2) = -k_1 \sqrt{1 - \mu_{12}^2}, \quad (3.119)$$

$$\mathbf{k}_1 \cdot \bar{\mathbf{e}}(\mathbf{k}_2) = 0, \quad (3.120)$$

$$\mathbf{k}_2 \cdot \mathbf{e}(\mathbf{k}_1) = k_2 \sqrt{1 - \mu_{12}^2} \cos \phi, \quad (3.121)$$

$$\mathbf{k}_2 \cdot \bar{\mathbf{e}}(\mathbf{k}_1) = k_2 \sqrt{1 - \mu_{12}^2} \sin \phi, \quad (3.122)$$

$$\mathbf{k}_2 \cdot \mathbf{e}(\mathbf{k}_3) = -\frac{k_1 k_2}{k_3} \sqrt{1 - \mu_{12}^2}, \quad (3.123)$$

$$\mathbf{k}_2 \cdot \bar{\mathbf{e}}(\mathbf{k}_3) = 0. \quad (3.124)$$

For the other possible permutations, we apply (3.82) to (3.95) and derive the following,

$$\begin{aligned} \mathbf{k}_1 \cdot \mathbf{e}(\mathbf{k}_3) &= -\mathbf{k}_2 \cdot \mathbf{e}(\mathbf{k}_3), & \mathbf{k}_2 \cdot \mathbf{e}(\mathbf{k}_1) &= -\mathbf{k}_3 \cdot \mathbf{e}(\mathbf{k}_1), & \mathbf{k}_3 \cdot \mathbf{e}(\mathbf{k}_2) &= -\mathbf{k}_1 \cdot \mathbf{e}(\mathbf{k}_2), \\ \mathbf{k}_1 \cdot \bar{\mathbf{e}}(\mathbf{k}_3) &= -\mathbf{k}_2 \cdot \bar{\mathbf{e}}(\mathbf{k}_3), & \mathbf{k}_2 \cdot \bar{\mathbf{e}}(\mathbf{k}_1) &= -\mathbf{k}_3 \cdot \bar{\mathbf{e}}(\mathbf{k}_1), & \mathbf{k}_3 \cdot \bar{\mathbf{e}}(\mathbf{k}_2) &= -\mathbf{k}_1 \cdot \bar{\mathbf{e}}(\mathbf{k}_2). \end{aligned} \quad (3.125)$$

We can now obtain the exact forms of (3.91) for the second-order vector kernel as,

$$\mathcal{V}_{123} = \left(\frac{k_1^2 - k_2^2}{k_3^2 k_1} \right) \left[\left(\frac{k_1}{k_2} + \mu_{12} \right) \sqrt{1 - \mu_1^2} \cos \omega - \mu_1 \sqrt{1 - \mu_{12}^2} \right] \sqrt{1 - \mu_{12}^2}, \quad (3.126)$$

$$\mathcal{V}_{231} = \left(\frac{k_3^2 - k_2^2}{k_3^2 k_2} \right) \sqrt{1 - \mu_1^2} \sqrt{1 - \mu_{12}^2} \cos \omega, \quad (3.127)$$

$$\mathcal{V}_{312} = \left(\frac{k_1^2 - k_3^2}{k_3^2 k_1} \right) \left[\mu_{12} \sqrt{1 - \mu_1^2} \cos \omega - \mu_1 \sqrt{1 - \mu_{12}^2} \right] \sqrt{1 - \mu_{12}^2}. \quad (3.128)$$

Equations (3.126)-(3.128) are 0 in the:

- Extreme squeezed limit, $\mu_{12} = -1$.
- Equilateral configuration, $k_1 = k_2 = k_3 = k$.

Therefore, there are no vector contributions to the galaxy number count bispectrum for the above configurations.

3.2.2.3 Tensors

The tensors can be expanded in Fourier space using the polarization tensors [86, 101],

$$e_{ij}(\mathbf{k}) = \frac{1}{\sqrt{2}} [e_i(\mathbf{k})e_j(\mathbf{k}) - \bar{e}_i(\mathbf{k})\bar{e}_j(\mathbf{k})], \quad \bar{e}_{ij}(\mathbf{k}) = \frac{1}{\sqrt{2}} [e_i(\mathbf{k})\bar{e}_j(\mathbf{k}) + \bar{e}_i(\mathbf{k})e_j(\mathbf{k})]. \quad (3.129)$$

The second-order tensors in the expression for the galaxy number count fluctuation is given by (2.98),

$$\Delta_{gT}^{(2)}(z, \mathbf{x}) = -\frac{1}{2} \left[(1 - \mathcal{Q}) + \frac{1}{\mathcal{H}} \frac{\partial}{\partial \eta} \right] h_{\parallel}^{(2)}(\mathbf{x}) . \quad (3.130)$$

Then,

$$h_{ij}^{(2)}(\mathbf{x}) = \int \frac{d^3k}{(2\pi)^3} [h(\mathbf{k})e_{ij}(\mathbf{k}) + \bar{h}(\mathbf{k})\bar{e}_{ij}(\mathbf{k})] e^{i\mathbf{k}\cdot\mathbf{x}} , \quad (3.131)$$

with,

$$h(\mathbf{k}) = \int d^3x h_{ij}(\mathbf{x}) e^{ij}(\mathbf{k}) e^{-i\mathbf{k}\cdot\mathbf{x}} , \quad \bar{h}(\mathbf{k}) = \int d^3x h_{ij}(\mathbf{x}) \bar{e}^{ij}(\mathbf{k}) e^{-i\mathbf{k}\cdot\mathbf{x}} . \quad (3.132)$$

Taking (3.131) we can write,

$$h_{\parallel}^{(2)}(\mathbf{x}) = n^i n^j h_{ij}^{(2)}(\mathbf{x}) = \int \frac{d^3k}{(2\pi)^3} [h(\mathbf{k})n^i n^j e_{ij}(\mathbf{k}) + \bar{h}(\mathbf{k})n^i n^j \bar{e}_{ij}(\mathbf{k})] e^{i\mathbf{k}\cdot\mathbf{x}} , \quad (3.133)$$

where $h(\eta, \mathbf{x})$ obeys,

$$h''(\eta, \mathbf{x}) - 2\mathcal{H}h'(\eta, \mathbf{x}) - \nabla^2 h(\eta, \mathbf{x}) = S(\eta, \mathbf{x}) , \quad (3.134)$$

obtained from projecting out the tensor part of the ij -component of the Einstein field equations. In Fourier space (3.134) is written as,

$$h''(\mathbf{k}) - 2\mathcal{H}h'(\mathbf{k}) + k^2 h(\mathbf{k}) = S(\mathbf{k}) , \quad (3.135)$$

where $S(\mathbf{k})$ is the source term. Following [102] $S_{ij}(\eta, \mathbf{x})$ is given as,

$$S_{ij}(\eta, \mathbf{x}) = 8 \left[\partial_i \Phi \partial_j \Phi + \frac{2}{8\pi G a^2 \rho} \partial_i (\Phi' + \mathcal{H}\Phi) \partial_j (\Phi' + \mathcal{H}\Phi) \right]^T , \quad (3.136)$$

where the superscript ‘T’ denotes the tensor part. Using $\Phi(\mathbf{x}) = g(\eta)\Phi_0(\mathbf{x})$, we can simplify (3.136) as,

$$S_{ij}(\mathbf{x}) = 8 \left[\partial_i \Phi \partial_j \Phi + \frac{1}{4\pi G a^2 \rho} \left(\frac{g'}{g} + \mathcal{H} \right)^2 \partial_i \Phi \partial_j \Phi \right]^T . \quad (3.137)$$

We can derive the following useful relation [72],

$$\frac{g'}{g\mathcal{H}} = f - 1 , \quad (3.138)$$

and use it to show that (3.135) becomes,

$$S_{ij}(\eta, \mathbf{x}) = 8 \left[1 + \frac{\mathcal{H}^2 f^2}{4\pi G a^2 \rho} \right] [\partial_i \Phi \partial_j \Phi]^T . \quad (3.139)$$

Since $4\pi G a^2 \rho = (3/2)\Omega_m \mathcal{H}^2$ we finally obtain,

$$S_{ij}(\eta, \mathbf{x}) = 8 \left[1 + \frac{2f^2}{3\Omega_m} \right] [\partial_i \Phi \partial_j \Phi]^\top . \quad (3.140)$$

The Fourier transform of (3.140) gives,

$$S_{ij}(\mathbf{k}_3) = -3\Omega_m \mathcal{H}^4 (3\Omega_m + 2f^2) \int d(\mathbf{k}_1, \mathbf{k}_2, \mathbf{k}_3) \frac{1}{k_1^2 k_2^2} [k_{1i} k_{2j} + k_{2i} k_{1j}] . \quad (3.141)$$

Then the source term S is given by,

$$\begin{aligned} S(\mathbf{k}_3) &= e^{ij}(\mathbf{k}_3) S_{ij}(\mathbf{k}_3) \\ &= -3\Omega_m \mathcal{H}^4 (3\Omega_m + 2f^2) \int d(\mathbf{k}_1, \mathbf{k}_2, \mathbf{k}_3) \frac{1}{k_1^2 k_2^2} [k_{1i} k_{2j} + k_{2i} k_{1j}] e^{ij}(\mathbf{k}_3) . \end{aligned} \quad (3.142)$$

Because $k_{1i} k_{2j} e^{ij} = k_{2i} k_{1j} e^{ij}$ we can write (3.142) as,

$$S(\mathbf{k}_3) = -6\Omega_m \mathcal{H}^4 (3\Omega_m + 2f^2) \int d(\mathbf{k}_1, \mathbf{k}_2, \mathbf{k}_3) \frac{k_{1i} k_{2j}}{k_1^2 k_2^2} e^{ij}(\mathbf{k}_3) . \quad (3.143)$$

In general, the solution to (3.135) for the amplitude of the second-order tensor, $h(\mathbf{k})$, is given by an integral over the Green's function, $\mathcal{G}(\eta, k)$, written in spherical Bessel functions [102],

$$h(\eta, \mathbf{k}) = \frac{1}{a} \int_0^\eta d\tilde{\eta} \frac{\eta \tilde{\eta}}{k^2} [j_1(k\eta) y_1(k\tilde{\eta}) - j_1(k\tilde{\eta}) y_1(k\eta)] a(\tilde{\eta}) S(\tilde{\eta}, \mathbf{k}) . \quad (3.144)$$

However, for simplicity we consider the solution for $h(\mathbf{k})$ in the matter era where $S(\eta, \mathbf{k})$ is nearly constant in time at high redshift and therefore, we can approximate (3.144) to [86],

$$h(\eta, \mathbf{k}) \approx \frac{\mathcal{G}(\eta, k)}{k^2} S(\eta, \mathbf{k}) , \quad (3.145)$$

where,

$$\mathcal{G}(\eta, k) = 1 + \frac{3[k\eta \cos(k\eta) - \sin(k\eta)]}{(k\eta)^3} . \quad (3.146)$$

Using the results of (3.143) and (3.145) in (3.133) and (3.130) we obtain the Fourier transform as follows,

$$\Delta_{g\Gamma}^{(2)}(\mathbf{x}) = \int \frac{d^3 k_3}{(2\pi)^3} \Delta_{g\Gamma}^{(2)}(\mathbf{k}_3) e^{i\mathbf{k}_3 \cdot \mathbf{x}} , \quad (3.147)$$

where,

$$\Delta_{g\Gamma}^{(2)}(\mathbf{k}_3) = \int d(\mathbf{k}_1, \mathbf{k}_2, \mathbf{k}_3) \mathcal{K}_\Gamma^{(2)}(\mathbf{k}_1, \mathbf{k}_2, \mathbf{k}_3) . \quad (3.148)$$

$\mathcal{K}_T^{(2)}$ is the second-order kernel for tensor perturbations and takes the form,

$$\begin{aligned} \mathcal{K}_T^{(2)}(\mathbf{k}_1, \mathbf{k}_2, \mathbf{k}_3) = \frac{3\Omega_m \mathcal{H}^4}{k_3^2} & \left\{ \left[(3\Omega_m + 2f^2) \left(2f - \mathcal{Q} + \frac{2\mathcal{H}'}{\mathcal{H}^2} \right) + 4f \frac{f'}{\mathcal{H}} - 3\Omega_m \left(1 + \frac{2\mathcal{H}'}{\mathcal{H}^2} \right) \right] \mathcal{G}(\eta, k_3) \right. \\ & \left. + (3\Omega_m + 2f^2) \frac{\mathcal{G}'(\eta, k_3)}{\mathcal{H}} \right\} \mathcal{T}_{123}, \end{aligned} \quad (3.149)$$

where,

$$\mathcal{T}_{123} = \frac{1}{k_1^2 k_2^2} \left[e^{ij}(\mathbf{k}_3) k_{1i} k_{2j} n^l n^m e_{lm}(\mathbf{k}_3) + \bar{e}^{ij}(\mathbf{k}_3) k_{1i} k_{2j} n^l n^m \bar{e}_{lm}(\mathbf{k}_3) \right]. \quad (3.150)$$

Equation (3.150) requires the following:

- The projection of the polarization tensors along the line of sight which gives,

$$\mathbf{e}_{ij}(\mathbf{k}_1) n^i n^j = \frac{1}{\sqrt{2}} (1 - \mu_1^2) \cos 2\phi_n, \quad (3.151)$$

$$\bar{\mathbf{e}}_{ij}(\mathbf{k}_1) n^i n^j = \frac{1}{\sqrt{2}} (1 - \mu_1^2) \sin 2\phi_n, \quad (3.152)$$

$$\begin{aligned} \mathbf{e}_{ij}(\mathbf{k}_2) n^i n^j = \frac{1}{\sqrt{2}} & \left[(1 - \mu_{12}^2) \sin^2 \omega - \mu_{12}^2 (1 - \mu_1^2) \cos^2 \omega \cos \omega \right. \\ & \left. + 2\mu_1 \mu_{12} \sqrt{1 - \mu_1^2} \sqrt{1 - \mu_{12}^2} - \mu_1^2 (1 - \mu_{12}^2) \right], \end{aligned} \quad (3.153)$$

$$\bar{\mathbf{e}}_{ij}(\mathbf{k}_2) n^i n^j = \frac{1}{\sqrt{2}} \left[\mu_{12} (1 - \mu_1^2) \sin 2(\omega - 2\mu_1 \sqrt{1 - \mu_1^2} \sqrt{1 - \mu_{12}^2} \sin \omega) \right], \quad (3.154)$$

$$\begin{aligned} \mathbf{e}_{ij}(\mathbf{k}_3) n^i n^j = \frac{1}{\sqrt{2}} & \left\{ (1 - \mu_1^2) \sin^2 \omega - \frac{k_2^2}{k_3^2} \left[\left(\frac{k_1}{k_2} + \mu_{12} \right) (1 - \mu_1^2) \cos^2 \omega \right. \right. \\ & \left. \left. + \mu_1^2 (1 - \mu_{12}^2) \right] - 2 \left(\frac{k_1}{k_2} + \mu_{12} \right) \mu_1 \sqrt{1 - \mu_1^2} \sqrt{1 - \mu_{12}^2} \cos \omega \right\}, \end{aligned} \quad (3.155)$$

$$\bar{\mathbf{e}}_{ij}(\mathbf{k}_3) n^i n^j = \frac{1}{\sqrt{2}} \frac{k_2}{k_3} \left[- (1 - \mu_1^2) \left(\frac{k_1}{k_2} + \mu_{12} \right) \sin 2\omega + 2\mu_1 \sqrt{1 - \mu_1^2} \sqrt{1 - \mu_{12}^2} \sin \omega \right]. \quad (3.156)$$

- The contraction of the polarization tensors with the mode vectors as,

$$e^{ij}(\mathbf{k}_3)k_{1i}k_{2j} = -\frac{k_1^2 k_2^2}{\sqrt{2}k_3^2}(1 - \mu_{12}^2), \quad (3.157)$$

$$\bar{e}^{ij}(\mathbf{k}_3)k_{1i}k_{2j} = 0, \quad (3.158)$$

$$e^{ij}(\mathbf{k}_2)k_{1i}k_{3j} = -\frac{1}{\sqrt{2}}k_1^2(1 - \mu_{12}^2), \quad (3.159)$$

$$\bar{e}^{ij}(\mathbf{k}_2)k_{1i}k_{3j} = 0, \quad (3.160)$$

$$e^{ij}(\mathbf{k}_1)k_{2i}k_{3j} = -\frac{1}{\sqrt{2}}k_2^2(1 - \mu_{12}^2)\cos 2\phi, \quad (3.161)$$

$$\bar{e}^{ij}(\mathbf{k}_1)k_{2i}k_{3j} = -\frac{1}{\sqrt{2}}k_2^2(1 - \mu_{12}^2)\sin 2\phi. \quad (3.162)$$

Here also, the cyclic symmetry over the \mathbf{k}_i 's is broken and therefore, we give the explicit forms of the different permutations,

$$\begin{aligned} \mathcal{T}_{123} = \frac{1}{4k_3^4}(1 - \mu_{12}^2) & \left[k_3^2 - k_1^2 + (k_1^2 - 2k_2^2 - k_3^2)\mu_1^2 + (2k_1k_2\mu_1^2 - 2k_1k_2)\mu_{12} + (3k_2^2\mu_1^2 - k_2^2)\mu_{12}^2 \right. \\ & + 4k_2(k_1 + k_2\mu_{12})\mu_1\sqrt{1 - \mu_1^2}\sqrt{1 - \mu_{12}^2}\cos\omega \\ & \left. - (1 - \mu_1^2)(k_1^2 + 2k_1k_2\mu_{12} + k_2^2\mu_{12}^2 + k_3^2)\cos 2\omega \right], \end{aligned} \quad (3.163)$$

$$\mathcal{T}_{231} = -\frac{1}{2k_3^2}(1 - \mu_1^2)(1 - \mu_{12}^2)\cos 2\omega, \quad (3.164)$$

$$\begin{aligned} \mathcal{T}_{312} = \frac{1}{4k_3^2}(1 - \mu_{12}^2) & \left[(1 - \mu_{12}^2)(1 - 3\mu_1^2) + 4\mu_1\mu_{12}\sqrt{1 - \mu_1^2}\sqrt{1 - \mu_{12}^2}\cos\omega \right. \\ & \left. - (1 - \mu_1^2)(1 + \mu_{12}^2)\cos 2\omega \right], \end{aligned} \quad (3.165)$$

where we have eliminated the \sin^2 and \cos^2 terms by using the trigonometric identities,

$$\sin^2\theta = \frac{1}{2}(1 - \cos 2\theta), \quad \cos^2\theta = \frac{1}{2}(1 + \cos 2\theta). \quad (3.166)$$

In the extreme squeezed limit ($\mu_{12} = -1$), (3.163)-(3.165) are 0 and therefore, there are no tensor contributions to the galaxy number count bispectrum.

3.3 The galaxy power spectrum

The dark matter overdensity, $\delta_T(\mathbf{x})$ is usually modeled as a random field which is homogeneous and isotropic. This does not necessarily mean that it is Gaussian. Its Fourier transform $\delta_T(\mathbf{k})$ follows a simple relation [103, 104],

$$\langle \delta_T(\mathbf{k})\delta_T(\mathbf{k}') \rangle = (2\pi)^3 P_m(k)\delta^D(\mathbf{k} + \mathbf{k}'), \quad (3.167)$$

for some function $P_m(k)$ which is known as the matter power spectrum. It only depends on the magnitude of \mathbf{k} and not on its direction [105]. The notation “ $\langle \rangle$ ” denotes the ensemble average over all possible realizations. At tree-level, the matter power spectrum involves only the first-order δ_T and therefore,

$$\langle \delta_T^{(1)}(\mathbf{k}) \delta_T^{(1)}(\mathbf{k}') \rangle = (2\pi)^3 P(k) \delta^D(\mathbf{k} + \mathbf{k}') , \quad (3.168)$$

where $P(k)$ is the first-order matter power spectrum in T-gauge. Its expression is given in [38],

$$P(z, k) = \frac{9}{25} \frac{1}{\Omega_{m0}^2} \left(\frac{k}{H_0} \right)^4 T^2(k) D^2(z) P_{\Phi_P}(k) , \quad (3.169)$$

where we have restored the redshift dependence. $T(k)$ is the transfer function. It ensures that the amplitude of the k -modes of the gravitational field Φ which enter the Hubble sphere during radiation era, are suppressed relative to the modes which re-enter later, during the matter era. The plot for $T(k)$ is shown in Figure 3.5 below. We have used

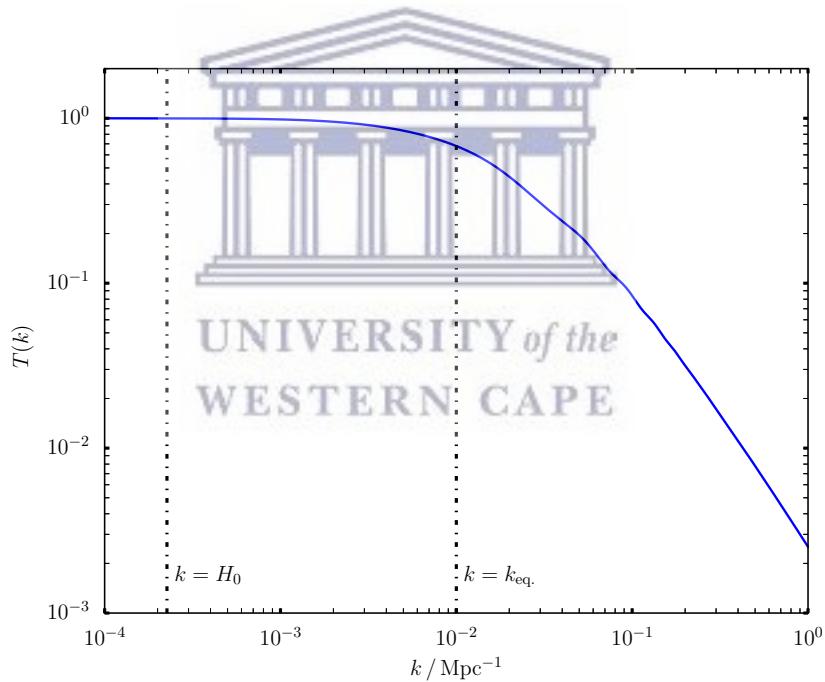


FIGURE 3.5: The transfer function T versus the wavenumber k / Mpc^{-1} . The wiggles show the effect of the baryons. The two critical scales are: the matter-radiation equality scale, $k_{\text{eq.}} \approx 10^{-2} \text{ Mpc}^{-1}$ and the Hubble scale at present time, $H_0 \approx 2.26 \times 10^{-4} \text{ Mpc}^{-1}$.

the fitting formula provided by [106],

$$T(k) = \frac{\Omega_{b0}}{\Omega_{m0}} T_b(k) + \frac{\Omega_{c0}}{\Omega_{m0}} T_c(k) , \quad (3.170)$$

which is a very good approximation. It splits the transfer function into baryonic and cold dark matter (CDM) parts where, $T_b(k)$ and $T_c(k)$ are the baryonic and CDM transfer

functions respectively. Ω_{b0} and Ω_{c0} are the densities of baryon and CDM defined today respectively. Ω_{m0} is the total matter density where,

$$\Omega_{m0} = \Omega_{b0} + \Omega_{c0} . \quad (3.171)$$

The other variables in (3.169) are:

- $D(z)$ is the growth factor and,
- P_{Φ_P} is the power spectrum of the primordial gravitational field Φ_P determined from inflation. It is given by [38],

$$P_{\Phi_P}(k) = \frac{50\pi^2}{9k^3} \left(\frac{k}{H_0} \right)^{n-1} \delta_H^2 \left[\frac{\Omega_{m0}}{D(z=0)} \right]^2 . \quad (3.172)$$

where $n = 0.9677$ is the spectral index [16]. The parameter δ_H is the curvature perturbation at horizon crossing during inflation and it can be parameterized by [106],

$$\delta_H = 1.94 \times 10^{-5} \Omega_{m0}^{-0.785-0.05 \ln \Omega_{m0}} e^{-0.95(n-1)-0.169(n-1)^2} . \quad (3.173)$$

For the tree-level galaxy power spectrum we can write [28],

$$\langle \Delta_g^{(1)}(\mathbf{k}) \Delta_g^{(1)}(\mathbf{k}') \rangle = (2\pi)^3 P_g(\mathbf{k}) \delta^D(\mathbf{k} + \mathbf{k}') . \quad (3.174)$$

where $\Delta_g^{(1)}$ is the first-order galaxy number count fluctuation. Using the Fourier transform of $\Delta_g^{(1)}$ given in (3.16) and the definition of the linear dark matter power spectrum in (3.168), we can show that (3.174) leads to [28],

$$P_g(\mathbf{k}) = \mathcal{K}^{(1)}(\mathbf{k}) \mathcal{K}^{(1)}(-\mathbf{k}) P(k) . \quad (3.175)$$

The galaxy power spectrum is also a real-valued function but unlike the matter power spectrum, it depends both on the magnitude and direction of \mathbf{k} . This is because the kernel $\mathcal{K}^{(1)}$ contains the first-order relativistic lightcone projection effects (see (3.17) and (3.18)) which depend on the direction cosine parameter $\mu = \hat{\mathbf{k}} \cdot \hat{\mathbf{n}}$. $\mathcal{K}^{(1)}$ is of the following form,

$$\mathcal{K}^{(1)} \sim [\mathcal{O}(k^0) + \mathcal{O}(k^{-2})] + i\mathcal{O}(k^{-1}) , \quad (3.176)$$

and therefore, we find that the linear galaxy power spectrum can be written as a series in k^{-n} ,

$$\frac{P_g(\mathbf{k})}{P(k)} \sim \frac{[\dots]}{k^0} + \frac{[\dots]}{k^2} + \frac{[\dots]}{k^4} . \quad (3.177)$$

where $n = 0, 1, 2, 3, 4$. We can work out the full expression of P_g by using the exact forms of $\mathcal{K}^{(1)}$ given by (3.17) and (3.18). We then obtain,

$$\frac{P_g(\mathbf{k})}{P(k)} = (b_1 + f\mu^2)^2 + [\mu^2(\gamma_1^2 + 2f\gamma_2) + 2b_1\gamma_2] \frac{1}{k^2} + \frac{4\gamma_2^2}{k^4}. \quad (3.178)$$

Since the galaxy power spectrum is a function of k and μ , it can be decomposed into its multipole moments, $P_g^\ell(k)$ using the special Legendre polynomials, $\mathcal{L}_\ell(\mu)$. This is written as follows [72, 107–109],

$$P_g(\mathbf{k}) = \sum_{\ell=0}^{\ell=4} P_g^\ell(k) \mathcal{L}_\ell(\mu), \quad (3.179)$$

where ℓ is the multipole index. It follows from (3.178) that the non-zero multipoles are $\ell = 0, 2$ and 4 . The corresponding multipoles are obtained as [109],

$$P_g^\ell(k) = \frac{(2\ell + 1)}{4\pi} \int_0^{2\pi} d\phi \int_{-1}^{+1} d\mu P_g(\mathbf{k}) \mathcal{L}_\ell(\mu). \quad (3.180)$$

Integrating over the azimuthal angle ϕ yields [72, 108],

$$P_g^\ell(k) = \frac{(2\ell + 1)}{2} \int_{-1}^{+1} d\mu P_g(\mathbf{k}) \mathcal{L}_\ell(\mu). \quad (3.181)$$

Here, we have assumed the “local plane-parallel approximation” as explained in [110]. In this approximation, the position vectors $(\mathbf{x}, \mathbf{x}')$ of a pair of galaxies separated by relevant scales are locally parallel i.e., $\mathbf{k} \cdot \mathbf{x} \approx \mathbf{k} \cdot \mathbf{x}'$ [109].

We consider the case of the monopole i.e., $\ell = 0$ and $\mathcal{L}_0(\mu) = 1$. Using (3.178) in (3.181) we find that,

$$\frac{P_g^0(k)}{P(k)} = \mathcal{P}_0 + \frac{\mathcal{P}_2}{k^2} + \frac{\mathcal{P}_4}{k^4}, \quad (3.182)$$

where,

$$\mathcal{P}_0 = b_1^2 + \frac{2}{3}fb_1 + \frac{f^2}{5}, \quad (3.183)$$

$$\mathcal{P}_2 = \frac{\gamma_1^2}{3} + 2\gamma_2 \left(b_1 + \frac{f}{3} \right), \quad (3.184)$$

$$\mathcal{P}_4 = 4\gamma_2^2. \quad (3.185)$$

In the Newtonian limit, $\gamma_1 = \gamma_2 = 0$ and hence, $\mathcal{P}_2 = \mathcal{P}_4 = 0$. Then (3.182) recovers the result presented in [108],

$$\frac{P_{gN}^0(k)}{P(k)} = \mathcal{P}_0 = b_1^2 + \frac{2}{3}fb_1 + \frac{f^2}{5}. \quad (3.186)$$

where the subscript ‘N’ denotes Newtonian. We show the numerics below in Figure 3.6 and Figure 3.7. We have used the latest Planck best-fit values [16], in particular for

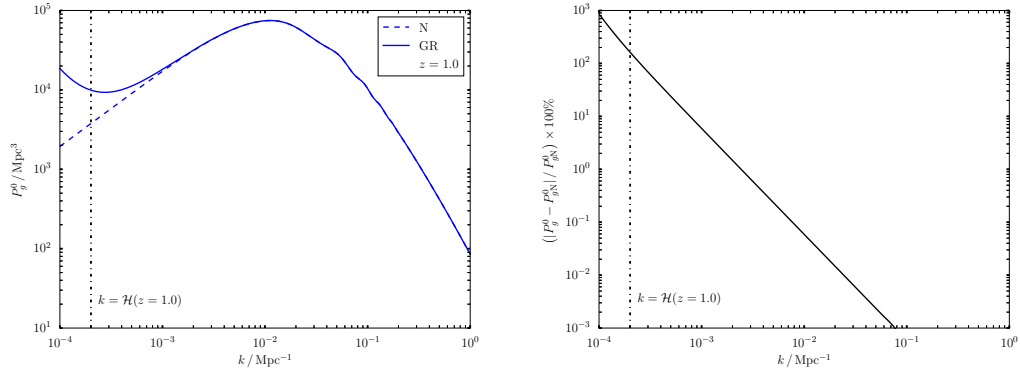


FIGURE 3.6: *Left*: The monopole of the linear galaxy power spectrum at $z = 1.0$. The solid curve is the full relativistic (GR) case given by (3.182). The dashed curve is the Newtonian (N) case given by (3.186). *Right*: The percentage difference relative to the Newtonian curve.

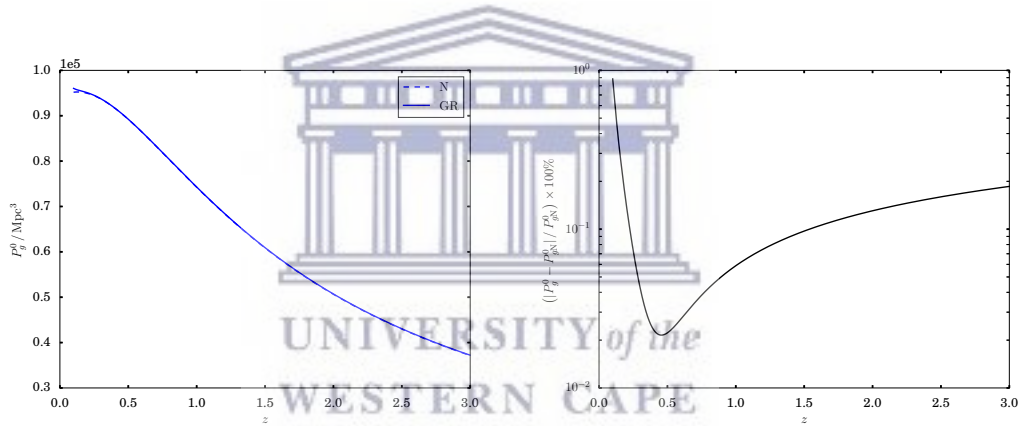


FIGURE 3.7: *Left*: The redshift evolution of the monopole of the linear galaxy power spectrum. *Right*: The percentage difference relative to the Newtonian curve.

$h = 0.678$ and $\Omega_{m0} = 1 - \Omega_{\Lambda0} = 0.308$. For the first-order galaxy bias we have chosen,

$$b_1 = \sqrt{1+z}, \quad (3.187)$$

and we have set the evolution bias and magnification bias to 0, i.e., $b_e = Q = 0$. We have neglected all the integrated terms. The *left* plot in Figure 3.6 shows the Newtonian approximation (dashed) and the full relativistic curve (solid). The GR effects boost the galaxy power spectrum on large scales with a percentage contribution of $\sim 0.1\%$ on equality scales and $\gtrsim 10\%$ on Gpc scales (*right* plot). The *left* plot in Figure 3.7 shows the redshift evolution of the monopole at $k_{\text{eq.}} = 10^{-2} \text{ Mpc}^{-1}$. The percentage difference varies between 0.01% and 1% (*right* plot).

3.4 The galaxy bispectrum

We begin with the Fourier definition of the bispectrum [104, 111, 112],

$$\langle \Delta_X(z, \mathbf{k}_1) \Delta_X(z, \mathbf{k}_2) \Delta_X(z, \mathbf{k}_3) \rangle = (2\pi)^3 B_X(z, \mathbf{k}_1, \mathbf{k}_2, \mathbf{k}_3) \delta^D(\mathbf{k}_1 + \mathbf{k}_2 + \mathbf{k}_3), \quad (3.188)$$

where Δ_X is the Fourier transform of the number density field of any biased objects. At tree-level the only combinations of terms that contribute to the bispectrum are,

$$\langle \Delta_X(\mathbf{k}_1) \Delta_X(\mathbf{k}_2) \Delta_X(\mathbf{k}_3) \rangle = \frac{1}{2} \langle \Delta_X^{(1)}(\mathbf{k}_1) \Delta_X^{(1)}(\mathbf{k}_2) \Delta_X^{(2)}(\mathbf{k}_3) \rangle + 2 \text{ cyc. perm.}, \quad (3.189)$$

where we suppress the redshift dependence for brevity. The factor 1/2 comes from the perturbative expansion of Δ_X ,

$$\Delta_X = \Delta_X^{(1)} + \frac{1}{2} \Delta_X^{(2)}. \quad (3.190)$$

The “2 cyc. perm.” indicates two cyclic permutations of the \mathbf{k} -vectors. Hence, for the galaxy number count fluctuation we can write,

$$\frac{1}{2} \langle \Delta_g^{(1)}(\mathbf{k}_1) \Delta_g^{(1)}(\mathbf{k}_2) \Delta_g^{(2)}(\mathbf{k}_3) \rangle + 2 \text{ cyc. perm.} = (2\pi)^3 B_g(\mathbf{k}_1, \mathbf{k}_2, \mathbf{k}_3) \delta^D(\mathbf{k}_1 + \mathbf{k}_2 + \mathbf{k}_3), \quad (3.191)$$

where B_g is the tree-level galaxy bispectrum. Applying the Newtonian-GR split (refer to Section 2.6) to the perturbations on the left-hand side of (3.191), we obtain the following,

$$\begin{aligned} \langle \Delta_g^{(1)}(\mathbf{k}_1) \Delta_g^{(1)}(\mathbf{k}_2) \Delta_g^{(2)}(\mathbf{k}_3) \rangle &= \langle \Delta_{gN}^{(1)}(\mathbf{k}_1) \Delta_{gN}^{(1)}(\mathbf{k}_2) \Delta_{gN}^{(2)}(\mathbf{k}_3) \rangle + \langle \Delta_{gGR}^{(1)}(\mathbf{k}_1) \Delta_{gGR}^{(1)}(\mathbf{k}_2) \Delta_{gGR}^{(2)}(\mathbf{k}_3) \rangle \\ &+ \langle \Delta_{gN}^{(1)}(\mathbf{k}_1) \Delta_{gN}^{(1)}(\mathbf{k}_2) \Delta_{gGR}^{(2)}(\mathbf{k}_3) \rangle + \langle \Delta_{gGR}^{(1)}(\mathbf{k}_1) \Delta_{gGR}^{(1)}(\mathbf{k}_2) \Delta_{gN}^{(2)}(\mathbf{k}_3) \rangle \\ &+ 2 \left[\langle \Delta_{gN}^{(1)}(\mathbf{k}_1) \Delta_{gGR}^{(1)}(\mathbf{k}_2) \Delta_{gN}^{(2)}(\mathbf{k}_3) \rangle + \langle \Delta_{gN}^{(1)}(\mathbf{k}_1) \Delta_{gGR}^{(1)}(\mathbf{k}_2) \Delta_{gGR}^{(2)}(\mathbf{k}_3) \rangle \right] \\ &+ 2 \text{ cyc. perm.}, \end{aligned} \quad (3.192)$$

where the first line splits into pure Newtonian and GR parts while the last two lines show the Newtonian-GR cross correlations.

3.4.1 Wick’s theorem

It is possible to express the galaxy bispectrum in terms of the kernels $\mathcal{K}^{(1)}$ and $\mathcal{K}^{(2)}$ by using the Wick’s theorem. To begin, we use the Fourier transforms of $\Delta_g^{(1)}$ and $\Delta_g^{(2)}$ given by (3.16) and (3.62) respectively in the left-hand side of (3.191). We obtain the

following,

$$\begin{aligned} \frac{1}{2} \langle \Delta_g^{(1)}(\mathbf{k}_1) \Delta_g^{(1)}(\mathbf{k}_2) \Delta_g^{(2)}(\mathbf{k}_3) \rangle &= \frac{1}{2} \int \frac{d^3 k'_1}{(2\pi)^3} \int d^3 k'_2 \mathcal{K}^{(1)}(\mathbf{k}_1) \mathcal{K}^{(1)}(\mathbf{k}_2) \mathcal{K}^{(2)}(\mathbf{k}'_1, \mathbf{k}'_2, \mathbf{k}_3) \\ &\quad \times \langle \delta_T^{(1)}(\mathbf{k}_1) \delta_T^{(1)}(\mathbf{k}_2) \delta_T^{(1)}(\mathbf{k}'_1) \delta_T^{(1)}(\mathbf{k}'_2) \rangle \\ &\quad \times \delta^D(\mathbf{k}'_1 + \mathbf{k}'_2 - \mathbf{k}_3) \\ &= \frac{1}{2} \left[\delta^D(\mathbf{k}_3) \langle \Delta_g^{(2)} \rangle \right] \langle \Delta_g^{(1)}(\mathbf{k}_1) \Delta_g^{(1)}(\mathbf{k}_2) \rangle, \end{aligned} \quad (3.193)$$

where the ensemble average of $\Delta_g^{(2)}$ in the last line is given by [72],

$$\langle \Delta_g^{(2)} \rangle = \int \frac{d^3 k}{(2\pi)^3} P(k) \mathcal{K}^{(2)}(\mathbf{k}, -\mathbf{k}, \mathbf{0}). \quad (3.194)$$

We apply the Wick's theorem [113–115] in the first line of (3.193) to split the 4-point correlators as products of 2-point correlators,

$$\begin{aligned} \langle \delta_T^{(1)}(\mathbf{k}_1) \delta_T^{(1)}(\mathbf{k}_2) \delta_T^{(1)}(\mathbf{k}'_1) \delta_T^{(1)}(\mathbf{k}'_2) \rangle &= \langle \delta_T^{(1)}(\mathbf{k}_1) \delta_T^{(1)}(\mathbf{k}_2) \rangle \langle \delta_T^{(1)}(\mathbf{k}'_1) \delta_T^{(1)}(\mathbf{k}'_2) \rangle \\ &\quad + \langle \delta_T^{(1)}(\mathbf{k}'_1) \delta_T^{(1)}(\mathbf{k}_1) \rangle \langle \delta_T^{(1)}(\mathbf{k}'_2) \delta_T^{(1)}(\mathbf{k}_2) \rangle \\ &\quad + \langle \delta_T^{(1)}(\mathbf{k}_1) \delta_T^{(1)}(\mathbf{k}'_2) \rangle \langle \delta_T^{(1)}(\mathbf{k}_2) \delta_T^{(1)}(\mathbf{k}'_1) \rangle. \end{aligned} \quad (3.195)$$

Use the definition of the first-order matter power spectrum given in (3.168), we show that (3.195) becomes,

$$\begin{aligned} \langle \delta_T^{(1)}(\mathbf{k}_1) \delta_T^{(1)}(\mathbf{k}_2) \delta_T^{(1)}(\mathbf{k}'_1) \delta_T^{(1)}(\mathbf{k}'_2) \rangle &= (2\pi)^6 \left[P^{(4)}(k_1) P^{(1)}(k'_1) \delta^D(\mathbf{k}_1 + \mathbf{k}_2) \delta^D(\mathbf{k}'_1 + \mathbf{k}'_2) \right. \\ &\quad + P^{(1)}(k'_1) P^{(1)}(k'_2) \delta^D(\mathbf{k}'_1 + \mathbf{k}_1) \delta^D(\mathbf{k}'_2 + \mathbf{k}_2) \\ &\quad \left. + P^{(1)}(k_1) P^{(1)}(k_2) \delta^D(\mathbf{k}_1 + \mathbf{k}'_2) \delta^D(\mathbf{k}_2 + \mathbf{k}'_1) \right]. \end{aligned} \quad (3.196)$$

We then use (3.196) in the first line of (3.193) and perform the integrals. We use the symmetrical property of the Dirac-delta function i.e., $\delta^D(-\mathbf{k}) = \delta^D(\mathbf{k})$ and we obtain the following,

$$\begin{aligned} \frac{1}{2} (2\pi)^3 P^{(1)}(k_1) \delta^D(\mathbf{k}_1 + \mathbf{k}_2) \mathcal{K}^{(1)}(\mathbf{k}_1) \mathcal{K}^{(1)}(\mathbf{k}_2) \delta^D(-\mathbf{k}_3) &\left[\int \frac{d^3 k'_1}{(2\pi)^3} P^{(1)}(k'_1) \mathcal{K}^{(2)}(\mathbf{k}'_1, -\mathbf{k}'_1, \mathbf{0}) \right] \\ + (2\pi)^3 \mathcal{K}^{(1)}(\mathbf{k}_1) \mathcal{K}^{(1)}(\mathbf{k}_2) \mathcal{K}^{(2)}(\mathbf{k}_1, \mathbf{k}_2, \mathbf{k}_3) &P^{(1)}(k_1) P^{(1)}(k_2) \delta^D(-\mathbf{k}_1 - \mathbf{k}_2 - \mathbf{k}_3), \end{aligned}$$

where the first line is just,

$$\frac{1}{2} \left[\delta^D(\mathbf{k}_3) \langle \Delta_g^{(2)} \rangle \right] \langle \Delta_g^{(1)}(\mathbf{k}_1) \Delta_g^{(1)}(\mathbf{k}_2) \rangle,$$

which cancels with the second term in (3.193). Therefore, we are finally left with,

$$\begin{aligned} \frac{1}{2} \langle \Delta_g^{(1)}(\mathbf{k}_1) \Delta_g^{(1)}(\mathbf{k}_2) \Delta_g^{(2)}(\mathbf{k}_3) \rangle &= (2\pi)^3 \mathcal{K}^{(1)}(\mathbf{k}_1) \mathcal{K}^{(1)}(\mathbf{k}_2) \mathcal{K}^{(2)}(\mathbf{k}_1, \mathbf{k}_2, \mathbf{k}_3) P^{(1)}(k_1) P^{(1)}(k_2) \\ &\quad \times \delta^D(\mathbf{k}_1 + \mathbf{k}_2 + \mathbf{k}_3). \end{aligned} \quad (3.197)$$

Then (3.191) and (3.197) imply that,

$$B_g(\mathbf{k}_1, \mathbf{k}_2, \mathbf{k}_3) = \mathcal{K}^{(1)}(\mathbf{k}_1) \mathcal{K}^{(1)}(\mathbf{k}_2) \mathcal{K}^{(2)}(\mathbf{k}_1, \mathbf{k}_2, \mathbf{k}_3) P^{(1)}(k_1) P^{(1)}(k_2) + 2 \text{ cyc. perm.}, \quad (3.198)$$

and splitting the kernels into Newtonian and GR parts leads to,

$$\begin{aligned} B_g(\mathbf{k}_1, \mathbf{k}_2, \mathbf{k}_3) &= \left[\mathcal{K}_N^{(1)}(\mathbf{k}_1) \mathcal{K}_N^{(1)}(\mathbf{k}_2) \mathcal{K}_N^{(2)}(\mathbf{k}_1, \mathbf{k}_2, \mathbf{k}_3) + \mathcal{K}_{GR}^{(1)}(\mathbf{k}_1) \mathcal{K}_{GR}^{(1)}(\mathbf{k}_2) \mathcal{K}_{GR}^{(2)}(\mathbf{k}_1, \mathbf{k}_2, \mathbf{k}_3) \right. \\ &\quad + \mathcal{K}_N^{(1)}(\mathbf{k}_1) \mathcal{K}_N^{(1)}(\mathbf{k}_2) \mathcal{K}_{GR}^{(2)}(\mathbf{k}_1, \mathbf{k}_2, \mathbf{k}_3) + \mathcal{K}_{GR}^{(1)}(k_1) \mathcal{K}_{GR}^{(1)}(k_2) \mathcal{K}_N^{(2)}(\mathbf{k}_1, \mathbf{k}_2, \mathbf{k}_3) \\ &\quad \left. + 2 \mathcal{K}_N^{(1)}(\mathbf{k}_1) \mathcal{K}_{GR}^{(1)}(\mathbf{k}_2) \left\{ \mathcal{K}_N^{(2)}(\mathbf{k}_1, \mathbf{k}_2, \mathbf{k}_3) + \mathcal{K}_{GR}^{(2)}(\mathbf{k}_1, \mathbf{k}_2, \mathbf{k}_3) \right\} \right] P(k_1) P(k_2) \\ &\quad + 2 \text{ cyc. perm.}, \end{aligned} \quad (3.199)$$

where $\mathcal{K}_{GR}^{(2)} = \mathcal{K}_S^{(2)} + \mathcal{K}_V^{(2)} + \mathcal{K}_T^{(2)}$ and we write P for $P^{(1)}$ from now on. The equation above is the full expression for the galaxy bispectrum. If we neglect the GR lightcone projection effects, then the only term surviving in (3.199) is the first term which is the Newtonian galaxy bispectrum,

$$B_{gN}(\mathbf{k}_1, \mathbf{k}_2, \mathbf{k}_3) = \mathcal{K}_N^{(1)}(\mathbf{k}_1) \mathcal{K}_N^{(1)}(\mathbf{k}_2) \mathcal{K}_N^{(2)}(\mathbf{k}_1, \mathbf{k}_2, \mathbf{k}_3) P(k_1) P(k_2) + 2 \text{ cyc. perm.} \quad (3.200)$$

3.4.2 The multipoles of the galaxy bispectrum

In Section 3.2 we have seen that the kernels are complex and therefore, they can be represented as follows,

$$\mathcal{K}^{(1)} = \mathcal{K}_R^{(1)} + i\mathcal{K}_I^{(1)} \quad \text{and} \quad \mathcal{K}^{(2)} = \mathcal{K}_R^{(2)} + i\mathcal{K}_I^{(2)}. \quad (3.201)$$

This makes the galaxy bispectrum to be a complex function. We can work out the real and imaginary parts by using (3.201) in (3.198). We find that the real part is,

$$\begin{aligned} B_{gR} &= \left[\mathcal{K}_{123R}^{(2)} \left(\mathcal{K}_{1R}^{(1)} \mathcal{K}_{2R}^{(1)} - \mathcal{K}_{1I}^{(1)} \mathcal{K}_{2I}^{(1)} \right) - \mathcal{K}_{123I}^{(2)} \left(\mathcal{K}_{1R}^{(1)} \mathcal{K}_{2I}^{(1)} + \mathcal{K}_{1I}^{(1)} \mathcal{K}_{2R}^{(1)} \right) \right] P(k_1) P(k_2) \\ &\quad + 2 \text{ cyc. perm.}, \end{aligned} \quad (3.202)$$

and the imaginary part is,

$$B_{gI} = \left[\mathcal{K}_{123R}^{(2)} \left(\mathcal{K}_{1R}^{(1)} \mathcal{K}_{2I}^{(1)} + \mathcal{K}_{1I}^{(1)} \mathcal{K}_{2R}^{(1)} \right) + \mathcal{K}_{123I}^{(2)} \left(\mathcal{K}_{1R}^{(1)} \mathcal{K}_{2R}^{(1)} - \mathcal{K}_{1I}^{(1)} \mathcal{K}_{2I}^{(1)} \right) \right] P(k_1) P(k_2) + 2 \text{ cyc. perm. } , \quad (3.203)$$

where $\mathcal{K}_i^{(1)} \equiv \mathcal{K}^{(1)}(\mathbf{k}_i)$ and $\mathcal{K}_{ijk}^{(2)} \equiv \mathcal{K}^{(2)}(\mathbf{k}_i, \mathbf{k}_j, \mathbf{k}_k)$. Both B_{gR} and B_{gI} depend on the three mode vectors and angles (μ_1, ω) i.e.,

$$B_{gR} \equiv B_{gR}(k_1, k_2, k_3, \mu_1, \omega) , \quad B_{gI} \equiv B_{gI}(k_1, k_2, k_3, \mu_1, \omega) . \quad (3.204)$$

The dependence on μ_1 and ω can be expanded in spherical harmonics, $Y_{\ell m}(\mu_1, \omega)$. The spherical harmonics are a set of basis functions for solutions of the Laplace equation,

$$\nabla_{\Omega}^2 Y_{\ell m}(\mu_1, \omega) = 0 , \quad (3.205)$$

defined on a sphere. They are related to the Legendre function $\mathcal{L}_{\ell}(\mu_1)$ as [116, 117],

$$Y_{\ell m}(\mu_1, \omega) = (-1)^m \sqrt{\frac{(2\ell+1)(\ell-m)!}{4\pi(\ell+m)!}} \mathcal{L}_{\ell}(\mu_1) e^{im\omega} , \quad (3.206)$$

and follow the orthogonal rule [117],

$$\int d\Omega Y_{\ell m}(\mu_1, \omega) Y_{\ell' m'}(\mu_1, \omega) = \delta_{\ell\ell'} \delta_{mm'} , \quad (3.207)$$

where $\ell = 0, 1, 2, 3, \dots$, $m = -\ell, -\ell+1, \dots, \ell-1, \ell$ and $d\Omega = -d\mu_1 d\omega$. We expand the real and imaginary parts of the galaxy bispectrum as,

$$B_{gR}(k_1, k_2, k_3, \mu_1, \omega) = \sum_{\ell=0}^{\infty} \sum_{m=-\ell}^{\ell} B_{gR}^{\ell m}(k_1, k_2, k_3) Y_{\ell m}(\mu_1, \omega) , \quad (3.208)$$

$$B_{gI}(k_1, k_2, k_3, \mu_1, \omega) = \sum_{\ell=0}^{\infty} \sum_{m=-\ell}^{\ell} B_{gI}^{\ell m}(k_1, k_2, k_3) Y_{\ell m}(\mu_1, \omega) . \quad (3.209)$$

Inverting (3.208) and (3.209) leads to [117],

$$B_{gR}^{\ell m}(k_1, k_2, k_3) = \sqrt{\frac{1}{4\pi(2\ell+1)}} \int_0^{2\pi} d\omega \int_{-1}^{+1} d\mu_1 B_{gR}(k_1, k_2, k_3, \mu_1, \omega) Y_{\ell m}^*(\mu_1, \omega) , \quad (3.210)$$

$$B_{gI}^{\ell m}(k_1, k_2, k_3) = \sqrt{\frac{1}{4\pi(2\ell+1)}} \int_0^{2\pi} d\omega \int_{-1}^{+1} d\mu_1 B_{gI}(k_1, k_2, k_3, \mu_1, \omega) Y_{\ell m}^*(\mu_1, \omega) , \quad (3.211)$$

where $(B_{gR}^{\ell m}, B_{gI}^{\ell m})$ are the multipoles and $Y_{\ell m}^*(\mu_1, \omega)$ is the complex conjugate of $Y_{\ell m}(\mu_1, \omega)$. The integration over μ_1 and ω moves the xyz -axes around \mathbf{n} covering all the possible triangular orientations. If we consider the spherical harmonics as a set of real functions, usually known as *tesseral spherical harmonics*, then (3.206) is written as,

$$Y_{\ell m}(\mu_1, \omega) = (-1)^m \sqrt{2} \sqrt{\frac{(2\ell+1)(\ell-|m|)!}{4\pi(\ell+|m|)!}} \mathcal{L}_\ell(\mu_1) \sin |m|\omega \quad \text{for } m < 0, \quad (3.212)$$

$$Y_{\ell 0}(\mu_1) = \sqrt{\frac{(2\ell+1)}{4\pi}} \mathcal{L}_\ell(\mu_1) \quad \text{for } m = 0, \quad (3.213)$$

$$Y_{\ell m}(\mu_1, \omega) = (-1)^m \sqrt{2} \sqrt{\frac{(2\ell+1)(\ell-m)!}{4\pi(\ell+m)!}} \mathcal{L}_\ell(\mu_1) \cos m\omega \quad \text{for } m > 0. \quad (3.214)$$

In this thesis, we work with $m = 0$ for simplicity. Most of the information is in the $m = 0$ modes [118]. Therefore, (3.213) shows that the spherical harmonics are proportional to the Legendre polynomials i.e.,

$$Y_{\ell 0}(\mu_1) = Y_{\ell 0}^*(\mu_1) \propto \mathcal{L}_\ell(\mu_1), \quad (3.215)$$

which have even powers of μ_1 for even ℓ 's and odd powers of μ_1 for odd ℓ 's. With *SymPy* (Symbolic Python), it is possible to obtain the exact expressions for the real and imaginary parts of the galaxy bispectrum (neglecting vectors and tensors for simplicity) as,

$$B_{gR}(k_1, k_2, k_3, \mu_{12}, \mu_1, \omega) = \sum_{i=\text{even}} \sum_{j=\text{even}} \mathcal{R}_{ij}(k_1, k_2, k_3, \mu_{12}) \mu_1^i \cos^j(\omega) + \sum_{i'=\text{odd}} \sum_{j'=\text{odd}} \mathcal{R}_{i'j'}(k_1, k_2, k_3, \mu_{12}) \mu_1^{i'} \sqrt{1-\mu_1^2} \cos^{j'}(\omega), \quad (3.216)$$

$$B_{gI}(k_1, k_2, k_3, \mu_{12}, \mu_1, \omega) = \sum_{i=\text{odd}} \sum_{j=\text{even}} \mathcal{I}_{ij}(k_1, k_2, k_3, \mu_{12}) \mu_1^i \cos^j(\omega) + \sum_{i'=\text{odd}} \sum_{j'=\text{even}} \mathcal{I}_{i'j'}(k_1, k_2, k_3, \mu_{12}) \mu_1^{j'} \sqrt{1-\mu_1^2} \cos^{i'}(\omega). \quad (3.217)$$

Then, the integration over μ_1 and ω in (3.210) and (3.211) admits,

$$B_{gR}^{\ell 0}(k_1, k_2, k_3) = 0, \quad B_{gI}^{\ell 0}(k_1, k_2, k_3) \neq 0, \quad \text{for } \ell = 1, 3, 5, \dots \quad (3.218)$$

$$B_{gR}^{\ell 0}(k_1, k_2, k_3) \neq 0, \quad B_{gI}^{\ell 0}(k_1, k_2, k_3) = 0, \quad \text{for } \ell = 0, 2, 4, \dots \quad (3.219)$$

For the monopole, $\ell = 0$ and $\mathcal{L}_0(\mu_1) = 1$. Then we have,

$$B_g^0(k_1, k_2, k_3) = B_{gR}^{00}(k_1, k_2, k_3), \quad (3.220)$$

where we define the shorthand notation $B_g^\ell \equiv B_g^{\ell 0}$. We find that the monopole is always real. For the case of the dipole ($\ell = 1$) we have,

$$B_g^1(k_1, k_2, k_3) = B_{gI}^{10}(k_1, k_2, k_3), \quad (3.221)$$

which is purely imaginary. Future work will look at the different multipoles of the galaxy bispectrum in more details.

3.4.3 The monopole in the squeezed configuration

We derive the analytical expressions for the monopole in the squeezed limit ($\theta_{12} = 180^\circ \implies \mu_{12} = -1$). In that configuration we have,

$$\mathbf{k}_2 \approx -\mathbf{k}_1 = -\mathbf{k}_S, \quad \mathbf{k}_3 = \mathbf{k}_L, \quad \mathbf{k}_S \cdot \mathbf{k}_L \approx 0, \quad \mu_2 \approx -\mu_1 = -\mu_S, \quad \mu_3 = \mu_L, \quad (3.222)$$

and for the magnitudes of the mode vectors,

$$k_1 \approx k_2 = k_S \gg k_3 = k_L, \quad (3.223)$$

where S and L denote the short and long modes respectively. To obtain μ_L , we start by defining ε ($\ll 1$) which is the angle between $\mathbf{k}_1 = \mathbf{k}_S$ and $\mathbf{k}_2 \approx -\mathbf{k}_S$ in the head-tail configuration for a closed triangle with the third side $\mathbf{k}_3 = \mathbf{k}_L$. Since θ_{12} is the angle between \mathbf{k}_1 and \mathbf{k}_2 when they are tail to tail then,

$$\theta_{12} = \arccos \hat{\mathbf{k}}_1 \cdot \hat{\mathbf{k}}_2 = \pi - \varepsilon. \quad (3.224)$$

Applying (3.222) to the identities given in (3.104) and (3.106) we obtain,

$$\mu_2 = \mu_S \left(-1 + \frac{\varepsilon^2}{2} \right) + \varepsilon \sqrt{1 - \mu_S^2} \cos \omega + \mathcal{O}(\varepsilon^3), \quad (3.225)$$

$$k_L^2 = k_S^2 \varepsilon^2 + \mathcal{O}(\varepsilon^4). \quad (3.226)$$

Neglecting the higher powers for ε leads to,

$$\mu_2 = -\mu_S + \varepsilon \sqrt{1 - \mu_S^2} \cos \omega \quad \text{and} \quad k_L = \varepsilon k_S. \quad (3.227)$$

Then, using the conservation for the mode vectors given by (3.105) we have,

$$\mu_L = -(\mu_S + \mu_2) \frac{k_S}{k_L} = -\sqrt{1 - \mu_S^2} \cos \omega . \quad (3.228)$$

We can now obtain the exact expressions for the kernels. At first order (see (3.16)),

$$\mathcal{K}^{(1)}(\mathbf{k}_S) = b_{1S} + i\gamma_1 \frac{\mu_S}{k_S} + \mathcal{O}(k_S^{-2}) \quad \text{and} \quad \mathcal{K}^{(1)}(\mathbf{k}_L) = b_{1L} + i\gamma_1 \frac{\mu_L}{k_L} + \frac{\gamma_2}{k_L^2} , \quad (3.229)$$

where we define,

$$b_{1S} = b_1 + f\mu_S^2 \quad \text{and} \quad b_{1L} = b_1 + f\mu_L^2 . \quad (3.230)$$

At second-order, the F_2 and G_2 kernels (see (3.27) and (3.28)) become,

$$F_2(\mathbf{k}_S, -\mathbf{k}_S) = 0 , \quad F_2(\mathbf{k}_S, \mathbf{k}_L) = \frac{10}{7} , \quad G_2(\mathbf{k}_S, -\mathbf{k}_S) = 0 \quad \text{and} \quad G_2(\mathbf{k}_S, \mathbf{k}_L) = \frac{6}{7} . \quad (3.231)$$

We neglect the tidal term for simplicity. Then, the Newtonian kernel in (3.63) gives,

$$\mathcal{K}_N^{(2)}(\mathbf{k}_S, -\mathbf{k}_S, \mathbf{k}_L) = b_2 , \quad (3.232)$$

$$\mathcal{K}_N^{(2)}(\mathbf{k}_L, \mathbf{k}_S, -\mathbf{k}_S) = b_{SL} + fb_{1S}\mu_S\mu_L \frac{k_S}{k_L} , \quad (3.233)$$

$$\mathcal{K}_N^{(2)}(-\mathbf{k}_S, \mathbf{k}_L, \mathbf{k}_S) = \mathcal{K}_N^{(2)}(\mathbf{k}_L, \mathbf{k}_S, -\mathbf{k}_S) \Big|_{\mu_S \rightarrow -\mu_S} , \quad (3.234)$$

where,

$$b_{SL} = \frac{10}{7}b_1 + b_2 + \frac{6}{7}\mu_S^2 + b_1f(\mu_S^2 + \mu_L^2) + 2f^2\mu_S^2\mu_L^2 . \quad (3.235)$$

For the second-order scalars (S) given by (3.65) we obtain,

$$\mathcal{K}_S^{(2)}(\mathbf{k}_S, -\mathbf{k}_S, \mathbf{k}_L) = \mathcal{O}(k_S^{-2}) , \quad (3.236)$$

$$\begin{aligned} \mathcal{K}_S^{(2)}(\mathbf{k}_L, \mathbf{k}_S, -\mathbf{k}_S) &= \Gamma_5 \frac{\mu_S\mu_L}{k_S k_L} + \frac{(\Gamma_7 + \Gamma_8\mu_S^2)}{k_L^2} + i \left[\Gamma_2 \frac{\mu_S}{k_S k_L^2} + (\Gamma_9 + \Gamma_{12}\mu_S^2)\mu_S \frac{k_S}{k_L^2} \right. \\ &\quad \left. + (\Gamma_{11} + \Gamma_{13}\mu_S^2) \frac{\mu_L}{k_L} \right] + \mathcal{O}(k_S^{-2}) , \end{aligned} \quad (3.237)$$

$$\mathcal{K}_S^{(2)}(-\mathbf{k}_S, \mathbf{k}_L, \mathbf{k}_S) = \mathcal{K}_S^{(2)}(\mathbf{k}_L, \mathbf{k}_S, -\mathbf{k}_S) \Big|_{\mu_S \rightarrow -\mu_S} . \quad (3.238)$$

For the vectors and tensors (see Section 3.2.2.2 and Section 3.2.2.3) we obtain exactly 0 (squeezed limit $\implies \mu_{12} = -1$) i.e.,

$$\mathcal{K}_V^{(2)}(\mathbf{k}_S, -\mathbf{k}_S, \mathbf{k}_L) = \mathcal{K}_V^{(2)}(\mathbf{k}_L, \mathbf{k}_S, -\mathbf{k}_S) = \mathcal{K}_V^{(2)}(-\mathbf{k}_S, \mathbf{k}_L, \mathbf{k}_S) = 0 , \quad (3.239)$$

$$\mathcal{K}_T^{(2)}(\mathbf{k}_S, -\mathbf{k}_S, \mathbf{k}_L) = \mathcal{K}_T^{(2)}(\mathbf{k}_L, \mathbf{k}_S, -\mathbf{k}_S) = \mathcal{K}_T^{(2)}(-\mathbf{k}_S, \mathbf{k}_L, \mathbf{k}_S) = 0 . \quad (3.240)$$

We now have all the tools to derive the analytical expressions for the galaxy bispectrum in the squeezed limit,

$$\begin{aligned}
B_g^{\text{sq}} &= \mathcal{K}^{(1)}(\mathbf{k}_S)\mathcal{K}^{(1)}(-\mathbf{k}_S) \left[\mathcal{K}_N^{(2)}(\mathbf{k}_S, -\mathbf{k}_S, \mathbf{k}_L) + \mathcal{K}_{\text{GR}}^{(2)}(\mathbf{k}_S, -\mathbf{k}_S, \mathbf{k}_L) \right] [P^{(1)}(k_S)]^2 \\
&+ \mathcal{K}^{(1)}(-\mathbf{k}_S)\mathcal{K}^{(1)}(\mathbf{k}_L) \left[\mathcal{K}_N^{(2)}(-\mathbf{k}_S, \mathbf{k}_L, \mathbf{k}_S) + \mathcal{K}_{\text{GR}}^{(2)}(-\mathbf{k}_S, \mathbf{k}_L, \mathbf{k}_S) \right] P^{(1)}(k_S)P^{(1)}(k_L) \\
&+ \mathcal{K}^{(1)}(\mathbf{k}_L)\mathcal{K}^{(1)}(\mathbf{k}_S) \left[\mathcal{K}_N^{(2)}(\mathbf{k}_L, \mathbf{k}_S, -\mathbf{k}_S) + \mathcal{K}_{\text{GR}}^{(2)}(\mathbf{k}_L, \mathbf{k}_S, -\mathbf{k}_S) \right] P^{(1)}(k_L)P^{(1)}(k_S),
\end{aligned} \tag{3.241}$$

where $\mathcal{K}_{\text{GR}}^{(2)} = \mathcal{K}_S^{(2)} + \mathcal{K}_V^{(2)} + \mathcal{K}_T^{(2)}$. We drop the first line in (3.241) because the coupling between two short modes is negligible compared to the coupling between a short- and long mode i.e., $[P^{(1)}(k_S)]^2 \ll P^{(1)}(k_S)P^{(1)}(k_L)$. For the scalars we find,

$$\begin{aligned}
\frac{B_{gS}^{\text{sq}}}{P^{(1)}(k_L)P^{(1)}(k_S)} &= \left(b_{1L} + i\gamma_1 \frac{\mu_L}{k_L} + \frac{\gamma_2}{k_L^2} \right) \left(b_{1S} + i\gamma_1 \frac{\mu_S}{k_S} \right) \left\{ b_{SL} + f b_{1S} \mu_S \mu_L \frac{k_S}{k_L} + \Gamma_5 \frac{\mu_S \mu_L}{k_S k_L} \right. \\
&+ \left. \frac{(\Gamma_7 + \Gamma_8 \mu_S^2)}{k_L^2} + i \left[\Gamma_2 \frac{\mu_S}{k_S k_L^2} + (\Gamma_9 + \Gamma_{12} \mu_S^2) \mu_S \frac{k_S}{k_L^2} + (\Gamma_{11} + \Gamma_{13} \mu_S^2) \frac{\mu_L}{k_L} \right] \right\} \\
&+ \left(b_{1L} + i\gamma_1 \frac{\mu_L}{k_L} + \frac{\gamma_2}{k_L^2} \right) \left(b_{1S} - i\gamma_1 \frac{\mu_S}{k_S} \right) \left\{ b_{SL} - f b_{1S} \mu_S \mu_L \frac{k_S}{k_L} - \Gamma_5 \frac{\mu_S \mu_L}{k_S k_L} \right. \\
&+ \left. \frac{(\Gamma_7 + \Gamma_8 \mu_S^2)}{k_L^2} + i \left[-\Gamma_2 \frac{\mu_S}{k_S k_L^2} - (\Gamma_9 + \Gamma_{12} \mu_S^2) \mu_S \frac{k_S}{k_L^2} + (\Gamma_{11} + \Gamma_{13} \mu_S^2) \frac{\mu_L}{k_L} \right] \right\}
\end{aligned} \tag{3.242}$$

The expansion of (3.242) gives,

$$\begin{aligned}
\frac{B_{gS}^{\text{sq}}}{2P^{(1)}(k_L)P^{(1)}(k_S)} &= b_{1S}b_{1L}b_{SL} + \left[b_{1S}(b_{SL}\gamma_2 - f\gamma_1^2\mu_S^2\mu_L^2) + b_{1S}b_{1L}(\Gamma_7 + \Gamma_8\mu_S^2) \right. \\
&- \left. b_{1L}\gamma_1(\Gamma_9 + \Gamma_{12}\mu_S^2)\mu_S^2 - b_{1S}\gamma_1(\Gamma_{11} + \Gamma_{13}\mu_S^2)\mu_L^2 \right] \frac{1}{k_L^2} \\
&+ \gamma_2 \left[b_{1S}(\Gamma_7 + \Gamma_8\mu_S^2) - \gamma_1(\Gamma_9 + \Gamma_{12}\mu_S^2)\mu_S^2 \right] \frac{1}{k_L^4},
\end{aligned} \tag{3.243}$$

where we neglect the terms proportional to odd powers of μ_S and μ_L because,

$$\frac{1}{2} \int_{-1}^{+1} d\mu_S (\mu_S)^n = \frac{1}{2\pi} \int_0^{2\pi} d\omega (\mu_L)^n = 0 \quad \text{for odd } n. \tag{3.244}$$

We average (3.243) over ω to eliminate μ_L^2 since (3.228) shows that,

$$\frac{1}{2\pi} \int_0^{2\pi} d\omega \mu_L^2 = 1 - \mu_S^2. \tag{3.245}$$

Then, we average over μ_S to obtain the monopole as,

$$\frac{B_{gS}^{\text{sq } 0}}{2P^{(1)}(k_L)P^{(1)}(k_S)} = \mathcal{B}_0 + \frac{\mathcal{B}_2}{k_L^2} + \frac{\mathcal{B}_4}{k_L^4}, \quad (3.246)$$

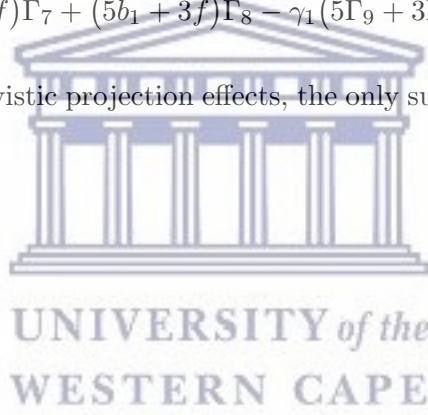
where,

$$\begin{aligned} \mathcal{B}_0 = & \frac{20}{7}b_1^3 + \frac{52}{21}b_1^2b_2 + 2b_1^2b_2 + \frac{4}{3}b_1b_2f + \frac{68}{105}b_1f^2 + \frac{4}{3}b_1^3f + \frac{4}{3}b_1^2f + \frac{12}{35}b_1f^3 \\ & + \frac{12}{15}b_2f^2 + \frac{12}{245}f^3 + \frac{4}{105}f^4, \end{aligned} \quad (3.247)$$

$$\begin{aligned} \mathcal{B}_2 = & \frac{2}{105} \left\{ \gamma_2(80b_1f + 42b_1f^2 + 105b_1^2 + 70b_1^2f + 105b_1b_2 + 35b_2f + 18f^2 + 6f^3) \right. \\ & + 7b_1 \left[5(3b_1 + f)\Gamma_7 + (5b_1 + 3f)\Gamma_8 \right] - \gamma_1 \left[(35b_1 + 7f)\Gamma_{11} + (7b_1 + 3f)\Gamma_{13} \right] \\ & + f \left[(35b_1 + 7f)\Gamma_7 + (7b_1 + 3f)\Gamma_8 \right] - \gamma_1 \left[(7b_1 + 3f)f\gamma_1 + 7(5b_1 + f)\Gamma_9 \right. \\ & \left. \left. + 3(7b_1 + f)\Gamma_{12} \right] \right\}, \end{aligned} \quad (3.248)$$

$$\mathcal{B}_4 = \frac{2}{15}\gamma_2 \left[5(3b_1 + f)\Gamma_7 + (5b_1 + 3f)\Gamma_8 - \gamma_1(5\Gamma_9 + 3\Gamma_{12}) \right]. \quad (3.249)$$

In the absence of relativistic projection effects, the only surviving term is the Newtonian term \mathcal{B}_0 .



Chapter 4

The GR projection effects in the Gaussian galaxy bispectrum

In this chapter we present the numerical results. We are using our own Fortran code which computes the galaxy bispectrum for any triangular shapes, including all the second-order local relativistic effects discussed in Chapter 3. We choose an isosceles configuration,

$$k_1 = k_2 = k_S \quad \text{and} \quad k_3 = k_L = k_S \sqrt{2(1 + \mu_{12})}. \quad (4.1)$$

where we have set $r = 1$ in (3.107). For the astrophysical parameters, we use:

$$b_1(z) = \sqrt{1+z}, \quad b_2(z) = -0.1\sqrt{1+z}, \quad b_e = \mathcal{Q} = 0, \quad (4.2)$$

and consider $z = 1$. We want to show the contributions of the second-order scalars (S), vectors (V) and tensors (T) in the monopole³. Since the vectors vanish for an equilateral shape (see (3.126)-(3.128)), therefore we choose a moderately squeezed shape with $\mu_{12} = -0.999$ ($\theta_{12} = 177^\circ$). Then, from (4.1) we find that $k_3 \approx k_S/16$.

4.1 Method of computation

- We define:

- The Newtonian galaxy bispectrum $B_{gN}(\mathbf{k}_1, \mathbf{k}_2, \mathbf{k}_3)$ as,

$$\mathcal{K}_N^{(1)}(\mathbf{k}_1)\mathcal{K}_N^{(1)}(\mathbf{k}_2)\mathcal{K}_N^{(2)}(\mathbf{k}_1, \mathbf{k}_2, \mathbf{k}_3)P^{(1)}(k_1)P^{(1)}(k_2) + 2 \text{ cycl. perm.} \quad (4.3)$$

³The imaginary part of the monopole of B_g is always 0 (refer to Section 3.4.3).

- The GR galaxy bispectrum with second-order scalars $B_{gS}(\mathbf{k}_1, \mathbf{k}_2, \mathbf{k}_3)$ as,

$$\mathcal{K}^{(1)}(\mathbf{k}_1)\mathcal{K}^{(1)}(\mathbf{k}_2)\mathcal{K}_S^{(2)}(\mathbf{k}_1, \mathbf{k}_2, \mathbf{k}_3)P^{(1)}(k_1)P^{(1)}(k_2) + 2 \text{ cycl. perm.} \quad (4.4)$$

where $\mathcal{K}^{(1)} = \mathcal{K}_N^{(1)} + \mathcal{K}_{GR}^{(1)}$.

- The GR galaxy bispectrum with second-order vectors $B_{gV}(\mathbf{k}_1, \mathbf{k}_2, \mathbf{k}_3)$ as,

$$\mathcal{K}^{(1)}(\mathbf{k}_1)\mathcal{K}^{(1)}(\mathbf{k}_2)\mathcal{K}_V^{(2)}(\mathbf{k}_1, \mathbf{k}_2, \mathbf{k}_3)P^{(1)}(k_1)P^{(1)}(k_2) + 2 \text{ cycl. perm.} \quad (4.5)$$

- The GR galaxy bispectrum with second-order tensors $B_{gT}(\mathbf{k}_1, \mathbf{k}_2, \mathbf{k}_3)$ as,

$$\mathcal{K}^{(1)}(\mathbf{k}_1)\mathcal{K}^{(1)}(\mathbf{k}_2)\mathcal{K}_T^{(2)}(\mathbf{k}_1, \mathbf{k}_2, \mathbf{k}_3)P^{(1)}(k_1)P^{(1)}(k_2) + 2 \text{ cycl. perm.} \quad (4.6)$$

- The full GR galaxy bispectrum $B_g(\mathbf{k}_1, \mathbf{k}_2, \mathbf{k}_3)$ as,

$$\mathcal{K}^{(1)}(\mathbf{k}_1)\mathcal{K}^{(1)}(\mathbf{k}_2)\mathcal{K}^{(2)}(\mathbf{k}_1, \mathbf{k}_2, \mathbf{k}_3)P^{(1)}(k_1)P^{(1)}(k_2) + 2 \text{ cycl. perm.} \quad (4.7)$$

where $\mathcal{K}^{(2)} = \mathcal{K}_N^{(2)} + \mathcal{K}_S^{(2)} + \mathcal{K}_V^{(2)} + \mathcal{K}_T^{(2)}$.

- We compute the following two cases:

- **Method 1:** The absolute value of (3.220) i.e., $|B_g^0|$.
- **Method 2:** The monopole of the absolute value,

$$B_g^{\text{abs},0} = \int_{-1}^{+1} d\mu_1 \int_0^{2\pi} d\omega |B_g(k_1, k_2, k_3, \mu_1, \omega)|, \quad (4.8)$$

where $B_g = B_{gR} + iB_{gI}$. This method receives contributions from all the multipoles of B_g .

4.2 The effect of the tidal term

We begin with (4.3),

$$B_{gN}(\mathbf{k}_1, \mathbf{k}_2, \mathbf{k}_3) = \mathcal{K}_N^{(1)}(\mathbf{k}_1)\mathcal{K}_N^{(1)}(\mathbf{k}_2)\mathcal{K}_N^{(2)}(\mathbf{k}_1, \mathbf{k}_2, \mathbf{k}_3)P^{(1)}(k_1)P^{(1)}(k_2) + 2 \text{ cycl. perm.} \quad (4.9)$$

which is the Newtonian galaxy bispectrum. The first- and second-order kernels are given by (3.17) and (3.63) respectively. We list them down again,

$$\mathcal{K}_N^{(1)}(\mathbf{k}_1) = b_1 + f\mu_1^2, \quad (4.10)$$

$$\begin{aligned} \mathcal{K}_N^{(2)}(\mathbf{k}_1, \mathbf{k}_2, \mathbf{k}_3) &= b_1 F_2(\mathbf{k}_1, \mathbf{k}_2) + b_2 + f G_2(\mathbf{k}_1, \mathbf{k}_2) \mu_3^2 - \frac{2}{7}(b_1 - 1) S_2(\mathbf{k}_1, \mathbf{k}_2) \\ &\quad + f^2 \frac{\mu_1 \mu_2}{k_1 k_2} (\mu_1 k_1 + \mu_2 k_2)^2 + b_1 \frac{f}{k_1 k_2} \left[(\mu_1^2 + \mu_2^2) k_1 k_2 + \mu_1 \mu_2 (k_1^2 + k_2^2) \right]. \end{aligned} \quad (4.11)$$

where the expression for the tidal bias coefficient is given in [64],

$$b_{\text{Tidal}} = -\frac{2}{7}(b_1 - 1). \quad (4.12)$$

We can use (4.10) and (4.11) in (4.9) and isolate the tidal term such that we obtain,

$$\underbrace{B_{gN}(\mathbf{k}_1, \mathbf{k}_2, \mathbf{k}_3)}_{\text{standard Newtonian}} \rightarrow B_{gN}(\mathbf{k}_1, \mathbf{k}_2, \mathbf{k}_3) + B_{g\text{Tidal}}(\mathbf{k}_1, \mathbf{k}_2, \mathbf{k}_3), \quad (4.13)$$

where,

$$\begin{aligned} B_{g\text{Tidal}}(\mathbf{k}_1, \mathbf{k}_2, \mathbf{k}_3) &= -\frac{2}{7}(b_1 - 1) \left[b_1^2 + b_1 f (\mu_1^2 + \mu_2^2) + f^2 \mu_1^2 \mu_2^2 \right] S_2(\mathbf{k}_1, \mathbf{k}_2) P(k_1) P(k_2) \\ &\quad + 2 \text{ cycl. perm.} \end{aligned} \quad (4.14)$$

Figure 4.1 shows the plots. The Newtonian galaxy bispectrum is purely real. The *top left* plot is the absolute value of the monopole. The tidal term makes the standard Newtonian curve (B_{gN} , orange) to go negative on large scales (red curve). We use dashed line to indicate negative.

Explanation: We are considering $z = 1$ and this gives $b_1 \approx 1.41$. Therefore, in (4.14) the only term which controls the overall sign of $B_{g\text{Tidal}}$ must be S_2 because all the other terms are positive. In the exact squeezed limit we have,

$$S_2(\mathbf{k}_S, -\mathbf{k}_S) = \frac{2}{3} \quad \text{and} \quad S_2(-\mathbf{k}_S, \mathbf{k}_L) = S_2(\mathbf{k}_L, \mathbf{k}_S) = -\frac{1}{3}, \quad (4.15)$$

which leads to,

$$B_{g\text{Tidal}}(\mathbf{k}_S, -\mathbf{k}_S, \mathbf{k}_L) = -[\dots] P(k_S) P(k_S), \quad (4.16)$$

$$B_{g\text{Tidal}}(-\mathbf{k}_S, \mathbf{k}_L, \mathbf{k}_S) = B_{g\text{Tidal}}(\mathbf{k}_L, \mathbf{k}_S, -\mathbf{k}_S) = +[\dots] P(k_S) P(k_L). \quad (4.17)$$

The $P(k_S)P(k_S)$ term in (4.16) is neglected since it is very small. Hence, $B_{g\text{Tidal}}$ is positive and makes the overall B_{gN} in (4.13) always positive. However, in moderate

squeezed configurations, S_2 grows positive on large scales [119]. The $P(k_S)P(k_S)$ term does contribute to $B_{g\text{Tidal}}$ and dominates over the $P(k_S)P(k_L)$ term. This results in the overall B_{gN} to be negative on large scales.

In the coming sections on GR effects we include the tidal term throughout.

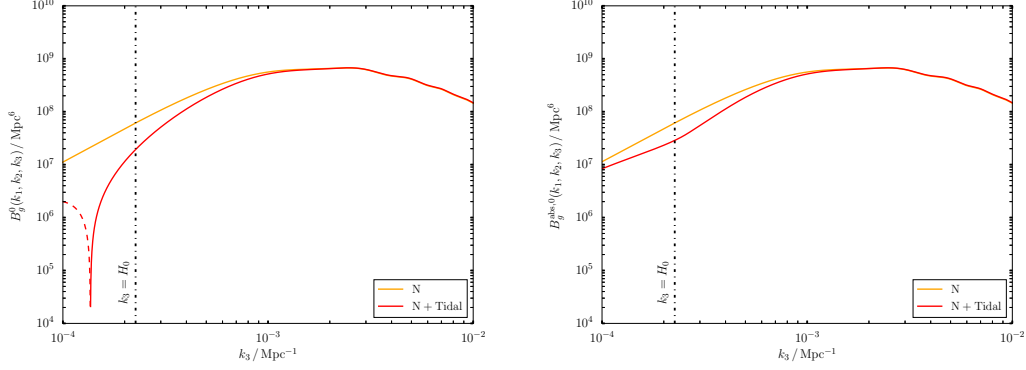


FIGURE 4.1: The monopole of the galaxy bispectrum at $z = 1$ in the Newtonian approximation. The triangular configuration is a moderately squeezed shape ($k_1 = k_2 = k_S$, $k_3 \approx k_S/16$). We use solid line for positive and dashed line for negative. *Left:* Monopole computed using **Method 1**. *Right:* Monopole computed using **Method 2**.

4.3 Correlations in the galaxy bispectrum

The complete expression for the relativistic galaxy bispectrum contains various 3-point correlations as given in (3.199),

$$\begin{aligned}
 B_g(\mathbf{k}_1, \mathbf{k}_2, \mathbf{k}_3) = & \left[\mathcal{K}_N^{(1)}(\mathbf{k}_1) \mathcal{K}_N^{(1)}(\mathbf{k}_2) \mathcal{K}_N^{(2)}(\mathbf{k}_1, \mathbf{k}_2, \mathbf{k}_3) + \mathcal{K}_{GR}^{(1)}(\mathbf{k}_1) \mathcal{K}_{GR}^{(1)}(\mathbf{k}_2) \mathcal{K}_{GR}^{(2)}(\mathbf{k}_1, \mathbf{k}_2, \mathbf{k}_3) \right. \\
 & + \mathcal{K}_N^{(1)}(\mathbf{k}_1) \mathcal{K}_N^{(1)}(\mathbf{k}_2) \mathcal{K}_{GR}^{(2)}(\mathbf{k}_1, \mathbf{k}_2, \mathbf{k}_3) + \mathcal{K}_{GR}^{(1)}(\mathbf{k}_1) \mathcal{K}_{GR}^{(1)}(\mathbf{k}_2) \mathcal{K}_N^{(2)}(\mathbf{k}_1, \mathbf{k}_2, \mathbf{k}_3) \\
 & \left. + 2\mathcal{K}_N^{(1)}(\mathbf{k}_1) \mathcal{K}_{GR}^{(1)}(\mathbf{k}_2) \left\{ \mathcal{K}_N^{(2)}(\mathbf{k}_1, \mathbf{k}_2, \mathbf{k}_3) + \mathcal{K}_{GR}^{(2)}(\mathbf{k}_1, \mathbf{k}_2, \mathbf{k}_3) \right\} \right] P(k_1)P(k_2) \\
 & + 2 \text{ cyc. perm. } , \tag{4.18}
 \end{aligned}$$

where $\mathcal{K}_{GR}^{(2)} = \mathcal{K}_S^{(2)} + \mathcal{K}_V^{(2)} + \mathcal{K}_T^{(2)}$. The correlations which are unaffected by the second-order GR projection effects (S, V and T) are,

$$\langle \Delta_N^{(1)}(\mathbf{k}_1) \Delta_N^{(1)}(\mathbf{k}_2) \Delta_N^{(2)}(\mathbf{k}_3) \rangle, \quad \langle \Delta_N^{(1)}(\mathbf{k}_1) \Delta_{GR}^{(1)}(\mathbf{k}_2) \Delta_N^{(2)}(\mathbf{k}_3) \rangle, \quad \langle \Delta_{GR}^{(1)}(\mathbf{k}_1) \Delta_{GR}^{(1)}(\mathbf{k}_2) \Delta_N^{(2)}(\mathbf{k}_3) \rangle . \tag{4.19}$$

We show the plots below in Figure 4.2. The pure Newtonian correlation (red) dominates on small scales. The correlation having only one first-order GR projection term i.e., $\langle \Delta_N^{(1)}(\mathbf{k}_1) \Delta_{GR}^{(1)}(\mathbf{k}_2) \Delta_N^{(2)}(\mathbf{k}_3) \rangle$ (cyan), is the most dominant on super-equality scales.

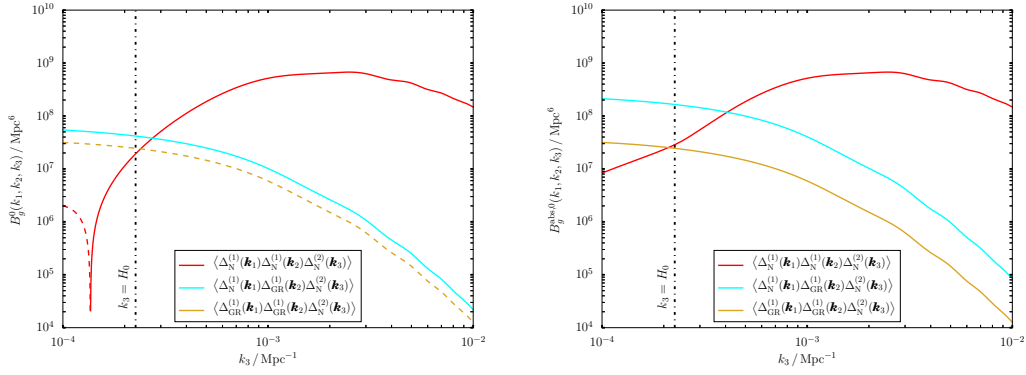


FIGURE 4.2: The monopole for the 3-point correlations listed in (4.19) at $z = 1$. The triangular configuration is a moderately squeezed shape ($k_1 = k_2 = k_S$, $k_3 \approx k_S/16$). We use solid line for positive and dashed line for negative. *Left*: Monopole computed using **Method 1**. *Right*: Monopole computed using **Method 2**.

If we omit the first-order GR projection effects, we will definitely miss this contribution to the full squeezed galaxy bispectrum.

The remaining correlations which contain information about the second-order relativistic effects are,

$$\langle \Delta_{\text{GR}}^{(1)}(\mathbf{k}_1) \Delta_{\text{GR}}^{(1)}(\mathbf{k}_2) \Delta_{\text{GR}}^{(2)}(\mathbf{k}_3) \rangle, \quad \langle \Delta_{\text{N}}^{(1)}(\mathbf{k}_1) \Delta_{\text{GR}}^{(1)}(\mathbf{k}_2) \Delta_{\text{GR}}^{(2)}(\mathbf{k}_3) \rangle, \quad \langle \Delta_{\text{N}}^{(1)}(\mathbf{k}_1) \Delta_{\text{N}}^{(1)}(\mathbf{k}_2) \Delta_{\text{GR}}^{(2)}(\mathbf{k}_3) \rangle. \quad (4.20)$$

It is important to isolate these correlations because they help to identify the dominant relativistic terms in the full galaxy bispectrum. Here, we study these correlations in details as follows:

- We split $\Delta_{\text{GR}}^{(2)}$ into scalars (S), vectors (V) and tensors (T).
- We look at the scalars which contain the quadratic first-order and intrinsic second-order terms (refer to Section 1.6.3 and Section 3.2.2).
- Then, we consider the vectors and tensors.

We do not show plots for the monopole of the imaginary part of B_g because it is always 0 (by definition, B_g^{abs} has no imaginary part). For other multipoles, the imaginary part can be non-zero. We leave this topic for future work.

4.3.1 Quadratic first-order and intrinsic GR second-order scalars

We start by looking at the scalars. In that case the kernels to be used are:

1. The first-order kernels, $\mathcal{K}_N^{(1)}$ and $\mathcal{K}_{GR}^{(1)}$ are given by (3.17) and (3.18) respectively.
2. The second-order Newtonian kernel, $\mathcal{K}_N^{(2)}$ is given by (4.11).
3. The second-order kernel for the local relativistic scalars ($\mathcal{K}_{GR}^{(2)} = \mathcal{K}_S^{(2)}$) is given by (3.65).
 - At first, we set the $\tilde{\Gamma}$'s to 0 in order to remove the intrinsic GR second-order scalars (see Section 3.2.2). In this case, the second-order scalars are computed in the Newtonian approximation.
 - Then, we include the $\tilde{\Gamma}$'s and show their importance by computing the percentage fractional difference.

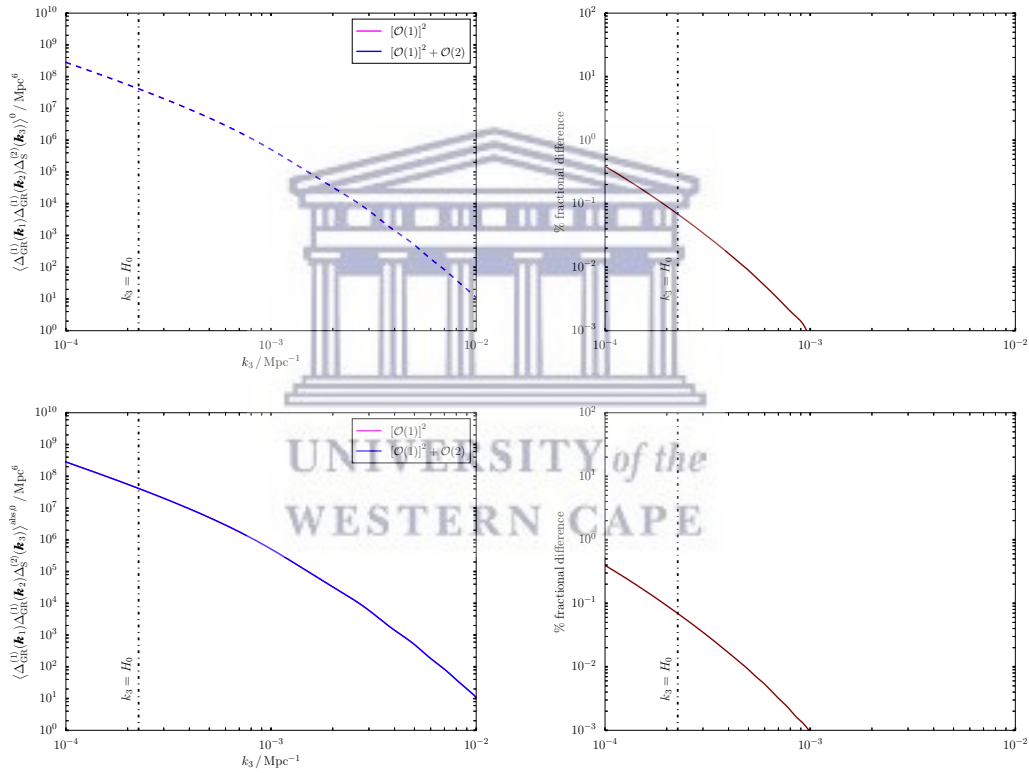


FIGURE 4.3: *Left panel:* The monopole for the 3-point correlation $\langle \Delta_{GR}^{(1)}(\mathbf{k}_1) \Delta_{GR}^{(1)}(\mathbf{k}_2) \Delta_{GR}^{(2)}(\mathbf{k}_3) \rangle$ at $z = 1$. The triangular configuration is a moderately squeezed shape ($k_1 = k_2 = k_S$, $k_3 \approx k_S/16$). We use solid line for positive and dashed line for negative. The magenta curve is for the quadratic first-order terms. The blue curve includes the intrinsic second-order terms. *Top left panel:* Monopole computed using **Method 1**. *Bottom left panel:* Monopole computed using **Method 2**. *Right panel:* The percentage fractional difference between the blue and magenta curves.

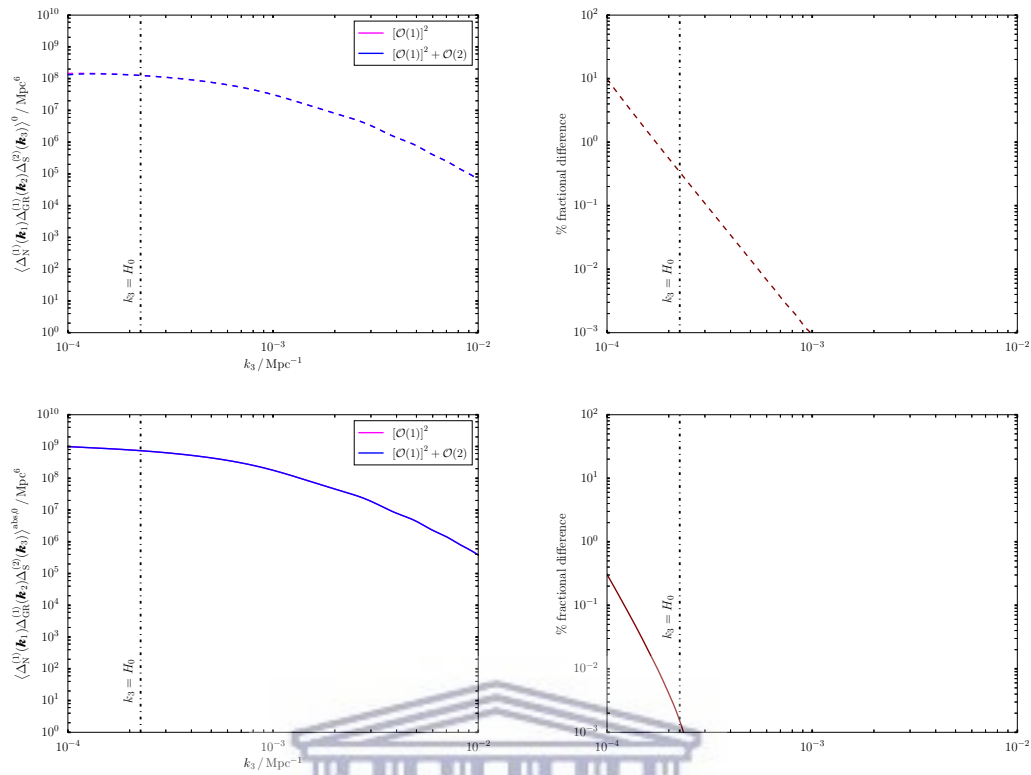


FIGURE 4.4: *Left panel:* The monopole for the 3-point correlation $\langle \Delta_N^{(1)}(\mathbf{k}_1) \Delta_{GR}^{(1)}(\mathbf{k}_2) \Delta_{GR}^{(2)}(\mathbf{k}_3) \rangle$ at $z = 1$. The triangular configuration is a moderately squeezed shape ($k_1 = k_2 = k_S$, $k_3 \approx k_S/16$). We use solid line for positive and dashed line for negative. The magenta curve is for the quadratic first-order terms. The blue curve includes the intrinsic second-order terms. *Top left panel:* Monopole computed using **Method 1**. *Bottom left panel:* Monopole computed using **Method 2**. *Right panel:* The percentage fractional difference between the blue and magenta curves.

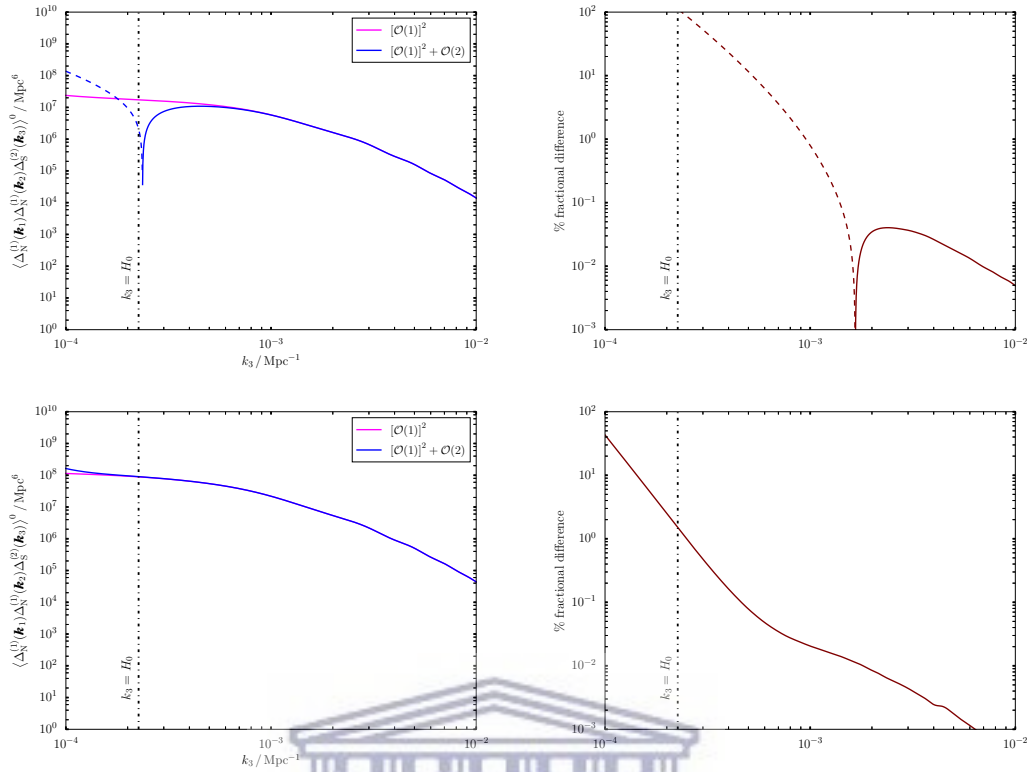


FIGURE 4.5: *Left panel:* The monopole for the 3-point correlation $\langle \Delta_N^{(1)}(\mathbf{k}_1) \Delta_N^{(1)}(\mathbf{k}_2) \Delta_{GR}^{(2)}(\mathbf{k}_3) \rangle$ at $z = 1$. The triangular configuration is a moderately squeezed shape ($k_1 = k_2 = k_S$, $k_3 \approx k_S/16$). We use solid line for positive and dashed line for negative. The magenta curve is for the quadratic first-order terms only. The blue curve includes the intrinsic second-order terms. *Top left panel:* Monopole computed using **Method 1**. *Bottom left panel:* Monopole computed using **Method 2**. *Right panel:* The percentage fractional difference between the blue and magenta curves.

The plots in Figure 4.3, Figure 4.4 and Figure 4.5 show that the intrinsic GR second-order scalars becomes non-negligible on fairly large scales which are still within the horizon. Failing to include these terms will lead to a wrong estimation when computing the galaxy bispectrum. At this stage onwards, we take into account both the quadratic first-order and intrinsic GR second-order terms when we consider the second-order scalars (S).

4.3.2 Vectors and tensors

The second-order kernels for the vectors (V) and tensors (T) are given in (3.126)-(3.128) and (3.163)-(3.165) respectively. We show the V-T contributions for the different correlations given by (4.20) below in Figure 4.6. We can see that the second-order scalars (blue) largely dominate over the vectors (green) and tensors (purple).

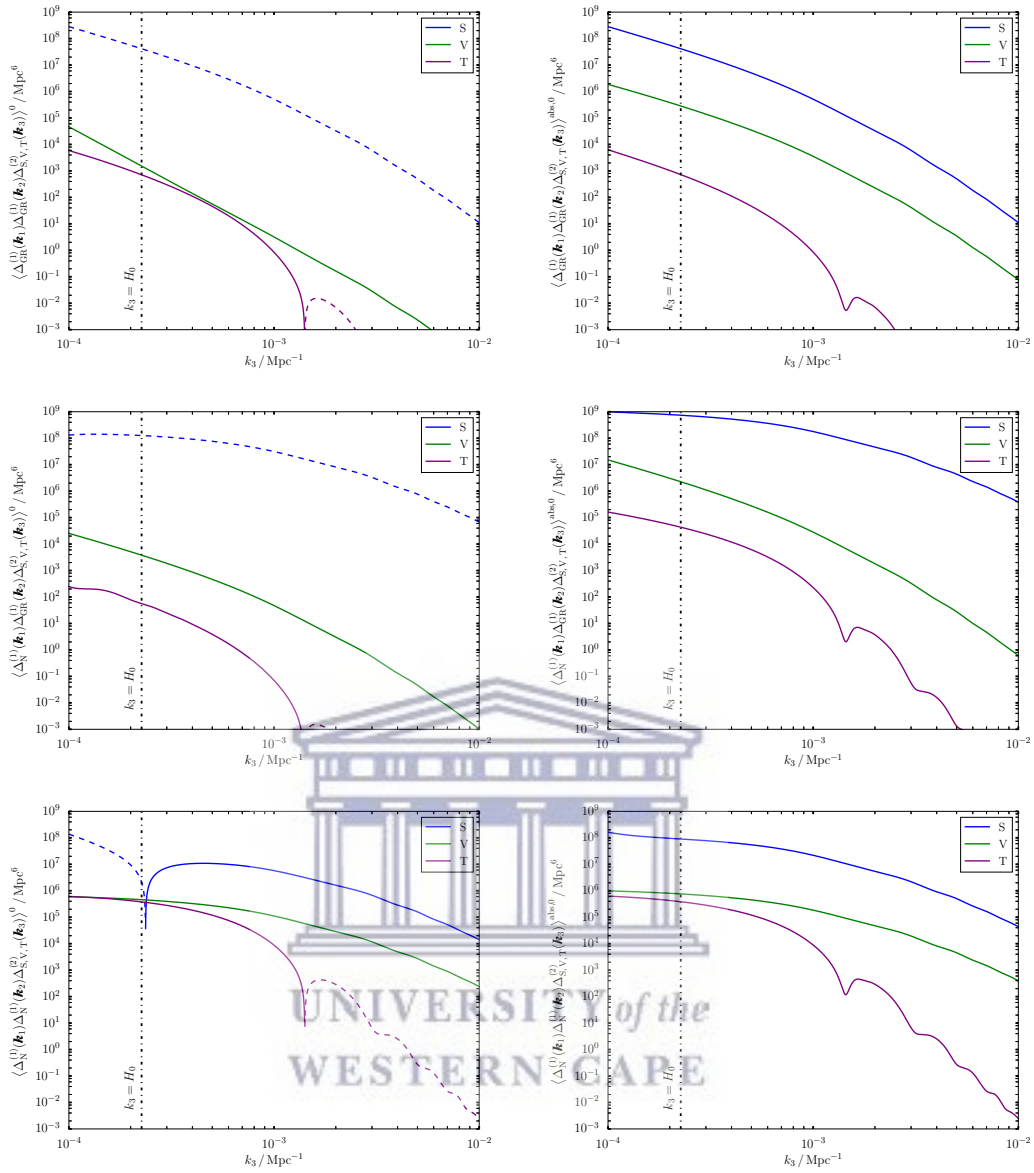


FIGURE 4.6: V-T contributions in the monopole of the 3-point correlations listed in (4.20) at $z = 1$. The triangular configuration is a moderately squeezed shape ($k_1 = k_2 = k_S$, $k_3 \approx k_S/16$). We use solid line for positive and dashed line for negative. *Left panel:* Monopole computed using **Method 1**. *Right panel:* Monopole computed using **Method 2**.

4.4 The full local relativistic galaxy bispectrum

In Figure 4.7, we compute the monopole for the expression given in (4.7) which is for the case of the full GR. We also show the percentage difference relative to the Newtonian approximation. On scales around equality, we can find a power-law fit for the fractional

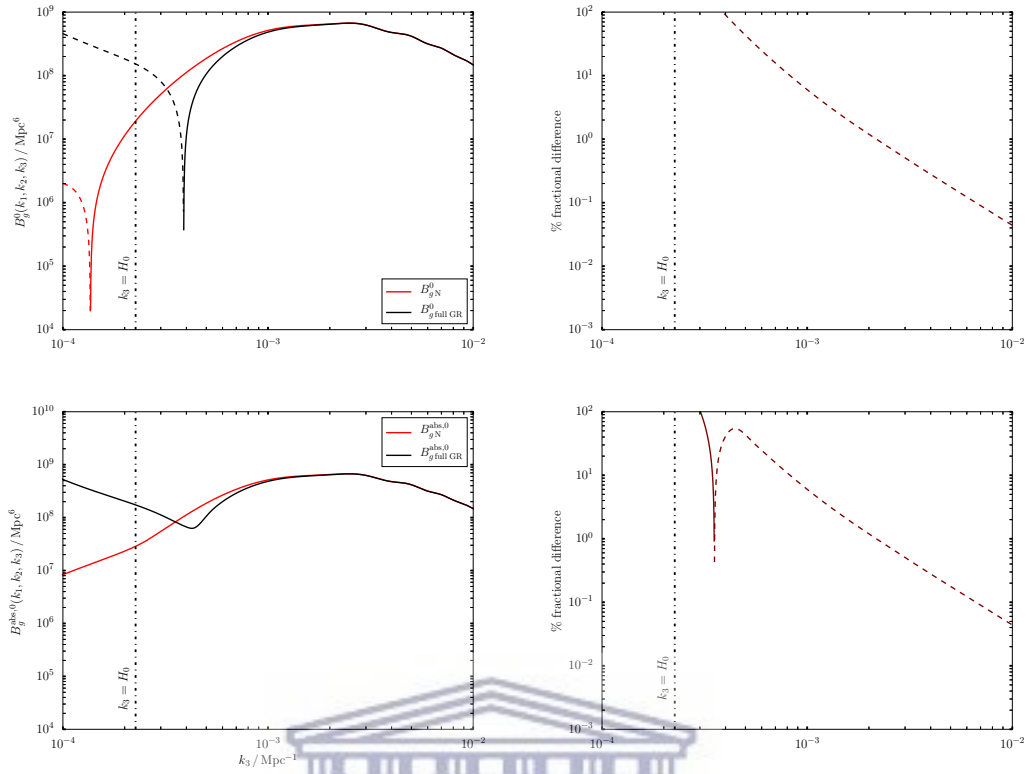


FIGURE 4.7: The monopole at $z = 1$. The triangular configuration is a moderately squeezed shape ($k_1 = k_2 = k_S$, $k_3 \approx k_S/16$). We use solid line for positive and dashed line for negative. The red curve is the Newtonian approximation. The black curve is the full local relativistic galaxy bispectrum. *Top left panel:* Monopole computed using **Method 1**. *Bottom left panel:* Monopole computed using **Method 2**. *Right panel:* The percentage fractional difference relative to the Newtonian approximation.

GR corrections to the Newtonian prediction:

$$B_g^0 = B_{gN}^0 \left[1 + \Delta B \right], \quad \Delta B = \epsilon \left(\frac{k_3}{k_{\text{eq}}} \right)^{-n}, \quad 0.007 \text{ Mpc}^{-1} \lesssim k_3 \lesssim 0.07 \text{ Mpc}^{-1}. \quad (4.21)$$

TABLE 4.1: Amplitude of the fractional GR corrections at $k_3 \sim 0.01 \text{ Mpc}^{-1}$ for Figure 4.7.

ΔB	$\epsilon \times 10^2$	n
Method 1	-0.0408	2.01
Method 2	0.0408	2.01

4.5 2-D colour plot

To explore other triangular configurations, we generate a colour intensity map where we impose the condition $k_1 \geq k_2 \geq k_3$ to avoid redundancy and choose $k_1 = 0.01 \text{ Mpc}^{-1}$. The maps are given in Figure 4.8 with the colours being normalized. We show the monopoles for the Newtonian (N) and full GR galaxy bispectra as defined in (4.3) and (4.7) respectively. We also show the percentage difference relative to the Newtonian approximation. The difference is greatest close the squeezed limit.

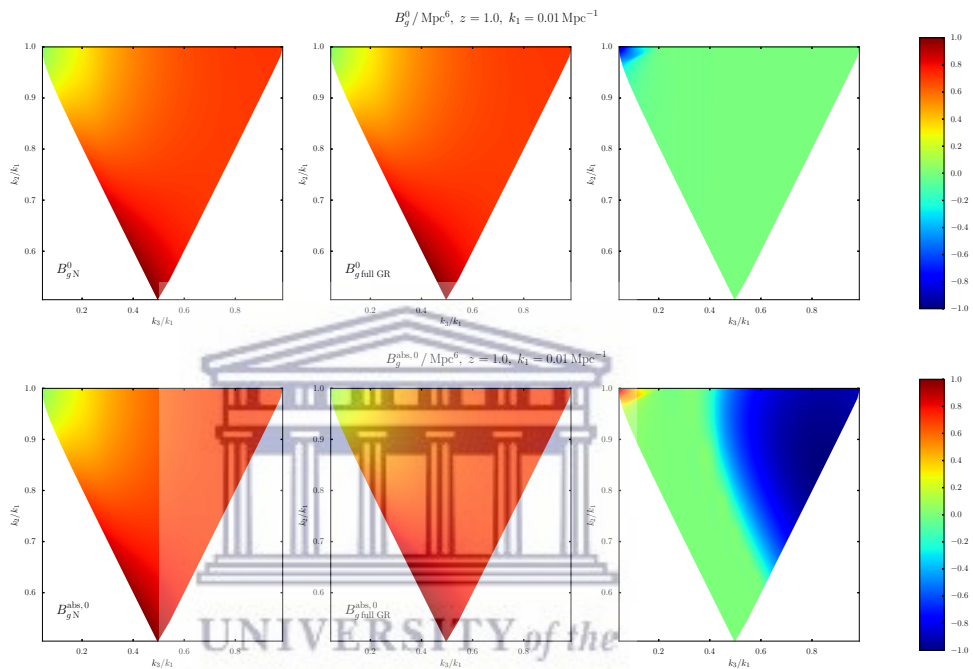


FIGURE 4.8: The monopole of the galaxy bispectrum with $k_1 = 0.01 \text{ Mpc}^{-1}$ at $z = 1.0$. The upper left tip of the wedge is the squeezed limit ($k_1 = k_2, k_3 \rightarrow 0$) and the upper right tip is the equilateral shape ($k_1 = k_2 = k_3$). *Top panel:* Monopole computed using **Method 1**. *Bottom panel:* Monopole computed using **Method 2**. *Left column:* The Newtonian monopole (N). *Middle column:* The monopole for the full GR case. *Right column:* The percentage fractional difference relative to the Newtonian approximation.

In Figure 4.9 we show the colour plots for the monopoles with V (*left*) and T (*middle*) only. We also compute the difference between the two plots (*right*) to show that the second-order vectors and tensors contribute differently to the monopole.

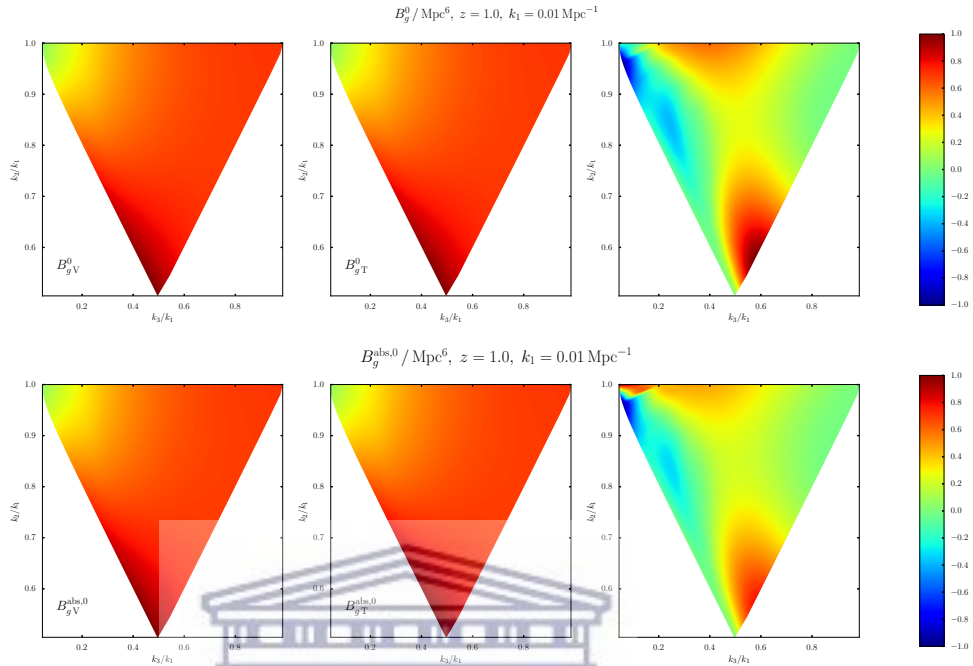


FIGURE 4.9: The monopole of the galaxy bispectrum with $k_1 = 0.01 \text{ Mpc}^{-1}$ at $z = 1.0$. The upper left tip of the wedge is the squeezed limit ($k_1 = k_2, k_3 \rightarrow 0$) and the upper right tip is the equilateral shape ($k_1 = k_2 = k_3$). *Top panel:* Monopole computed using **Method 1**. *Bottom panel:* Monopole computed using **Method 2**. *Left column:* The monopole with second-order vectors (V). *Middle column:* The monopole with second-order tensors (T). *Right column:* The difference between V and T.

F Chapter 5

Chapter 5

The GR projection effects in the non-Gaussian galaxy bispectrum

5.1 Local primordial non-Gaussianity

The galaxy 2-point correlation function (2PCF) in real space or equivalently the galaxy power spectrum in Fourier space is a powerful statistical tool which has been used to put constraints on cosmological parameters extracted from galaxy surveys. In linear perturbation theory, the statistical properties of the perturbations are often taken to be Gaussian and therefore, they are fully explained by the power spectrum. On very large scales, it is possible to detect non-Gaussian contributions to cosmological correlations. The galaxy power spectrum already provides constraints on the amount of non-Gaussianity on large scales. For better constraints, we have to go beyond the power spectrum and the next level in the galaxy correlation function is the bispectrum (3PCF).

Future galaxy surveys e.g., the SKA, will increasingly make use of the galaxy bispectrum to do the forecasts on cosmological parameters. These surveys will probe higher redshifts and bigger volumes in the Universe at scales beyond the equality scale ($k_{\text{eq}} \sim 10^{-2} \text{ Mpc}^{-1}$). Those scales contain fossil records from the primordial Universe. These are non-Gaussian features in the primordial gravitational potential $\Phi_{\text{p}}(\mathbf{x})$. The most studied example is the local form of primordial non-Gaussianity (PNG) in which Φ_{p} is expressed as a power series of a single primordial Gaussian field $\varphi(\mathbf{x})$ [120–122],

$$- \Phi_{\text{p}}(\mathbf{x}) = \varphi(\mathbf{x}) + f_{\text{NL}} (\varphi^2(\mathbf{x}) - \langle \varphi^2 \rangle) + \dots, \quad (5.1)$$

where the constant f_{NL} measures the amount of non-Gaussianity. The minus sign arises because of our convention for the first-order Φ and Ψ in (1.43). This local form of PNG

shows high signatures in the galaxy bispectrum for the squeezed configuration. Different models of inflation predict different values of f_{NL} . In many multi-field inflationary models, f_{NL} is predicted to be of $\mathcal{O}(\gtrsim 1)$ [123]. The single field slow-roll inflation predicts a very small value for non-Gaussianity in the squeezed limit of the bispectrum [24]. Planck 2015 measurements of the Cosmic Microwave Background (CMB) bispectrum gives $-9.2 < f_{\text{NL}} < 10.8$ at 95% confidence level [124].

5.2 Second-order dark matter and velocity kernels in the presence of PNG

In Fourier space, the dark matter density field δ and velocity divergence $\theta = \nabla \cdot \mathbf{v}$ have perturbative solutions [28],

$$\delta(\eta, \mathbf{k}) = \sum_{n=1}^{\infty} \int d(\mathbf{k}_1, \mathbf{k}_2, \dots, \mathbf{k}_n) F_n(\mathbf{k}_1, \mathbf{k}_2, \dots, \mathbf{k}_n), \quad (5.2)$$

$$\theta(\eta, \mathbf{k}) = -\mathcal{H}f \sum_{n=1}^{\infty} \int d(\mathbf{k}_1, \mathbf{k}_2, \dots, \mathbf{k}_n) G_n(\mathbf{k}_1, \mathbf{k}_2, \dots, \mathbf{k}_n), \quad (5.3)$$

where F_n and G_n are the n^{th} -order Fourier kernels. The first-order ($n = 1$) solutions are obtained by setting $F_1 = G_1 = 1$ and this gives,

$$\delta(\eta, \mathbf{k}) = \delta_{\text{T}}^{(1)}(\eta, \mathbf{k}) \quad \text{and} \quad \theta(\eta, \mathbf{k}) = -\mathcal{H}f \delta_{\text{T}}^{(1)}(\eta, \mathbf{k}), \quad (5.4)$$

which we have seen in Chapter 3 (“T” denotes the total matter gauge). We relate $\delta_{\text{T}}^{(1)}$ to the primordial Gaussian gravitational potential φ via the Poisson equation [28],

$$\delta_{\text{T}}^{(1)}(\eta, \mathbf{k}) = \alpha(\eta, k) \varphi(\mathbf{k}), \quad (5.5)$$

where,

$$\alpha(\eta, k) = \frac{2k^2 T(k) D(\eta)}{3\Omega_{m0} H_0^2}. \quad (5.6)$$

Note that $\varphi = -\Phi^{(1)}$. Then at second-order we can find that [28],

$$\delta_{\text{T}}^{(2)}(\eta, \mathbf{k}) = \int d(\mathbf{k}_1, \mathbf{k}_2, \mathbf{k}) \left[F_2(\mathbf{k}_1, \mathbf{k}_2) + f_{\text{NL}} \frac{\alpha(\eta, k)}{\alpha(\eta, k_1) \alpha(\eta, k_2)} \right], \quad (5.7)$$

$$\theta^{(2)}(\eta, \mathbf{k}) = -\mathcal{H}f \int d(\mathbf{k}_1, \mathbf{k}_2, \mathbf{k}) \left[G_2(\mathbf{k}_1, \mathbf{k}_2) + f_{\text{NL}} \frac{\alpha(\eta, k)}{\alpha(\eta, k_1) \alpha(\eta, k_2)} \right], \quad (5.8)$$

where f_{NL} introduces mode coupling. If it is 0, we recover (3.21) and (3.22).

5.3 Galaxy overdensity with PNG

Apart from the Planck CMB data, galaxy surveys are also good tracers for the underlying dark matter and velocity fields. The continuity equation gives the relation between these two fields as [64],

$$D_\eta \delta(\eta, \mathbf{q}) = -\theta(\eta, \mathbf{q}) [1 + \delta(\eta, \mathbf{q})], \quad (5.9)$$

where $D_\eta = D/D\eta$ is the convective derivative and \mathbf{q} is the Lagrangian coordinate. If we assume that there is no velocity bias between the galaxies and dark matter then,

$$D_\eta \delta_g(\eta, \mathbf{q}) = -\theta(\eta, \mathbf{q}) [1 + \delta_g(\eta, \mathbf{q})], \quad (5.10)$$

where δ_g is the galaxy overdensity. We equate (5.9) and (5.10) and obtain the following differential equation,

$$\frac{D_\eta \delta_g}{(1 + \delta_g)} = -\theta = \frac{D_\eta \delta}{(1 + \delta)}. \quad (5.11)$$

In the Lagrangian frame, the convective derivative becomes a partial derivative (see Table 5 in [64]) and therefore integrating (5.11) gives,

$$\ln [1 + \delta_g(\eta, \mathbf{x})] = \ln [1 + \delta(\eta, \mathbf{x})] + \ln \left[\frac{1 + \delta_g(\eta_f, \mathbf{x}_f)}{1 + \delta(\eta_f, \mathbf{x}_f)} \right], \quad (5.12)$$

where we have fixed the integration constant with the galaxy overdensity, $\delta_g(\eta_f, \mathbf{x}_f)$, defined on the formation time slice with $\eta = \eta_f$ and $\mathbf{x} = \mathbf{x}_f$. Here, \mathbf{x} is the Eulerian coordinate corresponding to a fixed Lagrangian position, $\mathbf{q} = \mathbf{x}(\eta = 0)$. Therefore, \mathbf{x}_f corresponds to the position on the formation time slice. The mapping between the Lagrangian and Eulerian coordinates is as follows [27, 28, 64],

$$\mathbf{x} = \mathbf{q} + \mathbf{\Upsilon}^{(1)}(\mathbf{q}, \eta), \quad (5.13)$$

where $\mathbf{\Upsilon}^{(1)}$ is the first order Lagrangian displacement and $\mathbf{\Upsilon}^{(1)}(\mathbf{q}, \eta = 0) = 0$. We can write (5.12) as,

$$1 + \delta_g(\eta, \mathbf{x}) = \left[\frac{1 + \delta(\eta, \mathbf{x})}{1 + \delta_f} \right] 1 + \delta_{gf}, \quad (5.14)$$

and expand up to second-order as,

$$\begin{aligned} 1 + \delta_g^{(1)} + \frac{1}{2} \delta_g^{(2)} &= 1 + \delta^{(1)} - \delta_f^{(1)} + \delta_{gf}^{(1)} \\ &+ \frac{1}{2} \delta^{(2)} - \frac{1}{2} \delta_f^{(2)} + \frac{1}{2} \delta_{gf}^{(2)} + [\delta_f^{(1)}]^2 - \delta^{(1)} \delta_f^{(1)} + \delta^{(1)} \delta_{gf}^{(1)} - \delta_f^{(1)} \delta_{gf}^{(1)}, \end{aligned} \quad (5.15)$$

where the subscript ‘f’ denotes quantities evaluated on the formation time slice (η_f, \mathbf{x}_f), while those without a subscript ‘f’ are evaluated at (η, \mathbf{x}) . To simplify the right-hand

side of (5.15) we begin with $\Upsilon^{(1)}$ and express it in terms of $\delta^{(1)}$ as [64, 125],

$$\Upsilon^{(1)}(\eta, \mathbf{x}) = -\frac{\nabla}{\nabla^2}\delta^{(1)}(\eta, \mathbf{x}) = -\frac{\nabla}{\nabla^2}D(\eta)\delta_0^{(1)}(\mathbf{x}), \quad (5.16)$$

where D is the linear matter growth factor and ‘0’ denotes present time. Then using (5.13) we have at first-order,

$$\mathbf{x}_f = \mathbf{x} + \left(\frac{D_f}{D} - 1\right)\Upsilon^{(1)}(\eta, \mathbf{x}). \quad (5.17)$$

With (5.17) we can obtain the following expansion,

$$\delta_f^{(1)} = \left(\frac{D_f}{D}\right)\delta^{(1)} + \left(\frac{D_f}{D}\right)\left(\frac{D_f}{D} - 1\right)\Upsilon_i^{(1)}\partial^i\delta^{(1)}, \quad (5.18)$$

$$\delta_f^{(2)} = \left(\frac{D_f}{D}\right)^2\delta^{(2)} + \left(\frac{D_f}{D}\right)^2\left(\frac{D_f}{D} - 1\right)\Upsilon_i^{(1)}\partial^i\delta^{(2)}. \quad (5.19)$$

Lastly, we need a bias prescription for the galaxy overdensity, δ_{gf} , and we use the following [28],

$$\delta_{gf}^{(1,2)} = \left[b_{10}\left(\delta^{(1)} + \frac{1}{2}\delta^{(2)}\right) + b_{01}\varphi - b_{01}\Upsilon_i^{(1)}\partial^i\varphi + \frac{1}{2}b_{20}[\delta^{(1)}]^2 + \frac{1}{2}b_{02}\varphi^2 + b_{11}\delta^{(1)}\varphi + \frac{1}{2}b_{\text{Tidal}}[K_{ij}]^2 \right]_f, \quad (5.20)$$

where K_{ij} is given by (2.88). We can again use (5.17) to express the right-hand side in terms of quantities evaluated at (η, \mathbf{x}) . Then we substitute (5.18), (5.19) and (5.20) in (5.15), and collect the first- and second-order terms as,

$$\delta_g^{(1)} = \left[1 + \frac{D_f}{D}(b_{10}^f - 1) \right] \delta^{(1)} + \frac{D_f}{D}b_{01}^f\varphi, \quad (5.21)$$

$$\begin{aligned} \delta_g^{(2)} = & \left[1 + \left(\frac{D_f}{D}\right)^2(b_{10}^f - 1) \right] \delta^{(2)} + \left[2b_{10}^f\frac{D_f}{D}\left(1 - \frac{D_f}{D}\right) + \left(\frac{D_f}{D}\right)^2b_{20}^f \right] [\delta^{(1)}]^2 \\ & + \left(\frac{D_f}{D}\right)^2b_{\text{Tidal}}^f[K_{ij}]^2 + \frac{D_f}{D}\left(\frac{D_f}{D} - 1\right)(b_{10}^f - 1)\Upsilon_i^{(1)}\partial^i\delta^{(1)} \\ & - 2b_{01}^f\frac{D_f}{D}\left(1 + \frac{D_f}{D}\right)\Upsilon_i^{(1)}\partial^i\varphi + \left(\frac{D_f}{D}\right)^2b_{02}^f\varphi^2 \\ & + 2\left[b_{01}^f\frac{D_f}{D}\left(1 - \frac{D_f}{D}\right) + \left(\frac{D_f}{D}\right)^2b_{11}^f\right]\delta^{(1)}\varphi. \end{aligned} \quad (5.22)$$

The definition for the Lagrangian displacement in (5.13) enables us to obtain an alternative way of writing the second-order solution of (5.7) as [27],

$$\delta^{(2)} = \frac{34}{21}[\delta^{(1)}]^2 + \frac{2}{7}[K_{ij}]^2 - \Upsilon_i^{(1)}\partial^i\delta^{(1)}, \quad (5.23)$$

where we have multiplied the first term by 2 to keep the consistency of our notation. If we allow $\eta_f \rightarrow 0$ (implying $D_f/D \rightarrow 0$), but define finite values for the Lagrangian bias

as [64],

$$\begin{aligned} b_{10}^L &= \frac{D_f}{D} b_{10}^f, & b_{01}^L &= \frac{D_f}{D} b_{10}^f, & b_{11}^L &= \left(\frac{D_f}{D}\right)^2 b_{11}^f, & b_{02}^L &= \left(\frac{D_f}{D}\right)^2 b_{02}^f, & b_{20}^L &= \left(\frac{D_f}{D}\right)^2 b_{20}^f, \\ b_{\text{Tidal}}^L &= \left(\frac{D_f}{D}\right)^2 b_{\text{Tidal}}^f, \end{aligned} \quad (5.24)$$

and use (5.23) to eliminate $\Upsilon_i^{(1)} \partial^i \delta^{(1)}$ in (5.22) we obtain,

$$\delta_g^{(1)} = (1 + b_{10}^L) \delta^{(1)} + b_{01}^L \varphi, \quad (5.25)$$

$$\begin{aligned} \delta_g^{(2)} &= (1 + b_{10}^L) \delta^{(2)} + \left[\frac{8}{21} b_{10}^L + b_{20}^L \right] [\delta^{(1)}]^2 + \left[b_{\text{Tidal}}^L - \frac{2}{7} b_{10}^L \right] [K_{ij}]^2 - 2b_{01}^L \Upsilon_i^{(1)} \partial^i \varphi \\ &\quad + b_{02}^L \varphi^2 + 2(b_{01}^L + b_{11}^L) \delta^{(1)} \varphi. \end{aligned} \quad (5.26)$$

b_{01}^L , b_{11}^L and b_{02}^L are obtained from the combinations of the two independent Lagrangian bias parameters, b_{10}^L and b_{20}^L as [27, 126, 127],

$$b_{01}^L = 2f_{\text{NL}} \delta_c b_{10}^L, \quad b_{11}^L = 2f_{\text{NL}} (\delta_c b_{20}^L - b_{10}^L) \quad \text{and} \quad b_{02}^L = 4f_{\text{NL}}^2 \delta_c (\delta_c b_{20}^L - 2b_{10}^L), \quad (5.27)$$

where δ_c is the threshold density in the halo mass function given by [128],

$$\delta_c(z) = \frac{3(12\pi)^{2/3}}{20} [1 + 0.0123 \lg \Omega_m(z)]. \quad (5.28)$$

We can obtain the definition for the Eulerian bias parameters from (5.25) and (5.26) (see Section 2 in [64]) as,

$$\begin{aligned} b_{10}^E &= 1 + b_{10}^L, & b_{01}^E &= b_{01}^L, & b_{20}^E &= \frac{8}{21} b_{10}^L + b_{20}^L, & b_{11}^E &= b_{01}^L + b_{11}^L, & b_{02}^E &= b_{02}^L, \\ b_{\text{Tidal}}^E &= b_{\text{Tidal}}^L - \frac{2}{7} (b_{10}^E - 1), \end{aligned} \quad (5.29)$$

and this leads to,

$$\delta_g^E = b_{10}^E \left(\delta^{(1)} + \frac{1}{2} \delta^{(2)} \right) + b_{01}^E \varphi - b_{01}^E \Upsilon_i^{(1)} \partial^i \varphi + \frac{1}{2} b_{20}^E [\delta^{(1)}]^2 + \frac{1}{2} b_{02}^E \varphi^2 + b_{11}^E \delta^{(1)} \varphi + \frac{1}{2} b_{\text{Tidal}}^E [K_{ij}]^2, \quad (5.30)$$

where δ_g^E is the galaxy overdensity in the Eulerian frame. We set $b_{\text{Tidal}}^L = 0$ in (5.29) to obtain the limit of the local Lagrangian bias [64]. Using (5.27) and (5.29) we obtain,

$$b_{01}^E = 2f_{\text{NL}} \delta_c (b_{10}^E - 1), \quad (5.31)$$

$$b_{11}^E = 2f_{\text{NL}} \left[\delta_c b_{20}^E + \left(\frac{13}{21} \delta_c - 1 \right) (b_{10}^E - 1) \right], \quad (5.32)$$

$$b_{02}^E = 4f_{\text{NL}}^2 \delta_c \left[\delta_c b_{20}^E - 2 \left(\frac{4}{21} \delta_c + 1 \right) (b_{10}^E - 1) \right]. \quad (5.33)$$

5.4 PNG in the squeezed Newtonian galaxy bispectrum

The Fourier transform of (5.30) gives,

$$\begin{aligned} \delta_g^E(\mathbf{k}_3) &= \left[b_{10}^E + \frac{b_{01}^E}{\alpha(k_3)} \right] \delta^{(1)}(\mathbf{k}_3) \\ &+ \frac{1}{2} \int d(\mathbf{k}_1, \mathbf{k}_2, \mathbf{k}_3) \left[b_{10}^E \left(F_2(\mathbf{k}_1, \mathbf{k}_2) + f_{\text{NL}} \frac{\alpha(k)}{\alpha(k_1)\alpha(k_2)} \right) + b_{20}^E \right. \\ &\quad \left. - b_{01}^E \left(\frac{N_2(\mathbf{k}_2, \mathbf{k}_1)}{\alpha(k_1)} + \frac{N_2(\mathbf{k}_1, \mathbf{k}_2)}{\alpha(k_2)} \right) + \frac{b_{02}^E}{\alpha(k_1)\alpha(k_2)} \right. \\ &\quad \left. + b_{11}^E \left(\frac{1}{\alpha(k_1)} + \frac{1}{\alpha(k_2)} \right) - \frac{2}{7} (b_{10}^E - 1) S_2(\mathbf{k}_1, \mathbf{k}_2) \right]. \end{aligned} \quad (5.34)$$

The first line of (5.34) shows the scale-dependent part of the linear galaxy bias, $b_{01}^E/\alpha(k)$ which is proportional to f_{NL}/k^2 . In the second line we have the non-linear effects of PNG with the following:

- N_2 is the Fourier kernel generated by the convective term, $\Upsilon_i^{(1)} \partial^i \varphi$ in (5.30). It is given by [28],

$$2\Upsilon_i^{(1)}(\mathbf{k}_3) \partial^i \varphi(\mathbf{k}_3) = \int d(\mathbf{k}_1, \mathbf{k}_2, \mathbf{k}_3) \left(\frac{N_2(\mathbf{k}_2, \mathbf{k}_1)}{\alpha(k_1)} + \frac{N_2(\mathbf{k}_1, \mathbf{k}_2)}{\alpha(k_2)} \right), \quad (5.35)$$

where,

$$N_2(\mathbf{k}_1, \mathbf{k}_2) = \frac{\mathbf{k}_1 \cdot \mathbf{k}_2}{k_1^2}. \quad (5.36)$$

- The terms in b_{01}^E and b_{11}^E are proportional to f_{NL}/k^2 .
- The term in b_{02}^E is proportional to f_{NL}^2/k^4 .

The above modifies the first- and second-order Gaussian Newtonian kernels given in (4.10) and (4.11) respectively as,

$$\mathcal{K}_{\text{NnG}}^{(1)}(\mathbf{k}_1) = b_{10}^{\text{E}} + f\mu_1^2 + \frac{b_{01}^{\text{E}}}{\alpha(k_1)}, \quad (5.37)$$

$$\begin{aligned} \mathcal{K}_{\text{NnG}}^{(2)}(\mathbf{k}_1, \mathbf{k}_2, \mathbf{k}_3) &= b_{10}^{\text{E}} \left[F_2(\mathbf{k}_1, \mathbf{k}_2) + f_{\text{NL}} \frac{\alpha(k_3)}{\alpha(k_1)\alpha(k_2)} \right] + b_{20}^{\text{E}} \\ &+ f^2 \left[2\mu_1^2\mu_2^2 + \mu_1\mu_2 \left(\mu_1^2 \frac{k_1}{k_2} + \mu_2^2 \frac{k_2}{k_1} \right) \right] \\ &+ fb_{10}^{\text{E}} \left[\mu_1^2 + \mu_2^2 + \mu_1\mu_2 \left(\frac{k_1}{k_2} + \frac{k_2}{k_1} \right) \right] - \frac{2}{7}(b_{10}^{\text{E}} - 1)S_2(\mathbf{k}_1, \mathbf{k}_2) \\ &+ f\mu_3^2 \left[G_2(\mathbf{k}_1, \mathbf{k}_2) + f_{\text{NL}} \frac{\alpha(k_3)}{\alpha(k_1)\alpha(k_2)} \right] + b_{11}^{\text{E}} \left(\frac{1}{\alpha(k_1)} + \frac{1}{\alpha(k_2)} \right) \\ &- b_{01}^{\text{E}} \left(\frac{N_2(\mathbf{k}_2, \mathbf{k}_1)}{\alpha(k_1)} + \frac{N_2(\mathbf{k}_1, \mathbf{k}_2)}{\alpha(k_2)} \right) + \frac{b_{02}^{\text{E}}}{\alpha(k_1)\alpha(k_2)} \\ &+ fb_{01}^{\text{E}} \left[\frac{\mu_1^2}{\alpha(k_2)} + \frac{\mu_2^2}{\alpha(k_1)} + \mu_1\mu_2 \left(\frac{k_1}{\alpha(k_1)k_2} + \frac{k_2}{\alpha(k_2)k_1} \right) \right]. \quad (5.38) \end{aligned}$$

Henceforth, we suppress the superscript ‘E’ to reduce clutter. In the squeezed limit,

$$N_2(\mathbf{k}_S, -\mathbf{k}_S) = -1, \quad N_2(-\mathbf{k}_S, \mathbf{k}_L) = 0, \quad N_2(\mathbf{k}_L, \mathbf{k}_S) = 0. \quad (5.39)$$

We again omit the tidal term for simplicity. Then at first-order,

$$\mathcal{K}_{\text{NnG}}^{(1)}(\mathbf{k}_S) = \mathcal{K}_{\text{NnG}}^{(1)}(-\mathbf{k}_S) = b_{10} + f\mu_S^2 + \frac{b_{01}}{\alpha(k_S)}, \quad (5.40)$$

$$\mathcal{K}_{\text{NnG}}^{(1)}(\mathbf{k}_L) = b_{10} + f\mu_L^2 + \frac{b_{01}}{\alpha(k_L)}. \quad (5.41)$$

At second-order,

$$\mathcal{K}_{\text{NnG}}^{(2)}(\mathbf{k}_S, -\mathbf{k}_S, \mathbf{k}_L) = b_{20} + \frac{2}{\alpha(k_S)}(b_{11} - b_{01}), \quad (5.42)$$

$$\begin{aligned} \mathcal{K}_{\text{NnG}}^{(2)}(-\mathbf{k}_S, \mathbf{k}_L, \mathbf{k}_S) &= b_{10} \left[\frac{10}{7} + \frac{f_{\text{NL}}}{\alpha(k_L)} \right] + b_{20} + f\mu_S^2 \left[\frac{6}{7} + \frac{f_{\text{NL}}}{\alpha(k_L)} \right] \\ &+ fb_{10} \left[\mu_S^2 + \mu_L^2 - \mu_S\mu_L \left(\frac{k_S}{k_L} + \frac{k_L}{k_S} \right) \right] \\ &+ f^2 \left[2\mu_S^2\mu_L^2 - \mu_S\mu_L \left(\mu_S^2 \frac{k_S}{k_L} + \mu_L^2 \frac{k_L}{k_S} \right) \right] \\ &+ b_{11} \left[\frac{1}{\alpha(k_S)} + \frac{1}{\alpha(k_L)} \right] + \frac{b_{02}}{\alpha(k_S)\alpha(k_L)} \\ &+ fb_{01} \left[\frac{\mu_S^2}{\alpha(k_L)} + \frac{\mu_L^2}{\alpha(k_S)} - \mu_S\mu_L \left(\frac{k_S}{\alpha(k_S)k_L} + \frac{k_L}{\alpha(k_L)k_S} \right) \right], \quad (5.43) \end{aligned}$$

$$\begin{aligned}
\mathcal{K}_{\text{NnG}}^{(2)}(\mathbf{k}_L, \mathbf{k}_S, -\mathbf{k}_S) &= b_{10} \left[\frac{10}{7} + \frac{f_{\text{NL}}}{\alpha(k_L)} \right] + b_{20} + f\mu_S^2 \left[\frac{6}{7} + \frac{f_{\text{NL}}}{\alpha(k_L)} \right] \\
&+ fb_{10} \left[\mu_S^2 + \mu_L^2 - \mu_S\mu_L \left(\frac{k_S}{k_L} + \frac{k_L}{k_S} \right) \right] \\
&+ f^2 \left[2\mu_S^2\mu_L^2 + \mu_S\mu_L \left(\mu_S^2 \frac{k_S}{k_L} + \mu_L^2 \frac{k_L}{k_S} \right) \right] \\
&+ b_{11} \left[\frac{1}{\alpha(k_S)} + \frac{1}{\alpha(k_L)} \right] + \frac{b_{02}}{\alpha(k_S)\alpha(k_L)} \\
&+ fb_{01} \left[\frac{\mu_S^2}{\alpha(k_L)} + \frac{\mu_L^2}{\alpha(k_S)} + \mu_S\mu_L \left(\frac{k_S}{\alpha(k_S)k_L} + \frac{k_L}{\alpha(k_L)k_S} \right) \right].
\end{aligned} \tag{5.44}$$

We can now work the analytical expression for the non-Gaussian Newtonian galaxy bispectrum in the squeezed limit,

$$\begin{aligned}
B_{g\text{NnG}}^{\text{sq}} &= \mathcal{K}_{\text{NnG}}^{(1)}(\mathbf{k}_S)\mathcal{K}_{\text{NnG}}^{(1)}(-\mathbf{k}_S)\mathcal{K}_{\text{NnG}}^{(2)}(\mathbf{k}_S, -\mathbf{k}_S, \mathbf{k}_L) [P^{(1)}(k_S)]^2 \\
&+ \mathcal{K}_{\text{NnG}}^{(1)}(-\mathbf{k}_S)\mathcal{K}_{\text{NnG}}^{(1)}(\mathbf{k}_L)\mathcal{K}_{\text{NnG}}^{(2)}(-\mathbf{k}_S, \mathbf{k}_L, \mathbf{k}_S) P^{(1)}(k_S)P^{(1)}(k_L) \\
&+ \mathcal{K}_{\text{NnG}}^{(1)}(\mathbf{k}_L)\mathcal{K}_{\text{NnG}}^{(1)}(\mathbf{k}_S)\mathcal{K}_{\text{NnG}}^{(2)}(\mathbf{k}_L, \mathbf{k}_S, -\mathbf{k}_S) P^{(1)}(k_L)P^{(1)}(k_S).
\end{aligned} \tag{5.45}$$

In doing so, we neglect the following:

- $[P^{(1)}(k_S)]^2$ because $[P^{(1)}(k_S)]^2 \ll P^{(1)}(k_S)P^{(1)}(k_L)$.
- $1/\alpha(k_S)$ because it is proportional to $(1/k_S^2) \ll 1$.

For the long mode k_L we have $T(k_L) \approx 1$ (refer to Figure 3.5). Hence,

$$\alpha(k_L) \approx \frac{2k_L^2(1+z)D(z)}{3\Omega_m\mathcal{H}^2}. \tag{5.46}$$

We average (5.45) over ω and μ_S to obtain the monopole as,

$$B_{g\text{NnG}}^{\text{sq}0} = \left[\mathcal{B}_0 + \frac{\mathcal{D}_1}{k_L^2} + \frac{\mathcal{D}_2}{k_L^4} \right] P^{(1)}(k_S)P^{(1)}(k_L), \tag{5.47}$$

where the first term is the same \mathcal{B}_0 given by (3.247),

$$\begin{aligned}
\mathcal{B}_0 &= \frac{20}{7}b_{10}^3 + \frac{52}{21}b_{10}^2f + 2b_{10}^2b_{20} + \frac{4}{3}b_{10}b_{20}f + \frac{68}{105}b_{10}f^2 + \frac{4}{3}b_{10}^3f + \frac{4}{3}b_{10}^2f + \frac{12}{35}b_{10}f^3 \\
&+ \frac{12}{15}b_{20}f^2 + \frac{12}{245}f^3 + \frac{4}{105}f^4,
\end{aligned} \tag{5.48}$$

which is the monopole of the galaxy bispectrum in the Newtonian approximation with initial Gaussian conditions (refer to Chapter 3). The others are the PNG coefficients,

$$\mathcal{D}_1 = \frac{1}{35} \frac{\Omega_m \mathcal{H}^2}{(1+z)D(z)} \left[(6f^2 + 54b_{10}f^2 + 210b_{10}^2f + 210b_{10}^3) f_{\text{NL}} + 70b_{20}b_{01}(f + 3b_{10}) \right. \\ \left. + 3b_{01}f(3f^2 + 28b_{10}f + 35b_{10}^2) + 7b_{11}(f^2 + 10b_{10}f + 15b_{10}^2) \right], \quad (5.49)$$

$$\mathcal{D}_2 = \frac{3}{70} \frac{\Omega_m^2 \mathcal{H}^4}{(1+z)^2 D^2(z)} \left[b_{01}f(3f + 5b_{10})(28f_{\text{NL}} + b_{01}) + 35b_{01}b_{11}(f + 3b_{10}) \right], \quad (5.50)$$

which give 0 when $f_{\text{NL}} = 0$. Equations (5.49) and (5.50) are in agreement with [28, 99].

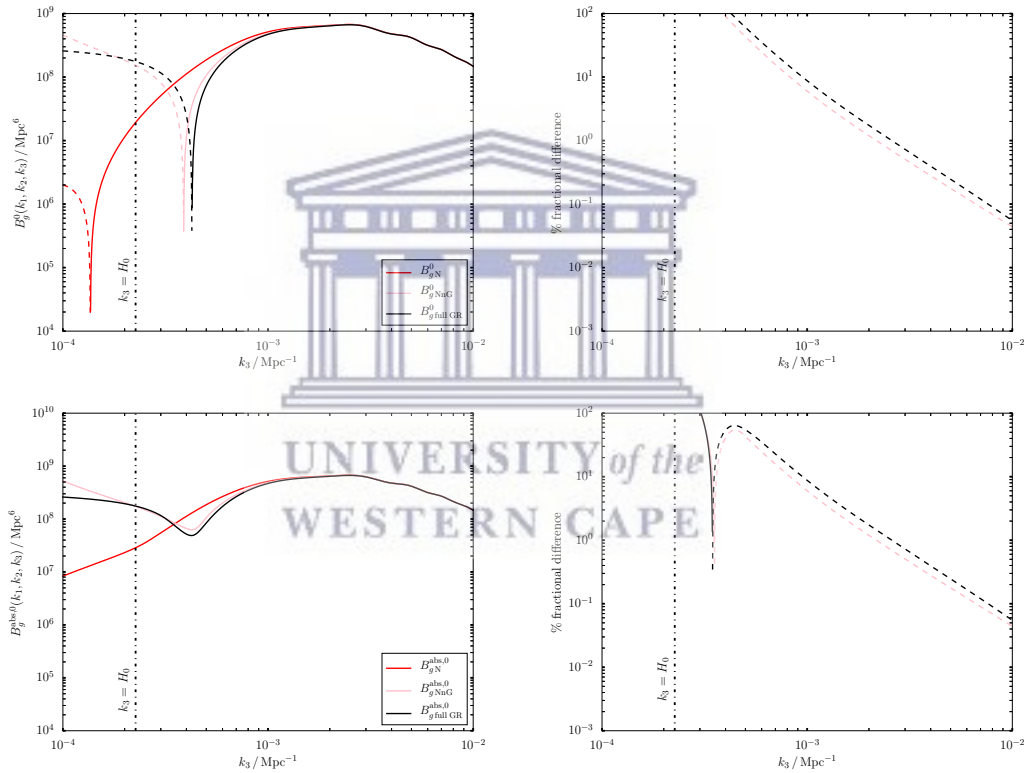


FIGURE 5.1: *Left panel:* The monopole at $z = 1.0$. We use solid line for positive and dashed line for negative. The red curve is the Gaussian Newtonian galaxy bispectrum. The pink curve is the non-Gaussian Newtonian galaxy bispectrum. The black curve is the full Gaussian relativistic galaxy bispectrum in Chapter 4. *Top left panel:* Monopole computed using **Method 1**. *Bottom left panel:* Monopole computed using **Method 2**. *Right panel:* The percentage fractional difference relative to the Gaussian Newtonian curve.

Figure 5.1 shows the plots for the moderately squeezed configuration ($k_1 = k_2 = k_S$, $k_3 \approx k_S/16$). We choose a value of $f_{\text{NL}} = 0.5$ to get the non-Gaussian Newtonian curve close to the full Gaussian GR curve (this value is consistent with [99]). The left plots show that the non-Gaussian Newtonian curve (pink) is trying to mimic the

full Gaussian GR curve (black).

The percentage fractional difference relative to the Gaussian Newtonian curve shows that the non-Gaussian Newtonian and full Gaussian GR curves are roughly the same order of magnitudes. This shows that it is possible to find a value of f_{NL} (which will depend on the galaxy bias, evolution bias, magnification bias and redshift) that closely matches the effect of the second-order relativistic corrections to the Gaussian Newtonian prediction. Therefore, neglecting the second-order GR projection effects in the galaxy bispectrum will lead to a misinterpretation of primordial Universe. This is because on the false basis of a Newtonian interpretation, we will conclude that the primordial Universe is significantly non-Gaussian and that the non-Gaussianity is of the local type [96]. This has already been shown in [31, 34] for the case of the galaxy power spectrum.

5.5 PNG in the full relativistic galaxy bispectrum

f_{NL} does not affect the second-order kernels for the vectors and tensors but, it does modify that of the second-order scalars in large proportion. The changes to the Newtonian kernels are already given in (5.37) and (5.38). For the second-order GR scalars, we begin with the kernel in the Gaussian case given by (3.65) in Chapter 3 as,

$$\begin{aligned} \mathcal{K}_S^{(2)}(\mathbf{k}_1, \mathbf{k}_2, \mathbf{k}_3) = & \frac{1}{k_1^2 k_2^2} \left\{ \Gamma_1 + \tilde{\Gamma}_1 + E_2(\mathbf{k}_1, \mathbf{k}_2, \mathbf{k}_3) \tilde{\Gamma}_2 \right. \\ & + i(\mu_1 k_1 + \mu_2 k_2) \Gamma_2 + \frac{k_1^2 k_2^2}{k_3^2} \left[F_2(\mathbf{k}_1, \mathbf{k}_2) \Gamma_3 + G_2(\mathbf{k}_1, \mathbf{k}_2) \Gamma_4 \right] \\ & + (\mu_1 k_1 \mu_2 k_2) \Gamma_5 + (\mathbf{k}_1 \cdot \mathbf{k}_2) \Gamma_6 + (k_1^2 + k_2^2) \Gamma_7 + (\mu_1^2 k_1^2 + \mu_2^2 k_2^2) \Gamma_8 \\ & + i \left[(\mu_1 k_1^3 + \mu_2 k_2^3) \Gamma_9 + (\mu_1 k_1 + \mu_2 k_2) (\mathbf{k}_1 \cdot \mathbf{k}_2) \Gamma_{10} \right. \\ & + k_1 k_2 (\mu_1 k_2 + \mu_2 k_1) \Gamma_{11} + (\mu_1^3 k_1^3 + \mu_2^3 k_2^3) \Gamma_{12} \\ & \left. \left. + \mu_1 \mu_2 k_1 k_2 (\mu_1 k_1 + \mu_2 k_2) \Gamma_{13} + \mu_3 \frac{k_1^2 k_2^2}{k_3} G_2(\mathbf{k}_1, \mathbf{k}_2) \Gamma_{14} \right] \right\}. \end{aligned} \quad (5.51)$$

Below, we list the changes that PNG brings to (5.51):

- By (5.7) and (5.8), F_2 and G_2 need to be modified as,

$$F_2(\mathbf{k}_1, \mathbf{k}_2) \rightarrow F_2(\mathbf{k}_1, \mathbf{k}_2) + f_{\text{NL}} \frac{\alpha(k_3)}{\alpha(k_1)\alpha(k_2)}, \quad G_2(\mathbf{k}_1, \mathbf{k}_2) \rightarrow G_2(\mathbf{k}_1, \mathbf{k}_2) + f_{\text{NL}} \frac{\alpha(k_3)}{\alpha(k_1)\alpha(k_2)}. \quad (5.52)$$

- We have additional terms to the dynamical correction $\tilde{\Gamma}_1$ as follows:

$$\tilde{\Gamma}_1 \rightarrow \tilde{\Gamma}_1 + \bar{\Gamma}_1, \quad (5.53)$$

where,

$$\begin{aligned} \frac{\bar{\Gamma}_1}{\mathcal{H}^4} &= \frac{27}{10} \Omega_m^2 f_{\text{NL}} \left[-1 + 2f + b_e - 4\mathcal{Q} - \frac{2(1-\mathcal{Q})}{\bar{\chi}\mathcal{H}} - \frac{\mathcal{H}'}{\mathcal{H}^2} \right] \\ &+ \frac{9}{5} \Omega_m f f_{\text{NL}} \left[5 - 2f - 4\mathcal{Q} - \frac{2(1-\mathcal{Q})}{\bar{\chi}\mathcal{H}} - \frac{3\mathcal{H}'}{\mathcal{H}^2} \right] \\ &+ \frac{6}{5} f f_{\text{NL}} (3 - b_e) - \frac{9}{5} \Omega_m f_{\text{NL}} \frac{f'}{\mathcal{H}}. \end{aligned} \quad (5.54)$$

- Because f_{NL} introduces coupling between the short and long modes, we have to restore the long modes $v_{\text{GR}}^{(2)}$ and $\delta_{\text{TGR}}^{(2)}$.

- We have the Doppler term $\partial_{\parallel} v_{\text{GR}}^{(2)}$ that leads to a term of the form,

$$i\mu_3 k_3 [\bar{\Gamma}_2(z) + E_2(\mathbf{k}_1, \mathbf{k}_2, \mathbf{k}_3) \bar{\Gamma}_3(z)] / (k_1 k_2)^2, \quad (5.55)$$

where,

$$\frac{\bar{\Gamma}_2}{\mathcal{H}^3} = \frac{9}{2} \Omega_m f \left[-b_e + 2\mathcal{Q} + \frac{2(1-\mathcal{Q})}{\bar{\chi}\mathcal{H}} + \frac{\mathcal{H}'}{\mathcal{H}^2} \right] \left[1 - \frac{2}{5} f_{\text{NL}} \left(1 + \frac{2f}{3\Omega_m} \right) \right], \quad (5.56)$$

$$\frac{\bar{\Gamma}_3}{\mathcal{H}^3} = 3\Omega_m f \left[b_e - 2\mathcal{Q} - \frac{2(1-\mathcal{Q})}{\bar{\chi}\mathcal{H}} - \frac{\mathcal{H}'}{\mathcal{H}^2} \right]. \quad (5.57)$$

- We have the GR correction to the second-order Kaiser term $-\mathcal{H}^{-1} \partial_{\parallel}^2 v_{\text{GR}}^{(2)}$ which gives,

$$\mu_3^2 k_3^2 [\bar{\Gamma}_4(z) + E_2(\mathbf{k}_1, \mathbf{k}_2, \mathbf{k}_3) \bar{\Gamma}_5(z)] / (k_1 k_2)^2, \quad (5.58)$$

where,

$$\frac{\bar{\Gamma}_4}{\mathcal{H}^2} = -\frac{9}{2} \Omega_m f \left[1 - \frac{2}{5} f_{\text{NL}} \left(1 + \frac{2f}{3\Omega_m} \right) \right], \quad \frac{\bar{\Gamma}_5}{\mathcal{H}^2} = 3\Omega_m f. \quad (5.59)$$

- $\delta_{\text{TGR}}^{(2)}$ modifies Γ_6 and Γ_7 as follows,

$$\Gamma_6 \rightarrow \Gamma_6 + \bar{\Gamma}_6(z), \quad \Gamma_7 \rightarrow \Gamma_7 + \bar{\Gamma}_7(z), \quad (5.60)$$

where,

$$\frac{\bar{\Gamma}_6}{\mathcal{H}^2} = \frac{3}{2}\Omega_m \left[1 + \frac{2f}{3\Omega_m} + \frac{12}{5}f_{\text{NL}} \left(1 + \frac{2f}{3\Omega_m} \right) \right], \quad (5.61)$$

$$\frac{\bar{\Gamma}_7}{\mathcal{H}^2} = -3\Omega_m \left[1 + \frac{2f}{3\Omega_m} - \frac{3}{5}f_{\text{NL}} \left(1 + \frac{2f}{3\Omega_m} \right) \right]. \quad (5.62)$$

- The first line in (5.34) shows the linear galaxy bias which can be written as,

$$b_1(z, k) = b_{10}(z) + \frac{b_{01}(z)}{\alpha(k)}. \quad (5.63)$$

Due to the scale dependent part of (5.63) we have the following extra terms:

$$\frac{1}{(k_1 k_2)^2} \left\{ \left(\frac{k_1^2}{\alpha(k_1)} + \frac{k_2^2}{\alpha(k_2)} \right) \bar{\Gamma}_8(z) + i \left[\left(\frac{\mu_1 k_1^3}{\alpha(k_1)} + \frac{\mu_2 k_2^3}{\alpha(k_2)} \right) \bar{\Gamma}_9(z) + k_1 k_2 \left(\frac{\mu_1 k_2}{\alpha(k_2)} + \frac{\mu_2 k_1}{\alpha(k_1)} \right) \bar{\Gamma}_{10}(z) \right] \right\}, \quad (5.64)$$

where,

$$\begin{aligned} \frac{\bar{\Gamma}_8}{\mathcal{H}^2} &= \frac{3}{2}\Omega_m \left[b_{01} \left(1 - f + b_e - 4\mathcal{Q} - \frac{2(1-\mathcal{Q})}{\bar{\chi}\mathcal{H}} - \frac{3\mathcal{H}'}{\mathcal{H}^2} \right) + \frac{b'_{01}}{\mathcal{H}} + 2 \left(1 - \frac{1}{\bar{\chi}\mathcal{H}} \right) \frac{\partial b_{01}}{\partial \ln \bar{L}} \right] \\ &\quad - f \left[b_{01} \left(-4 + b_e - \frac{2\mathcal{H}'}{\mathcal{H}^2} \right) + \frac{b'_{01}}{\mathcal{H}} \right], \end{aligned} \quad (5.65)$$

$$\frac{\bar{\Gamma}_9}{\mathcal{H}} = -\frac{3}{2}\Omega_m b_{01}, \quad (5.66)$$

$$\frac{\bar{\Gamma}_{10}}{\mathcal{H}} = f \left[b_{01} \left(-1 + b_e - 2\mathcal{Q} - \frac{2(1-\mathcal{Q})}{\bar{\chi}\mathcal{H}} - \frac{3\mathcal{H}'}{\mathcal{H}^2} \right) + \frac{b'_{01}}{\mathcal{H}} + 2 \left(1 - \frac{1}{\bar{\chi}\mathcal{H}} \right) \frac{\partial b_{01}}{\partial \ln \bar{L}} \right]. \quad (5.67)$$

Therefore (5.51) becomes,

$$\begin{aligned}
\mathcal{K}_S^{(2)}(\mathbf{k}_1, \mathbf{k}_2, \mathbf{k}_3) = & \frac{1}{k_1^2 k_2^2} \left\{ \Gamma_1 + \tilde{\Gamma}_1 + \bar{\Gamma}_1 + E_2(\mathbf{k}_1, \mathbf{k}_2, \mathbf{k}_3) \tilde{\Gamma}_2 \right. \\
& + i \left[(\mu_1 k_1 + \mu_2 k_2) \Gamma_2 + \mu_3 k_3 (\bar{\Gamma}_2 + E_2(\mathbf{k}_1, \mathbf{k}_2, \mathbf{k}_3) \bar{\Gamma}_3) \right] \\
& + \frac{k_1^2 k_2^2}{k_3^2} \left(F_2(\mathbf{k}_1, \mathbf{k}_2) + f_{\text{NL}} \frac{\alpha(k_3)}{\alpha(k_1) \alpha(k_2)} \right) \Gamma_3 \\
& + \frac{k_1^2 k_2^2}{k_3^2} \left(G_2(\mathbf{k}_1, \mathbf{k}_2) + f_{\text{NL}} \frac{\alpha(k_3)}{\alpha(k_1) \alpha(k_2)} \right) \Gamma_4 \\
& + (\mu_1 k_1 \mu_2 k_2) \Gamma_5 + \mu_3^2 k_3^2 (\bar{\Gamma}_4 + E_2(\mathbf{k}_1, \mathbf{k}_2, \mathbf{k}_3) \bar{\Gamma}_5) \\
& + (\mathbf{k}_1 \cdot \mathbf{k}_2) (\Gamma_6 + \bar{\Gamma}_6) + (k_1^2 + k_2^2) (\Gamma_7 + \bar{\Gamma}_7) \\
& + \left(\frac{k_1^2}{\alpha(k_1)} + \frac{k_2^2}{\alpha(k_2)} \right) \bar{\Gamma}_8 + (\mu_1^2 k_1^2 + \mu_2^2 k_2^2) \Gamma_8 \\
& + i \left[(\mu_1 k_1^3 + \mu_2 k_2^3) \Gamma_9 + \left(\frac{\mu_1 k_1^3}{\alpha(k_1)} + \frac{\mu_2 k_2^3}{\alpha(k_2)} \right) \bar{\Gamma}_9 \right. \\
& \quad + (\mu_1 k_1 + \mu_2 k_2) (\mathbf{k}_1 \cdot \mathbf{k}_2) \Gamma_{10} + k_1 k_2 (\mu_1 k_2 + \mu_2 k_1) \Gamma_{11} \\
& \quad + k_1 k_2 \left(\frac{\mu_1 k_2}{\alpha(k_2)} + \frac{\mu_2 k_1}{\alpha(k_1)} \right) \bar{\Gamma}_{10} + (\mu_1^3 k_1^3 + \mu_2^3 k_2^3) \Gamma_{12} \\
& \quad + \mu_1 \mu_2 k_1 k_2 (\mu_1 k_1 + \mu_2 k_2) \Gamma_{13} \\
& \quad \left. + \mu_3 \frac{k_1^2 k_2^2}{k_3} \left(G_2(\mathbf{k}_1, \mathbf{k}_2) + f_{\text{NL}} \frac{\alpha(k_3)}{\alpha(k_1) \alpha(k_2)} \right) \Gamma_{14} \right] \left. \right\}. \tag{5.68}
\end{aligned}$$

Figure 5.2 shows the comparison between the Gaussian and non-Gaussian galaxy bispectra. We are still working with $f_{\text{NL}} = 0.5$. The Gaussian Newtonian curve (red) goes negative on super-Hubble scale due to the tidal term. With f_{NL} , this negative part is pulled within the horizon scale (pink). For the case of the full Gaussian relativistic curve (black), it goes negative on large scales because the second-order scalars are negative. Adding the effect of f_{NL} moves the negative part towards the right i.e., further within the horizon scale (grey).

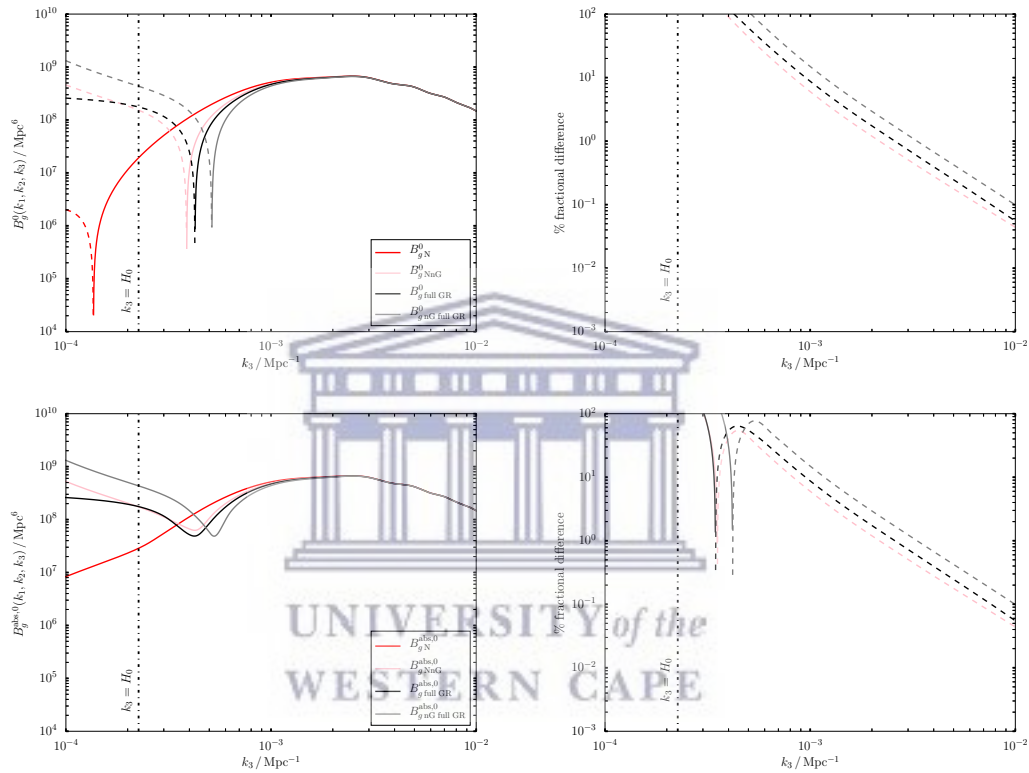


FIGURE 5.2: The monopole at $z = 1.0$. We use solid line for positive and dashed line for negative. The red and black curves are the Gaussian Newtonian and full relativistic galaxy bispectra (refer to Chapter 4). The pink and grey curves are the non-Gaussian Newtonian and full relativistic galaxy bispectra respectively. *Top left panel:* Monopole computed using **Method 1**. *Bottom left panel:* Monopole computed using **Method 2**. *Right panel:* The percentage fractional difference relative to the Gaussian Newtonian curve.

Chapter 6

Conclusion and future work

First we highlight the main findings of the project.

6.1 Summary

We begin by giving a summary of each chapter:

- Chapter 1 starts with the fundamentals of cosmology. It talks about the standard model of the background Universe and gives the relevant important equations for an expanding FLRW Universe. It then explores the first- and second-order perturbation theory in the Λ CDM model. It also summarizes the essential cosmological-related sciences of the SKA.
- Chapter 2 shows a detailed derivation on the first-order relativistic corrections in the galaxy number count. At second-order, it uses the general formula provided by [49] and breaks down the highly complex equation into simple parts: scalars, vectors and tensors. All integrated terms are omitted since we work with the Fourier galaxy bispectrum at a fixed redshift so that we necessarily are within the plane-parallel approximation where integrated and wide-angle effects cannot be simply incorporated. In order to include these effects we need to use the angular bispectrum which also would allow for the correlation of different redshift bins (we work at fixed redshift). The initial condition for the primordial gravitation potential is assumed to be Gaussian.
- Chapter 3 derives all the Fourier kernels for the first- and second-order terms discussed in Chapter 2. It then shortly introduces the galaxy power spectrum and fully derives the galaxy bispectrum, giving the analytical expressions in the

squeezed limit. Unlike the galaxy power spectrum which is always a real quantity, the galaxy bispectrum has real and imaginary parts. With $m = 0$, the even multipoles of the bispectrum are always real whilst the odd multipoles are always imaginary.

- Chapter 4 looks at the monopole of the galaxy bispectrum for a moderately squeezed configuration with $k_1 = k_2 = k_S$ and $k_3 = k_L \approx k_S/16$. It explores the different correlations in the galaxy bispectrum, showing the contributions from the scalars (S), vectors (V) and tensors (T). For the chosen configuration, the scalars dominate over the vectors and tensors, and provide a good approximation to the full GR galaxy bispectrum.
- Chapter 5 complements the results presented in Chapter 4. First, it adds the effect of non-Gaussianity i.e., the f_{NL} parameter to the Newtonian prediction. We find that at $z = 1.0$, the non-Gaussian Newtonian curve with $f_{\text{NL}} = 0.5$ mimics the full Gaussian GR curve on large scales (*top left* plot in Figure 5.1). Finally, it shows the full non-Gaussian GR curve where a value of $f_{\text{NL}} = 0.5$ pulls the negative part of the curve well inside the Horizon scale as compared to the full Gaussian GR case (*top left* plot in Figure 5.2).

6.2 Major findings of the project

The effect of non-Gaussianity in the galaxy distribution is generated by the following:

- Primordial nature of the gravitational field Φ .
- Intrinsic second-order GR projection effects.
- Quadratic first-order GR projection effects.

The standard Newtonian galaxy bispectrum takes care of redshift space distortions and excludes all other relativistic projection effects. This has further been explored in [129] where they consider the GR effect arising from weak lensing and omit all the other lightcone effects. This PhD thesis complements their work by computing for the first time the galaxy bispectrum for a primordial Gaussian Universe, including all the local GR projection effects up to second order. We assume the plane-parallel approximation in Fourier space which breaks down on the ultra-large transverse scales. The galaxy bispectrum is very sensitive to the galaxy bias parameters. To avoid spurious gauge effects, we incorporate a careful treatment of the galaxy bias on ultra-large scales. We choose to work with the local model for the non-linear bias which includes the tidal effect

[64]. This leads to a relativistic bias relation for the Poisson-gauge galaxy overdensity contrast given by (2.89).

We give a full analysis on the second-order scalars (S), vectors (V) and tensors (T) in the galaxy bispectrum. We present all the details on the Fourier geometry in Chapter 3. We give the explicit forms of the kernels for S, V and T in (3.65), (3.126)-(3.128) and (3.163)-(3.165) respectively. We also provide the analytical formula for the squeezed galaxy bispectrum in (3.246). We show the plots for a moderately squeezed configuration ($k_1 = k_2 = k_S$, $k_3 \approx k_S/16$) in Figure 4.7. The GR lightcone effects can be significant e.g., when the short modes are at equality scale ($k_S = 0.01 \text{ Mpc}^{-1}$) we have a percentage GR correction of $\mathcal{O}(50\%)$ in the bispectrum monopole at $z = 1.0$. To show information on other triangular configurations, we generate 2-D colour intensity maps as shown in Figure 4.8 and Figure 4.9. These maps show the percentage difference between the GR and Newtonian galaxy bispectra. The difference is greater near the squeezed limit.

We also look at the Newtonian galaxy bispectrum in a non-Gaussian Universe. We show in Chapter 5 a full description on the non-linearities due f_{NL} . The bias relation is given by (5.30) and the Fourier kernels are presented in (5.37) and (5.38). We derive the analytical expression for the non-Gaussian Newtonian monopole in (5.47). At $z = 1.0$, we find that the non-Gaussian Newtonian monopole with a value of $f_{\text{NL}} = 0.5$ mimics the full local GR effects in the Gaussian case. This is shown in the *top* panel of Figure 5.1. Then we attempt to include the effect of f_{NL} in the full local relativistic galaxy bispectrum. This leads to the modification of the kernel for the second-order scalars which is given by (5.68). The vectors and tensors are unaffected by f_{NL} . We show the plot for the case of a moderately squeezed configuration in Figure 5.2.

6.3 Upcoming projects

We have taken the first step towards a complete analysis of the second-order lightcone projection effects in the galaxy bispectrum. Our results are incomplete because we have omitted:

- Second-order effect of the radiation era on initial conditions for sub-equality modes.
- Non-local projection effects i.e., the integrated GR effects.
- Wide-angle and radial (cross-bin) correlations.

The first point will require the use of a second-order Boltzmann code, as in [98]. The last two points will be the hardest ones to achieve since they will require an angular

bispectrum analysis on the past lightcone. This will involve a high degree of complexity [129]. Other possible interesting projects in the pipeline for publications will be:

- Extracting information from the other multipoles of the galaxy bispectrum.
- Applying our derived second-order Fourier kernels to the case of HI intensity mapping. This will require setting,

$$\mathcal{Q} = 1, \quad \frac{d\mathcal{Q}}{d \ln \bar{L}} = 0 \quad \text{and} \quad (6.1)$$

inputting a proper model for the evolution bias as in [130],

$$b_e = -\frac{d \ln [(1+z)^{-3} \bar{n}_g]}{d \ln (1+z)} \quad \text{with} \quad \bar{n}_g = (1+z)^2 \mathcal{H} \bar{T}_{\text{HI}}, \quad (6.2)$$

where the background HI brightness temperature is given by the fitting formula [131],

$$\bar{T}_{\text{HI}}(z) = 5.5919 \times 10^{-2} + 2.3242 \times 10^{-1} z - 2.4136 \times 10^{-2} z^2 \text{ mK}. \quad (6.3)$$



Bibliography

- [1] A. K. Singal, *Horizon, homogeneity and flatness problems ? do their resolutions really depend upon inflation?*, in *Proceedings, National Conference on Current Issues in Cosmology, Astrophysics and High Energy Physics (CICAHEP): Dibrugarh, India, November 2-5, 2015*, (Dibrugarh, India), pp. 94–99, Dibrugarh Univ., Dibrugarh Univ., 2016. [arXiv:1603.01539](#).
- [2] G. Veneziano, *A Simple / short introduction to pre - big bang physics / cosmology*, in *Highlights of subnuclear physics: 50 years later. Proceedings, 35th Course of the International School of Subnuclear Physics, Erice, Italy, August 26-September 4, 1997*, pp. 364–380, 1997. [hep-th/9802057](#).
- [3] S. S. Bayin, *Is the Universe Flat?*, [arXiv:1309.5815](#).
- [4] J.-P. Uzan, *The big-bang theory: construction, evolution and status*, 2016. [arXiv:1606.06112](#).
- [5] L. Senatore, *Lectures on Inflation*, in *Proceedings, Theoretical Advanced Study Institute in Elementary Particle Physics: New Frontiers in Fields and Strings (TASI 2015): Boulder, CO, USA, June 1-26, 2015*, pp. 447–543, 2017. [arXiv:1609.00716](#).
- [6] S. Chongchitnan, *Reheating in an inflation model parametrized by the Hubble radius*, [arXiv:1709.03482](#).
- [7] A. R. Liddle, *An Introduction to cosmological inflation*, in *Proceedings, Summer School in High-energy physics and cosmology: Trieste, Italy, June 29-July 17, 1998*, pp. 260–295, 1999. [astro-ph/9901124](#).
- [8] J. Martin, C. Ringeval, R. Trotta, and V. Vennin, *The Best Inflationary Models After Planck*, *JCAP* **1403** (2014) 039, [[arXiv:1312.3529](#)].
- [9] W. J. Handley, S. D. Brechet, A. N. Lasenby, and M. P. Hobson, *Kinetic Initial Conditions for Inflation*, *Phys. Rev.* **D89** (2014), no. 6 063505, [[arXiv:1401.2253](#)].

- [10] N. Yoshida, *Structure Formation in the Early Universe*, [arXiv:0906.4372](https://arxiv.org/abs/0906.4372).
- [11] V. Springel, C. S. Frenk, and S. D. M. White, *The large-scale structure of the Universe*, *Nature* **440** (2006) 1137, [[astro-ph/0604561](https://arxiv.org/abs/astro-ph/0604561)].
- [12] M. Iye, *High redshift galaxy surveys*, *Proc. SPIE Int. Soc. Opt. Eng.* **7016** (2008) 701602, [[arXiv:0809.0050](https://arxiv.org/abs/0809.0050)].
- [13] J. W. Fowler et al., *CMB observations with a compact heterogeneous 150-GHz interferometer in Chile*, *Astrophys. J. Suppl.* **156** (2005) 1, [[astro-ph/0403137](https://arxiv.org/abs/astro-ph/0403137)].
- [14] J. Borrill, *The challenge of data analysis for future CMB observations*, *AIP Conf. Proc.* **476** (1999), no. 1 277–282, [[astro-ph/9903204](https://arxiv.org/abs/astro-ph/9903204)].
- [15] **WMAP** Collaboration, C. L. Bennett et al., *Nine-Year Wilkinson Microwave Anisotropy Probe (WMAP) Observations: Final Maps and Results*, *Astrophys. J. Suppl.* **208** (2013) 20, [[arXiv:1212.5225](https://arxiv.org/abs/1212.5225)].
- [16] **Planck** Collaboration, P. A. R. Ade et al., *Planck 2015 results. XIII. Cosmological parameters*, *Astron. Astrophys.* **594** (2016) A13, [[arXiv:1502.01589](https://arxiv.org/abs/1502.01589)].
- [17] J. Miralda-Escude, *The dark age of the universe*, *Science* **300** (2003) 1904–1909, [[astro-ph/0307396](https://arxiv.org/abs/astro-ph/0307396)].
- [18] Lucian Dorneanu, *Nuclear chemistry of the big bang*, 2007. [Online; accessed February 28, 2018].
- [19] D. H. Lyth and A. Riotto, *Particle physics models of inflation and the cosmological density perturbation*, *Phys. Rept.* **314** (1999) 1–146, [[hep-ph/9807278](https://arxiv.org/abs/hep-ph/9807278)].
- [20] C. Bonvin and R. Durrer, *What galaxy surveys really measure*, *Phys. Rev.* **D84** (2011) 063505, [[arXiv:1105.5280](https://arxiv.org/abs/1105.5280)].
- [21] V. Tansella, G. Jelic-Cizmek, C. Bonvin, and R. Durrer, *COFFE: a code for the full-sky relativistic galaxy correlation function*, [arXiv:1806.11090](https://arxiv.org/abs/1806.11090).
- [22] X. Chen, *Primordial Non-Gaussianities from Inflation Models*, *Adv. Astron.* **2010** (2010) 638979, [[arXiv:1002.1416](https://arxiv.org/abs/1002.1416)].
- [23] V. Acquaviva, N. Bartolo, S. Matarrese, and A. Riotto, *Second order cosmological perturbations from inflation*, *Nucl. Phys.* **B667** (2003) 119–148, [[astro-ph/0209156](https://arxiv.org/abs/astro-ph/0209156)].

- [24] J. M. Maldacena, *Non-Gaussian features of primordial fluctuations in single field inflationary models*, *JHEP* **05** (2003) 013, [[astro-ph/0210603](#)].
- [25] N. Bartolo, J. P. B. Almeida, S. Matarrese, M. Pietroni, and A. Riotto, *Signatures of Primordial non-Gaussianities in the Matter Power-Spectrum and Bispectrum: the Time-RG Approach*, *JCAP* **1003** (2010) 011, [[arXiv:0912.4276](#)].
- [26] S. Das, *Primordial non-Gaussianity as a signature of pre-inflationary radiation era*, [arXiv:1302.0172](#).
- [27] M. Tellarini, A. J. Ross, G. Tasinato, and D. Wands, *Non-local bias in the halo bispectrum with primordial non-Gaussianity*, *JCAP* **1507** (2015), no. 07 004, [[arXiv:1504.00324](#)].
- [28] M. Tellarini, A. J. Ross, G. Tasinato, and D. Wands, *Galaxy bispectrum, primordial non-Gaussianity and redshift space distortions*, *JCAP* **1606** (2016), no. 06 014, [[arXiv:1603.06814](#)].
- [29] F. Schmidt and M. Kamionkowski, *Halo Clustering with Non-Local Non-Gaussianity*, *Phys. Rev.* **D82** (2010) 103002, [[arXiv:1008.0638](#)].
- [30] C. Carbone, O. Mena, and L. Verde, *Cosmological Parameters Degeneracies and Non-Gaussian Halo Bias*, *JCAP* **1007** (2010) 020, [[arXiv:1003.0456](#)].
- [31] M. Bruni, R. Crittenden, K. Koyama, R. Maartens, C. Pitrou, and D. Wands, *Disentangling non-Gaussianity, bias and GR effects in the galaxy distribution*, *Phys. Rev.* **D85** (2012) 041301, [[arXiv:1106.3999](#)].
- [32] D. Jeong, F. Schmidt, and C. M. Hirata, *Large-scale clustering of galaxies in general relativity*, *Phys. Rev.* **D85** (2012) 023504, [[arXiv:1107.5427](#)].
- [33] S. Camera, M. G. Santos, and R. Maartens, *Probing primordial non-Gaussianity with SKA galaxy redshift surveys: a fully relativistic analysis*, *Mon. Not. Roy. Astron. Soc.* **448** (2015), no. 2 1035–1043, [[arXiv:1409.8286](#)].
- [34] S. Camera, R. Maartens, and M. G. Santos, *Einstein's legacy in galaxy surveys*, *Mon. Not. Roy. Astron. Soc.* **451** (2015), no. 1 L80–L84, [[arXiv:1412.4781](#)].
- [35] P. Schneider, *Weak gravitational lensing*, in *Proceedings, 33rd Advanced Saas Fee Course on Gravitational Lensing: Strong, Weak, and Micro: Les Diablerets, Switzerland, April 7-12, 2003*, pp. 269–451, 2006. [astro-ph/0509252](#).
- [36] S. M. Carroll, *Lecture notes on general relativity*, [gr-qc/9712019](#).

- [37] K. Liao, Z. Li, G.-J. Wang, and X.-L. Fan, *Test of the FLRW metric and curvature with strong lens time delays*, *Astrophys. J.* **839** (2017), no. 2 70, [[arXiv:1704.04329](#)].
- [38] S. Dodelson, *Modern Cosmology*. Academic Press, Amsterdam, 2003.
- [39] **Supernova Search Team** Collaboration, A. G. Riess et al., *Observational evidence from supernovae for an accelerating universe and a cosmological constant*, *Astron. J.* **116** (1998) 1009–1038, [[astro-ph/9805201](#)].
- [40] N. G. Busca et al., *Baryon Acoustic Oscillations in the Ly- α forest of BOSS quasars*, *Astron. Astrophys.* **552** (2013) A96, [[arXiv:1211.2616](#)].
- [41] **DES** Collaboration, T. Abbott et al., *The dark energy survey*, [astro-ph/0510346](#).
- [42] M. Visser, *General relativistic energy conditions: The Hubble expansion in the epoch of galaxy formation*, *Phys. Rev.* **D56** (1997) 7578–7587, [[gr-qc/9705070](#)].
- [43] **Planck** Collaboration, N. Aghanim et al., *Planck 2018 results. VI. Cosmological parameters*, [arXiv:1807.06209](#).
- [44] D. W. Hogg, *Distance measures in cosmology*, [astro-ph/9905116](#).
- [45] C. Clarkson, O. Umeh, R. Maartens, and R. Durrer, *What is the distance to the CMB?*, *JCAP* **1411** (2014), no. 11 036, [[arXiv:1405.7860](#)].
- [46] Bsouter, *Back to the future: Cosmic distance measurements just got better!*, 2012. [Online; accessed February 28, 2017].
- [47] Wikipedia, *Cosmic microwave background*, 2017. [Online; accessed February 28, 2017].
- [48] K. A. Malik and D. R. Matravers, *A Concise Introduction to Perturbation Theory in Cosmology*, *Class. Quant. Grav.* **25** (2008) 193001, [[arXiv:0804.3276](#)].
- [49] D. Bertacca, *Observed galaxy number counts on the light cone up to second order: III. Magnification bias*, *Class. Quant. Grav.* **32** (2015), no. 19 195011, [[arXiv:1409.2024](#)].
- [50] L. Sberna and P. Pani, *Nonsingular solutions and instabilities in Einstein-scalar-Gauss-Bonnet cosmology*, *Phys. Rev.* **D96** (2017), no. 12 124022, [[arXiv:1708.06371](#)].
- [51] H. E. S. Velten, R. F. vom Marttens, and W. Zimdahl, *Aspects of the cosmological ?coincidence problem?*, *Eur. Phys. J.* **C74** (2014), no. 11 3160, [[arXiv:1410.2509](#)].

- [52] L. Amendola and S. Tsujikawa, *Dark energy: theory and observations*. Cambridge University Press, Cambridge, 2010.
- [53] R. Durrer, *Cosmological perturbation theory, Lect. Notes Phys.* **653** (2004) 31–70, [[astro-ph/0402129](#)]. [,31(2004)].
- [54] D. Duniya, D. Bertacca, and R. Maartens, *Clustering of quintessence on horizon scales and its imprint on HI intensity mapping, JCAP* **1310** (2013) 015, [[arXiv:1305.4509](#)].
- [55] D. G. A. Duniya, D. Bertacca, and R. Maartens, *Probing the imprint of interacting dark energy on very large scales, Phys. Rev.* **D91** (2015) 063530, [[arXiv:1502.06424](#)].
- [56] L. Perivolaropoulos, *Consistency of Λ CDM with Geometric and Dynamical Probes, J. Phys. Conf. Ser.* **222** (2010) 012024, [[arXiv:1002.3030](#)].
- [57] T. Baker, P. G. Ferreira, and C. Skordis, *A Fast Route to Modified Gravitational Growth, Phys. Rev.* **D89** (2014), no. 2 024026, [[arXiv:1310.1086](#)].
- [58] M. J. Hudson and S. J. Turnbull, *The growth rate of cosmic structure from peculiar velocities at low and high redshifts, Astrophys. J.* **751** (2013) L30, [[arXiv:1203.4814](#)].
- [59] L. Samushia et al., *The clustering of galaxies in the SDSS-III Baryon Oscillation Spectroscopic Survey: measuring growth rate and geometry with anisotropic clustering, Mon. Not. Roy. Astron. Soc.* **439** (2014), no. 4 3504–3519, [[arXiv:1312.4899](#)].
- [60] E. V. Linder and R. N. Cahn, *Parameterized Beyond-Einstein Growth, Astropart. Phys.* **28** (2007) 481–488, [[astro-ph/0701317](#)].
- [61] O. Umeh, *The influence of structure formation on the evolution of the universe*. PhD thesis, University of Cape Town, 2013.
- [62] K. Nakamura, *Second-order gauge invariant cosmological perturbation theory: Einstein equations in terms of gauge invariant variables, Prog. Theor. Phys.* **117** (2007) 17–74, [[gr-qc/0605108](#)].
- [63] F. Bernardeau, S. Colombi, E. Gaztanaga, and R. Scoccimarro, *Large scale structure of the universe and cosmological perturbation theory, Phys. Rept.* **367** (2002) 1–248, [[astro-ph/0112551](#)].
- [64] V. Desjacques, D. Jeong, and F. Schmidt, *Large-Scale Galaxy Bias, arXiv:1611.09787*.

- [65] **Cosmology SWG** Collaboration, F. B. Abdalla et al., *Cosmology from HI galaxy surveys with the SKA*, [arXiv:1501.04035](#).
- [66] D. Jeong, L. Dai, M. Kamionkowski, and A. S. Szalay, *The redshift-space galaxy two-point correlation function and baryon acoustic oscillations*, *Mon. Not. Roy. Astron. Soc.* **449** (2015), no. 3 3312–3322, [[arXiv:1408.4648](#)].
- [67] M. Lopez-Corredoira, *Alcock-Paczynski cosmological test*, *Astrophys. J.* **781** (2014), no. 2 96, [[arXiv:1312.0003](#)].
- [68] A. Raccanelli et al., *Measuring redshift-space distortions with future SKA surveys*, [arXiv:1501.03821](#).
- [69] M. G. Santos et al., *Cosmology with a SKA HI intensity mapping survey*, [arXiv:1501.03989](#).
- [70] A. Challinor and A. Lewis, *The linear power spectrum of observed source number counts*, *Phys. Rev.* **D84** (2011) 043516, [[arXiv:1105.5292](#)].
- [71] D. Alonso, P. Bull, P. G. Ferreira, R. Maartens, and M. Santos, *Ultra large-scale cosmology in next-generation experiments with single tracers*, *Astrophys. J.* **814** (2015), no. 2 145, [[arXiv:1505.07596](#)].
- [72] S. Jolicoeur, O. Umeh, R. Maartens, and C. Clarkson, *Imprints of local lightcone projection effects on the galaxy bispectrum. II*, *JCAP* **1709** (2017) 040, [[arXiv:1703.09630](#)].
- [73] C. Bonvin, *Isolating relativistic effects in large-scale structure*, *Class. Quant. Grav.* **31** (2014), no. 23 234002, [[arXiv:1409.2224](#)].
- [74] J. Yoo, *Relativistic Effect in Galaxy Clustering*, *Class. Quant. Grav.* **31** (2014) 234001, [[arXiv:1409.3223](#)].
- [75] K. A. Malik, *Cosmological perturbations in an inflationary universe*. PhD thesis, Portsmouth U., 2001. [astro-ph/0101563](#).
- [76] Yu. L. Bolotin, V. A. Cherkaskiy, G. I. Ivashkevych, O. A. Lemets, and D. A. Yerokhin, *Dynamics of the Universe in Problems*, [arXiv:0904.0382](#).
- [77] W. H. Kinney, *Cosmology, inflation, and the physics of nothing*, *NATO Sci. Ser. II* **123** (2003) 189–243, [[astro-ph/0301448](#)].
- [78] C. Bonvin, R. Durrer, and M. A. Gasparini, *Fluctuations of the luminosity distance*, *Phys. Rev.* **D73** (2006) 023523, [[astro-ph/0511183](#)]. [Erratum: *Phys. Rev.* **D85**,029901(2012)].

- [79] F. R. G. Ellis, R. Maartens, and A. H. M. MacCallum, *Relativistic cosmology*. Cambridge University Press, Cambridge, 2012.
- [80] D. Duniya, *Large-scale imprint of relativistic effects in the cosmic magnification*, *Phys. Rev. D* **93** (2016), no. 10 103538, [[arXiv:1604.03934](https://arxiv.org/abs/1604.03934)]. [Addendum: *Phys. Rev. D* **93**, no. 12, 129902 (2016)].
- [81] D. Duniya, *Understanding the relativistic overdensity of galaxy surveys*, [arXiv:1606.00712](https://arxiv.org/abs/1606.00712).
- [82] D. Bertacca, N. Bartolo, M. Bruni, K. Koyama, R. Maartens, S. Matarrese, M. Sasaki, and D. Wands, *Galaxy bias and gauges at second order in General Relativity*, *Class. Quant. Grav.* **32** (2015), no. 17 175019, [[arXiv:1501.03163](https://arxiv.org/abs/1501.03163)].
- [83] E. Villa and C. Rampf, *Relativistic perturbations in Λ CDM: Eulerian & Lagrangian approaches*, *JCAP* **1601** (2016), no. 01 030, [[arXiv:1505.04782](https://arxiv.org/abs/1505.04782)].
- [84] D. Bertacca, R. Maartens, and C. Clarkson, *Observed galaxy number counts on the lightcone up to second order: I. Main result*, *JCAP* **1409** (2014), no. 09 037, [[arXiv:1405.4403](https://arxiv.org/abs/1405.4403)].
- [85] T. H.-C. Lu, K. Ananda, C. Clarkson, and R. Maartens, *The cosmological background of vector modes*, *JCAP* **0902** (2009) 023, [[arXiv:0812.1349](https://arxiv.org/abs/0812.1349)].
- [86] J.-C. Hwang, D. Jeong, and H. Noh, *Gauge dependence of gravitational waves generated from scalar perturbations*, *Astrophys. J.* **842** (2017), no. 1 46, [[arXiv:1704.03500](https://arxiv.org/abs/1704.03500)].
- [87] S. Saga, D. Yamauchi, and K. Ichiki, *Weak lensing induced by second-order vector mode*, *Phys. Rev. D* **92** (2015), no. 6 063533, [[arXiv:1505.02774](https://arxiv.org/abs/1505.02774)].
- [88] M. Bojowald and G. M. Hossain, *Cosmological vector modes and quantum gravity effects*, *Class. Quant. Grav.* **24** (2007) 4801–4816, [[arXiv:0709.0872](https://arxiv.org/abs/0709.0872)].
- [89] L. Dai, D. Jeong, and M. Kamionkowski, *Anisotropic imprint of long-wavelength tensor perturbations on cosmic structure*, *Phys. Rev. D* **88** (2013), no. 4 043507, [[arXiv:1306.3985](https://arxiv.org/abs/1306.3985)].
- [90] D. Bertacca, R. Maartens, and C. Clarkson, *Observed galaxy number counts on the lightcone up to second order: II. Derivation*, *JCAP* **1411** (2014), no. 11 013, [[arXiv:1406.0319](https://arxiv.org/abs/1406.0319)].
- [91] L. Dai, E. Pajer, and F. Schmidt, *On Separate Universes*, *JCAP* **1510** (2015), no. 10 059, [[arXiv:1504.00351](https://arxiv.org/abs/1504.00351)].

- [92] N. Bartolo, D. Bertacca, M. Bruni, K. Koyama, R. Maartens, S. Matarrese, M. Sasaki, L. Verde, and D. Wands, *A relativistic signature in large-scale structure*, *Phys. Dark Univ.* **13** (2016) 30–34, [[arXiv:1506.00915](#)].
- [93] R. de Putter, O. Doré, and D. Green, *Is There Scale-Dependent Bias in Single-Field Inflation?*, *JCAP* **1510** (2015), no. 10 024, [[arXiv:1504.05935](#)].
- [94] J. A. S. Lima, V. Zanchin, and R. H. Brandenberger, *On the Newtonian cosmology equations with pressure*, *Mon. Not. Roy. Astron. Soc.* **291** (1997) L1–L4, [[astro-ph/9612166](#)].
- [95] J. C. Hidalgo, A. J. Christopherson, and K. A. Malik, *The Poisson equation at second order in relativistic cosmology*, *JCAP* **1308** (2013) 026, [[arXiv:1303.3074](#)].
- [96] O. Umeh, S. Jolicoeur, R. Maartens, and C. Clarkson, *A general relativistic signature in the galaxy bispectrum: the local effects of observing on the lightcone*, *JCAP* **1703** (2017) 003, [[arXiv:1610.03351](#)].
- [97] S. Jolicoeur, O. Umeh, R. Maartens, and C. Clarkson, *Imprints of local lightcone projection effects on the galaxy bispectrum. Part III. Relativistic corrections from nonlinear dynamical evolution on large-scales*, *JCAP* **1803** (2018), no. 03 036, [[arXiv:1711.01812](#)].
- [98] T. Tram, C. Fidler, R. Crittenden, K. Koyama, G. W. Pettinari, and D. Wands, *The Intrinsic Matter Bispectrum in Λ CDM*, *JCAP* **1605** (2016), no. 05 058, [[arXiv:1602.05933](#)].
- [99] K. Koyama, O. Umeh, R. Maartens, and D. Bertacca, *The observed galaxy bispectrum from single-field inflation in the squeezed limit*, [[arXiv:1805.09189](#)].
- [100] T. Baldauf, U. Seljak, V. Desjacques, and P. McDonald, *Evidence for Quadratic Tidal Tensor Bias from the Halo Bispectrum*, *Phys. Rev.* **D86** (2012) 083540, [[arXiv:1201.4827](#)].
- [101] K. N. Ananda, C. Clarkson, and D. Wands, *The Cosmological gravitational wave background from primordial density perturbations*, *Phys. Rev.* **D75** (2007) 123518, [[gr-qc/0612013](#)].
- [102] D. Baumann, P. J. Steinhardt, K. Takahashi, and K. Ichiki, *Gravitational Wave Spectrum Induced by Primordial Scalar Perturbations*, *Phys. Rev.* **D76** (2007) 084019, [[hep-th/0703290](#)].

- [103] Y. Li, M. Schmittfull, and U. Seljak, *Galaxy power-spectrum responses and redshift-space super-sample effect*, *JCAP* **1802** (2018), no. 02 022, [[arXiv:1711.00018](#)].
- [104] R. Scoccimarro, S. Colombi, J. N. Fry, J. A. Frieman, E. Hivon, and A. Melott, *Nonlinear evolution of the bispectrum of cosmological perturbations*, *Astrophys. J.* **496** (1998) 586, [[astro-ph/9704075](#)].
- [105] M. Tegmark, A. J. S. Hamilton, M. A. Strauss, M. S. Vogeley, and A. S. Szalay, *Measuring the galaxy power spectrum with future redshift surveys*, *Astrophys. J.* **499** (1998) 555–576, [[astro-ph/9708020](#)].
- [106] D. J. Eisenstein and W. Hu, *Baryonic features in the matter transfer function*, *Astrophys. J.* **496** (1998) 605, [[astro-ph/9709112](#)].
- [107] A. Taruya, S. Saito, and T. Nishimichi, *Forecasting the Cosmological Constraints with Anisotropic Baryon Acoustic Oscillations from Multipole Expansion*, *Phys. Rev.* **D83** (2011) 103527, [[arXiv:1101.4723](#)].
- [108] J. Yoo and U. Seljak, *Wide Angle Effects in Future Galaxy Surveys*, *Mon. Not. Roy. Astron. Soc.* **447** (2015), no. 2 1789–1805, [[arXiv:1308.1093](#)].
- [109] C. Blake, P. Carter, and J. Koda, *Power spectrum multipoles in a curved sky: an application to the 6-degree Field Galaxy Survey*, [[arXiv:1801.04969](#)].
- [110] **BOSS** Collaboration, F. Beutler et al., *The clustering of galaxies in the SDSS-III Baryon Oscillation Spectroscopic Survey: Testing gravity with redshift-space distortions using the power spectrum multipoles*, *Mon. Not. Roy. Astron. Soc.* **443** (2014), no. 2 1065–1089, [[arXiv:1312.4611](#)].
- [111] S. Yokoyama, T. Matsubara, and A. Taruya, *Halo/galaxy bispectrum with primordial non-Gaussianity from integrated perturbation theory*, *Phys. Rev.* **D89** (2014), no. 4 043524, [[arXiv:1310.4925](#)].
- [112] R. E. Smith, P. I. R. Watts, and R. K. Sheth, *The impact of halo shapes on the bispectrum in cosmology*, *Mon. Not. Roy. Astron. Soc.* **365** (2006) 214–230, [[astro-ph/0508382](#)].
- [113] C. A. Valenzuela-Toledo, Y. Rodriguez, and J. P. Beltran Almeida, *Feynman-like Rules for Calculating n-Point Correlators of the Primordial Curvature Perturbation*, *JCAP* **1110** (2011) 020, [[arXiv:1107.3186](#)].
- [114] S. Weinberg, *Cosmology*. Oxford University Press, 2008.

- [115] D. H. Lyth and A. R. Liddle, *The primordial density perturbation: Cosmology, inflation and the origin of structure*. Cambridge University Press, 2009.
- [116] A. F. Heavens and A. N. Taylor, *A Spherical Harmonic Analysis of Redshift Space*, *Mon. Not. Roy. Astron. Soc.* **275** (1995) 483–497, [[astro-ph/9409027](#)].
- [117] Y. Nan, K. Yamamoto, and C. Hikage, *Higher multipoles of the galaxy bispectrum in redshift space*, [arXiv:1706.03515](#).
- [118] P. Gagrani and L. Samushia, *Information Content of the Angular Multipoles of Redshift-Space Galaxy Bispectrum*, *Mon. Not. Roy. Astron. Soc.* **467** (2017), no. 1 928–935, [[arXiv:1610.03488](#)].
- [119] D. Karagiannis, A. Lazanu, M. Liguori, A. Raccanelli, N. Bartolo, and L. Verde, *Constraining Primordial non-Gaussianity with Bispectrum and Power Spectrum from Upcoming Optical and Radio Surveys*, [arXiv:1801.09280](#).
- [120] A. Gangui, F. Lucchin, S. Matarrese, and S. Mollerach, *The Three point correlation function of the cosmic microwave background in inflationary models*, *Astrophys. J.* **430** (1994) 447–457, [[astro-ph/9312033](#)].
- [121] L. Verde, L.-M. Wang, A. Heavens, and M. Kamionkowski, *Large scale structure, the cosmic microwave background, and primordial non-gaussianity*, *Mon. Not. Roy. Astron. Soc.* **313** (2000) L141–L147, [[astro-ph/9906301](#)].
- [122] N. Bartolo, E. Komatsu, S. Matarrese, and A. Riotto, *Non-Gaussianity from inflation: Theory and observations*, *Phys. Rept.* **402** (2004) 103–266, [[astro-ph/0406398](#)].
- [123] B. A. Bassett, S. Tsujikawa, and D. Wands, *Inflation dynamics and reheating*, *Rev. Mod. Phys.* **78** (2006) 537–589, [[astro-ph/0507632](#)].
- [124] **Planck** Collaboration, P. A. R. Ade et al., *Planck 2015 results. XVII. Constraints on primordial non-Gaussianity*, *Astron. Astrophys.* **594** (2016) A17, [[arXiv:1502.01592](#)].
- [125] F. R. Bouchet, S. Colombi, E. Hivon, and R. Juszkiewicz, *Perturbative Lagrangian approach to gravitational instability*, *Astron. Astrophys.* **296** (1995) 575, [[astro-ph/9406013](#)].
- [126] T. Giannantonio and C. Porciani, *Structure formation from non-Gaussian initial conditions: multivariate biasing, statistics, and comparison with N-body simulations*, *Phys. Rev.* **D81** (2010) 063530, [[arXiv:0911.0017](#)].

- [127] T. Baldauf, U. Seljak, and L. Senatore, *Primordial non-Gaussianity in the Bispectrum of the Halo Density Field*, *JCAP* **1104** (2011) 006, [[arXiv:1011.1513](https://arxiv.org/abs/1011.1513)].
- [128] T. Kitayama and Y. Suto, *Semianalytical predictions for statistical properties of x-ray clusters of galaxies in cold dark matter universes*, *Astrophys. J.* **469** (1996) 480, [[astro-ph/9604141](https://arxiv.org/abs/astro-ph/9604141)].
- [129] E. Di Dio, R. Durrer, G. Marozzi, and F. Montanari, *The bispectrum of relativistic galaxy number counts*, *JCAP* **1601** (2016) 016, [[arXiv:1510.04202](https://arxiv.org/abs/1510.04202)].
- [130] R. Maartens, C. Clarkson, and S. Chen, *The kinematic dipole in galaxy redshift surveys*, [arXiv:1709.04165](https://arxiv.org/abs/1709.04165).
- [131] **MeerKLASS** Collaboration, M. G. Santos et al., *MeerKLASS: MeerKAT Large Area Synoptic Survey*, 2017. [arXiv:1709.06099](https://arxiv.org/abs/1709.06099).

